IMMUNOPATHOGENESIS AND CONTROL OF SINDBIS VIRUS IN THE CENTRAL NERVOUS SYSTEM DURING NONFATAL ALPHAVIRUS ENCEPHALOMYELITIS

by
Victoria Kate Baxter

A dissertation submitted to Johns Hopkins University in conformity with the requirements for the degree of Doctor of Philosophy

Baltimore, Maryland

January 2016

ABSTRACT

Sindbis virus (SINV), the prototypic alphavirus, is neurotropic in mice, providing a valuable model for studying nonfatal alphavirus encephalomyelitis. Infectious virus is cleared from the brain within a week after infection, but viral RNA is cleared slowly and persists for the life of the animal. To better understand the immunopathogenesis and control of SINV infection, C57BL/6 mice were infected with the nonfatal TE strain of SINV, and clinical disease, virus clearance, and the immune response were examined. During the height of active infection, mice developed clinical signs of encephalomyelitis and exhibited neurological deficits. Following recovery from clinical disease, hippocampus-dependent memory deficits persisted, concurrent with the presence of viral RNA. Treatment with 6-diazo-5-oxo-l-norleucine (DON), a glutamine antagonist that inhibits both lymphocyte proliferation and glutamate excitotoxicity, partially prevented development of clinical disease and neurological sequelae. Mice treated with DON exhibited decreased CNS inflammation and pathology but delayed virus clearance, indicating that the immune response mediates both processes. Previous studies have shown that clearance of SINV is cooperatively facilitated by anti-SINV antibody and the cytokine interferon gamma (IFN-γ). To further examine the role IFN-γ plays in SINV clearance and control, neuronal cell cultures and mice deficient in IFN-γ (*Ifng*$^{-/-}$) or IFN-γ receptor (*Ifngr1*$^{-/-}$) were infected with SINV TE. IFN-γ facilitated clearance of both infectious virus and viral RNA *in vitro*, but mice with impaired IFN-γ signaling displayed accelerated viral RNA clearance from the CNS despite delayed clearance of infectious virus, suggesting IFN-γ-induced immunomodulation. IFN-γ promoted local production of

anti-SINV antibody but inhibited infiltration of granzyme B-producing CD8+ T cells. Memory T cells, which persist in the brain following clearance of infectious virus, were also affected by IFN-γ signaling, with *Ifng*$^{-/-}$ and *Ifngr1*$^{-/-}$ mice possessing fewer CD8+ tissue resident memory T cells. Therefore, IFN-γ plays a multi-faceted role in SINV clearance and control during CNS infection.

THESIS ADVISORY COMMITTEE

Thesis Advisor: Dr. Diane E. Griffin

Thesis Committee: Dr. Jay Bream

Dr. Alan Scott

Dr. M. Christine Zink (chair, reader)

ACKNOWLEDGEMENTS

I have been incredibly fortunate to have a strong support group throughout the course of this thesis work, both inside and outside the lab. I first and foremost want to thank my mentor Diane Griffin for guiding me throughout this process. She had the experience and foresight to let me think critically and independently but not let me flounder and waste my time. She also has been incredibly encouraging and understanding of my postdoctoral fellowship, and I would have never been able to have passed my ACLAM specialty boards without her support. I am very fortunate to have such an incredible scientist and role model for a mentor.

I would also like to thank my thesis committee. Drs. Jay Bream and Alan Scott helped me piece together the immunology aspects of my project while consistently providing support and encouragement. Dr. Chris Zink assisted with the pathogenesis and virology. In addition to serving as my committee chair and thesis reader, she also served as the director of my laboratory animal postdoctoral fellowship. I truly appreciate her for all the helpful discussions, both regarding science and life outside of Hopkins and am very lucky to have her as a role model in veterinary science.

The Griffin lab members made my day-to-day life in the lab truly enjoyable. In particular, I would like to thank Drs. Kimberly Schultz and Kirsten Kulcsar. We shared lab space for the majority of my thesis work, and I will cherish all the laughs we shared together. Many wonderful lab members have moved on to bigger things: Dr. Sivabalan Manivannan, Dr. Rupak Shivakoti, Dr. Wen-Hsuan Lin, Steve Goldstein, Niki Putnam, and Julia Zhao. And several current lab members continue to make coming in to work

each day enjoyable: Debbie Hauer (our wonderful lab manager/"lab mother"), Dr. Gui Nilarantanakul, Ashley Nelson, Nina Martin, Elizabeth Troisi, and Jane Xie. I also would like to thank all of the too-numerous-to-name members of labs throughout MMI whom I worked with each day. I really enjoyed talking science and animal models with them, and they definitely helped make my PhD experience a special one. I would be terribly remiss to not acknowledge the wonderful animal caretakers who kept my thesis work (i.e., my lab mice) alive and well, DJ Johnson and Chris Wright. Their investment in and concern for the welfare of the research animals are truly inspiring, and I was incredibly lucky to have them caring for my mice.

Much of the work seen in this thesis was accomplished through shared effort with other researchers at Johns Hopkins. Michelle Potter and Barbara Slusher of the Brain Science Institute spoiled me with such a positive collaborative experience, and I am proud of how productive our collaborations have turned out to be. The Retrovirus lab in the MCP department, particularly Drs. Joe Mankowski, Kelly Metcalf Pate, and Lisa Mangus, were incredibly generous to give their time helping me with microscopy and immunohistochemistry techniques and well as general experimental design. I knew if I ever needed anything, they would always be available and willing to help me.

I would also like to thank the administrative team in the Cellular and Molecular Medicine program. Dr. Raijni Rao was always supportive, and I appreciate her guidance and encouragement throughout the process. Program "mothers" Leslie Lichter and Colleen Graham were incredibly kind and understanding and always made sure I was on track. I always knew I could count on them for a hug and some words of encouragement.

I also had an incredible CMM class to matriculate in with, and I look forward to seeing how far everyone goes in their careers.

Throughout my PhD career, I had the unique opportunity to participate in another aspect of research: my postdoctoral fellowship in lab animal medicine. As previously mentioned, Dr. Chris Zink provided an incredible amount of support and encouragement as I juggled both programs at the same time, and LAM faculty members Drs. Bob Adams and Julie Watson provided excellent mentorship to make me the best clinical vet I could be. I also was very fortunate to have an incredible cohort of lab animal trainees to share my clinical experience with. Past residents Drs. Eric Hutchinson, Nicole Azene, Kelly Rice (my wonderful friend and resident-mate), Tracey Graham, Theresa Meade, Caroline Garrett, and Pete Otovic have all moved on to bigger and better things, and current residents Drs. Rachael Cohen, Meghan Vermillion, Cassie Moats, Jess Izzi, Anna Goodroe, Logan France, and Adam Werts continue to make my experience at Hopkins a fun and special one. I truly appreciate being able to spend time with RAR and the MCP department when I wasn't in lab and will cherish all the memories we made. I especially want to thank Kelly Metcalf Pate and Zach Freeman, my wonderful resident-mates and good friends. Having them for friends and confidants has made even my worst days bearable, and I am thankful to have them in my life.

Finally, I would like to thank my family. My parents Dave and Karen have always supported me, even though I "could get a job with just my DVM". They raised me to be the confident and independent person I am, and I am so proud and thankful to be their daughter. My sisters Bree and Kelley have always provided their support and encouragement, while making sure I'm not being overconfident or getting a big head.

And I especially want to thank my wonderful husband Josh. He has spent the majority of our almost 12-year relationship supporting me throughout the phases of my career. He not only supported me when I suddenly announced I was going to go to vet school, but also completed two master's degrees so that he could stay in College Station during the four years I spent earning my DVM. He supported me when we decided moving away from Texas and to Baltimore was the best move for my career. And he is supporting me now as we look to the next chapter of my career and our lives. Josh has always been loving and encouraging while simultaneously being my "reality check" throughout everything. He has been with me through many good times and a few bad times, and I am truly thankful to go through life with him as my partner.

TABLE OF CONTENTS

ABSTRACT…… ii

ACKNOWLEDGEMENTS……..….....iv

TABLE OF CONTENTS…….....…..viii

CHAPTER 1: GENERAL INTRODUCTION……....……...… 1

ALPHAVIRUSES WORLDWIDE……...……....… 2

SINDBIS VIRUS.....4

SINDBIS VIRUS INFECTION OF THE CENTRAL NERVOUS SYSTEM.....5

PATHOLOGY OF ALPHAVIRUS INFECTION..... 8

IMMUNE RESPONSE TO VIRUS INFECTION IN THE CENTRAL NERVOUS SYSTEM..... 10

VIRUS CLEARANCE.....12

INTERFERON GAMMA..... 15

LONG-TERM MAINTENANCE OF CELLULAR IMMUNITY DURING VIRAL INFECTION.....16

FIGURES..... 20

CHAPTER 2: INFECTION WITH SINDBIS VIRUS RESULTS IN PERSISTENT NEUROLOGICAL SEQUELAE FOLLOWING RECOVERY FROM CLINICAL ALPHAVIRUS ENCEPHALOMYELITIS..... 22

INTRODUCTION.....23

MATERIALS AND METHODS.....24

RESULTS.....30

DISCUSSION..... 32

FIGURES..... 35

CHAPTER 3: GLUTAMINE ANTAGONISM DECREASES PATHOLOGY BUT DELAYS VIRUS CLEARANCE DURING NONFATAL ALPHAVIRUS ENCEPHALOMYELITIS 40

INTRODUCTION.....41

MATERIALS AND METHODS..... 43

RESULTS.....53

DISCUSSION..... 66

FIGURES..... 71

CHAPTER 4: MODULATION OF THE IMMUNE RESPONSE BY INTERFERON GAMMA DURING NONFATAL ALPHAVIRUS ENCEPHALOYMYELITIS ALTERS VIRUS CLEARANCE IN THE CENTRAL NERVOUS SYSTEM..... 87

INTRODUCTION.....88

MATERIALS AND METHODS..... 90

RESULTS.....99

DISCUSSION.....118

FIGURES.....129

TABLES..... 150

CHAPTER 5: MEMORY T CELLS REMAIN IN THE BRAIN LONG-TERM FOLLOWING ALPHAVIRUS CLEARANCE..... 151

INTRODUCTION..... 152

MATERIALS AND METHODS.....154

RESULTS.....158

DISCUSSION.....164

FIGURES.....169

CHAPTER 6: GENERAL DISCUSSION AND CONCLUSIONS.....179

FIGURES.....190

TABLES.....192

APPENDICES......194

APPENDIX A.....195

APPENDIX B.....214

REFERENCES.....217

CURRICULUM VITAE.....265

CHAPTER 1:

GENERAL INTRODUCTION

ALPHAVIRUSES WORLDWIDE

Arboviruses, particularly members of the Togaviridae and Flaviviridae families, represent an emerging threat of disabling disease worldwide. Alphaviruses, members of Togaviridae, are generally divided into two major groups based on geographical location and typical disease manifestation[1]. Old World alphaviruses, which include Sindbis virus (SINV), Chikungunya virus (CHIKV), Ross River virus, and Semliki Forest virus (SFV), are normally found in Europe, Africa, Asia, and Australia. When humans are infected, clinical disease typically manifests as fever, rash, and arthritis[2]. In contrast, the New World alphaviruses, which include eastern equine encephalitis virus (EEEV), western equine encephalitis virus (WEEV), and Venezuelan equine encephalitis virus (VEEV), are generally found in North and South America. When humans are naturally infected, they tend to develop encephalitis and meningitis. Occasionally other disease manifestations are seen with alphavirus infection, such as encephalomyelitis induced by CHIKV or SFV[3,4]. Despite alphaviruses being considered to cause acute infections, large percentages of people report development of debilitating long-term maladies, such as myalgia and arthralgia, that last months to years following recovery from the initial clinical illness[5-7].

Mosquitoes transmit alphaviruses, and like other arboviruses such as flaviviruses and bunyaviruses, they represent a remerging threat to populations worldwide as vectors expand into new territories. New World alphaviruses are typically maintained in a sylvatic cycle, with passerine or aquatic birds and small mammals serving as reservoir hosts[8]. However, promiscuity by permissive mosquitos species, which include *Aedes* and

Culex spp, occasionally results in infection of other species, particularly humans and horses. These large mammals are typically dead-end hosts, though VEEV is capable of replicating at high enough titers in the blood to permit continued transmission[2].

Human cases of EEE, WEE, and VEE are only sporadically reported in the United States each year, though outbreaks of EEE and VEE over the last few decades have increased and are being diagnosed in previously unreported locations. An outbreak of VEE in the mid-1990's in Venezuela and Columbia affected an estimated 75,000 to 100,000 people[9]. The number of human cases of EEE in the northeastern United States has markedly increased in the last decade, with states such as Vermont and Maine reporting locally-acquired human cases for the first time[10,11]. Mortality associated with New World alphavirus infection varies by species. While most people infected with WEEV remain asymptomatic, EEE carries a substantial death rate, ranging from 30 to 70% depending on the source[8,12,13]. People who survive the clinical illness, especially those infected as infants or children, tend to develop lifelong neurological deficits[14-18].

Currently, no treatments beyond symptomatic care are available for people who contract EEE, WEE, or VEE[19]. A licensed combination vaccine for EEEV, WEEV, and VEEV is available for horses, but no effective vaccine is approved for non-military use in humans[20]. Because of the reemerging public health concern and propensity for these viruses to cause lasting physical debilitations, it is increasingly important to understand the pathogenesis of alphavirus encephalomyelitis so that better preventatives and treatments may be developed.

SINDBIS VIRUS

Sindbis virus (SINV) is the prototypic member of the alphaviruses. Like other members of the genus, it is enveloped with a positive-sense, single-stranded RNA genome[21,22]. The 70nm virion consists of capsid proteins surrounding a single RNA genome, and two transmembrane glycoproteins, E1 and E2, facilitate entry into cells by endocytosis via a currently unknown receptor(s). The 11.7kb genome contains a 5'methylguanylate cap and 3'polyadenylated tail and encodes both structural and nonstructural proteins. The four nonstructural proteins (nsp1, nsp2, nsp3, and nsp4) are encoded at the 5' end, and the five structural proteins, which include the capsid and E1 and E2 glycoproteins, are encoded at the 3' end. Like other positive-sense RNA viruses, the genomic RNA of SINV is infectious, meaning when in a permissive cell, it can automatically replicate and produce infectious virus particles.

Upon entry into a permissive cell, the viral envelope fuses with the cell membrane, and the virion core disassembles, revealing the genomic RNA that serves as messenger RNA from which the nonstructural proteins are translated[22,23]. Virus replication occurs within cytopathic vacuoles that form in the cytoplasm on the surface of lysosomes and endosomes. The nonstructural proteins are translated as a polyprotein and, following multiple cleavage events, facilitate replication of a complementary, negative sense, full-length RNA genome (Fig1-1). Additional full-length, positive-sense, single-stranded RNA genomes are then transcribed from this negative-sense genome for incorporation into new virus particles. The negative-sense genome also encodes a promoter from which a subgenomic RNA is transcribed. Translation of the subgenomic

RNA results in production of a structural polyprotein that includes capsid, E3, E2, 6K, and E1. Following post-translational processing of the polyprotein, the capsid proteins assemble around a single positive-sense RNA genome. The capsid then buds from the plasma membrane, acquiring the envelope proteins that were processed in the endoplasmic reticulum. The two glycoproteins form heterodimeric trimers, creating a Class II fusion system, with E2 serving as the ligand for receptor binding and E1 containing the fusion peptide. E2 also contains most of the known epitopes for neutralizing antibodies[24,25].

SINV was first isolated in 1952 from *Culex univittatus* mosquitoes in Egypt and was named after the village in which it was first identified[26]. It is categorized as an Old World alphavirus, and upon natural infection by mosquitos, humans develop a flu-like illness with rash and arthralgia. However, upon infection of mice with laboratory-adapted strains of SINV, the virus is neurotropic and causes encephalomyelitis[27]. This provides a valuable model of disease typically produced by the New World alphaviruses, allowing for the study of pathogenesis of virus infection and the resulting host immune response.

SINDBIS VIRUS INFECTION IN THE CENTRAL NERVOUS SYSTEM

Several host and virus strain factors can affect virulence during SINV infection; one of these is maturity of neurons and mice. Susceptibility to alphavirus infection is age-dependent, with maturation associated with decreased virus replication and less severe clinical disease. While neonatal mice infected with SINV die within three to four days

following infection, mice infected at weanling age with the same strain are able to clear the virus and recover from clinical disease[28]. These disparate outcomes are not due to changes in the immune response, but instead are due to increased resistance of neurons to infection as the cells mature[29-31]. Differentiation of neurons *in vitro* is associated with increased expression of antiviral genes and with decreased replication of infectious virus and production of viral proteins and RNA during infection[32].

Several strains of SINV have been adapted in the laboratory and produce clinical disease of varying severity in mice. The cell culture-adapted HRSP strain is the least virulent, reaching lower peak virus titers *in vivo* than other strains and capable of being fully cleared when injected into mice[33]. On the other end of the spectrum, neuroadapted Sindbis virus (NSV) causes 100% mortality in susceptible strains of mice. Neuroadapted Sindbis virus was created through intracranially inoculating mice with the original SINV isolate from mosquitoes, AR339, and serially passaging it through the brains of alternating neonatal and weanling mice six times[34]. Infection of susceptible weanling mice with NSV causes encephalomyelitis with ascending paralysis and results in 100% mortality by ten days post infection (DPI)[35]. Amino acid changes in the E1 (V72A and G313D) and E2 (G55H and L209G) proteins of NSV are determinants of its increased virulence[36]. Of intermediate virulence is the TE strain of SINV, which is a recombinant virus strain containing the E2 gene of NSV and the E1 gene of AR339[36,37]. While infection of suckling mice results in 100% mortality, infection of weanling mice only rarely progresses to death[37]. These seemingly minor changes in glycoprotein sequence can alter the virus's ability to bind surface receptors of permissive cells, resulting in altered virus replication and thus facilitating increased virulence[36-38].

Finally, the strain of mouse used also affects the outcome of SINV infection. SJL mice infected with the nonfatal AR339 strain of SINV develop more severe disease than BALB/c mice and have higher levels of inflammation and reduced IL-4 mRNA expression[39]. When infected with NSV strain of SINV, C57BL/6 mice develop ascending paralysis and 100% mortality by 14 days, while BALB/c mice only develop mild disease and survive[40]. Brains of C57BL/6 mice have increased inflammation and apoptosis with amplified proinflammatory cytokine expression and production, while BALB/c mice possess more infiltrating regulatory T cells and increased levels of anti-SINV antibody[41]. Unlike age receptiveness to SINV infection, differences in virus susceptibility in mouse strains appear to be immune-mediated.

When C57BL/6 mice are intracranially infected with the nonfatal TE strain of SINV, the course of virus infection in the brain can be divided into three main phases (Fig 1-2)[42]. Phase 1 occurs in the first week of infection, and during this time, both infectious virus titers and viral RNA levels reach their peak, around 3 to 5 DPI. Infectious virus titers then fall precipitously, dropping below detectable levels by about 7 to 8 DPI, while viral RNA levels remain at high copy number. During Phase 2 of infection, which occurs from about 10 to 60 DPI, infectious virus titers are no longer consistently detectable by plaque assay in the brain. Viral RNA levels start out at high copy number but steadily decline throughout the rest of the phase. Phase 3 of infection starts at around 60 DPI and continues for at least a year following infection and presumably for the remaining life of the animal[43,44]. Infectious virus continues to be undetectable, but viral RNA reaches a low level steady-state that is consistently detectable by qRT-PCR[42].

PATHOLOGY OF ALPHAVIRUS INFECTION

When neurons are infected with a virus, there are three possible outcomes that may occur[45]. First, the virus may directly kill the neuron by inducing processes such as apoptosis or necrosis[46-48]. Second, the neuron may be damaged or die through a secondary process, such as by inflammatory effects or by glutamate excitotoxicity[49,50]. Activation of nearby microglia and astrocytes that release reactive oxygen and nitrogen species and infiltration of monocytes, neutrophils, and lymphocytes releasing cytokines may all facilitate neuronal damage[51]. And lastly, virus infection of the neuron may be controlled through a noncytolytic mechanism, and the cell survives. Because viral RNA continues to persist within the cell, the immune system must continually control virus reactivation by some mechanism currently unknown.

Histopathological changes in the brains of New World alphavirus-infected humans and horses are characterized by acute neuronal degeneration and classic encephalitic features. Early in the disease process, massive numbers of neutrophils infiltrate the brain, though lymphocytes soon replace them as the predominant immune cell population[52,53]. In brains of C57BL/6 mice infected with NSV, marked loss of neurons, particularly in the CA regions of hippocampus, is the hallmark feature[54]. Perivascular cuffing and parenchymal infiltration of mononuclear cells is also considerable. Grossly, hydrocephalus and dilation of the lateral ventricles may also be seen. Together, these pathologic changes result in the neurologic deficits seen with alphavirus encephalomyelitis.

The immune system response to alphavirus infection in the central nervous system (CNS) presents a double-edged sword: while the immune response is necessary for bringing virus replication and production under control, it is also responsible for many of the pathological changes and neurological damage produced. When SCID mice, which are deficient in both B cells and T cells, are infected with the AR339 strain of SINV, they do not develop signs of neurological disease in contrast to their wild-type counterparts[24]. When mice lacking various components of cellular immunity are infected with NSV, mortality significantly decreases, indicating T cells play an important role in the process[55]. Furthermore, NSV-induced clinical disease development and mortality coincide with infiltration of CD4+ and CD8+ T cells into the brain[56]. These studies point towards the immune response playing an overwhelmingly significant role in alphavirus encephalomyelitis.

Another secondary consequence of virus infection that contributes to neuronal damage and death is glutamate excitotoxicity. Glutamate is a major excitatory neurotransmitter that binds to three different receptors on recipient neurons: 2-amino-3-(5-methyl-3-oxo-1,2-oxazol-4-yl) propranoic acid (AMPA), N-methyl-D-aspartic acid (NMDA), and kainate receptors[57]. Over-activation of these receptors results in a substantial influx of calcium into the post-synaptic neuron, which in turn triggers a cascade resulting in free radical production and mitochondrial dysfunction, and ultimately, cell death[58,59]. Hippocampal neurons in the brain and motor neurons in the spinal cord are especially sensitive to glutamate excitotoxicity[60-63], and the process plays a role in SINV-induced pathology[64,65]. Furthermore, treatment with an AMPA receptor antagonist protects mice from NSV-induced death, indicating a significant role for

glutamate excitotoxicity in the pathologic process occurring during alphavirus encephalomyelitis[49].

IMMUNE RESPONSE TO VIRUS INFECTION IN THE CENTRAL NERVOUS SYSTEM

Response to viral infections of the CNS poses a unique problem for the immune system. The restrictive nature of the blood brain barrier limits the ability of proteins and immune cells to enter into the brain and spinal cord in response to a virus infection[66]. Resident cells of the CNS, particularly neurons, have a limited-to-nonexistent capacity to express MHC molecules[67]. And arguably most important, preservation of neuronal function requires that infected neurons be allowed to survive, necessitating immune cells to employ special noncytolytic mechanisms to control virus infection.

Upon establishment of a new virus infection in the CNS, activation of the innate immune response is triggered. Type I interferons (IFNs), particularly IFN beta (IFN-β), are rapidly produced by neurons and glial cells[68]. Local production of IFN-β and IFN alpha (IFN-α) decreases virus replication and restricts virus spread from cell to cell by activating antiviral genes and neuroprotective factors[69-71]. Clinical disease in mice with impaired type I IFN signaling is more severe for several viruses that infect the CNS, including SINV, West Nile virus (WNV), neurotropic coronavirus, and Theiler's murine encephalitis virus (TMEV)[69,71-75]. Activated microglia and astrocytes secrete a wide range of cytokines and chemokines, including proinflammatory cytokines IL-6, IL-1β, and

TNF, and leukocyte chemoattractants CCL-1, CCL-2, CCL-5 (RANTES), CXCL9, and CXCL10[76-78]. Secretion of these molecules enhances leukocyte adhesion and migration to the site of infection and up-regulation of MHC molecules on microglia. These innate immune processes restrict early virus replication until the adaptive immune response can be mounted to further control and clear virus[79].

Response of adaptive immune cells to infection in the CNS is initiated a few days into the course of infection. Antigen presentation in the parenchyma of the CNS is severely limited, so most lymphocyte activation occurs in peripheral lymph nodes[80]. In the case of the brain, the draining lymph nodes are the superficial and deep cervical lymph nodes (CLNs)[81]. In C57BL/6 mice infected with SINV TE, CD8+ T cells first enter the brain around 5 DPI and peak in number at 7 DPI[42]. CD4+ T cells and B cells soon follow, peaking around 10 DPI. T cells initially accrue around vessels in the brain, forming perivascular cuffs, but parenchymal cellularity soon increases. CD4+ T cells mostly accumulate around the vessels, while CD8+ T cells travel further into the parenchyma[82]. Cell numbers slowly decrease during Phase 2 of infection, returning to baseline by four months[42].

The T cells present in the brain have a variety of antiviral effector functions. CD8+ T cells have cytotoxic activity and secrete effector molecules such as IFN-γ and granzyme B. While neurons only rarely express MHC I molecules, CD8+ T cells have been shown to directly interact with TMEV-infected neurons, providing a possible MHC-independent mechanism for CD8+ T cell-mediated virus control[83]. CD4+ T cells support migration and survival of CD8+ T cells and secrete a variety of cytokines, including IFN-γ[84]. Resident B cells in the brain secrete antibody directed against the virus; IgM is

initially produced, followed by IgG and IgA[42,85]. Together, these responses lead to clearance of virus.

VIRUS CLEARANCE

Because neurons are a valuable yet finite nonrenewable population of cells, clearance of viruses that infect them requires a noncytolytic process to avoid permanent long-term neurological deficits[86]. Virus clearance is a multi-component process. Virus spread must be inhibited, production of both infectious virus and viral RNA must be diminished, and reactivation from persistent viral remnants must be controlled. Mechanisms of virus clearance are also cell type- and tissue region-specific.

While innate production of type I IFN, particularly IFN-β, can help with the early control of SINV replication and spread, the adaptive immune response is responsible for long-term virus clearance[69,70]. While wild-type C57BL/6 mice are able to clear infectious SINV by 7 to 8 DPI, SCID mice still possess high titers in CNS tissue at 35 DPI. μMT mice, which lack mature B cells and thus antibody, have decreased virus titers but cannot fully clear infectious virus, and mice deficient in IFN-γ or IFN-γ receptor show reactivation of infectious virus after initial clearance. The course of SINV infection of mice double-knockout for antibody and IFN-γ is intermediate between that of SCID mice and μMT mice. Therefore, SINV clearance from the CNS is achieved by a synergistic cooperation between SINV-specific antibody and IFN-γ[70].

Several studies have shown that antibody directed against the E2 glycoprotein of SINV plays an important role in clearance of virus. When hyperimmune serum is transferred to persistently infected SCID mice, virus clearance occurs within 48 hours[24]. This still occurs in the absence of complement and NK cells, and when sensitized T cells are similarly adoptively transferred, no change in virus replication occurs. Viral RNA levels also decrease with passive transfer of hyperimmune serum. The most potent antibodies for clearance are those directed against the SINV E2 glycoprotein. When cells are treated *in vitro* with monoclonal antibodies against SINV E2, virus production decreases, and Na^+K^+ATPase function and membrane potential are restored[24,87]. However, when passively transferred antibodies are allowed to naturally decay over time, virus production resumes, indicating replication-competent viral RNA persists in infected cells[43]. While inflammation reduces the blood brain barrier restrictions to entry of immunoglobulins into the brain parenchyma during acute SINV infection, the amount found in the brain interstitium following initial clearance of infectious virus is 100 to 200 times less than that found in the serum[88,89]. This amount is unlikely to be sufficient to suppress virus reactivation, suggesting that a considerable amount of antibody is locally produced by resident B cells[90]. Antibody-secreting B cells remain in the brain following initial clearance of infectious virus, likely contributing to long-term control of virus reactivation[44,91].

Though unable to clear infectious virus from the entire brain, uMT mice are capable of clearing virus from the brain stem and from the spinal cord[92]. SCID mice are incapable of clearing virus from these regions, suggesting T cells play a significant clearance role in certain areas of the brain and in the spinal cord[70]. Both CD4+ and CD8+

T cells are required for full virus clearance in these regions, suggesting that an antiviral cytokine response produced by both cell types facilitates this process rather than a cytotoxic effector response, which would exacerbate CNS pathological changes[92]. SCID mice were infected with recombinant SINV viruses expressing constructs for either IFN-γ or TNF-α, the two cytokines produced by both CD4+ and CD8+ T cells with antiviral activity. Virus clearance in the spinal cord was achieved with the IFN-γ recombinant virus, but not the one expressing TNF-α, indicating IFN-γ plays a prominent role in virus clearance. Treatment of differentiated neuronal CSM14.1 cells with IFN-γ results in decreased production of infectious virus and viral RNA and initiation of virus clearance[93]. SINV-infected athymic nude mice have decreased B cells and antibody levels in the CNS, particularly IgG, suggesting T cells influence B cell recruitment into the brain and immunoglobulin isotype switching as well[85,94].

Because SINV can reactivate in the brain once anti-SINV antibody decays in SCID mice, persistent viral RNA is capable of renewing virus production[43]. Therefore, immune-mediated decreases of viral RNA during Phase 2 of infection is likely very important to prevent renewed virus production. Currently the mechanisms by which viral RNA is cleared are very poorly understood. When infected with NSV, viral RNA levels in the brains and spinal cords of both CD8 and B2m knockout mice remain elevated longer than in wild-type mice[67]. This suggests CD8+ T cells play an important role in viral RNA clearance, likely through secretion of an effector protein, such as IFN-γ. Mice that are deficient in either IFN-γ or IFN-γ receptor tend to show reactivation of infectious virus after initial virus clearance during Phase 2 of infection, around 18 to 21 DPI, suggesting IFN-γ is required for decreasing viral RNA levels during this time[70]. Because

CD8+ T cells in the brain contract considerably at the start of Phase 2 of infection, CD4+ T cells may predominantly produce IFN-γ during this time[42].

INTERFERON GAMMA

IFN-γ is predominantly produced by activated CD4+ and CD8+ T cells and by natural killer (NK) cells[95,96]. Because these cells, particularly the T cells, do not enter the brain until 3 to 4 DPI, IFN-γ likely exerts its effects by combatting virus already within cells, as opposed to preventing virus infection of naïve cells[76]. In addition to SINV, several different neurotropic viruses have been implicated to be cleared at least in part by IFN-γ, including measles virus, lymphocytic choriomeningitis virus (LCMV), vesicular stomatitis virus (VSV), mouse hepatitis virus (MHV), enterovirus 71, Theiler's murine encephalitis virus (TMEV), and bornavirus[97-102].

IFN-γ, the classic proinflammatory cytokine, exerts its effects by inducing IFN-stimulated genes (ISGs) through its signaling pathway. The IFN-γ receptor consists of a heterotetramer made up of the ligand-binding IFN-γR1 and signaling IFN-γR2[103]. During SINV infection, IFN-γ signals through its receptor to activate the Jak/Stat pathway, and phosphorylated Stat proteins, particularly STAT1, translocate to the nucleus where they bind to gamma-associated site (GAS) elements on genes[104]. IFN-γ signaling has been shown to activate over 200 ISGs with varying functions, resulting in multifaceted modulation of the immune response[103,105]. These include cellular effects on immune cell trafficking, T helper cell differentiation, antigen presentation, IgG class switching, and

macrophage activation, and more direct intracellular antiviral activities, such as the upregulation of dsRNA-activated protein kinase (PKR) and 2'-5' oligoadenylate synthetase (2-5A synthetase)[106-108]. The IFN-γ receptor is expressed on many different cell types, including neurons[103].

During SINV infection in neuronal cell culture *in vitro*, STAT1 is phosphorylated at both Tyr_{701} and Ser_{727}[104]. Viral protein and RNA production transiently increases before decreasing markedly, and host protein synthesis is restored[93,104]. IFN-γ signaling also leads to improved cell survival. If cells are treated with Jak inhibitor 1, these effects are reversed, indicating the importance of IFN-γ-induced Jak-STAT signaling in SINV clearance and cell survival[93].

LONG-TERM MAINTENANCE OF CELLULAR IMMUNITY DURING VIRAL INFECTION

In acute virus infections, infectious virus is cleared after a few days to weeks by the immune system. The T cell response to a virus infection can be divided into three major stages: clonal expansion, contraction, and memory formation[109]. Upon introduction of an antigen, naïve T cells are activated through MHC I-CD8 or MHC II-CD4 interactions with antigen presenting cells, which primarily occur in the peripheral lymph nodes during neuronal infections due to the restrictive nature of the blood brain barrier[80]. Upon activation, T cells acquire effector functions, which for CD8+ T cells include expression of cytokines such as IFN-γ and TNF-α and chemokines such as RANTES and

cytotoxic capability through the granzyme/perforin system[110]. CD4+ T cells differentiate into T helper (Th) cell subsets and produce a wide array of cytokines, including some with antiviral properties, such as IFN-γ and TNF-α[111]. These activated T cells then clonally expand, mainly through signaling with IL-2, and migrate to the site of infection. These short-term effector T cells (T_{EFF}) have a high capacity for effector function and work towards clearing virus through cytolytic and/or noncytolytic means, depending on the nature and site of infection.

After acute virus infection is brought under control, the T_{EFF} population contracts considerably, mainly through apoptotic pathways[112,113]. Approximately five to ten percent on these cells will survive, going on to mature into memory cells[114,115]. These memory T cells are generally divided into two main groups: effector memory (T_{EM}) and central memory (T_{CM}) T cells[116]. T_{CM} cells have high proliferative and secretory IL-2 potential, but little effector capacity[109]. These cells tend to express L-selectin (CD62L) and CCR7, allowing them to home to lymph nodes and other secondary lymphoid organs where they perform immunosurveillance activities. T_{EM} cells in contrast have little to no proliferative potential but are capable of immediately producing effector proteins, such as antiviral cytokines IFN-γ and TNF-α, and inducing cytotoxic activity. They lack L-selectin or CCR7 and so readily circulate through the secondary lymph nodes and previous sites of infection via the blood and lymph. These memory T cells establish an effective and permanent mechanism to combat future pathogen infections and control persistent virus from reactivating.

A memory T cell population that has only been characterized within the last decade is the tissue resident memory (T_{RM}) T cell. These cells express CD103, an integrin

protein that serves as a receptor for e-cadherin. E-cadherin is an adhesion molecule found on epithelial cells, and so the interaction between e-cadherin and CD103 is thought to help T_{RM} cells remain in non-lymphoid tissues and avoid circulation throughout the lymphatic system[117-119]. They develop transcriptional and phenotypic signatures distinct from T_{CM} and T_{EM} cells that are dependent on the tissue in which they reside[120]. Upon restimulation, these cells secrete cytokines that rapidly activate the immune response, including resident B and T cells, dendritic cells, and NK cells[121]. T_{RM} cells are most commonly seen in barrier tissues such as the skin, gastrointestinal (GI) muscosa, and female reproductive tissue but have also been reported in immunoprivileged sites such as the brain[117,121-126].

Maintenance and survival of memory T cells are primarily regulated by two cytokines: IL-7 and IL-15[127]. The receptor for IL-7 (CD127) is expressed on naïve and memory T cells, but is downregulated on T_{EFF} cells[127,128]. IL-7 is considered to be important for maintenance of memory T cell survival, and is thought to be mediated, at least in part, through promoting expression of BCL-2, the anti-apoptotic protein[129-131]. IL-15, in contrast, is thought to mainly regulate low-grade proliferation and renewal of memory T cells[132-134]. Together, these two cytokines ensure that memory T cell populations remain stable so that they can properly respond to pathogen reintroduction.

Exhaustion of T cells was first characterized in CD8+ T cells during chronic persistent LCMV infection[135]. During the exhaustion process, T cells progressively lose effector functions. For CD8+ T cells, cytotoxic activity, IL-2 secretion, and proliferation potential are first lost, followed by TNF-α and IFN-γ production[109,136,137]. Over time, expression of inhibitory T cell markers, such as PD-1, LAG-3, and TIM-3, also

increase[138,139]. Apoptosis of memory T cells becomes more frequent, and if persistent viral load is excessively high or infection prolonged, the memory populations may be completely eliminated, leading to loss of T cell-mediated virus control[136,140]. Both CD8+ and CD4+ T cells can lose effector function during chronic infection, but CD4+ T cell exhaustion is less well understood[141-144]. T cell exhaustion is commonly found in chronic virus infection, such as with hepatitis C virus (HCV), human immunodeficiency virus (HIV), LCMV, and hepatitis B virus (HBV), but less is known regarding its role during acute virus infections where viral RNA may persist, such as with SINV infection[145,146].

FIGURES

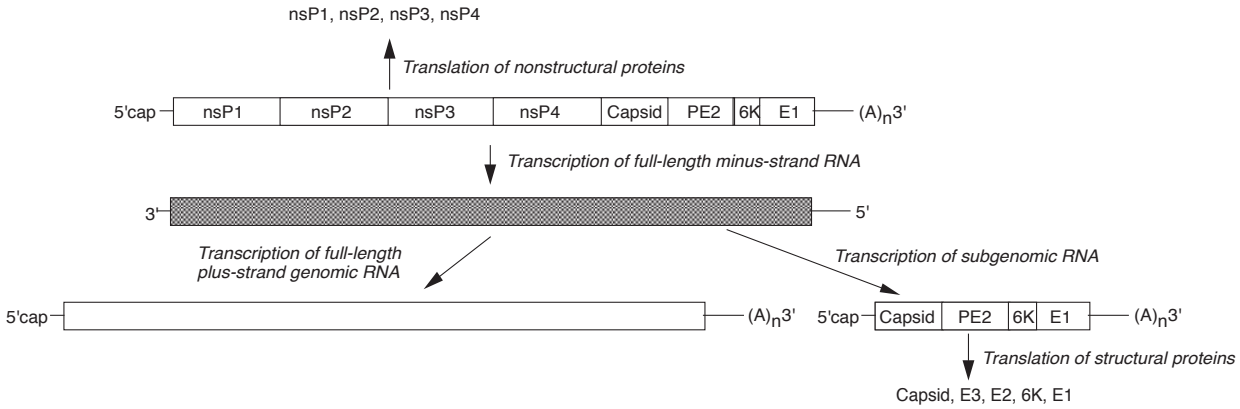

Figure 1-1. Replication of SINV. The full-length, positive-sense genome encodes four structural proteins at the 5' end and five structural proteins at the 3' end. Nonstructural proteins are first translated from the full length, positive-sense genome and then complementary minus-strand RNA is transcribed. New full length, plus-strand genomes are transcribed from the minus-strand RNA for encapsidation into new virons. Subgenomic mRNA is transcribed from a subgenomic promoter found in the minus-strand RNA, and the structural proteins that assemble to form new virions are translated as a polyprotein from it. This figure was reproduced from Diane Griffin, 2014.

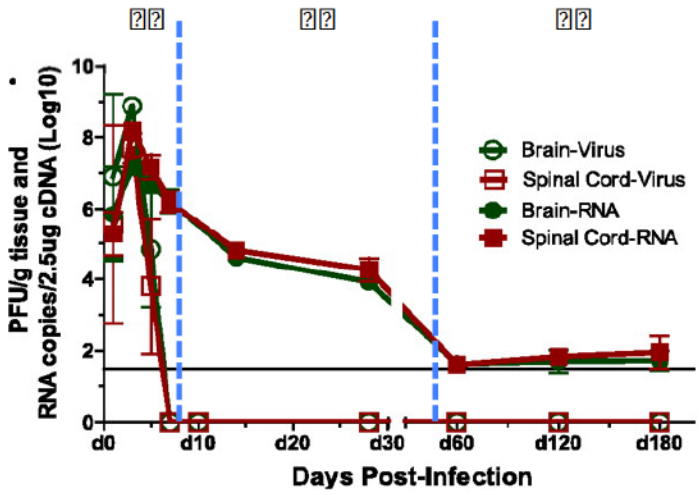

Figure 1-2. Course of SINV infection in C57BL/6 mouse brains. SINV occurs in three phases. In Phase 1, both infectious virus and viral RNA levels peak, but infectious virus titers soon drop below detectable levels. In Phase 2, viral RNA levels slowly decline over time, until they reach a low level steady state in Phase 3. This figure was reproduced and adapted from Metcalf and Griffin, 2011.

CHAPTER 2:

INFECTION WITH SINDBIS VIRUS RESULTS IN PERSISTENT NEUROLOGICAL SEQUELAE FOLLOWING RECOVERY FROM CLINICAL ALPHAVIRUS ENCEPHALOMYELITIS

INTRODUCTION

(from Potter and Baxter, *et al*, 2015)

Arthropod-borne alphaviruses and flaviviruses are plus-strand enveloped RNA viruses that pose an increasing worldwide threat to human populations as disease vectors expand into new geographic locations[20,147-150]. The New World alphaviruses, which include eastern equine encephalitis virus (EEEV), western equine encephalitis virus (WEEV), and Venezuelan equine encephalitis virus (VEEV), cause encephalomyelitis in humans and horses with varying rates of mortality[8,13]. Many patients who recover from the acute clinical disease, especially infants and children, are left with lifelong debilitating neurological defects, such as cognitive deficits, impaired motor control, and emotional and behavioral disturbances[14-18,151]. Currently, no treatments beyond symptomatic care are available, and no licensed human vaccines exist[20]. All three viruses are endemic in the Americas, and encephalomyelitis outbreaks caused by EEEV and VEEV have increased over the last few decades[9,152]. Therefore, it is increasingly important to understand the mechanisms responsible for the long-term consequences of alphavirus infection and to develop therapeutic interventions.

Sindbis virus (SINV), the prototypic alphavirus, produces rash and arthritis in humans but is neurotropic in mice and provides a valuable model for studying alphavirus-induced encephalomyelitis. In susceptible mice, nonlethal SINV infection consists of three phases in the brain: (1) presence of high levels of both infectious virus and viral RNA until about 7– 8 days post-infection (DPI); (2) undetectable infectious virus with significant yet declining viral RNA levels from about 10 to 60 DPI; and (3) chronic low-

but-detectable steady-state viral RNA levels from 60 DPI on, presumably for the remaining life of the animal[42]. However, it is currently unknown whether SINV infection results in cognitive dysfunction in mice. The aim of this study was to use this mouse model of alphavirus encephalomyelitis to determine the impact of viral infection on cognitive function and relate that to changes in brain structure and function. Motor, anxiety, and neurocognitive function were tested at each of the three different phases of SINV infection in mice. These data were correlated with the presence of infectious virus and viral RNA in the brain, along with severity of neuroinflammation and cell death.

MATERIALS & METHODS

Sindbis Virus Infection of Mice

Five to six-week-old male C57BL/6 mice (Jackson labs) were infected intranasally with 10^5 pfu of the nonfatal TE strain of SINV in 20μL PBS or 20μL PBS vehicle for control while under light isoflurane anesthesia[37]. At 5, 28, or 90 DPI, mice underwent a battery of behavioral tests (see below). Following behavioral testing, mice were euthanized by isoflurane overdose and perfused with 15mL ice cold PBS. For RNA and plaque assay analysis, brains were collected, flash-frozen in liquid nitrogen, and stored at -80°C. For histopathology and immunohistochemistry, mice were perfused with 40mL cold 4% paraformaldehyde (PFA), and brains were cut into three coronal sections using a using an Adult Mouse Brain Slicer (Zivic Instruments) and fixed overnight in 4 % PFA at 4°C. Brains were washed in ice cold PBS and embedded in paraffin. All studies

were approved by the Johns Hopkins University Institutional Animal Care and Use Committee.

Open Field (from Potter and Baxter, *et al,* 2015)

Animals were placed in the center of the open field arena (San Diego Instruments) at the beginning of the test and left undisturbed for 30 minutes. A 16 X 16 photobeam configuration was used to track the subject's path within the arena. The total number of beams broken was used as a measure of locomotor activity, and the ratio of center to periphery breaks was used as a measure of anxiety[153,154]. The investigator was blinded to the experimental conditions throughout testing. These experiments were performed in collaboration with Michelle C. Potter, PhD.

Elevated Plus Maze

The mice were placed in the center of the plus maze (two opposite arms open and the other two opposite arms closed), and the time spent in each arm was monitored for five minutes[155]. Anxiety was evaluated by calculating the ratio of time spent in the closed versus open arms. The investigator was blinded to the experimental conditions throughout testing. These experiments were performed in collaboration with Michelle C. Potter, PhD.

Rotarod

Mice were placed on the rotarod for five minutes, and the average time it took for mice to fall from the apparatus over three trials was measured. The investigator was

blinded to the experimental conditions throughout testing. These experiments were performed in collaboration with Michelle C. Potter, PhD.

Y-Maze (from Potter and Baxter, *et al,* 2015)

The Y-maze consisted of three arms of equal length interconnected at 120°. This test measured working memory by scoring the number of alternations the mouse completed (animal visits all three arms without going into the same arm twice in a row) over five minutes[156]. The investigator was blinded to the experimental conditions throughout testing. These experiments were performed in collaboration with Michelle C. Potter, PhD.

Contextual and Cued Fear Conditioning (from Potter and Baxter, *et al,* 2015)

On day 1, mice were placed in the testing chamber for a total of 300 seconds; baseline was recorded from 0–120 seconds, and then three tone-shock pairings were applied. The first tone was given for 30 seconds between 120 and 150 seconds, which was paired with a two-second foot shock (0.5mA) during the last two seconds of the tone (148–150 seconds). The second tone was given for 30 seconds between 180 and 210 seconds with the shock administered during the last 2 seconds (208–210 seconds). Finally, the third tone was given for 30 seconds between 240 and 270 seconds, with the shock between 268 and 270 seconds. On day 2, mice were placed into the same testing chamber and scored for percentage of freezing for five minutes during which time no tone or shock was given (contextual fear conditioning). Three hours after contextual testing, the mice were introduced to the same testing chamber with altered context. After

a 300 second baseline (pretone), five tones were given for 30 seconds each at one-minute intervals without the shock pairing (tone). The percent time the mouse spent freezing was recorded during the tone phase just described and used as a measure of cued fear conditioning[155]. The investigator was blinded to the experimental conditions throughout testing. These experiments were performed in collaboration with Michelle C. Potter, PhD.

Histology and Immunohistochemistry

Three to four 10μm brain sections per mouse were stained with hematoxylin and eosin (H&E), coded, and scored blindly as previously described[39] using a 0–3 scale. A score of 0 was given for slides with no detectable inflammation, a score of 1 for one to two small inflammatory foci per section, a score of 2 for moderate inflammatory foci in up to 50% of 10X magnification fields, and a score of 3 for moderate to large inflammatory foci in greater than 50% of 10X magnification fields. If excessive parenchymal cellularity was present, an additional point was added, allowing for a maximal score of 4.

For SINV antigen staining, 10μm sections of brain were rehydrated and treated with 1mg/mL proteinase K (1:200 in distilled water) for 20 minutes, and endogenous peroxide was quenched in methanol + 3% H_2O_2 for ten minutes. Tissues were blocked with 10% normal goat serum (NGS) in PBS for 20 minutes and stained with NSV anti-sera (1:200 in PBS + 5% NGS + 0.04% Triton-X)(Jackson 1987) for 60 minutes, biotinylated anti-rabbit IgG secondary (Vector labs, 5mg/mL in PBS + 5% + 0.04% Triton-X) for 30 minutes, and avidin-biotin complex (VECTASTAIN Elite ABC kit,

Vector Labs) for 40 minutes developed in 3,3'-diaminobenzidine (Vector Labs) for eight minutes. Slides were counterstained with hematoxylin for 60 seconds, dehydrated, and mounted with Permount (Fisher Scientific).

For TUNEL staining, 10μm brain sections were rehydrated and treated with 1mg/mL proteinase K (1:200 in deionized water) for 30 minutes, and endogenous peroxide was quenched in 3% H_2O_2 for five minutes. Sections were immersed in TdT Labeling Buffer and stained with TdT Labeling Reaction mix for 60 minutes at 37°C in a humidity chamber, immersed in TdT Stop Buffer, and stained with strep-HRP solution for ten minutes (TACS 2 TdT kit, Trevigen Inc). Brains were developed in 3,3'-diaminobenzidine (Vector Labs) for seven minutes, counterstained with hematoxylin for 60 seconds, dehydrated, and mounted with Permount (Fisher Scientific). Stained sections were coded, and the whole visible hippocampus on one brain section per mouse was outlined to determine the hippocampus area using a Nikon Eclipse E600 microscope and StereoInvestigator software (MBF Bioscience). All TUNEL-positive cells, as indicated by brown staining, were counted blindly within the outlined area, and results were graphed as TUNEL-positive cells per mm^2 hippocampus.

Quantification of Infectious Virus

Ice-cold PBS was added to the left halves of brains previously flash frozen and stored at -80°C to a concentration of 20% weight per volume (w/v) in Lysing Matrix A tubes (MP Biomedicals). Brains were homogenized at 6.0 M/s for 40 sec using a FastPrep-24 homogenizer (MP Biomedicals) and clarified by centrifuging at 13,200 rpm for 15 minutes at 4°C. Supernatant fluids were collected and serially diluted ten-fold in

DMEM + 1% FBS. Diluted homogenates were incubated on baby hamster kidney (BHK) cells for one hour, and an agarose overlay was applied. Assay plates were incubated at 37°C, 5% CO_2 for 48 hours, and plaques were counted using 10% neutral red solution to aid visualization.

Viral RNA Quantification by qRT-PCR

Right brain halves were placed in Lysing Matrix D tubes (MP Biomedicals), and samples were homogenized in 1.0mL Qiazol at 6.0 M/s for 40 sec using a FastPrep-24 homogenizer (MP Biomedicals). RNA was isolated using the Qiagen RNeasy Lipid Mini kit, and cDNA was synthesized with random primers using a Life Technologies High Capacity cDNA Reverse Transcription Kit following manufacturer's instructions. Quantitative real-time PCR (qRT-PCR) was performed using TaqMan Universal PCR Master Mix and TaqMan probe (5'–6-carboxyfluorescein [FAM]-CGCATACAGACTTCCGCCCAGT–6-carboxytetramethylrhodamine [TAMRA]-3', Applied Biosystems) with primers to the SINV E2 gene (forward, nt 8732-5'-TGGGACGAAGCGGACGATAA-3'-nt 8752; reverse, nt 8805-5'-CTGCTCCGCTTTGGTCGTAT-3'-nt 8786). cDNA was amplified for 50 cycles using a 7500 Fast Real-Time PCR System, and data were analyzed using Sequence Detector software, version 1.4 (Applied Biosystems). SINV E2 copies were quantified using a standard curve made of ten-fold dilutions of a plasmid containing the SINV subgenomic region and normalized to endogenous mouse *Gapdh* mRNA.

Statistics

Statistical analyses were performed using Graphpad Prism 6 software. For behavioral tests, an unpaired Student's *t*-test was used for two-group comparisons and a one-way ANOVA or two-way repeated measures ANOVA with Fisher's PLSD post-hoc analysis was used to compare three or more groups. A p value of < 0.05 was considered significant in all analyses.

RESULTS

SINV-infected mice have hippocampus-dependent memory deficits that persist beyond recovery from clinical disease

To assess the neurocognitive integrity of mice infected with SINV at each phase of infection, a battery of behavioral tests was performed on mice infected with the TE strain of SINV or mock-infected with PBS at 5, 28, and 90 DPI. SINV-infected mice showed increased motor activity (Fig 2-1A) and decreased anxiety (Fig 2-1B) at 5 DPI, but these effects were not seen at 28 or 90 DPI. Though SINV-infected mice trended towards showing decreased anxiety at 5 DPI as assessed by elevated plus maze (Fig 2-1C; $p = 0.07$, Student's t test), this finding was not significant. To assess motor coordination, SINV-infected and mock-infected mice were tested on the rotarod, but no difference between groups was found (Fig 2-1D).

The effect of SINV infection on working and hippocampus-dependent memory was measured using Y maze and fear conditioning, respectively. Working memory, as measured by percent spontaneous alterations on the Y maze, was not affected by SINV

infection at any of the assessed time points (Fig 2-1E). Mice showed decreased percent time spent freezing at 5 DPI for both contextual (Fig 2-1F) and cued (Fig 2-1G) fear conditioning. A significant decrease in percent time spent freezing continued to be seen at 28 and 90 DPI for contextual fear conditioning ($p < 0.05$, Student's t test), but not for cued fear conditioning. These data show that behavioral deficits continue during Phases 2 and 3 of SINV infection.

Inflammation and cell death in the brain peak during Phase 1 of infection

To better understand the mechanisms behind the behavioral testing results, brain sections of SINV-infected and mock-infected mice were examined. Inflammatory cells present around vessels and in the brain parenchyma were easily detectable at 5 DPI in SINV-infected mice, though less so at later time points and in mock-infected mice (Fig 2-2A). H&E-stained brains were evaluated for inflammation using a four point scoring system, and SINV-infected mice had higher scores at 5 DPI compared to mock-infected mice or at later time points (Fig 2-2C). To evaluate cell death in brains, TUNEL staining was performed at each time point in both mock-infected and SINV-infected mice, and the number of TUNEL-positive cells within the hippocampus was counted. TUNEL-positive cells in hippocampus were readily measured in the brains of SINV-infected mice at 5 DPI, but not at later time points or in mock-infected brains (Figs 2-2B and 2-2D). Based on these results, both inflammation and cell death peak during the period when behavioral deficits are most apparent in SINV-infected mice.

Detectable SINV peaks during Phase 1 of infection

To correlate SINV infection with behavioral tests and histological findings, infectious virus, viral protein, and viral RNA levels were assessed at each time point. Viral protein, as assessed by brain polyclonal anti-SINV antibody immunohistochemistry, was easily detectable at 5 DPI in SINV-infected mice, but not in mock-infected mice or at 28 or 90 DPI (Fig 2-3A). Infectious virus was detectable by plaque assay in brains at high levels at 5 DPI, but was undetectable at 28 or 90 DPI (Fig 2-3B). In contrast, viral RNA, as measured by qRT-PCR for the E2 structural gene, peaked at 5 DPI, but was still detectable, though at declining levels, at 28 and 90 DPI (Fig 2-3C). These data show that the most marked behavioral and histological changes occur when active virus replication is occurring. The persistent hippocampus-dependent memory deficits seen at 28 and 90 DPI occur when only viral RNA is present in brains of infected mice.

DISCUSSION

(from Potter and Baxter, *et al,* 2015)

In this study, we found that at the peak of active virus infection, SINV-infected mice demonstrated increased activity, reduced anxiety, and impaired hippocampus-dependent contextual and cued fear conditioning memory. Eleven weeks after the clearance of infectious virus when only viral RNA was present in the brain, SINV-infected mice continued to show significant memory impairment as indicated by contextual fear conditioning tests.

During the early stages of infection, SINV mice were hyperactive and less anxious in the open field test compared to uninfected mice. Epidemic encephalitis can lead to behavioral abnormalities similar to attention-deficit/hyperactivity disorder (ADHD), with damage to the brainstem suggested as a cause[157]. Other areas that are important for locomotor activity are the basal ganglia and the cerebellum. The amygdala is a central area of processing fear and anxiety[158]. Indeed, in cases of viral encephalitis such as from human herpesvirus 6 (HHV6), there was significant damage to the medial temporal lobe including the amygdala[159]. Neurological sequelae in patients surviving alphavirus encephalomyelitis have been reported to include hyperactivity, emotional disinhibition, and temperament disturbances[14,15,17,18], and symptoms similar to ADHD have been described in patients affected by encephalitis caused by other types of viruses, such as HIV[157,160].

The most profound and prolonged abnormalities were identified using fear conditioning. Contextual and cued fear conditioning involve different brain circuitry, with contextual fear conditioning being more associated with the hippocampus[161-165]. While SINV infects neurons in the cortex, brainstem, and spinal cord[35], previous studies of mice infected with a lethal neuroadapted strain of SINV (NSV) have noted that hippocampal neurons are particularly vulnerable to progressive damage[54]. Hippocampal neurons are also particularly susceptible to glutamate-induced excitotoxic damage, which plays a role in SINV-induced cell death[60,61,65]. In addition, the hippocampus plays a very important role in cognition, and factors affecting learning and memory processes can be probed using tasks such as fear conditioning[165,166]. In our study, deficits in fear conditioning at 5 DPI correlated with demonstration of active virus replication,

inflammation, and cell death in the hippocampus during the acute phase of infection. Impairments in contextual, but not cued, fear conditioning persisted for at least 90 days after infection, a time when the mice appeared to have fully recovered. Although virus-induced behavioral alterations in mice have been previously reported[167-169], to our knowledge, this is the first study of cognitive deficits and other behavioral abnormalities in a mouse model of alphavirus infection.

FIGURES

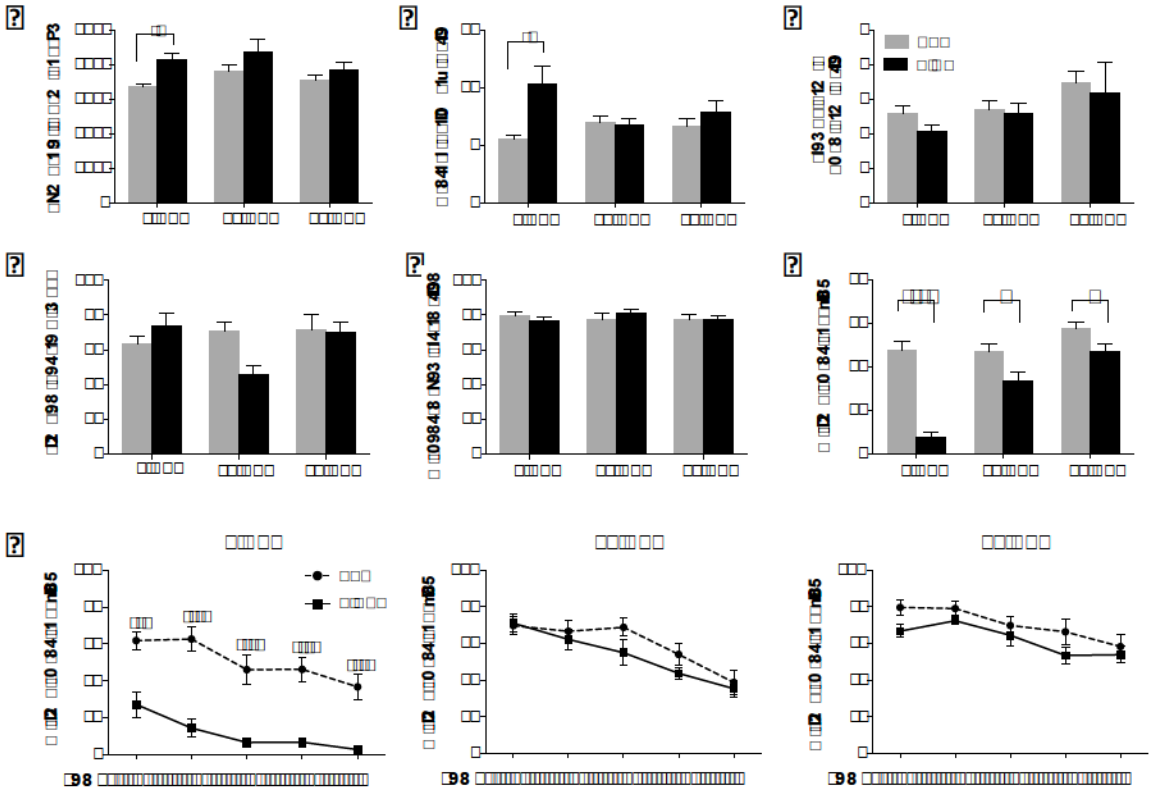

Figure 2-1. Assessment of locomotor activity, anxiety, and memory in SINV-infected mice. A battery of behavioral tests were performed on SINV-infected and mock-infected mice at 5, 28, and 90 DPI. (**A**) Locomotor activity was assessed by the open field test by measuring the number of beam breaks made by mice in 30 minutes. Anxiety was assessed by measuring the ratio of time mice spent in the center versus the periphery of the open field (**B**) and by measuring the ratio of time mice spent in the closed arm versus the open arm of the elevated plus maze (**C**). (**D**) Motor coordination was assessed by time to fall off the rotarod. (**E**) Working memory was measured as the percent of spontaneous alternation performed on the Y maze. Hippocampus-dependent memory was measured as the percent time spent freezing during contextual (**F**) and cued (**G**) fear conditioning (n = 12–15 mice per group; data presented as the mean ± SEM; *$p < 0.05$, **$p < 0.01$, ***$p <$

0.001, ****$p < 0.0001$, by repeated measures ANOVA for cued fear conditioning and unpaired t tests for all other tests;). These experiments were performed in collaboration with Michelle C. Potter, PhD. Figures 2-1A, 2-1B, 2-1C, 2-1F, and 2-1G were adapted from Potter and Baxter, *et al*, 2015.

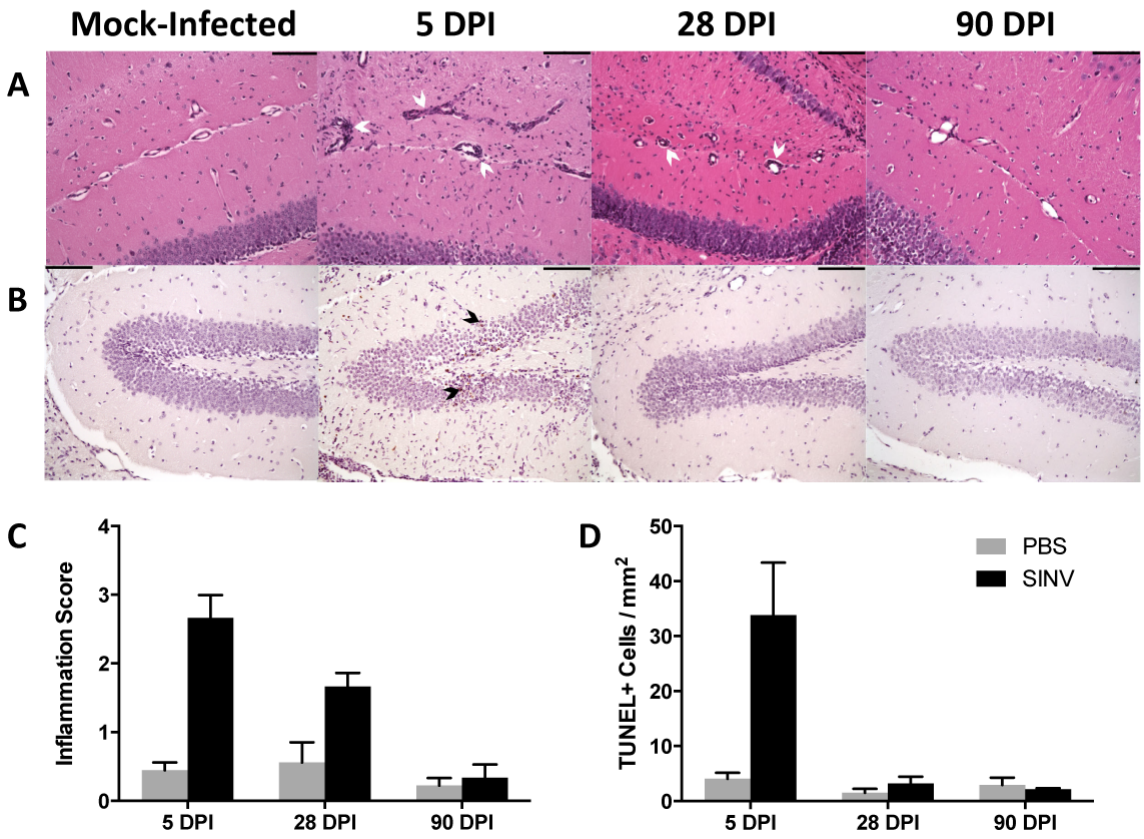

Figure 2-2. Inflammation and cell death in the brain over the course of SINV infection. (**A**) Representative photomicrographs of H&E-stained coronal brain sections from mock-infected mice and mice infected with SINV at 5, 28, or 90 DPI (white arrowheads denote perivascular cuffing; 200X magnification; scale bar = 100 μm). (**B**) Representative photomicrographs from TUNEL staining of the hippocampal dentate gyrus of mock-infected mice and mice infected with SINV at 5, 28, or 90 DPI (brown nuclear staining = TUNEL-positive [denoted by black arrowheads]; 200X magnification; scale bar = 100 μm). (**C**) Inflammation was assessed in mock-infected and SINV-infected mouse brains at 5, 28, and 90 DPI using a four point scoring system. (**D**) TUNEL-positive cells were quantified in the hippocampus of mock-infected and SINV-infected mouse brains at 5, 28, and 90 DPI (for all bar graphs, n = 3–4 mice per group per time

point; data presented as mean ± SEM). Figures were adapted from Potter and Baxter, *et al*, 2015.

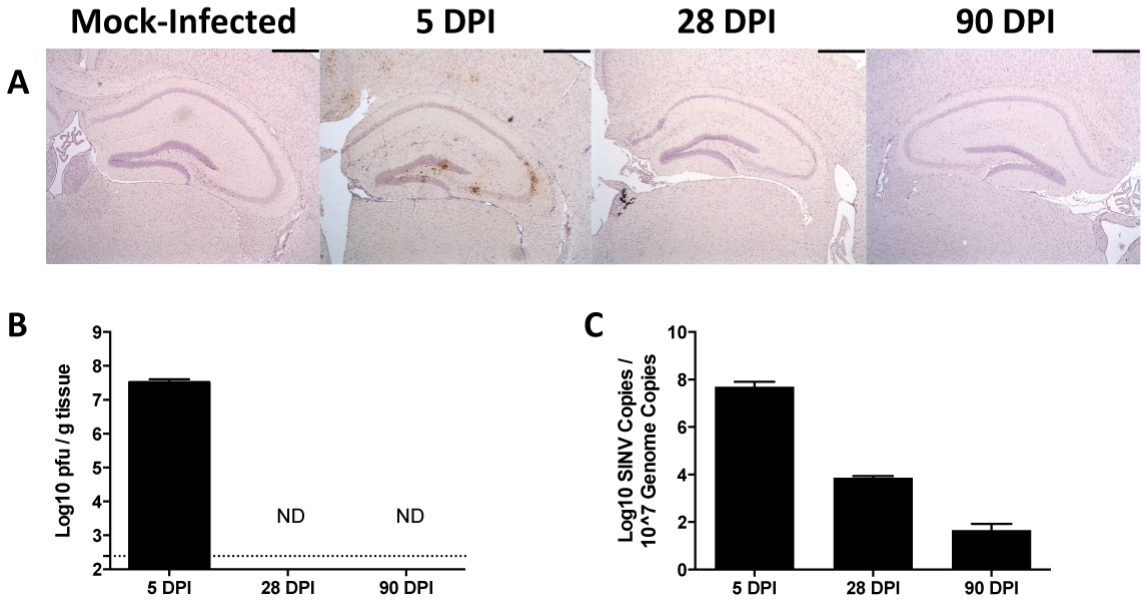

Figure 2-3. Detection of SINV and viral RNA in the brain over the course of SINV infection. (**A**) Representative photomicrographs of immunohistochemical staining for SINV antigen in mock-infected brains and brains of mice infected with SINV at 5, 28, or 90 DPI (brown staining=SINV protein; 40X magnification; scale bar=500 μm). Infectious virus (**B**) and viral RNA (**C**) were measured at 5, 28, and 90 DPI in SINV-infected mice by plaque assay and qRT-PCR, respectively (n = 3–4 mice per group per time point; data presented as mean ± SEM; dotted line represents limit of detection; ND, not detectable). Figures were adapted from Potter and Baxter, *et al*, 2015.

CHAPTER 3:

GLUTAMINE ANTAGONISM DECREASES PATHOLOGY BUT DELAYS VIRUS CLEARANCE DURING NONFATAL ALPHAVIRUS ENCEPHALOMYELITIS

INTRODUCTION

Recent epidemics of encephalomyelitis caused by the New World alphaviruses, including EEEV, WEEV, and VEEV demonstrate their capacity as a worldwide public health concern[9-11]. Currently no treatments beyond supportive care are available for alphavirus encephalomyelitis, and no licensed vaccines are approved for non-military human use[19]. Clinical disease induced by infection with New World alphaviruses can be severe[14,15,170-183]. When humans are infected with one of these viruses, the prodromal phase averages five days, but can last as long as four weeks. Patients tend to develop flu-like symptoms followed by abrupt onset of signs of encephalitis, such as headache, restlessness, seizures, and alterations in consciousness. Cerebrospinal fluid (CSF) often shows pleocytosis and elevated protein. Cerebral dysfunction is evident by electroencephalogram (EEG), and on MRI or CT scan, diffuse abnormalities in the parenchyma tend to be seen in the cortex, thalamus, basal ganglia, and brainstem. Mortality rates depend on the virus species. EEEV carries the higher mortality rate, ranging from 30 to 70%, while the death rate for WEEV is considerably lower, closer to 4%[15,173]. Fatalities are most common in infants and children. Neurological sequelae occur in approximately 25 to 35% of patients that recover, with higher rates in children[15,151,173].

On autopsy, brains of patients are grossly swollen and edematous[52,53,184]. Microscopically, meningoencephalitis is present with occasional vasculitis. Tissue destruction is marked with extensive neuronal death. Inflammatory infiltrates can be found around vessels and in the CNS parenchyma. Early in infection neutrophils are the primary infiltrating leukocyte, but lymphocytes soon predominate. Spinal cord

pathological changes are also commonly seen with EEEV infection. Similar clinical signs and pathological changes are seen in horses infected with one of the equine encephalitis viruses, though mortality rates tend to be higher compared to humans[185,186].

Neuronal damage resulting from alphavirus infection is due to both the immune response and glutamate excitotoxicity, and previous studies have shown that inhibition of these mechanisms can protect mice from fatal viral encephalomyelitis[49]. However, treatment has not been evaluated for prevention of sequelae in nonfatal infection. Because the glutamine antagonist, 6-diazo-5-oxo-L- norleucine (DON), affects both of these pathologic mechanisms[187-190], we tested the effects of treatment with DON on the development of neurological sequelae.

DON is an irreversible competitive inhibitor of several glutamine-utilizing enzymes[191]. During growth and proliferation, T cells preferentially use glutamine instead of glucose as an energy source, and rapidly dividing activated T cells show increased glutamine uptake and metabolism[192,193]. Therefore, glutamine antagonism can inhibit lymphocyte proliferation[190]. In the CNS, the excitatory neurotransmitter glutamate is synthesized from glutamine. Excess production of glutamate leads to neuronal death through glutamate excitotoxicity, so inhibition of glutamine metabolism might abrogate this process[57]. DON treatment has been shown to rescue mice from late-stage cerebral malaria, indicating it might be a viable treatment option for CNS infections that induce immune-mediated neuronal damage[194]. Therefore, we hypothesized that DON treatment would prevent SINV-infected mice from developing clinical disease with neurological deficits, and CNS pathological changes will be reduced due to decreased inflammation and glutamate excitotoxicity.

MATERIALS & METHODS

Sindbis Virus Infection and Clinical Evaluation of Mice

Four to six-week-old male C57BL/6 mice (Jackson labs) were infected intranasally with 10^5 pfu of the nonfatal TE strain of SINV in 20μL PBS or 20μL PBS vehicle for control while under light isoflurane anesthesia[37]. Mice were evaluated daily for presence of clinical signs indicative of encephalomyelitis (hunched posture, abnormal gait, paresis), and body weight was measured each day. At 5 DPI, mice underwent behavioral testing (see below), and at 5, 7, 9, or 11 DPI, mice were euthanized by isoflurane overdose and perfused with 15mL ice cold PBS following blood collection by cardiocentesis. Blood was allowed to coagulate in BD Microtainer serum separator tubes and centrifuged for 15 minutes at 1,500 RCF. The resulting serum layer was collected and stored at -20°C. For RNA and plaque assay analysis, brains and spinal cords were collected, flash-frozen in liquid nitrogen, and stored at -80°C. For histopathology and immunohistochemistry, mice were perfused with 40mL cold 4% PFA, and brains, spinal columns, and GI tracts were collected. Brains were cut into three coronal sections using a using an Adult Mouse Brain Slicer (Zivic Instruments), fixed overnight in 4 % PFA at 4°C, and washed in ice-cold PBS. Spinal columns were trimmed of excess soft tissue, fixed overnight in 4% PFA at 4°C, and then decalcified on a rotator for 24 to 36 hours in a 10% sodium citrate/22% formic acid solution. Spinal columns were washed in ice-cold PBS and cut to isolate the L4-L6 spinal cord regions. GI tracts were fixed overnight in 4% PFA, washed in ice-cold PBS, and placed in cassettes either as cross sections sampling each portion of the tract or complete using a closed Swiss roll technique.

Tissues were embedded in paraffin for sectioning and staining. The Johns Hopkins University Institutional Animal Care and Use Committee approved all studies.

Drug Administration (from Potter and Baxter, *et al,* 2015)

Daily intraperitoneal injections of DON (Sigma-Aldrich) were administered at doses of 0.3 or 0.6 mg/kg beginning the day of SINV inoculation (0 DPI) and continuing through 7 DPI. DON working solution was diluted in PBS each day from aliquots of a 100 mM stock solution in PBS stored at −80 °C. Control group animals received injections of PBS. On days of behavioral testing (5 and 6 DPI), the drug or vehicle was administered one hour prior to testing. Tissues were collected at two time points during drug administration (5 and 7 DPI) and at two time points following cessation of treatment (9 and 11 DPI).

DON Measurement in Tissues (from Potter and Baxter, *et al,* 2015)

DON was spiked into mouse sera or brains from untreated animals to generate standards at concentrations from 10 nM to 100 μM. DON was derivatized into a more stable and lipophilic analyte by adding butanol with 3 N HCl (250 μL) to standards and samples (50 μL). The brains were homogenized, and all samples were centrifuged at $16{,}000 \times g$ for five minutes to precipitate proteins. To carry out the derivatization reaction, an aliquot of supernatant (200 μL) was incubated at 60 °C for 30 minutes and dried at 45 °C under a nitrogen stream. Samples were resuspended in 50-μL 70 %/30 % water/acetonitrile, vortexed, and centrifuged again at $16{,}000 \times g$ for five minutes. Samples (2 μL) were subsequently injected and separated on an Agilent 1290 HPLC

equipped with a C18 column over a 5.5-min gradient from 30 to 70 % acetonitrile + 0.1 % formic acid and quantified on an Agilent 6520 QTOF mass spectrometer. Standards within the quantifiable range (30 nM–100 μM) were used to generate a standard curve. Samples below the limit of quantification were assigned a value of 0. These experiments were performed in collaboration with Jesse Alt and Camilo Rojas, PhD.

Open Field (from Potter and Baxter, *et al,* 2015)

Animals were placed in the center of the open field arena (San Diego Instruments) at the beginning of the test and left undisturbed for 30 minutes. A 16 X 16 photobeam configuration was used to track the subject's path within the arena. The total number of beams broken was used as a measure of locomotor activity, and the ratio of center to periphery breaks was used as a measure of anxiety[153,154]. The investigator was blinded to the experimental conditions throughout testing. These experiments were performed in collaboration with Michelle C. Potter, PhD.

Contextual and Cued Fear Conditioning (from Potter and Baxter, *et al,* 2015)

On Day 1 (5 DPI), mice were placed in the testing chamber for a total of 300 seconds; baseline was recorded from 0–120 seconds, and then three tone-shock pairings were applied. The first tone was given for 30 seconds between 120 and 150 seconds, which was paired with a two-second foot shock (0.5mA) during the last two seconds of the tone (148–150 seconds). The second tone was given for 30 seconds between 180 and 210 seconds with the shock administered during the last two seconds (208–210 seconds).

Finally, the third tone was given for 30 seconds between 240 and 270 seconds, with the shock between 268 and 270 seconds. On Day 2 (6 DPI), mice were placed into the same testing chamber and scored for percentage of freezing for five minutes during which time no tone or shock was given (contextual fear conditioning). Three hours after contextual testing, the mice were introduced to the same testing chamber with altered context. After a 300 second baseline (pretone), five tones were given for 30 seconds each at one-minute intervals without the shock pairing (tone). The percent time the mouse spent freezing was recorded during the tone phase just described and used as a measure of cued fear conditioning[155]. The investigator was blinded to the experimental conditions throughout testing. These experiments were performed in collaboration with Michelle C. Potter, PhD.

Histology and Immunohistochemistry

Three to four 10μm brain sections per mouse were stained with H&E, coded, and scored blindly as previously described[39] using a 0–3 scale. A score of 0 was given for slides with no detectable inflammation, a score of 1 for brains with one to two small inflammatory foci per section, a score of 2 for moderate inflammatory foci in up to 50% of 10X magnification fields, and a score of 3 for moderate to large inflammatory foci in greater than 50% of 10X magnification fields. If excessive parenchymal cellularity was present, an additional point was added, allowing for a maximal score of 4.

Three to four 10um lumbar spinal cord sections per mouse were stained with H&E, coded, and scored using a 0-2 scale adapted from the brain scoring system. A score of 0 was given for slides with no detectable inflammation, a score of 1 for spinal cord

sections with one to two small inflammatory foci per section, and a score of 2 for greater than two inflammatory foci per spinal cord or for spinal cords with moderate to marked inflammatory foci. An additional point was awarded if excessive parenchymal cellularity was present, allowing for a maximal score of 3.

For CD3 immunohistochemical staining, 10μm brain sections were rehydrated, and antigen retrieved by boiling in 0.01 M sodium citrate (pH 6.0) for ten minutes. After quenching endogenous peroxidases in methanol + 3% H_2O_2 for ten minutes, sections were blocked with 10 % NGS in PBS for 30 minutes. Tissues were incubated with polyclonal anti-human CD3 (Dako, 1:400 in PBS + 5 % NGS + 0.04 % Triton-X) for 60 minutes, biotinylated anti-rabbit IgG secondary (Vector labs, 5 mg/mL in PBS + 5 % NGS + 0.04 % Triton-X) for 30 minutes, and avidin-biotin-HRP complex (VECTASTAIN Elite ABC kit) for 40 minutes. Slides were developed with 3,3′-diaminobenzidine (Vector labs) for ten minutes, counterstained with hematoxylin for 60 seconds, dehydrated, and mounted with Permount (Fischer Scientific).

For TUNEL staining, 10μm brain or spinal cord sections were rehydrated and treated with 1mg/mL proteinase K (1:200 in deionized water) for 30 minutes, and endogenous peroxidases were quenched in methanol + 3% H_2O_2 for five minutes. Sections were immersed in TdT Labeling Buffer, stained with TdT Labeling Reaction mix for 60 minutes at 37°C in a humidity chamber, immersed in TdT Stop Buffer, and stained with strep-HRP solution for ten minutes (TACS 2 TdT kit, Trevigen Inc). Tissues were developed with 3,3'-diaminobenzidine (Vector Labs) for seven minutes, counterstained with hematoxylin for 60 sec, dehydrated, and mounted with Permount (Fisher Scientific).

Stained CD3 and TUNEL sections were coded, and the whole visible hippocampus on one brain section per mouse (both CD3 and TUNEL) or the entire spinal cord cross section per mouse (TUNEL only) was outlined to determine the tissue area using a Nikon Eclipse E600 microscope and StereoInvestigator software (MBF Bioscience). All CD3- or TUNEL-positive cells, as indicated by brown staining, were counted blindly within the outlined area, and results were graphed as CD3- or TUNEL-positive cells per mm^2 tissue. In TUNEL-stained 7 DPI brains, cells identified morphologically as neurons within the granule cell layer of the dentate gyrus and pyramidal cell layers of the CA regions were additionally counted.

For SINV antigen staining, 10μm sections of brain were rehydrated and treated with 1mg/mL proteinase K (Invitrogen, 1:200 in distilled water) for 20 minutes, and endogenous peroxide was quenched in methanol + 3% H_2O_2 for ten minutes. Tissues were blocked with 10% NGS in PBS for 20 minutes and stained with NSV anti-sera (1:200 in PBS + 5% NGS + 0.04% Triton-X)(Jackson 1988) for 60 minutes, biotinylated anti-rabbit IgG secondary (5mg/mL in PBS + 5% NGS + 0.04% Triton-X) for 30 minutes, and avidin-biotin complex (VECTASTAIN Elite ABC kit) for 40 minutes developed with 3,3'-diaminobenzidine (Vector Labs) for eight minutes. Slides were counterstained with hematoxylin for 60 seconds, dehydrated, and mounted with Permount.

Mononuclear Cell Isolation

Single cell suspensions were made from cervical lymph nodes (CLNs), brains, and spinal cords pooled from two to three mice per strain per time point. CLNs were

dissociated in RPMI + 1% FBS using gentleMACS C tubes and Dissociator (Miltenyi Biotech) and filtered through a 70μm-pore-size cell strainer. After pelleting by centrifugation, red blood cells were lysed using an ammonium chloride solution (Sigma-Aldrich). Remaining cells were filtered through another 70μm strainer, pelleted by centrifugation, and resuspended in PBS + 2mM EDTA (PE buffer) for counting. Brains and spinal cords were placed in RPMI media containing 1% FBS, 1 mg/mL collagenase D (Roche), and 0.1 mg/mL DNase I (Roche) and dissociated in C tubes using a gentleMACS Dissociator. Tissues were incubated for 30 minutes at 37°C with periodic agitation, and dissociated cells were filtered through a 70μm pore size cell strainer and pelleted by centrifugation. Cell pellets were resuspended in 30% supplemented Percoll (9:1 Percoll [GE Healthcare] : 10X salt solution of 80g NaCl, 3g KCl, 0.73g Na_2HPO_4, 0.2g KH_2PO_4, and 20g glucose in 1L dH_2O) in RPMI media in a 15mL conical tube and underlaid with 70% supplemented Percoll in RPMI media. Tubes were centrifuged at 850 x g at 4°C for 30 minutes with slow braking to create a gradient, and cells were collected from the 30/70% interface. Cells were pelleted by centrifugation and resuspended in PE buffer for counting. Live mononuclear cells were quantified by trypan blue exclusion.

Flow Cytometry

10^6 live cells were plated in a 96-well round bottom plate. A violet LIVE/DEAD Fixable Dead Cell Stain (Life Technologies) diluted in PE buffer was applied to cells for 30 minutes, followed by a 15-minute incubation with anti-mouse CD16/CD32 (BD Pharmingen) diluted in PE buffer to block Fc receptors. Cells were stained with monoclonal antibodies against CD45 (clone 30-F11), CD3 (clone 17A2), CD4 (clone

RM4-5), CD8a (clone 53-6.7), and CD19 (clone 1D3) from Ebioscience or BD Pharmingen diluted in PBS + 2mM EDTA + 0.5% BSA (FACS Buffer) for 30 minutes on ice. Cells were run on a BD FACSCanto II cytometer using BD FACSDiva software, version 8, and analyses were carried out using FlowJo software, version 8. Cells were characterized as follows: CD3 T cells ($CD45^{hi}$CD3+), CD4 T cells ($CD45^{hi}$CD3+CD4+), CD8 T cells ($CD45^{hi}$CD3+CD8+), and B cells ($CD45^{hi}$CD3-CD19+).

Quantification of Infectious Virus

Ice-cold PBS was added to left halves of brains (20% w/v) or whole spinal cords (10% w/v) previously flash frozen and stored at -80°C. Tissues were homogenized in MP Biomedicals Lysing Matrix A tubes at 6.0 M/s for 40 seconds using a FastPrep-24 homogenizer (MP Biomedicals) and clarified by centrifuging at 13,200 rpm for 15 minutes at 4°C. Supernatant fluids were collected and serially diluted ten-fold in DMEM + 1% FBS. Diluted homogenates were incubated on baby hamster kidney (BHK) cells for one hour, and an agarose overlay was applied. Assay plates were incubated at 37°C, 5% CO_2 for 48 hours, and plaques were counted using 10% neutral red solution to aid visualization.

Protein Quantification by Enzyme-Linked Immunosorbent Assay

Anti-SINV antibody was measured in serum and 20% w/v brain homogenates in three to six mice per strain per time point using an in-house enzyme-linked immunosorbent assay (ELISA). Maxisorp 96-well plates (Thermo Scientific Nunc) were coated with 10^6 pfu PEG-purified SINV TE diluted in 50mM $NaHCO_3$, pH 9.6 coating

buffer and incubated overnight at 4°C. Plates were blocked in PBS-0.05% Tween-20 + 10% FBS (PBST-10% FBS) for two hours at 37°C and incubated overnight at 4°C with samples diluted in PBST-10% FBS (1:100 [IgM] or 1:10 [IgG] for serum, 1:4 for brain homogenates). Wells were incubated with 1:1000 HRP-conjugated goat anti-mouse IgM or IgG (Southern Biotech) for two hours at room temperature, and plates were developed with a BD OptEIA TMB Substrate Reagent kit using 2M H_2SO_4 as stop solution. Plates were read at 450nm, and optical density (OD) values for mock-infected mice were subtracted from the OD values of infected mice.

Interferon gamma (IFN-γ) production was quantified in 20% w/v brain homogenates in three to five mice per strain per time point by commercial ELISA kit (Ebioscience Ready-SET- Go!). Assays were performed according to manufacturer's instructions, and data was presented as pg/g brain tissue with a 312pg/g limit of detection.

qRT-PCR Evaluation of IFN-γ mRNA Expression and Viral RNA Production

Right brain halves and whole spinal cords were placed in Lysing Matrix D tubes (MP Biomedicals), and samples were homogenized in 1.0mL Qiazol at 6.0 M/s for 40 seconds using a FastPrep-24 homogenizer (MP Biomedicals). RNA was isolated using the Qiagen RNeasy Lipid Mini kit, and cDNA was synthesized with random primers using a Life Technologies High Capacity cDNA Reverse Transcription Kit following manufacturer's instructions. qRT-PCR was performed using TaqMan Universal PCR Master Mix (Roche) on a 7500 Fast Real-Time PCR System for 50 cycles, and results were analyzed using Sequence Detector software, version 1.4. *Ifng* mRNA was measured using a commercially available TaqMan gene expression assay (Integrated DNA

Technologies), and relative gene quantification versus mock-infected mice was performed by the ΔΔCT method using mouse *Gapdh* for normalization. SINV RNA copies were measured using TaqMan probe (5'–6-carboxyfluorescein [FAM]-CGCATACAGACTTCCGCCCAGT–6-carboxytetramethylrhodamine [TAMRA]-3', Applied Biosystems) with primers to the SINV E2 gene (forward, 5'-TGGGACGAAGCGGACGATAA-3'; reverse, 5'-CTGCTCCGCTTTGGTCGTAT-3'). SINV E2 copies were quantified using a standard curve made of ten-fold dilutions of a plasmid containing the SINV subgenomic region and normalized to endogenous mouse *Gapdh*.

Statistics

Statistical analyses were performed using Graphpad Prism 6 software or Statview (SAS Institute Inc.). For clinical disease evaluation, a Mantel-Cox log-rank test was used to compare Kaplan-Meier curves, and for body weights, one-way ANOVA with Bonferroni's multiple comparisons post-test were employed. Behavioral tests were evaluated using a one-way ANOVA with Bonferroni's multiple comparisons post-hoc for open field and contextual fear conditioning and a two-way repeated measures ANOVA with Fisher's PLSD post-hoc for cued fear conditioning. Time-course studies were analyzed by two-way ANOVA with Tukey's multiple comparison post-test. Experiments comparing three or more groups at a single time point employed Kruskal-Wallis tests with Dunn's multiple comparisons post-hoc. A p value of <0.05 was considered significant in all analyses.

RESULTS

DON is easily detectable in serum, but less so in the brain one hour following administration

Previous studies have shown that the pathological changes seen during SINV infection is primarily due to a combination of glutamate toxicity and inflammatory effects produced by the immune response, rather than directly due to the virus itself[49]. To see if administration of a drug that counteracts both of these pathways would prevent development of clinical disease and CNS pathology, the glutamine antagonist DON was used to treat mice during SINV infection. Mice were intranasally infected with the TE strain of SINV and treated daily for the first 7 DPI with either a low (0.3mg/kg) dose or high (0.6mg/kg) dose of DON intraperitoneally.

One hour following drug administration on 7 DPI, serum and brains were collected, and DON concentration was measured by mass spectrometry. DON was not detectable in sera or brains of untreated mice, but was easily detected in the sera of mice treated with both the low (0.3mg/kg) and high (0.6mg/kg) dose of DON (Fig 3-1A). DON was detectable in the brains of mice treated with the high (0.6mg/kg) dose of DON, though at considerably lower concentrations than in the serum, and was not consistently measurable in brains of mice receiving the low (0.3mg/kg) dose of DON (Fig 3-2B). Mock-infected and SINV-infected mice showed similar concentrations of DON.

DON treatment partially prevents development of clinical disease but causes GI toxicity at high doses

To evaluate the effect of glutamine antagonism on development of clinical disease during SINV infection, mice were weighed and observed daily for the development of clinical signs throughout the period of DON administration. By 7 DPI, when almost all SINV-infected, untreated mice had development signs consistent with encephalomyelitis (hunched posture, abnormal gait, paresis), less than half of the DON-treated mice were showing clinical signs (Fig 3-2A; $p < 0.0001$, Mantel-Cox log rank test). Mock-infected mice did not develop signs of encephalomyelitis through 7 DPI. DON treatment did have a significant effect on body weight at 4, 5, 6, and 7 DPI among groups (Fig 3-2B; $p < 0.0001$, one-way ANOVA). While untreated, SINV-infected mice lost approximately 10-15% of their body weight by 7 DPI, SINV-infected mice receiving the low (0.3mg/kg) dose of DON lost significantly less weight ($p < 0.01$, Bonferroni's multiple comparisons test). Significantly more weight loss was seen in the SINV-infected, low (0.3mg/kg) dose DON-treated group compared to mock-infected, untreated and mock-infected, low (0.3mg/kg) dose DON-treated groups ($p < 0.0001$ and $p < 0.01$, respectively, Bonferroni's multiple comparisons test). Regardless of infection status, mice receiving high (0.6mg/kg) dose DON treatment lost the most body weight of any of the groups by 7 DPI.

Because DON has previously been reported to cause GI toxicity in human clinical trials[188,195-198], the intestines of the mice were examined for gross pathology and histopathology. Compared to mock-infected, untreated intestines, intestines from mock-infected mice receiving the high (0.6mg/kg) DON dose were grossly dilated. Histologically, large intestines of mice treated with the high (0.6mg/kg) dose of DON showed loss of architecture with dilation of glands and disruption of the epithelial layer

(Fig 3-2C). When examining body weights at 28 DPI of SINV-infected mice that had been treated with either low (0.3mg/kg) or high (0.6mg/kg) doses of DON through the first 7 DPI, mice regained the body weight they had initially lost (Fig 3-2D). These data show that DON treatment does partially prevent development of clinical disease in SINV-infected mice, though at high doses, drug administration causes GI toxicity, resulting in increased loss of body weight.

Glutamine antagonism partially prevents development of hippocampus dependent memory defects

To evaluate whether DON treatment prevents or mitigates development of neurological sequelae during SINV infection, open field and fear conditioning tests were performed at 5 DPI, the period when the most marked deficits were previously noted. In the open field test, there was a significant difference in the number of beam breaks recorded among groups (Fig 3-3A; $p < 0.0001$, one-way ANOVA), with untreated SINV-infected mice crossing more beams than all other groups ($p < 0.01$, Fisher's PLSD). Mice in the untreated, mock-infected and SINV-infected, low (0.3mg/kg) and high (0.6mg/kg) DON-treated groups did not significantly differ in the number of beam breaks recorded, though mock-infected, high (0.6mg/kg) dose DON-treated mice had significantly fewer recorded beam breaks than all other groups ($p < 0.01$, Fisher's PLSD). These results indicate that DON treatment can help prevent SINV-induced hyperlocomotion at 5 DPI, but long-term treatment may affect motor ability.

Anxiety was also assessed by the open field test at 5 DPI (Fig 3-3B). The ratio of time spent in the center of the open field compared to the periphery significantly differed

among groups ($p < 0.001$, one-way ANOVA), with untreated, SINV-infected mice showing a significantly increased ratio compared to all other groups ($p < 0.05$, Fisher's PLSD). The central:periphery ratio did not significantly differ among the other groups, indicating that DON protects mice from developing the disinhibitory behavior seen in during SINV infection in untreated mice at 5 DPI.

To evaluate hippocampus-dependent memory at 5 DPI, contextual (Fig 3-3C) and cued (Fig 3-3D) fear conditioning tests were performed on mice treated with DON. The percent time spent freezing significantly differed among the groups in both contextual and cued tests ($p < 0.0001$, one-way ANOVA). During contextual fear conditioning, SINV-infected mice treated with the high (0.6mg/kg) dose, but not the low (0.3mg/kg) dose, of DON showed a significant increase in the percent time spent freezing compared to the untreated, SINV-infected mice ($p < 0.01$, Fisher's PLSD). DON treatment did not affect cued fear conditioning performance among SINV-infected groups, though the effect seen previously between SINV-infected and mock-infected groups remained ($p < 0.0001$, Fisher's PLSD). Treatment of mice with the high (0.6mg/kg) dose of DON did not affect performance for either contextual or cued fear conditioning in mock-infected mice. These results show that high (0.6mg/kg) dose DON treatment prevents development of hippocampus-dependent memory deficits as measured by contextual, but not cued, fear conditioning in SINV-infected mice at 5 DPI.

Glutamine antagonism prevents lymphocyte proliferation in the CLNs and infiltration into CNS during SINV infection

After determining that DON treatment partially prevents the development of clinical neurological disease in SINV-infected mice, the mechanisms behind these effects were examined. Production of T cells and B cells was evaluated in the CLNs (representing the periphery), brains, and spinal cords of SINV-infected mice during DON administration (5 and 7 DPI) and after cessation of treatment (9 and 11 DPI). Trypan blue exclusion was used to count the total mononuclear cells (Fig 3-4A) in each tissue, and absolute counts of CD3+ T cells (Fig 3-4B), CD4+ T cells (Fig 3-4C), CD8+ T cells (Fig 3-4D), and CD19+ B cells (Fig 3-4E) were measured by flow cytometry.

In the CLNs, all cell types increased in untreated, SINV-infected mice, with total mononuclear cells and CD3+, CD4+, and CD8+ T cells peaking at 7 DPI, and CD19+ B cells peaking in number at 9 DPI. In the CLNs of mock-infected and SINV-infected, DON-treated mice, cell numbers did not increase during the period of DON treatment (5 and 7 DPI). Following cessation of treatment at 9 and 11 DPI, cell counts began to increase in SINV-infected mice that had been previously administered DON at the low (0.3mg/kg) dose. In the brains and spinal cords of untreated, SINV-infected mice, total mononuclear cell counts markedly increased starting at 7 DPI and peaked at 9 DPI. In both tissues, individual CD3+, CD4+, CD8+, and CD19+ cell populations steadily increased in number, peaking at 11 DPI. During the period of DON treatment at 5 and 7 DPI, infiltration of any cell population into the brain or spinal cord were not seen in SINV-infected mice receiving either the low (0.3mg/kg) or high (0.6mg/kg) dose of DON. However, at 9 DPI, total mononuclear cells and CD19+ B cells, and at 11 DPI, CD3+, CD4+, and CD8+ T cells began increasingly infiltrating the brains of SINV-infected mice previously treated with the low (0.3mg/kg) DON dose. Similar increases in

infiltrating cells into the spinal cords of DON-treated mice were not seen following cessation of treatment.

Infiltration of CD3+ T cells into the brains of DON-treated, SINV-infected mice was also evaluated by immunohistochemistry at 7 DPI. Positive-staining cells were readily detectable in untreated, SINV-infected mice, but less so in mock-infected mice or SINV-infected mice treated with either low (0.3mg/kg) or high (0.6mg/kg) DON (Fig 3-5A). Total counts of CD3+ cells in the hippocampi significantly differed among groups ($p < 0.05$, Kruskal-Wallis test), with more CD3+ cells found in untreated, SINV-infected mice (Fig 3-5B). Taken together, these findings indicate that DON treatment inhibits proliferation of T and B cells in the periphery in response to SINV infection, resulting in impaired infiltration of immune cells into the CNS. This effect is only transient though, because cessation of DON treatment resulted in gradual activation of the immune response.

Glutamine antagonism decreases CNS inflammation and pathology during SINV infection

To examine the effect of glutamine antagonism on CNS pathology during SINV infection, coronal brain sections and transverse lumbar spinal cord sections of SINV-infected mice treated with low (0.3mg/kg) dose or high (0.6mg/kg) dose DON were stained with H&E and evaluated for pathological changes. In the hippocampi (Fig 3-6A) and spinal cords (Fig 3-6B) of untreated, SINV-infected mice, perivascular cuffing and increased parenchymal cellularity were appreciable by 7 DPI. At 7 and 9 DPI, there was loss of neuronal architecture in the dentate gyrus of the hippocampus (Fig 3-6A), and at 9

DPI, tissue necrosis was noted in the lateral gray horn of the spinal cord (Fig 3-6B). Increased inflammation and pathological changes were no longer noted at 11 DPI. Compared to mock-infected controls (data not shown), increased inflammation and pathological changes were not noted in brains or spinal cords of SINV-infected mice receiving low (0.3mg/kg) dose or high (0.6mg/kg) dose DON during the period of drug administration. Following cessation of treatment at 9 and 11 DPI, perivascular cuffing became apparent in the hippocampi and spinal cords of SINV-infected mice previously treated with low (0.3mg/kg) dose and high (0.6mg/kg) dose DON. Disruption of normal architecture in the granule layer of the dentate gyrus was noted in SINV-infected mice previously treated with low (0.3mg/kg) dose DON at 11 DPI.

To further evaluate the level of inflammation in the brains and spinal cords of SINV-infected mice treated with DON, H&E-stained slides were blindly scored. Brain inflammation scores significantly differed among groups (Fig 3-6A; $p < 0.001$, two-way ANOVA), with untreated, SINV-infected mice having significantly higher scores than SINV-infected, low (0.3mg/kg) dose DON-treated mice at 5 and 7 DPI ($p < 0.001$, Tukey's multiple comparisons test), and SINV-infected, high (0.6mg/kg) dose DON-treated mice at 7 and 9 DPI ($p < 0.001$, Tukey's multiple comparisons test). Inflammation scores began to decrease at 11 DPI in untreated mice. Starting at 9 DPI, following cessation of DON treatment, brain inflammation scores in SINV-infected, low (0.3mg/kg) dose DON-treated mice began to increase, becoming significantly higher than those of SINV-infected, high (0.6mg/kg) dose DON-treated mice at 9 DPI ($p < 0.001$, Tukey's multiple comparisons test) and significantly higher than those of untreated, SINV-infected mice at 11 DPI ($p < 0.05$, Tukey's multiple comparisons test).

Inflammation scores in SINV-infected, high (0.6mg/kg) dose DON-treated mouse brains began to increase at 11 DPI.

Lumbar spinal cords scored for inflammation showed similar trends to brains (Fig 3-6D). Inflammation scores differed significantly among groups ($p < 0.001$, two-way ANOVA), with scores in untreated, SINV-infected mice significantly higher than those of SINV-infected, low (0.3mg/kg) dose DON-treated mice at 7 DPI ($p < 0.0001$, Tukey's multiple comparisons test) and significantly higher than those of SINV-infected, high (0.6mg/kg) dose DON-treated mice at 7 and 9 DPI ($p < 0.0001$, Tukey's multiple comparisons test). Following cessation of treatment, inflammation scores began to increase in SINV-infected, low (0.3m/kg) dose DON-treated and SINV-infected, high (0.6mg/kg) dose DON-treated mice at 9 and 11 DPI, respectively. By 11 DPI, spinal cord inflammation scores were comparable among treatment groups. These data show that glutamine antagonism transiently suppresses inflammation and CNS pathological changes during SINV infection, but cessation of treatment results in dose-dependent appearance of inflammation.

DON treatment decreases apoptosis in the CNS during SINV infection

Death of cells, particularly neurons, during viral infection results in significant organ dysfunction. To evaluate whether DON treatment affects cell death in the brain and spinal cord during SINV infection, coronal brain sections and transverse lumbar spinal cord sections in SINV-infected mice treated with low (0.3mg/kg) dose or high (0.6mg/kg) dose DON were examined by TUNEL assay. Increased numbers of TUNEL-positive cells were present at 7 and 9 DPI in the hippocampi of untreated, SINV-infected mice (Fig 3-

7A). During the period of DON treatment, TUNEL-positive cells were only rarely detectable in hippocampi of SINV-infected, low (0.3mg/kg) dose or high (0.6mg/kg) dose DON-treated mice, but positive cells increased in frequency at 9 DPI. At 11 DPI, TUNEL-positive cells were only rarely found in the hippocampi of all groups. TUNEL-positive cells were present throughout the spinal cord sections of untreated, SINV-infected mice at 7 and 9 DPI, but less so at 5 and 11 DPI (Fig 3-7B). In comparison, TUNEL-positive cells were only rarely seen in spinal cords of SINV-infected, low (0.3mg/kg) dose or high (0.6mg/kg) dose DON-treated mice at any of the time points.

Quantification of positive cells revealed untreated, SINV-infected mice had more apoptotic cells than SINV-infected, low (0.3mg/kg) dose or high (0.6mg/kg) dose DON-treated mice in the hippocampus at 7 DPI (Fig 3-7C; $p < 0.01$, Tukey's multiple comparisons test) and in the spinal cord at 7 and 9 DPI (Fig 3-7D; $p < 0.01$ for 7 DPI and $p < 0.001$ for 9 DPI, Tukey's multiple comparisons test). Cell death was comparable among groups at 5 and 11 DPI in both tissues. Further examination of TUNEL-positive neurons in the granule cell layer of the dentate gyrus and pyramidal cell layers of the CA regions in the hippocampus at 7 DPI revealed a significant difference among infection and treatment groups in number of apoptotic cells morphologically consistent with neurons (Fig 3-7E; $p < 0.05$, Kruskal-Wallis test), with more dead neurons found in the hippocampi of untreated, SINV-infected mice.

Glutamine antagonism suppresses antiviral effects of the immune response during SINV infection

Because glutamine antagonism suppresses lymphocyte proliferation[187,189,190], the antiviral effector function of these cells was evaluated during and following DON treatment during SINV infection. Previous studies have shown that clearance of infectious SINV from the CNS is facilitated synergistically by antibody directed against the SINV E2 glycoprotein and by IFN-γ, produced predominantly by B cells and T cells, respectively[24,92]. SINV-specific IgM and IgG were evaluated in the sera and brains of SINV-infected, DON-treated mice at 5, 7, 9 and 11 DPI by ELISA (Figs 3-8A-D). Serum IgM (Fig 3-8A) and IgG (Fig 3-8B) ODs significantly differed among treatment groups ($p < 0.01$ for IgM, $p < 0.0001$ for IgG, two-way ANOVA) and were both significantly higher in untreated mice compared to both low (0.3mg/kg) dose and high (0.6mg/kg) dose DON-treated mice at all timepoints for IgM ($p < 0.05$, Tukey's multiple comparisons test) and at 7, 9, and 11 DPI for IgG ($p < 0.05$, Tukey's multiple comparisons test). Increases in anti-SINV IgM and IgG were present in the sera of low (0.3mg/kg) dose and high (0.6mg/kg) dose DON-treated mice following cessation of treatment at 11 DPI.

Brain SINV-specific IgM (Fig 3-8C) and IgG (Fig 3-8D) ODs significantly differed among treatment groups ($p < 0.0001$ for both IgM and IgG, two-way ANOVA) but increases were delayed compared to the sera of corresponding mice. Brain anti-SINV ODs were significantly higher in untreated mice compared to both low (0.3mg/kg) dose and high (0.6mg/kg) dose DON-treated mice at 11 DPI for IgM ($p < 0.0001$, Tukey's multiple comparisons test) and at 9 and 11 DPI for IgG ($p < 0.0001$, Tukey's multiple comparisons test). Increases in anti-SINV IgM and IgG were present in the brains of low (0.3mg/kg) dose DON-treated, but not high (0.6mg/kg) dose DON-treated mice following

cessation of treatment at 11 DPI. These results show that glutamine antagonism decreases anti-SINV antibody production in the serum and brain during SINV infection, and that cessation of treatment allows increases in production. Additionally, development of anti-SINV IgM and IgG production is later in the brain than the serum.

IFN-γ represents the other main facilitator of virus clearance[92], and the effect of glutamine antagonism on its production in the brain during SINV infection was examined by measuring mRNA expression by qRT-PCR and protein levels by ELISA at 5, 7, 9, and 11 DPI. Overall IFN-γ mRNA expression, when normalized to that of untreated, mock-infected mouse brains, significantly differed among groups (Fig 3-8E; $p < 0.001$, two-way ANOVA), with untreated, SINV-infected mice having significantly increased expression at 7 DPI compared to low (0.3mg/kg) dose and high (0.6mg/kg) dose DON-treated mice ($p < 0.0001$, Tukey's multiple comparisons test). *Ifng* expression in brains of SINV-infected, low (0.3mg/kg) dose and high (0.6mg/kg) dose DON-treated mice was approximately 100- to 1,000-fold higher than untreated-mock-infected mice. Following cessation of DON treatment, *Ifng* expression increased in mice starting at 9 DPI, with SINV-infected, low (0.3mg/kg) dose DON-treated mice having significantly increased expression compared to untreated, SINV-infected mice at 11 DPI ($p < 0.05$, Tukey's multiple comparisons test). *Ifng* expression in mock-infected, high (0.6mg/kg) dose DON-treated mouse brains was comparable to that of untreated, mock-infected mouse brains (data not shown).

IFN-γ protein levels in the brain significantly differed among groups (Fig 3-8F; $p < 0.0001$, two-way ANOVA), with untreated, SINV-infected mice having significantly increased expression at 7 DPI compared to low (0.3mg/kg) dose and high (0.6mg/kg)

dose DON-treated mice ($p < 0.0001$, Tukey's multiple comparisons test). Following cessation of DON treatment, IFN-γ expression increased in mice previously treated starting at 9 DPI, with both SINV-infected, low (0.3mg/kg) dose and high (0.6mg/kg) dose DON-treated mice having significantly increased expression compared to untreated, SINV-infected mice at 11 DPI ($p < 0.01$, Tukey's multiple comparisons test). IFN-γ was not detected in the brains of mock-infected mice at any time point, regardless of treatment status (data not shown), nor was it detectable in brains of SINV-infected, low (0.3mg/kg) dose and high (0.6mg/kg) dose DON-treated mice during the period of drug administration at 5 and 7 DPI. These data show that glutamine antagonism impairs the two major adaptive antiviral responses involved in clearance of SINV.

DON treatment delays virus clearance in the brain and spinal cord

Because the two major avenues by which the immune response clears SINV from the CNS are affected by glutamine antagonism, virus production was examined over time in mice treated with DON. SINV protein production was visualized in coronal brain and lumbar spinal cord sections by immunohistochemistry. Positive staining for SINV antigen in the hippocampus (Fig 3-9A) and spinal cord (Fig 3-9B) of untreated mice was readily observed at 5, 7, and 9 DPI and 7 and 9 DPI, respectively. Comparable levels of positive SINV antigen staining were found in mice treated with low (0.3mg/kg) dose or high (0.6mg/kg) dose DON in both tissues at the above times. Additionally, SINV antigen was readily visualized in the brains and spinal cords of DON-treated, but not untreated, mice at 11 DPI. Following cessation of DON administration, levels of SINV

protein did begin to decrease in DON-treated mice at 9 and 11 DPI, indicating progress towards virus clearance.

Clearance of infectious virus was evaluated by measuring virus titers by plaque assay at 5, 7, 9, and 11 DPI. Infectious virus clearance was delayed in DON-treated mice in a dose-dependent manner, with titers significantly lower in untreated mice at 9 and 11 DPI in the brain (Fig 3-9C; $p < 0.05$ at 9 DPI and $p < 0.01$ for untreated vs low [0.3mg/kg] dose DON, $p < 0.001$ at 9 DPI and $p < 0.0001$ at 11 DPI for untreated vs high [0.6mg/kg] dose DON, $p < 0.0001$ at 11 DPI for low [0.3mg/kg] dose DON vs high [0.6mg/kg] dose DON, all Tukey's multiple comparisons test) and at 7, 9, and 11 DPI in the spinal cord (Fig 3-9D; $p < 0.05$ at 7 and 9 DPI for untreated vs low [0.3mg/kg] dose DON, $p < 0.05$ at 7 DPI and $p < 0.01$ at 9 and 11 DPI for untreated vs high [0.6mg/kg] dose DON, all Tukey's multiple comparisons test).

Initiation of viral RNA clearance was evaluated by measuring viral RNA levels by qRT-PCR at 5, 7, 9, and 11 DPI. Viral RNA clearance was delayed in DON-treated mice, with RNA copies significantly lower in untreated mice at 7, 9, and 11 DPI in the brain (Fig 3-9E; $p < 0.05$ at 7 DPI, $p < 0.01$ 9 DPI, and $p < 0.0001$ at 11 DPI for untreated vs low [0.3mg/kg] dose DON, $p < 0.01$ at 7 DPI, $p < 0.001$ 9 DPI, and $p < 0.0001$ at 11 DPI for untreated vs high [0.6mg/kg] dose DON, all Tukey's multiple comparisons test) and at 9 and 11 DPI in the spinal cord (Fig 3-9F; $p < 0.05$ at 9 DPI and $p < 0.01$ at 11 DPI for untreated vs low [0.3mg/kg] dose DON, $p < 0.05$ at 9 DPI and $p < 0.001$ at 11 DPI for untreated vs high [0.6mg/kg] dose DON, all Tukey's multiple comparisons test). Viral RNA levels did decrease in brains of DON-treated mice following cessation of drug administration, though not to the same dose-dependent effect

as was seen with infectious virus. These findings show that in addition to suppressing the immune response during SINV infection, glutamine antagonism delays virus clearance in the CNS.

DISCUSSION

(adapted from Potter and Baxter, et al, 2015)

Glutamatergic drugs such as AMPA and NMDA receptor antagonists have been previously shown to enhance survival of hippocampal neurons and increase lifespan in NSV-infected mice by prevention of immune-mediated damage and inhibition of excitotoxicity[49,65]. In the current study, we tested the effects of a glutamine antagonist, DON, for its potential to mitigate the consequences of nonfatal SINV infection seen at the peak of infection. DON blocks the conversion of glutamine to glutamate, thus decreasing the potential for glutamate excitotoxicity in the brain, but also suppresses proliferation of lymphocytes, which require glutamine to support rapid cell division induced by antigen stimulation[187,189,190]. DON was examined as a potential chemotherapeutic agent in the 1970s and 1980s, but it was not well tolerated in clinical trials due primarily to GI toxicity[188,195-198]. In our study, mice in the high (0.6 mg/kg) dose DON treatment group developed severe intestinal pathologic changes, likely explaining the marked weight loss seen regardless of infection status. These signs may also help explain why we observed a reduced motor ability in DON-treated mice. We do not believe that this influenced the cognitive tests since there was no difference in

freezing levels between mock-infected mice with or without DON during fear conditioning testing. Previous studies using DON[199,200] have also reported that issues with drug toxicity and dosing regimens were modified to counteract these negative side effects. In its present form, DON does not represent a viable treatment for alphavirus encephalomyelitis. However, by serving as a prototype, different glutamine antagonists or different formulations or derivatives of DON can be further evaluated as potential therapeutic options.

The glutamine antagonist DON partially prevented development of the deficit in contextual, but not cued, fear conditioning. This result suggests that cued and contextual conditioning are differentially susceptible to the effects of DON, which may be related to differences between anatomical structures and circuitry that support both types of learning. While the amygdala is essential for both cued and contextual fear conditioning, the hippocampus is not essential for cued fear conditioning but does contribute to contextual fear conditioning[161,201-204]. Indeed, this disconnect between effects on cued and contextual conditioning has been shown with other glutamate antagonists such as MK-801 [205,206].

Long-term persistence of a viral RNA reservoir in neurons presents the possibility of viral reactivation, relapse of disease, and progressive pathological changes[43]. Both infectious virus and SINV RNA typically peak in the brains of infected mice at 3–5 DPI, and while infectious virus quickly decreases to undetectable levels by 8–10 DPI, RNA levels slowly decline but remain measureable for at least a year[42]. DON had significantly higher titers and viral RNA levels than untreated mice, due to a delay in virus clearance likely associated with a decrease in immune cell infiltration into the CNS.

Previous studies using the more neurovirulent NSV strain of SINV have shown that the immune response to infection plays a significant role in the neuronal damage and death seen during fatal alphavirus encephalomyelitis[54], as well as in virus clearance. While neuronal cell death is independent of DNA fragmentation in motor neurons of the spinal cord during NSV infection, neuronal damage in the hippocampus appears to follow the classical apoptotic pathway and can be detected through TUNEL staining[48]. In the present study, treatment with DON resulted in decreased inflammatory cell infiltration, including CD3+ T cells, and lower levels of cell death in the brain, despite increased levels of infectious virus and comparable levels of viral antigen and RNA. Moreover, fewer DON-treated mice developed neurological signs by 7 DPI compared to untreated SINV-infected mice. The numbers of apoptotic neurons in the granule cell layer of the dentate gyrus and pyramidal cell layers of the CA regions differed between infection and treatment groups, with the highest number of positive cells seen in the untreated SINV-infected group. This loss of neurons across the hippocampal subfields, areas key to intact cognitive abilities, helps to explain the significantly impaired performance this group displayed in behavior tests.

Despite obtaining high serum levels, DON did not penetrate the brain well, suggesting that the drug's effect on alphavirus pathological changes primarily occurs through peripheral suppression of the antiviral immune response. DON treatment resulted in both decreased proliferation of T and B cells in the CLNs and fewer infiltrating T and B cells into the brain and spinal cord during the period of drug administration. Decreased inflammatory cell infiltration into the CNS reduces neuronal damage and thus explains the lack of clinical signs and weight loss in the low (0.3 mg/kg) dose DON group.

Following cessation of treatment, increased proliferation of lymphocytes in CLNs was seen at 9 DPI, while increased infiltration of cells into the brain was not observed until 11 DPI (and still not observed in the spinal cord), further supporting this hypothesis.

Previous studies have shown that alphavirus clearance from the CNS is primarily facilitated by antibody against the SINV E2 glycoprotein[24] and IFN-γ produced by NK cells and T cells[92]. In contrast to untreated, SINV-infected mice, SINV-specific antibody levels in sera and brains and *Ifng* expression and IFN-γ production in brains were considerably lower or undetectable in DON-treated mice during the period of drug administration. Following cessation of treatment, levels of antibody and IFN-γ increased, corresponding to increased proliferation and infiltration of immune cells into the CNS. While infectious virus titers and viral RNA levels were comparable among treatment groups during the period of DON administration, they remained significantly elevated in the brains and spinal cords of DON-treated mice compared to untreated mice at 9 and 11 DPI. However, they did decrease in titer and copy number during this period, indicating successful initiation of clearance. Therefore, while compromised immune cell proliferation in the periphery and infiltration into the brain and spinal cord results in decreased CNS pathological changes, it also results in impaired virus clearance from neurons. Once the immune response is no longer inhibited, virus clearance resumes. This supports the importance of the immune response in the pathogenesis of the less virulent SINV TE strain, as well as NSV, and suggests that immunosuppression in the periphery plays an important role in the mitigation of nonfatal alphavirus encephalomyelitis by glutamine antagonism.

The continued emergence of viral encephalomyelitis outbreaks around the world emphasizes the need to identify novel approaches to improve outcome using an animal model. These findings may also be applicable to treatment of other virus infections of the nervous system that share similar cognitive and pathological features including immune activation, inflammation, and excitotoxicity[207-209]. Additionally, the immunosuppressive nature of DON makes it a useful tool to further elucidate the mechanisms and pathogenesis of alphavirus-induced disease.

FIGURES

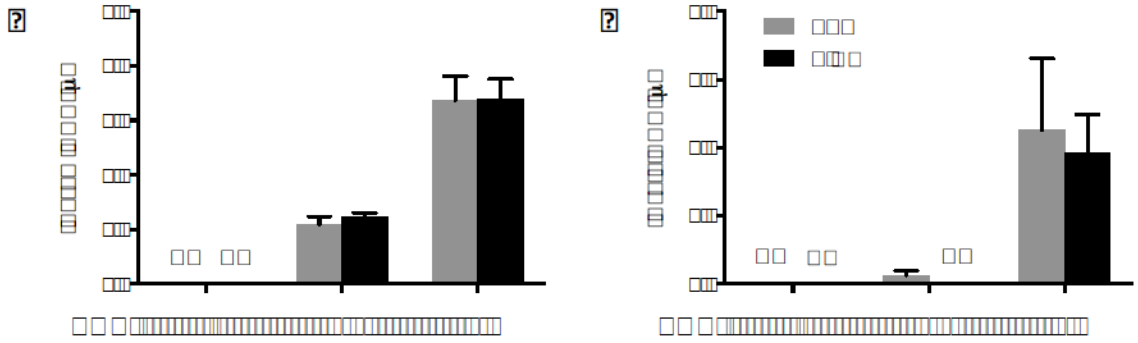

Figure 3-1. DON levels in tissues of SINV-infected and mock-infected mice. (**A, B**) Levels of DON were measured by HPLC in sera (**A**) and brains (**B**) of mock-infected (PBS) and SINV-infected mice receiving no treatment, low (0.3mg/kg) dose DON, or high (0.6mg/kg) dose DON (n = 3 mice per group; data presented as mean ± SEM; ND=not detectable). These experiments were performed in collaboration with Jesse Alt and Camilo Rojas, PhD. Figures were adapted from Potter and Baxter, *et al*, 2015.

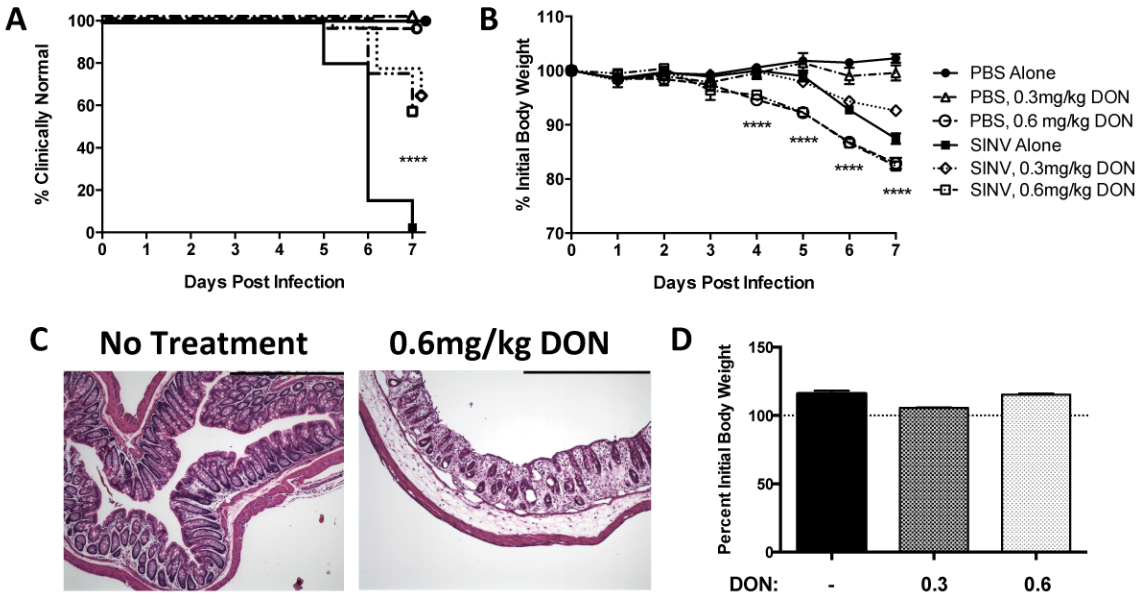

Figure 3-2. Clinical disease in DON-treated, SINV-infected mice. (**A**) Mock-infected (PBS) and SINV-infected mice receiving no treatment, low (0.3mg/kg) dose DON, or high (0.6mg/kg) dose DON were observed daily for the development of clinical signs (n = 9–32 mice over three separate independent experiments; ****$p < 0.0001$ by log-rank [Mantel-Cox] test). (**B**) Body weights were recorded daily in mock-infected (PBS) and SINV-infected mice receiving no treatment, low (0.3mg/kg) dose DON, or high (0.6mg/kg) dose DON (n = 9–32 mice over three separate independent experiments; ****$p < 0.0001$, one-way ANOVA with $p < 0.01$ by Bonferroni's multiple comparison tests). (**C**) Representative photomicrographs were taken of H&E-stained large intestine from untreated, mock-infected (left panel) and high (0.6mg/kg) dose DON-treated (right panel) mice (100X magnification; scale bar = 500μm). (**D**) Body weight was recorded in SINV-infected mice receiving no treatment, low (0.3mg/kg) dose DON, or high (0.6mg/kg) dose DON following recovery from clinical disease at 28 DPI (n = 3-4 mice

per group; data presented as mean ± SEM). Figures were adapted from Potter and Baxter, *et al*, 2015.

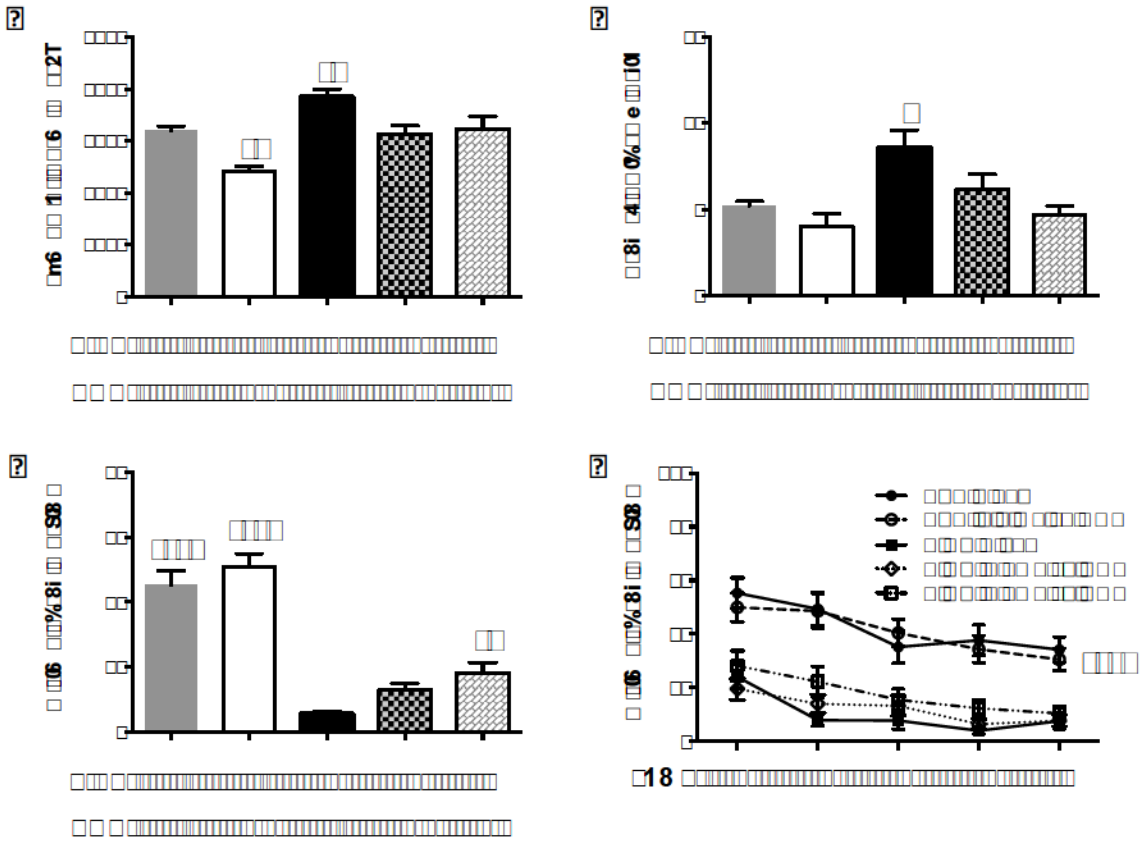

Figure 3-3. Effect of DON on locomotor activity, anxiety, and hippocampal dependent memory. (**A, B**) The open field test was used to assess locomotor activity (**A**) and anxiety (**B**) in mock-infected (PBS) and SINV-infected mice receiving no treatment, low (0.3mg/kg) dose DON, or high (0.6mg/kg) dose DON at 5 DPI by measuring the number of beam breaks made by mice in 30 minutes and the ratio of time mice spent in the center versus the periphery, respectively. (**C, D**) Hippocampus-dependent memory was assessed by contextual (**C**) and cued (**D**) fear conditioning in mock-infected (PBS) and SINV-infected mice receiving no treatment, low (0.3mg/kg) dose DON, or high (0.6mg/kg) dose DON at 5 DPI (n = 11-27 mice per group; data presented as mean ± SEM; *$p < 0.05$, **$p < 0.01$, ****$p < 0.0001$, ANOVA followed by Fisher's PLSD).

These experiments were performed in collaboration with Michelle C. Potter, PhD. Figures were adapted from Potter and Baxter, *et al*, 2015.

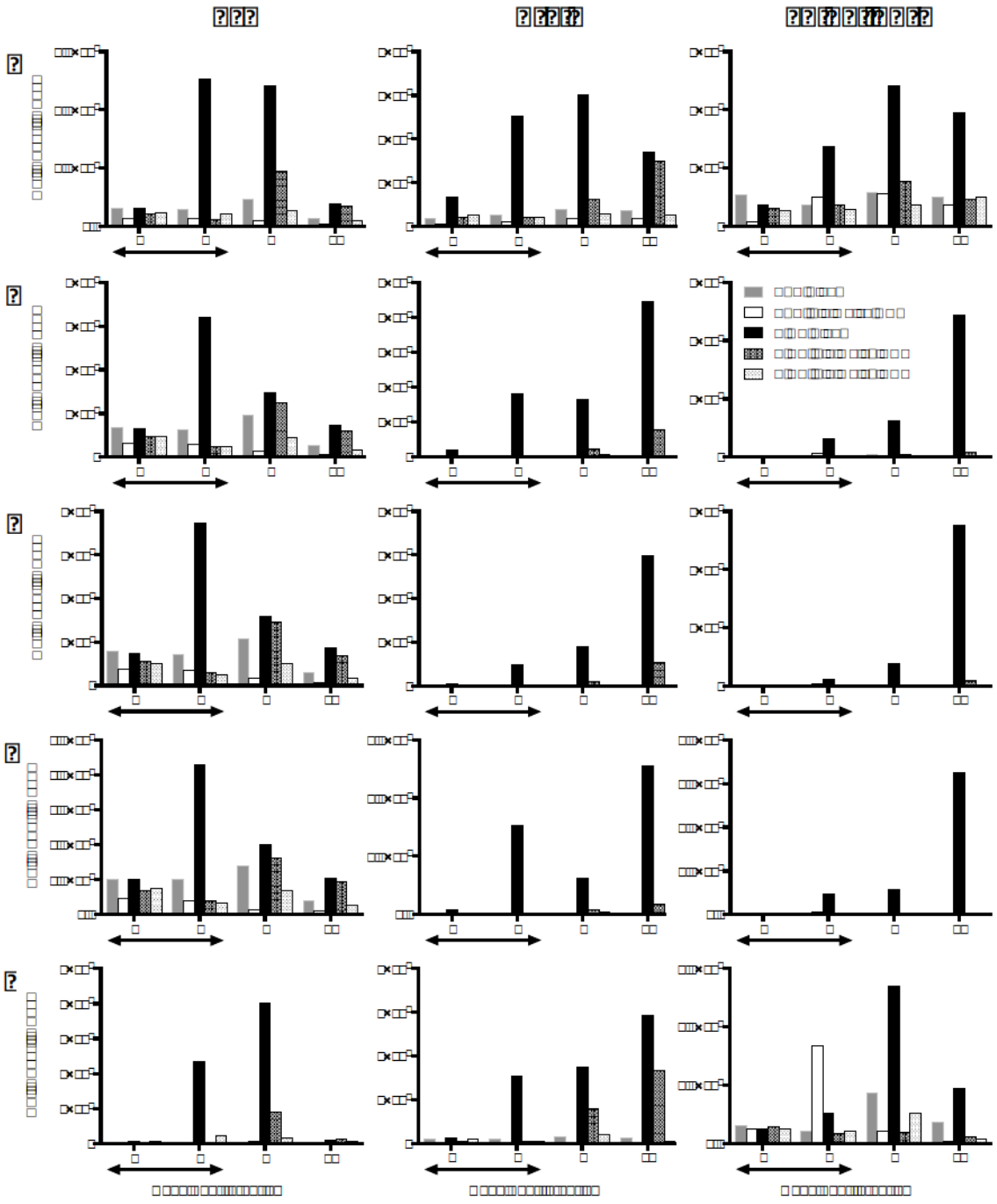

Figure 3-4. Effect of DON treatment on immune cell proliferation in the CLNs and infiltration into the CNS during SINV infection. (**A**) Total live mononuclear cells in the CLNs (left panel), brains (middle panel), and spinal cords (right panel) of mock-

infected and SINV-infected mice receiving no treatment, low (0.3mg/kg) dose DON, or high (0.6mg/kg) dose DON at 5, 7, 9, and 11 DPI by trypan blue exclusion. (**B-E**) Absolute numbers of CD3+ T cells (**B**), CD4+ T cells (**C**), CD8+ T cells (**D**), and B cells (**E**) in the CLNs (left panel), brains (middle panel), and spinal cords (right panel) by of mock-infected and SINV-infected mice receiving no treatment, low (0.3mg/kg) dose DON, or high (0.6mg/kg) dose DON at 5, 7, 9, and 11 DPI by flow cytometry (n = 2-3 pooled mice per group per time point; data presented as the mean ± SEM; double-headed arrows indicate the period of DON treatment).

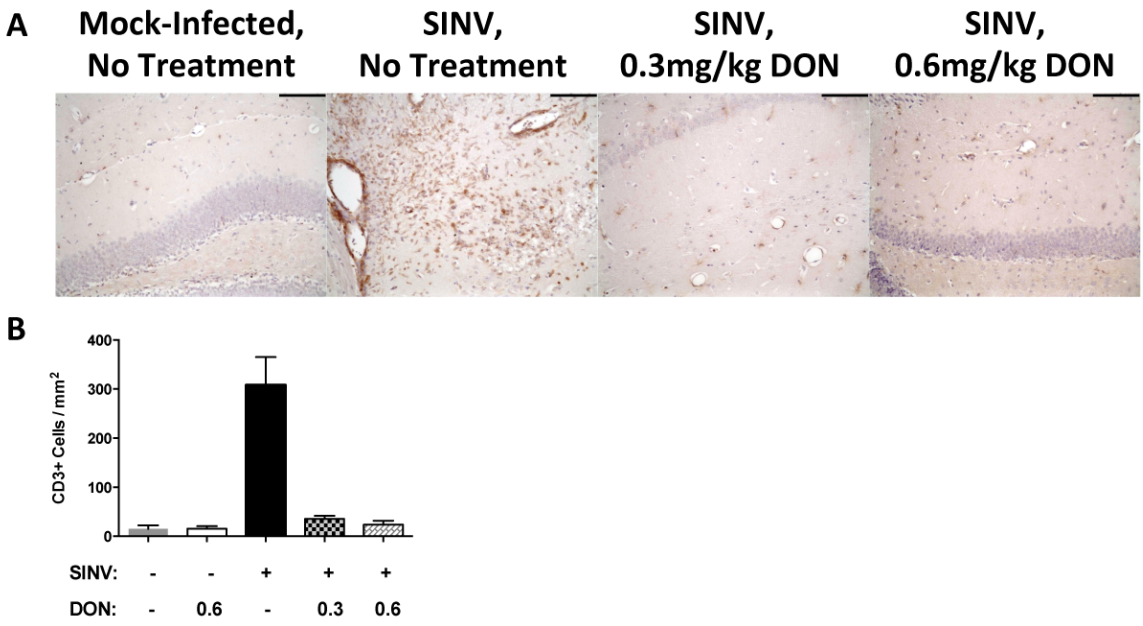

Figure 3-5. Effect of DON treatment on CD3+ T cell infiltration into the brain during SINV infection at 7 DPI. (**A**) Representative photomicrograph CD3+ staining of the hippocampus were taken of brains from mock-infected or SINV-infected mice receiving no treatment, low (0.3mg/kg) dose DON, or high (0.6mg/kg) dose DON at 7 DPI (CD3+ cells= brown staining; 200X magnification; scale bar=100 μm). (**B**) CD3+ cells were counted in the hippocampus of mock-infected or SINV-infected mice receiving no treatment, low (0.3mg/kg) dose DON, or high (0.6mg/kg) dose DON at 7 DPI (n = 3 mice per group per time point; data presented as the mean ± SEM; $p < 0.05$ by Kruskal-Wallis test). Figures were adapted from Potter and Baxter, *et al*, 2015.

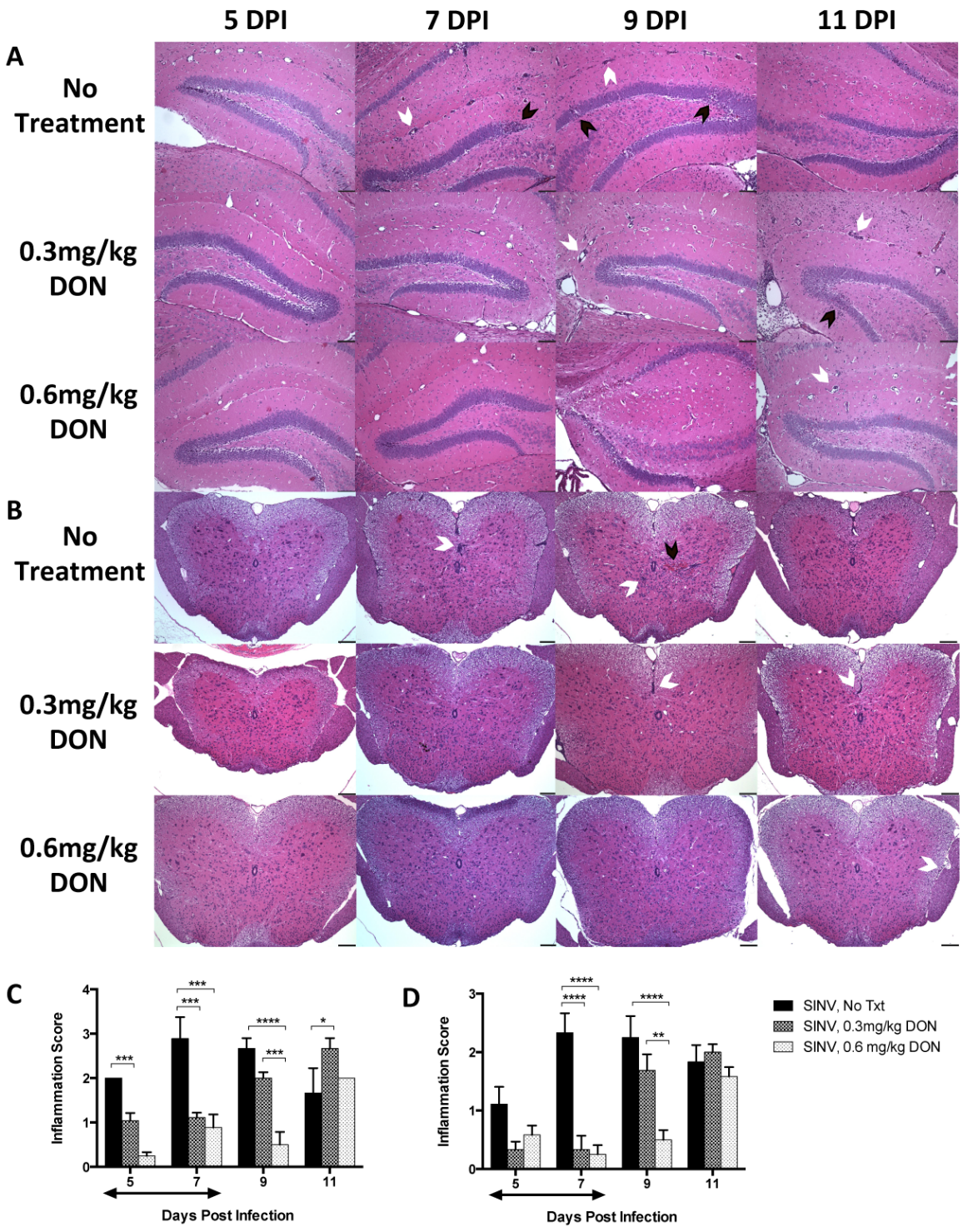

Figure 3-6. Effect of DON treatment on CNS inflammation and pathology during SINV infection. (**A, B**) Representative photomicrographs were taken of H&E sections of

the (**A**) brain and (**B**) spinal cord of SINV-infected mice receiving no treatment (top row), low (0.3mg/kg) dose DON (middle row), or high (0.6mg/kg) dose DON (bottom row) at 5, 7, 9 and 11 DPI. White arrowheads denote perivascular cuffing, and black arrowheads denote disruption of the granule cell layer of the hippocampus or loss of proper tissue architecture in the spinal cord (100X magnification; scale bar=100 μm). (**C, D**) H&E sections of brains (**C**) and spinal cords (**D**) of SINV-infected mice receiving no treatment, low (0.3mg/kg) dose DON, or high (0.6mg/kg) dose DON were scored for inflammation at 5, 7, 9 and 11 DPI using a four-point (brain) or three-point (spinal cord) system (n = 3-4 mice per group per time point; data presented as the mean ± SEM; double-headed arrows indicate the period of DON treatment; *$p < 0.05$, **$p < 0.01$, ***$p < 0.001$, ****$p < 0.0001$ by Tukey's multiple comparisons test).

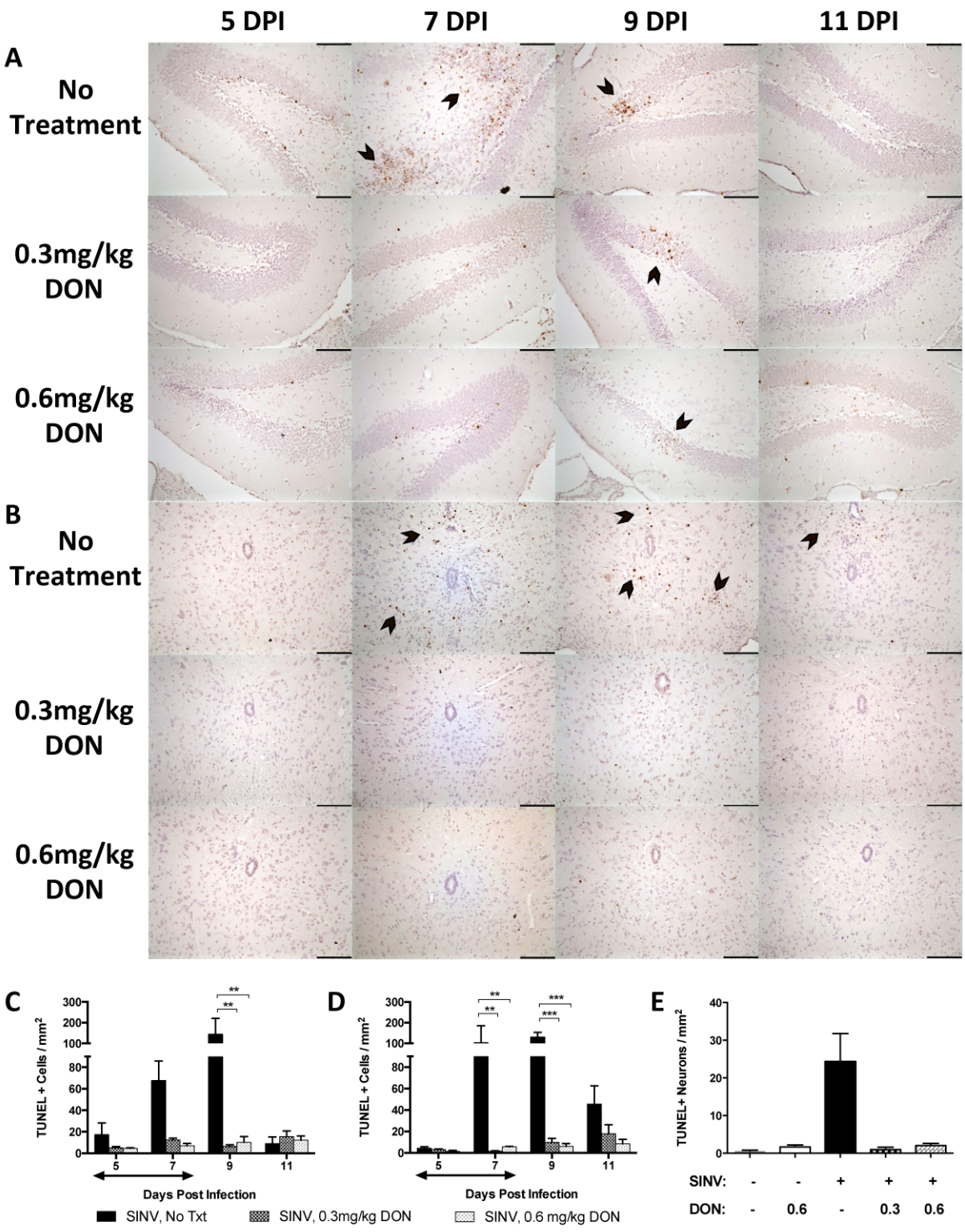

Figure 3-7. Effect of DON-treatment on cell death in the CNS during SINV infection. (**A, B**) Representative photomicrographs were taken of TUNEL staining in the

dentate gyrus in the hippocampus (**A**) and spinal cord (**B**) of SINV-infected mice receiving no treatment (top row), low (0.3mg/kg) dose DON (middle row), or high (0.6mg/kg) dose DON (bottom row) at 5, 7, 9 and 11 DPI (brown nuclear staining=TUNEL-positive [denoted by black arrowheads]; 200X magnification; scale bar=100 μm). (**C, D**) Quantification of TUNEL-positive cells in brains (**C**) and spinal cords (**D**) of SINV-infected mice receiving no treatment, low (0.3mg/kg) dose DON, or high (0.6mg/kg) dose DON at 5, 7, 9 and 11 DPI (n = 3-4 mice per group per time point; double-headed arrows indicate the period of DON treatment; $^{**}p < 0.01$, $^{***}p < 0.001$, by Tukey's multiple comparisons test). (**E**) Quantification of apoptotic/necrotic neuronal cell bodies in the granule layer of the dentate gyrus and pyramidal layer of the CA regions at 7 DPI (n = 3 mice per group; data presented as the mean ± SEM; $p < 0.05$ by Kruskal-Wallis test). Figure 3-7E was adapted from Potter and Baxter, *et al*, 2015.

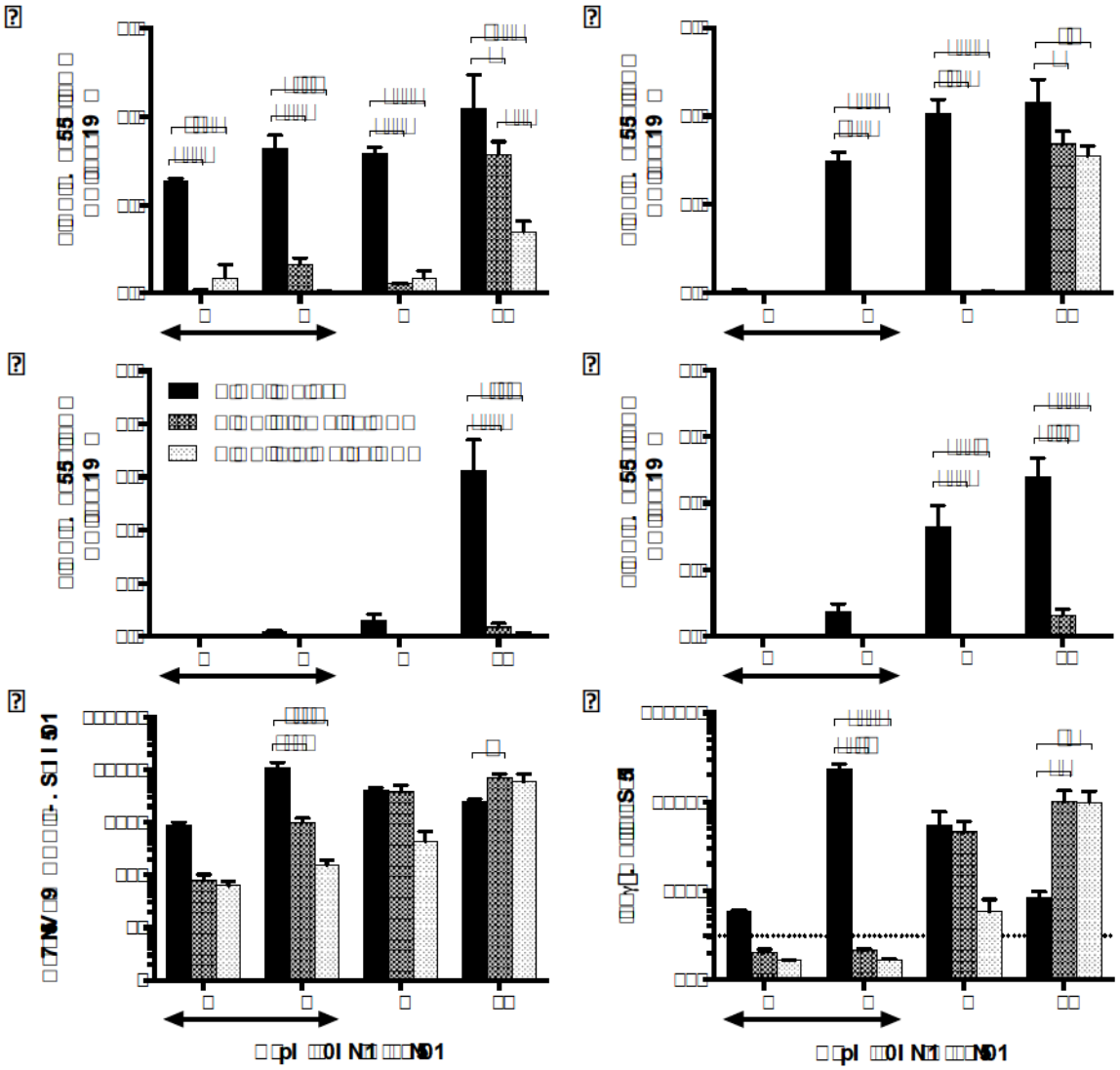

Figure 3-8. Effect of DON treatment on SINV-specific antibody and IFN-γ production. (**A-D**) SINV-specific IgM (**A, C**) and IgG (**B, D**) levels were measured by ELISA in the serum (**A, B**) and brain (**C, D**) of SINV-infected mice receiving no treatment, low (0.3mg/kg) dose DON, or high (0.6mg/kg) dose DON at 5, 7, 9 and 11 DPI. (**E, F**) *Ifng* mRNA expression (**E**) was measured by qPCR and IFN-γ protein levels (**F**) were measured by ELISA in the brains of SINV-infected mice receiving no treatment,

low (0.3mg/kg) dose DON, or high (0.6mg/kg) dose DON at 5, 7, 9 and 11 DPI (n = 3-4 mice per group per time point; data presented as the mean ± SEM; double-headed arrows indicate the period of DON treatment; dotted line indicates assay level of detection; *p < 0.05, **p < 0.01, ***p < 0.001, ****p < 0.0001 by Tukey's multiple comparisons test).

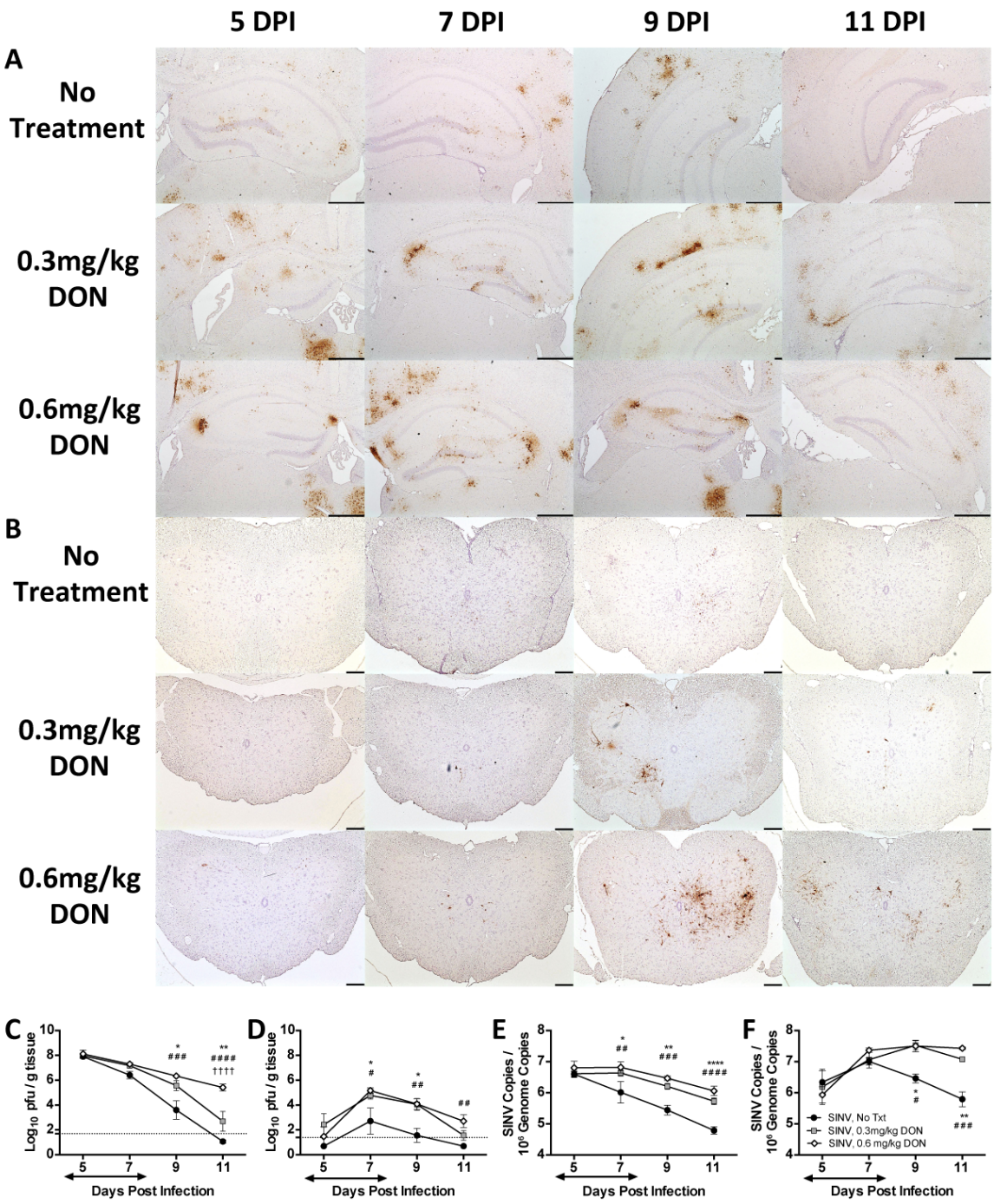

Figure 3-9. Effect of DON treatment on SINV production. (**A, B**) Representative photomicrographs of immunohistochemical staining for SINV antigen in SINV-infected mice receiving no treatment (top row), low (0.3mg/kg) dose DON (middle row), or high (0.6mg/kg) dose DON (bottom row) in the brain (**A**) and spinal cord (**B**) at 5, 7, 9, and 11

DPI (SINV antigen = brown staining; brain 40X magnification, scale bar=500μm; spinal cord 100X magnification, scale bar=100μm). (**C, D**) Infectious virus titers were measured by plaque assay in the brains (**C**) and spinal cords (**D**) of SINV-infected mice receiving no treatment (black circle and line), low (0.3mg/kg) dose DON (gray square and line), and high (0.6mg/kg) dose DON (white diamond and black line). (**E, F**) Viral RNA levels were measured by qRT-PCR in the brains (**E**) and spinal cords (**F**) of SINV-infected mice receiving no treatment (black circle and line), low (0.3mg/kg) dose DON (gray square and line), and high (0.6mg/kg) dose DON (white diamond and black line) (n = 3-6 mice per group per time point; data presented as the mean ± SEM; double-headed arrows indicate the period of DON treatment; dotted line indicates assay level of detection; $^{*}p < 0.05$, $^{**}p < 0.01$, $^{****}p < 0.0001$, untreated vs low [0.3 mg/kg] dose DON; $^{\#}p < 0.05$, $^{\#\#}p < 0.01$, $^{\#\#\#}p < 0.001$, $^{\#\#\#\#}p < 0.0001$, untreated vs high [0.6 mg/kg] dose DON; $^{††††}p < 0.0001$, low [0.3mg/kg] dose DON vs high [0.6mg/kg] dose DON, all by Tukey's multiple comparisons test).

CHAPTER 4:

MODULATION OF THE IMMUNE RESPONSE BY INTERFERON GAMMA DURING NONFATAL ALPHAVIRUS ENCEPHALOYMYELITIS ALTERS VIRUS CLEARANCE IN THE CENTRAL NERVOUS SYSTEM

INTRODUCTION

Mosquito-borne viruses that produce encephalomyelitis are becoming an increasing worldwide concern as arthropod vectors expand into new territories[147-150,210]. The New World alphaviruses, which include eastern, western, and Venezuelan equine encephalitis viruses, produce encephalomyelitis with varying fatality rates in dead-end hosts such as humans and horses[8,13]. However, humans who survive the initial disease syndrome, particularly those infected as infants or children, have a high probability of being left with debilitating life-long physical and mental disabilities[14-18]. Currently there are no treatments beyond supportive care for alphavirus encephalomyelitis[20].

Sindbis virus (SINV) is the prototypic member of the alphaviruses, and infection of susceptible mice with well characterized strains provides a valuable model for studying the pathogenesis of and host immune response to alphavirus encephalomyelitis. When C57BL/6 mice are intracranially infected with the nonfatal TE strain, the course of infection proceeds in three phases [42]. In Phase 1, which occurs through 7 to 8 days post infection (DPI), both infectious virus and viral RNA are readily detectable at high levels until infectious virus undergoes a precipitous drop in titers. In Phase 2, which occurs from approximately 10 to 60 DPI, infectious virus is no longer detectable, but viral RNA is still readily measureable at high but declining levels. Finally in Phase 3, which occurs from 60 DPI though at least a year following infection and presumably for the life of the animal, viral RNA reaches a low but detectable steady state in the CNS. Currently, the mechanisms that facilitate clearance of viral RNA are unknown. Understanding how the

immune response is able to clear both infectious virus and viral RNA while simultaneously controlling reactivation is critical to developing potential therapies.

As neurons are a valuable yet finite population with little regenerative capacity, clearance of virus by the immune system requires a noncytolytic mechanism to maintain functional neurological performance. While initial control of virus replication and production is dependent on type I interferon (IFN)[69,70,79], the adaptive immune response is responsible for later virus clearance and control. Previous work using SCID mice, which are incapable of naturally clearing SINV, has shown that treatment with hyperimmune serum results in successful clearance of both infectious virus and viral RNA from all regions of the CNS, indicating antibody directed against SINV plays a central role in clearance[24]. However, virus clearance from the brain stem and spinal cord is possible in antibody knockout mice, but requires IFN gamma (IFN-γ) produced by CD4+ and CD8+ T cells[92]. Mice that lack both antibody and IFN-γ produce an infectious virus titer profile similar to SCID mice and are less successful at clearing infectious virus compared to single antibody- or IFN-γ-knockout mice[70], indicating synergistic cooperation between the two in facilitating virus clearance. However, the mechanisms through which this occurs have not been elucidated.

IFN-γ, the sole type II IFNs, is primarily produced by activated T cells and natural killer (NK cells)[95,96]. Its antiviral activity is achieved through a Jak/STAT-dependent signaling pathway by binding IFN-γ to its heterotetrameric receptor, which is found on neurons [97,103,104]. IFN-γ signaling results in STAT activation and binding to gamma-associated sites (GAS) on over 200 genes, many with antiviral activity, including PKR and 2'-5' oligoadenylate synthetases[103,105]. IFN-γ also has immunomodulatory effects,

such as MHC class I induction, cytokine and chemokine secretion, and leukocyte activation and differentiation[106-108].

IFN-γ is known to help facilitate clearance of infectious virus during SINV infection. However, the mechanisms by which this occurs are not fully understood. Furthermore, the role IFN-γ plays in clearance of viral RNA has not yet been studied. We hypothesize that like infectious virus, IFN-γ facilitates clearance of viral RNA through induction of antiviral genes. By using both *in vitro* and *in vivo* systems, we sought to understand the antiviral and immunomodulatory role IFN-γ plays during SINV clearance in the CNS.

MATERIALS & METHODS

Cell Cultures

AP-7 cells, a gift from Dale Hunter at Tufts University[211], were derived from rat olfactory neurons and immortalized with a temperature-sensitive simian virus 40 (SV-40) T antigen. Cycling AP-7 (cAP-7) cells were grown at 33°C at 7% CO_2 in DMEM + 10% FBS + 2mM L-glutamine + 100U/mL penicillin + 100μg/mL streptomycin and for differentiation were transferred to 39°C at 5% CO_2 in DMEM + 10% FBS + 2mM L-glutamine + 100U/mL penicillin + 100μg/mL streptomycin + 1μg/mL insulin + 20 μM dopamine + 100μM ascorbic acid (dAP-7 cells). Cells were allowed to differentiate for five to seven days prior to infection.

CSM14.1 cells, a gift from Dale E. Bredesen of the Buck Institute of Age Research[212,213], were derived from rat nigral-striatal neurons and immortalized with a temperature-sensitive SV-40 T antigen. Cycling CSM14.1 cells were grown at 31°C at 5% CO_2 in DMEM + 10% FBS + 2mM L-glutamine + 100U/mL penicillin + 100µg/mL streptomycin and were transferred to 39°C at 5% CO_2 in DMEM + 1% FBS + 2mM L-glutamine + 100U/mL penicillin + 100µg/mL streptomycin for differentiation (dCSM14.1 cells). Cells were allowed to differentiate for at least three weeks prior to infection.

Virus and Infection of Cells

Titers of the TE strain of SINV[37] were determined by plaque assay using BHK cells. cAP-7, dAP-7, and dCSM14.1 cells were plated in six well culture dishes, and after forming a monolayer, were infected with SINV TE for one hour in DMEM + 1% FBS at a multiplicity of infection of 1 (cAP-7 and dAP-7 cells) or 5 (cAP-7, dAP-7, and dCSM14.1 cells). dAP-7 cells were treated for one hour with 500U/mL recombinant rat IFN-γ (PBL Interferon Source) in DMEM + 1% FBS at two hours prior to infection (IFN-γ Pre-Txt), two hours post infection (HPI, IFN-γ Txt 2 HPI), or 24 HPI (IFN-γ Txt 24 HPI). dCSM14.1 cells were treated at 24 HPI with 100U/mL recombinant rat IFN-γ in DMEM + 1% FBS for one hour. Supernatant fluids for plaque assays and cell pellets for protein and RNA were collected in triplicate at various time points following infection and stored at -80°C.

Sindbis Virus Infection of Mice

Four to six week-old wild-type C57BL/6 mice, mice deficient in IFN-γ receptor 1 (*Ifngr1*$^{-/-}$, strain B6.129S7-*Ifng*^{tm1Ts}/J), and mice deficient in IFN-γ (*Ifng*$^{-/-}$, strain B6.129S7-*Ifngr1*^{tm1Agt}/J, Jackson Labs) were intracranially inoculated with 10^3 pfu of the nonfatal TE strain of SINV diluted in 20μL PBS or 20μL PBS vehicle while under light isoflurane anesthesia. At sacrifice, mice were euthanized by an overdose of isoflurane anesthesia, and serum, cervical lymph nodes (CLNs), brains, and/or spinal cords were collected. Equal numbers of male and female mice were used in experiments whenever possible. The Johns Hopkins University Institutional Animal Care and Use Committee approved all studies performed.

Clinical Evaluation of Mice

Mice were weighed daily and evaluated for signs of encephalitis, characterized by kyphosis, abnormal gait, and paresis. For feed intake studies, mice were housed in groups of two or three, and total feed weight was recorded daily. The amount of feed consumed per day per mouse was calculated and normalized to that of mock-infected control mice for each strain. Body temperature was measured rectally each day using a Physitemp Thermalert TH-5 with a RET-3 rectal probe. Investigators were blinded to the strain or infection status of mice during these experiments, and evaluations were conducted at the same time of each day.

Quantification of Infectious Virus

Left-brain halves were placed in Lysing Matrix A tubes (MP Biomedicals), and 20% weight/volume (w/v) concentrations were made using ice-cold PBS. Alternatively,

whole spinal cords were placed in Lysing Matrix A tubes, and ice-cold PBS was added to make 10% w/v concentrations. Tissues were dissociated using a FastPrep-24 homogenizer (MP Biomedicals) at 6.0 M/s for 40 seconds and clarified by centrifugation for 15 minutes at 13,2000 rpm at 4°C. Supernatant fluids were collected and stored at -80°C for subsequent analyses. Infectious virus was quantified by plaque assay with homogenates or supernatant fluids from cell culture that were serially diluted 10-fold and incubated for one hour on BHK cells. An agar overlay was then applied, and cells were incubated at 37°C, 5% CO_2 for 48 hours, after which plaques were counted using 10% neutral red in PBS to help with visualization.

Immunoblot Analysis

Collected dAP-7 cells were incubated on ice for 30 minutes in RIPA buffer (50mM Tris, 150mM NaCl, 1% SDS, 1% NP-40, 0.5% Na-deoxycholate, 1mM EDTA) and centrifuged at 12,000 rpm for 15 minutes. Total protein was quantified by DC Protein assay (Bio-Rad) using a BSA standard curve, and ten μg was boiled in 6X SDS loading buffer (0.5M Tris [pH 6.8], 30% glycerol, 10% SDS, 0.12% bromophenol blue, 6% β-mercaptoethanol) for five minutes. Samples were run on a 10% SDS-polyacrylamide gel electrophoresis (PAGE) gel and transferred to a nitrocellulose membrane (Bio-Rad). Immunoblots were blocked in TBS-0.1% Tween-20 (TBST) + 5% milk for one hour at room temperature on a rocker and incubated overnight at 4°C on a rocker with primary antibody diluted in TBST + 5% BSA (1:2,000 rabbit polyclonal anti-nsp3; 1:10,000 rabbit polyclonal NSV anti-sera; 1:10,000 mouse monoclonal anti-β-actin, Millipore)[214,215]. Membranes were incubated with secondary antibody diluted in TBST +

5% milk (1:5,000 horseradish peroxidase (HRP)-conjugated donkey anti-rabbit IgG for nsp3 and poly-NSV, GE Healthcare; 1:5,000 HRP-conjugated sheep anti-mouse IgG for β-actin, GE Healthcare) for one hour at room temperature on a rocker and developed using Amersham ECL Western Blotting Detection Reagent (GE Healthcare) according to manufacturer's instructions.

Gene Expression Measurement by Real-Time PCR

RNA was isolated from dCSM1.1 and AP-7 cells using the Qiagen RNeasy or RNeasy Plus Mini kit following the manufacturer's directions. For mouse CNS tissue, right brain halves or whole spinal cords were homogenized in one mL QIAzol in Lysing Matrix D tubes (MP Biomedicals) at 6.0 M/s for 40 seconds using a FastPrep-24 homogenizer, and the Qiagen RNeasy Lipid Tissue Mini kit was used to isolate RNA. cDNA was synthesized using a High Capacity cDNA Reverse Transcription Kit with random primers (Life Technologies), and quantitative real-time PCR (qRT-PCR) was performed using TaqMan Universal PCR Master Mix (Roche) on a 7500 Fast Real-Time PCR System. SINV RNA copies were measured using TaqMan probe (5'–6-carboxyfluorescein [FAM]-CGCATACAGACTTCCGCCCAGT–6-carboxytetra-methylrhodamine [TAMRA]-3', Applied Biosystems) with primers to the SINV E2 gene (forward, 5'-TGGGACGAAGCGGACGATAA-3'; reverse, 5'-CTGCTCCGCTTTGGTCGTAT-3'). SINV E2 copies were quantified using a standard curve made of ten-fold dilutions of a plasmid containing the SINV subgenomic region genes and normalized to endogenous rodent *Gapdh*. mRNA was measured using commercially-available TaqMan gene expression assays (Applied Biosystems or

Integrated DNA Technologies), and relative quantification was performed by the ΔΔCT method using endogenous rodent *Gapdh* mRNA for normalization.

Microarray

dCSM14.1 cell pellets were submitted to the Johns Hopkins Malaria Research Institute Gene Array Core for microarray analysis using a rat exon library. Microarray data were analyzed with Partek Genomic Suite, version 6.6, using a 1.5 fold-change cutoff, and Ingenuity Pathway Analysis. Genes with putative antiviral function that were significantly upregulated with IFN-γ treatment were selected for further evaluation.

Comparative gene expression in WT B6, *Ifngr1*$^{-/-}$, and *Ifng*$^{-/-}$ mouse brains at 7 DPI was examined using the Mouse Innate & Adaptive Immune Responses RT² Profiler PCR Array (SABiosciences) according to manufacturer's instructions. RNA was pooled from three to four mice per strain. Results were analyzed using the online GeneGlobe Data Analysis Center (Qiagen), and genes with marked up- or down-regulation in *Ifngr1*$^{-/-}$ or *Ifng*$^{-/-}$ mice compared to WT B6 mice were selected for further evaluation.

Protein Quantification by Enzyme-Linked Immunosorbent Assay

Serum leptin was quantified by enzyme-linked immunosorbent assay (ELISA) using a commercial kit (Millipore) according to manufacturer's directions. Data was presented as ng/mL serum with a 0.2 ng/mL limit of detection.

Production of types I and II IFN was quantified by ELISA in 20% w/v brain homogenates. Verikine Mouse Interferon Alpha and Interferon Beta ELISA kits (PBL Interferon Source) were used to measure IFN alpha (IFN-α) and IFN beta (IFN-β),

respectively, and IFN-γ was measured using the mouse IFN gamma ELISA Ready-SET-Go! kit (Ebioscience). Assays were performed according to manufacturer's instructions, and data were presented as pg/g brain tissue with a 125, 156, and 312pg/g limit of detection for IFN- α, IFN- β, and IFN-γ, respectively.

Anti-SINV antibody was measured in serum, brain homogenates, and spinal cord homogenates using an in-house ELISA. Maxisorp 96-well plates (Thermo Scientific Nunc) were coated with 10^6 pfu PEG-purified SINV TE in coating buffer (50mM $NaHCO_3$, pH 9.6) and incubated overnight at 4°C. Plates were blocked in PBS-0.05% Tween-20 + 10% FBS (PBST-10% FBS) for two hours at 37°C and incubated overnight at 4°C with samples diluted in PBST-10% FBS (1:100 for serum, 1:4 for brain homogenates, 1:2 for spinal cord homogenates). Wells were incubated with 1:1000 HRP-conjugated goat anti-mouse IgG2a, IgG2b, or IgG3 or 1:2000 HRP-conjugated goat anti-mouse IgM, IgG, or IgG1 (Southern Biotech) for two hours at room temperature, and plates were developed with a BD OptEIA TMB Substrate Reagent kit using 2M H_2SO_4 as stop solution. Plates were read at 450nm, and optical density (OD) values for mock-infected mice of each strain were subtracted from the OD values of infected mice.

Mononuclear Cell Isolation

Single cell suspensions were made from cervical lymph nodes (CLNs) and brains pooled from three to seven mice per strain per time point. CLNs were dissociated in RPMI + 1% FBS using gentleMACS C tubes and Dissociator (Miltenyi Biotech) and filtered through a 70μm-pore-size cell strainer. After pelleting by centrifugation, red blood cells were lysed using an ammonium chloride solution (Sigma-Aldrich or

Ebioscience). Remaining cells were filtered through another 70μm strainer, pelleted by centrifugation, and resuspended in PBS + 2mM EDTA (PE buffer) for counting. Brains were placed in RPMI media containing 1% FBS, 1 mg/mL collagenase D (Roche), and 0.1 mg/mL DNase I (Roche) and dissociated in C tubes using a gentleMACS Dissociator. Tissues were incubated for 30 minutes at 37°C with periodic agitation, and dissociated cells were filtered through a 70μm-pore-size cell strainer and pelleted by centrifugation. Cell pellets were resuspended in 30% supplemented Percoll [9:1 Percoll (GE Healthcare) : 10X salt solution of 80g NaCl, 3g KCl, 0.73g Na_2HPO_4, 0.2g KH_2PO_4, and 20g glucose in 1L dH_2O] in RPMI media in a 15mL conical tube and underlaid with 70% supplemented Percoll in RPMI media. Tubes were centrifuged at 850 x g at 4°C for 30 minutes with slow braking, and cells were collected from the 30/70% interface. Cells were pelleted by centrifugation and resuspended in PE buffer for counting. Live mononuclear cells were quantified by trypan blue exclusion.

Flow Cytometry

10^6 live cells were placed in the wells of a 96-well round bottom plate. A violet LIVE/DEAD Fixable Dead Cell Stain (Life Technologies) diluted in PE buffer was applied to cells for 30 minutes, followed by a 15-minute incubation with anti-mouse CD16/CD32 (BD Pharmingen) diluted in PE buffer to block Fc receptors. Cells were stained with monoclonal antibodies against CD45 (clone 30-F11), CD3 (clone 17A2), CD4 (clone RM4-5), CD8 (clone 53-6.7), CD19 (clone 1D3), and CD25 (clone PC61.5) from Ebioscience or BD Pharmingen diluted in PBS + 2mM EDTA + 0.5% BSA (FACS Buffer) for 30 minutes on ice. For intracellular staining of Foxp3, cells were fixed for 20

minutes using Fixation/Permeabilization solution from the Ebioscience Foxp3/Transcription Factor Staining Buffer kit. Cells were stained for 30 minutes on ice with a monoclonal antibody against Foxp3 (clone FKJ-16S, BD Pharmingen) diluted in Permeabilization Buffer.

For intracytoplasmic cytokine staining (ICS), 2-3 x 10^6 cells were stimulated for four hours at 37°C with 50 ng/mL of phorbol-12-myristate 13-acetate (PMA, Sigma) and 1 μg/mL ionomycin (Sigma) in the presence of brefeldin A (GolgiPlug, BD Pharmingen) in RPMI + 1% FBS. Following LIVE/DEAD and surface antibody staining (see above), cells were fixed for 20 minutes using Fixation/Permeabilization solution from the BD Cytofix/Cytoperm kit. Cells were stained for 30 minutes on ice with monoclonal antibodies against IFN-γ (clone XMG1.2), IL-4 (clone 11B11), IL-17a (clone eBio17B7), granzyme B (clone NGZB), and TNF-α (clone MP6-XT22) from Ebioscience or BD Pharmingen diluted in BD Perm/Wash buffer.

Cells were resuspended in 200uL FACS Buffer and run on a BD FACSCanto II cytometer using BD FACSDiva software, version 8, and analyses were carried out using FlowJo software, version 8. Cells were characterized as follows: CD4 T cells ($CD45^{hi}$CD3+CD4+), CD8 T cells ($CD45^{hi}$CD3+CD4+), B cells ($CD45^{hi}$CD3-CD19+), Th1 cells (CD3+CD4+IFN-γ+), Th2 cells (CD3+CD4+IL-4+), Th17 cells (CD3+CD4+IL-17a+), and Tregs (CD3+CD4+CD25+Foxp3+). All flow cytometry data are averaged representations of three independent experiments.

Statistics

Statistical analyses were performed using Graphpad Prism 6 software. Time-

course studies were analyzed by two-way ANOVA with Bonferroni's or Tukey's multiple comparison post-test for two group and three group comparisons, respectively. Comparisons between three groups at a single time point were made using one-way ANOVA with Tukey's multiple comparisons post-test. Three outliers were identified in the IFN-γ protein production data by the ROUT method with a Q = 1% and removed from analyses (one data point each for WT B6 at 3 and 7 DPI and for *Ifngr1*$^{-/-}$ at 21 DPI). One outlier was identified at 11 DPI in the *Ifngr1*$^{-/-}$ group of the feed intake study by the same method as above and was removed from analysis. A p value of < 0.05 was considered significant for all analyses.

RESULTS

IFN-γ facilitates virus clearance in neurons *in vitro*

Because neurons are a valuable but finite and minimally renewable cell population, clearance of neurotropic viruses requires a noncytolytic process. Previous studies have shown that clearance of infectious virus is primarily facilitated through a cooperative effort between anti-SINV antibody and the cytokine IFN-γ, though the mechanisms by which this occurs remain to be fully understood[24,70,92]. To better elucidate the role IFN-γ plays in virus clearance, cultured AP-7 cells, which are derived from rat olfactory neurons, were selected for *in vitro* studies. cAP-7 cells, which morphologically resemble epithelial cells and represent immature neurons, and dAP-7 cells, which resemble mature neurons with bipolar morphology and dendrite-like processes[211], were

infected with the TE strain of SINV at a MOI of 5, and culture supernatant fluids were collected for assay of virus titers. Both cell types supported virus replication and production, though cAP-7 cells reached higher peak titers (Fig 4-1A). dAP-7 cells continued to produce virus through 72 HPI and were used for subsequent studies.

To examine the effect IFN-γ has on virus clearance in neurons, dAP-7 cells were infected with SINV TE at a MOI of 1, and cells were treated with 500U/mL rat recombinant IFN-γ at two hours prior to infection, at 2 HPI, or at 24 HPI. Virus readily replicated in all treatment groups, with titers peaking at about 32 HPI (Fig 4-1B). dAP-7 cells treated with IFN-γ prior to infection and at 2 HPI had significantly decreased virus titers relative to untreated cells at 24, 32, and 48 HPI, with the greatest effect seen in pretreated cells ($p < 0.0001$ for untreated vs IFN-γ Pre-Txt at 24, 32, and 48 HPI, $p < 0.05$, $p < 0.01$, and $p < 0.001$ for untreated vs IFN-γ Txt 2 HPI at 24, 32, and 48 HPI, respectively, all Tukey's multiple comparisons test). Treatment with IFN-γ at 24 HPI did not significantly alter virus titers.

Production of different SINV proteins was examined by immunoblot in dAP-7 cells infected with SINV alone or treated with 500U/mL IFN-γ at 2 HPI. In untreated SINV-infected cells, production of the nonstructural nsp3 protein and structural capsid protein reached high levels starting at 24 HPI (Fig 4-1C). Production of the structural glycoproteins E1 and E2 (along with the precursor to E2, pE2) was readily evident by 48 HPI. In contrast, production of SINV proteins in neurons treated with IFN-γ was markedly diminished. These results show that IFN-γ decreases the production of SINV proteins and can facilitate clearance of infectious virus.

Since IFN-γ is capable of clearing infectious virus by inhibiting production of SINV proteins, we next examined whether it could also facilitate clearance of viral RNA. dAP-7 cells infected with SINV TE at a MOI of 1 were treated with 500U/mL IFN-γ at 2 HPI, and cell pellets were collected to quantify viral RNA by qRT-PCR. Viral RNA copies were comparable between treated and untreated cells at 8 HPI, but copy number in untreated cells continued to rise, peaking at 72 HPI (Fig 4-1D). In contrast, SINV RNA levels plateaued in treated cells, and by 72 HPI had begun to decrease, indicating clearance. Overall viral RNA synthesis was significantly inhibited by IFN-γ treatment compared to untreated dAP-7 cells at 24, 32, 48, 56, and 72 HPI ($p < 0.0001$ for all time points, Bonferroni's multiple comparisons test). These studies show that IFN-γ signaling is capable of clearing both infectious virus and viral RNA from neurons *in vitro*.

IFN-γ induces expression of antiviral ISGs *in vitro*

Because IFN-γ is capable of clearing virus from neurons, we next examined what antiviral genes were activated by IFN-γ signaling during SINV infection. dCSM14.1 cells, a differentiated neuronal cell line derived from rat nigral-striatal cells, were infected with SINV TE at a MOI of 5 and treated with 100U/mL IFN-γ at 24 HPI. RNA from mock-infected cells, untreated SINV-infected cells collected at 24 and 27 HPI, and IFN-γ-treated, mock-infected and SINV-infected cells collected at 27 HPI were analyzed on a microarray, and results plotted using Partek Genomics Suite. Cluster analysis showed gene expression profiles were similar among cells treated with IFN-γ, regardless of SINV infection status (Fig 4-2A). Six hundred twenty-five genes were found to have at least a ±1.5 fold-change in gene expression among groups (Appendix A), and five genes with

putative antiviral function that were significantly up-regulated in SINV-infected, IFN-γ treated cells compared to mock-infected cells were selected for further examination (Table 4-1).

mRNA expression of the selected antiviral IFN-stimulated genes (ISGs) were examined by qRT-PCR for cAP-7 and dAP-7 cells that were infected with SINV TE at a MOI of 1 and treated with 500U/mL IFN-γ at 2 HPI. *Gbp2* (Fig 4-2B) and *Irgm* (Fig4-2C), two genes associated with autophagy[216], were highly expressed by SINV-infected dAP-7 cells treated with IFN-γ, as was *Oasl2* (Fig 4-2D), a member of the 2'-5'oligoadenylate/RNaseL system[217], and *Rsad2* (Fig 4-2E), which encodes viperin, a protein that interferes with assembly and release of many viruses[218]. *Zc3hav1* (Fig 4-2F), which encodes ZAP, a protein involved in viral RNA degradation and induction of the innate immune response[219], was less highly upregulated. All of these genes required IFN-γ for induction of any substantial expression, and SINV alone was generally not sufficient to mount a pronounced response. In cAP-7 cells, expression of each of these genes at 24 HPI was higher in mock-infected cells treated with IFN-γ compared to SINV-infected cells treated with IFN-γ. The opposite effect was seen in dAP-7 cells, highlighting the fact that the maturation status of neurons influences their ability to respond to infection and immune mediators.

Impaired IFN-γ signaling affects protein production, but not *Ifng* mRNA expression, in mice during SINV infection

To examine the role IFN-γ plays in the immunopathogenesis and clearance of alphavirus infection, production of IFN-γ in the brain was first examined. Relative to 0

DPI controls, during SINV infection, IFN-γ mRNA expression levels in WT B6 mouse brains increased sharply, peaking at 5 DPI (Fig 4-3A). Expression then slowly decreased but had not returned to baseline levels by 90 DPI. *Ifngr1*$^{-/-}$ mice showed a similar time course, with no significant difference in *Ifng* expression compared to the WT B6 mice ($p = 0.9988$, two-way ANOVA). IFN-γ protein production, as measured by ELISA, also sharply increased following SINV infection, peaking at 7 DPI in WT B6 mice before precipitously dropping to below detectable limits by 10 DPI (Fig 4-3B). In contrast to mRNA expression, production of IFN-γ over time differed between WT B6 and *Ifngr1*$^{-/-}$ mice ($p < 0.01$, two-way ANOVA), with *Ifngr1*$^{-/-}$ mouse brains having significantly higher peak production at 7 DPI ($p < 0.0001$, Bonferroni's multiple comparisons test). IFN-γ production also did not decrease as quickly in *Ifngr1*$^{-/-}$ *mice*, with protein still detectable through 14 DPI. These data suggest that while mRNA expression of IFN-γ does not differ between WT B6 and *Ifngr1*$^{-/-}$ mouse brains during SINV infection, impaired IFN-γ signaling results in a modified post-transcriptional regulation of protein production.

WT B6 mice lose more body weight than *Ifngr1*$^{-/-}$ or *Ifng*$^{-/-}$ mice during SINV infection due to changes in feed intake

After evaluating virus clearance and ISG induction in response to IFN-γ signaling during SINV infection *in vitro*, we sought to better understand the role of IFN-γ in virus immunopathogenesis and control *in vivo* by using mice deficient in either the IFN-γ receptor (*Ifngr1*$^{-/-}$) or IFN-γ itself (*Ifng*$^{-/-}$) and comparing them to mice with intact IFN-γ signaling (WT B6). While mice infected with the virulent NSV strain of SINV develop

progressive ascending paralysis prior to death, WT B6 mice infected with the less virulent TE strain of SINV generally do not progress beyond mild to moderate signs of encephalomyelitis. To assess the clinical disease produced by nonfatal SINV infection in *Ifngr1*$^{-/-}$ and *Ifng*$^{-/-}$ mice, animals were weighed and evaluated for signs of encephalomyelitis (a combination of abnormal posture and gait) daily. *Ifngr1*$^{-/-}$ and *Ifng*$^{-/-}$ mice developed clinical signs earlier than WT B6 mice (Fig 4-4A; median of 3 DPI vs 5 DPI). Almost all mice were showing clinical signs by 6 DPI, but *Ifngr1*$^{-/-}$ mice recovered from clinical disease earlier than *Ifng*$^{-/-}$ or WT B6 mice (median 11 DPI vs 13 DPI vs 14 DPI for *Ifngr1*$^{-/-}$, *Ifng*$^{-/-}$, and WT B6 mice, respectively). In all three strains, approximately 20% redeveloped clinical signs around 18 to 21 DPI.

Significant differences in body weight were seen in the different strains during SINV infection (Fig 4-4B; $p < 0.01$, two-way ANOVA). WT B6 mice lost approximately 13% of their initial body weight, reaching a nadir at 8 DPI, before recovering and surpassing their 0 DPI body weight by 17 DPI. In contrast, *Ifngr1*$^{-/-}$ and *Ifng*$^{-/-}$ mice lost an average of 7% and 1% of their initial body weight, respectively, by 6 DPI before recovering and surpassing their 0 DPI body weight by 11 and 7 DPI, respectively. While the rate of weight gain following recovery was approximately the same among strains, by 28 DPI, *Ifng*$^{-/-}$ mice were significantly heavier than the WT B6 and *Ifngr1*$^{-/-}$ mice that lost more weight ($p < 0.0001$ and $p < 0.01$ vs WT B6 and *Ifngr1*$^{-/-}$, respectively). No difference in body weights was found in mock-infected mice (Fig 4-4C). Prior to infection, WT B6 mice weighed slightly more than *Ifngr1*$^{-/-}$ mice but were not significantly heavier than *Ifng*$^{-/-}$ mice (mean body weight 17.9g, 16.9g, and 17.6g for WT

B6, *Ifngr1*$^{-/-}$, and *Ifng*$^{-/-}$, respectively; $p < 0.05$ for WT B6 vs *Ifngr1*$^{-/-}$, Tukey's multiple comparisons test; data not shown).

To determine the cause of the weight loss in SINV-infected mice, three parameters were measured: body temperature, feed intake, and serum leptin levels. The body temperature of all three strains did not increase or decrease with SINV infection, fluctuating only about 0.5 °C throughout the first 14 DPI (Fig 4-4D). When normalized to mock-infected strain controls at each day and then the amount of food consumed at 0 DPI, all three strains decreased their feed intake during the first week following infection (Fig 4-4E). However, while *Ifngr1*$^{-/-}$ and *Ifng*$^{-/-}$ mice increased the amount of feed they consumed starting at 7 DPI, WT B6 mice continued to show a decrease in daily feed consumption through 8 DPI. These patterns coincided with the times during which mice of each strain lost or regained body weight. To examine whether neurological changes in satiety were responsible for the weight loss, serum leptin was measured by ELISA at three time points following infection: when all three strains were losing weight (5 DPI), when *Ifngr1*$^{-/-}$ and *Ifng*$^{-/-}$, but not WT B6 mice were starting to recover body weight (7 DPI), and when all three strains were starting to recover (10 DPI) (Fig 4-4F). Despite serum being collected at the same time of day (mid-morning), no clear patterns were elucidated. Based on these data, the differences in body weight loss and gain among strains can likely be attributed to differences in the amount of feed consumed following infection.

Impaired IFN-γ signaling results in delayed clearance of infectious virus but earlier initiation of viral RNA clearance

As has been shown previously, clearance of infectious SINV from the CNS is altered in mice with impaired IFN-γ signaling. When examining infectious virus levels in the brains (Fig 4-5A) and spinal cords (Fig 4-5B) of WT B6, *Ifngr1*$^{-/-}$, and *Ifng*$^{-/-}$ mice by plaque assay, titers peaked at 1 to 3 DPI in all three strains, though brains reached 100-fold higher titers than spinal cords. However, while infectious virus titers were below detectable levels in WT B6 spinal cords by 7 DPI, infectious virus could still be detected in *Ifngr1*$^{-/-}$ and *Ifng*$^{-/-}$ mice. In both tissues of all three strains, infectious virus could periodically be detected through 28 DPI, but were only consistently detectable in the brains of *Ifngr1*$^{-/-}$ mice at 21 DPI. These data show that IFN-γ signaling is important in clearance of infectious virus, particularly from the spinal cord.

Because IFN-γ is capable of initiating clearance of viral RNA *in vitro*, its role *in vivo* was examined by quantifying SINV E2 RNA copies in brains and spinal cords of WT B6, *Ifngr1*$^{-/-}$, and *Ifng*$^{-/-}$ mice by qRT- PCR. Viral RNA peaked at 3 to 5 DPI in the brains (Fig 4-5C) and spinal cords (Fig 4-5D) of all three strains at comparable amounts. However, viral RNA levels were significantly lower in the brains of *Ifngr1*$^{-/-}$ and *Ifng*$^{-/-}$ mice compared to WT B6 mice at 7 DPI ($p < 0.001$ for WT B6 vs each strain, Tukey's multiple comparisons) and in the spinal cords of *Ifngr1*$^{-/-}$ and *Ifng*$^{-/-}$ mice compared to WT B6 mice at 5 and 7 DPI ($p < 0.001$ at 5 DPI and $p < 0.05$ at 7 DPI for WT B6 vs *Ifngr1*$^{-/-}$, $p < 0.01$ at 5 DPI and $p < 0.05$ at 7 DPI for WT B6 vs *Ifng*$^{-/-}$, all Tukey's multiple comparisons test). Viral RNA levels were comparable among strains throughout Phase 2 of infection; however, at occasional times during Phase 3, when viral RNA typically has reached a low-level steady state, viral RNA levels increased to those generally seen at Phase 2 time points, especially in *Ifng*$^{-/-}$ mice and in the spinal cord. The

results indicate that while impaired IFN-γ signaling results in delayed infectious virus clearance, it leads to accelerated initiation of viral RNA clearance. Furthermore, IFN-γ appears to prevent reactivation of viral RNA synthesis, and thus potentially infectious virus, during Phase 3 of infection, particularly in the spinal cord.

Ifngr1$^{-/-}$ and *Ifng*$^{-/-}$ mice have diminished induction of ISG expression in the CNS compared to WT B6 mice

As IFN-γ appeared to play a multi-dimensional role in virus clearance *in vivo*, we next examined the effect of impaired IFN-γ signaling on antiviral ISG expression. The five antiviral ISGs previously selected for *in vitro* analysis, *Gbp2*, *Irgm1*, *Oasl2*, *Rsad2*, and *Zc3hav1*, were examined by qPCR in the brains and spinal cords of WT B6, *Ifngr1*$^{-/-}$, and *Ifng*$^{-/-}$ mice infected intracranially with SINV TE. *Oas1a*, which encodes another protein associated with the 2'-5'oligoadenylate/RNaseL system considered to have more activity than *Oasl2* in mice[217], was additionally examined. Expression of each of these genes was considerably upregulated during SINV infection in all strains, regardless of IFN-γ signaling capacity, and returned to baseline levels by Phase 3 of infection. Peak expression levels of *Gbp2* (Fig 4-6A) and *Irgm1* (Fig 4-6B) at 7 DPI in the brain and 5 DPI in the spinal cord were significantly lower in *Ifngr1*$^{-/-}$ and *Ifng*$^{-/-}$ mice compared to WT B6 mice ($p < 0.0001$ for WT B6 vs both strains at both time points in both tissues, all Tukey's multiple comparisons test). Less pronounced, but still significant, differences in peak expression levels were seen with *Oasl2* (Fig 4-6C) and *Oas1a* (Fig 4-6D) at 3 DPI, though increased expression of *Oas1a* in WT B6 spinal cords was considerable ($p < 0.0001$ at 3 DPI for WT B6 vs both strains, Tukey's multiple comparisons test). *Rsad2*

(Fig 4-6E) and *Zc3hav1* (Fig 4-6F) expression both peaked at 7 DPI in the brain and at 3 DPI in the spinal cord, but significantly increased peak expression in WT B6 mice compared to both *Ifngr1*$^{-/-}$ and *Ifng*$^{-/-}$ mice was mostly found in the brains ($p < 0.001$ for *Rsad2* and $p < 0.0001$ for *Zc3hav1* for WT B6 vs *Ifngr1*$^{-/-}$, $p < 0.0001$ for both genes for WT B6 vs *Ifng*$^{-/-}$, all Tukey's multiple comparisons test). These results show that while ISGs are induced during SINV infection in the CNS of mice with impaired IFN-γ signaling, expression is generally diminished compared to that of mice with intact signaling.

Mice with impaired IFN-γ signaling have a modulated cytokine and chemokine immune response during SINV infection

One of the ways IFN-γ influences the immune response to virus infection is through its modulation of leukocyte differentiation and chemotaxis. To determine the role that IFN-γ signaling plays in the brains of SINV-infected mice, production and expression of cytokines and chemokines during the first two weeks following infection were examined. To narrow the numbers of genes examined, a microarray with 84 genes involved in the innate or adaptive immune response was first used to examine 7 DPI brains from SINV-infected mice of each strain (Fig 4-7A). Genes that were markedly up- or downregulated in *Ifngr1*$^{-/-}$ or *Ifng*$^{-/-}$ brains relative to WT B6 brains were selected for further examination by qRT-PCR in individual mice. The complete gene list and relative fold changes for both the brain and spinal cord at 7 DPI may be found in Appendix B.

Type I IFN protein production was examined by ELISA in the brains of WT B6, *Ifngr1*$^{-/-}$, and *Ifng*$^{-/-}$ mice. WT B6 mice produced the most IFN-α during SINV infection,

with levels peaking at 3 DPI (Fig 4-7B). Production was impaired in *Ifngr1*$^{-/-}$ and *Ifng*$^{-/-}$ brains, though IFN-α levels peaked in *Ifng*$^{-/-}$ mice earlier than the other two strains at 1 DPI. Following peak production, IFN-α quickly dropped to below detectable limits. In contrast, after reaching peak levels at 3 DPI, IFN-β production declined more slowly in WT B6 mice, dropping below detectable levels by 10 DPI (Fig 4-7C). IFN-β production was diminished in mice with impaired IFN-γ signaling, with levels only detectable at 5 and 1 DPI in *Ifngr1*$^{-/-}$ and *Ifng*$^{-/-}$ brains, respectively. IFN-γ signaling not only affects the amounts of IFN-α and IFN-β produced in brains during SINV infection but also the time of peak levels that corresponds with peak virus titers.

The immune response is responsible for virus clearance during SINV infection, but can also be neurotoxic, resulting in physiologic damage to neurons and thus clinical disease[54]. To determine how IFN-γ modulates immune response signaling, mRNA expression of several pro-inflammatory cytokines were examined by qRT-PCR and compared to mock-infected controls. A 7 DPI, when WT B6 mice no longer had detectable infectious virus in the brain but were still losing weight, brain mRNA expression of *Tnf* (Fig 4-7D) and *Csf2* (Fig 4-7E) were significantly higher compared to *Ifngr1*$^{-/-}$ and *Ifng*$^{-/-}$ mice ($p < 0.0001$ for WT B6 vs both strains, Tukey's multiple comparisons test). *Il6* mRNA expression (Fig 4-7F) was also significantly higher at 7 DPI in WT B6 mice compared to *Ifngr1*$^{-/-}$ and *Ifng*$^{-/-}$ mice ($p < 0.01$ and $p < 0.0001$ for WT B6 vs *Ifngr1*$^{-/-}$ and *Ifng*$^{-/-}$, respectively, Tukey's multiple comparisons test). While *Il1b* expression was highest in WT B6 mice (Fig 4-7G), mRNA expression was significantly lower in *Ifng*$^{-/-}$ mice at 7 DPI ($p < 0.0001$ and $p < 0.01$ for *Ifng*$^{-/-}$ vs WT B6 and *Ifngr1*$^{-/-}$, respectively, Tukey's multiple comparisons test).

The potential role of IFN-γ signaling for immune cell chemotaxis was examined by measuring mRNA expression for chemokines previously found to be regulated during nonfatal SINV infection in *Ifngr1*$^{-/-}$ and *Ifng*$^{-/-}$ mouse brains. *Ccl1* expression (Fig 4-7H) was significantly upregulated in *Ifng*$^{-/-}$ mice compared to both WT B6 and *Ifngr1*$^{-/-}$ mice at 5, 7, and 10 DPI ($p < 0.05$ at 5 DPI and $p < 0.0001$ at 7 and 10 DPI for *Ifng*$^{-/-}$ vs both WT B6 and *Ifngr1*$^{-/-}$, Tukey's multiple comparisons test). In contrast, WT B6 mice had higher mRNA expression of *Ccl2* (Fig 4-7I; $p < 0.0001$ for WT B6 vs both *Ifngr1*$^{-/-}$ and *Ifng*$^{-/-}$, Tukey's multiple comparisons) and *Ccl5* (Fig 4-7J; $p < 0.01$ and $p < 0.001$ for WT B6 vs *Ifngr1*$^{-/-}$ and *Ifng*$^{-/-}$, respectively, Tukey's multiple comparisons test) at 7 DPI. Alpha chemokine mRNAs *Cxcl9* (Fig 4-7K), *Cxcl10* (Fig 4-7L), and *Cxcl13* (Fig 4-7M) were all significantly upregulated in WT B6 mice at 7 DPI compared to *Ifngr1*$^{-/-}$ and *Ifng*$^{-/-}$ mice ($p < 0.0001$ for WT B6 vs both strains for all chemokines, Tukey's multiple comparison test). These data show that during SINV infection, IFN-γ likely plays an important role in stimulating the chemotaxis of inflammatory cells into the brain.

IFN-γ also influences differentiation of T helper (Th) cell subsets, and four cytokines associated with specific Th profiles, *Il2* (Fig 4-7N) for Th1 cells, *Il4* (Fig 4-7O) for Th2 cells, *Il17a* (Fig 4-7P) for Th17 cells, and *Il10* (Fig 4-7Q) for Tregs, were examined. At 7 DPI, mRNA expression of *Il2* and *Il10* was significantly lower in *Ifng*$^{-/-}$ mice ($p < 0.01$ for *Il2* and $p < 0.001$ for *Il10* for *Ifng*$^{-/-}$ vs both strains, Tukey's multiple comparisons test), and expression of *Il17a* was significantly higher in *Ifngr1*$^{-/-}$ mice ($p < 0.001$ for *Ifngr1*$^{-/-}$ vs both strains, Tukey's multiple comparisons test). *Il4* expression did not significantly differ among strains at 7 DPI. Th differentiation was further examined by measuring expression of transcription factors *Tbx21* (Fig 4-7R) for Th1 cells, *Gata3*

(Fig 4-7S) for Th2 cells, *Rorc* (Fig 4-7T) for Th17 cells, and *Foxp3* (Fig 4-7U) for Tregs. While significant differences were found between strains at various time points, no major trends were identified. These results show that at least at the cytokine level, IFN-γ signaling modulates Th profiles during SINV infection and warrants further examination.

Mice deficient in IFN-γ signaling have impaired expression of genes associated with pathogen recognition

IFN-γ has been reported to affect the ability of cells to sense pathogens[220]. To determine if IFN-γ plays a role in pathogen recognition and detection during SINV infection, mRNA expression of several surface and intracytoplasmic pattern recognition receptors (PRR's) was examined by qRT-PCR. Expression of four endosomal toll-like receptor genes, *Tlr3*, *Tlr7*, *Tlr8*, and *Tlr9*, and the associated adaptor protein *Myd88* were first examined (Fig 4-8A-E). Expression of *Tlr3* (Fig 4-8A), which recognizes dsRNA, and *Tlr9* (Fig 4-8D), which recognizes CpG DNA, were significantly higher in WT B6 mouse brains compared to *Ifngr1*$^{-/-}$ and *Ifng*$^{-/-}$ brains, as was *Myd88* (Figs 4-8A, 4-8D, and 4-8E; $p < 0.01$ and $p < 0.001$ for *Tlr3,* both $p < 0.0001$ for *Tlr9*, and $p < 0.01$ and $p < 0.00001$ for *MyD88* in WT B6 mice vs *Ifngr1*$^{-/-}$ and *Ifng*$^{-/-}$, respectively, all Tukey's multiple comparisons test). Differences in *Tlr7* (Fig 4-8B) and *Tlr8* (Fig 4-8C) expression, which both detect ssRNA, were less pronounced.

Expression of several proteins involved in intracellular pathogen recognition and signaling were next examined (Fig 4-8F-I). Nod-like receptor genes, *Nod1* and *Nlrp3*, which lead to NFkB activation and inflammasome formation, respectively, were both significantly upregulated in WT B6 mice relative to *Ifngr1*$^{-/-}$ and *Ifng*$^{-/-}$ mice at 7 DPI

(Figs 4-8F and 4-8G; $p < 0.0001$ for *Nod1* for WT B6 vs both *Ifngr1*$^{-/-}$ and *Ifng*$^{-/-}$, $p < 0.01$ and $p < 0.0001$ for *Nlrp3* for WT B6 vs *Ifngr1*$^{-/-}$ and *Ifng*$^{-/-}$, respectively, all Tukey's multiple comparisons test). IFN-γ has previously been found to mediate virus clearance through activation of the Jak/STAT signaling pathway, and expression of *Stat1* and *Stat3* were both significantly decreased in *Ifngr1*$^{-/-}$ and *Ifng*$^{-/-}$ mice compared to WT B6 mice at 7 DPI (Figs 4-8H and 4-8I; $p < 0.001$ and $p < 0.0001$ for *Stat1* and $p < 0.001$ and $p < 0.0001$ for *Stat3* in WT B6 mice vs *Ifngr1*$^{-/-}$ and *Ifng*$^{-/-}$, respectively, all Tukey's multiple comparisons test). Based on these data, IFN-γ signaling affects activation of the innate immune response through alteration of PRR gene expression.

IFN-γ signaling affects proliferation and infiltration of immune cells into the brain during SINV infection

Resident T cells secreting IFN-γ and B cells secreting SINV-specific antibody against the E2 glycoprotein in the are important facilitators of virus clearance[24,92]. To see if IFN-γ signaling affects recruitment and infiltration of T and B cells into the brain during SINV infection, quantification of total mononuclear cells by trypan blue exclusion and CD4+ T cells, CD8+ T cells, and CD19+ B cells by flow cytometry in the CLNs and brain during key times of the virus clearance process were performed. In the CLNs, WT B6 mice had significantly more total mononuclear cells than *Ifng*$^{-/-}$ mice at 5 DPI (Fig 4-9A; $p < 0.05$, Tukey's multiple comparisons test), but no significant differences among strains were found at 7 and 10 DPI. In the brain, *Ifngr1*$^{-/-}$ and *Ifng*$^{-/-}$ mice had significantly fewer total infiltrating mononuclear cells at 7 DPI compared to WT B6 mice (Fig 4-9B; $p < 0.01$ for WT B6 vs both strains, Tukey's multiple comparisons test). Neither the

percentage nor absolute number of CD4+ T cells (Fig 4-9C), CD8+ T cells (Fig 4-9E), or CD19+ B cells (Fig 4-9G) were affected by impaired IFN-γ signaling in CLNs, though numbers for each cell population generally decreased overall from 5 DPI to 10 DPI.

In contrast, differences in cell populations among mouse strains were found in the brain. Numbers of infiltrating CD8+ T cells peaked at 7 DPI, while infiltration of CD4+ T cells and B cells occurred later with peaks at 10 DPI. WT B6 mice had significantly more CD4+ T cells than *Ifng*$^{-/-}$ mice at 10 DPI (Fig 4-9D; $p < 0.01$, Tukey's multiple comparisons test). In contrast, both the percentage of live cells and absolute numbers of CD8+ T cells were higher in brains of *Ifngr1*$^{-/-}$ and *Ifng*$^{-/-}$ mice compared to WT B6 mice at 7 DPI (Fig 4-9F; $p < 0.01$ for WT B6 vs *Ifngr1*$^{-/-}$ [percentage only] and *Ifng*$^{-/-}$ [percentage and absolute count], Tukey's multiple comparisons test). This occurred despite WT B6 mice having more overall numbers of mononuclear cells in the brain at this time (Fig 4-9B). The percentage of live cells at 10 DPI and absolute number of B cells at 7 DPI and 10 DPI were significantly increased in WT B6 mice compared to *Ifngr1*$^{-/-}$ and *Ifng*$^{-/-}$ mice (Fig 4-9H; $p < 0.05$ for WT B6 vs both strains, Tukey's multiple comparisons test). Therefore, while the absence of IFN-γ signaling does not affect the proliferation of T and B cells in response to SINV infection, it does affect recruitment of these cells to the site of infection in the brain.

IFN-γ affects CD4+ and CD8+ T cell function in the brain during SINV infection

Because impaired IFN-γ signaling altered the numbers of CD4+ and CD8+ T cells infiltrating the brain during SINV infection, we sought to determine if the effector function of these cells was also affected. CD4+ T cells were further characterized by

measuring production of cytokines associated with different Th subsets in the brains of each strain at 7 DPI. IFN-γ was measured to evaluate Th1 cells, IL-4 for Th2 cells, and IL-17a for Th17 cells. Tregs were characterized as cells expressing both CD25 and producing Foxp3. IFN-γ was not produced by CD4+ T cells in *Ifng*$^{-/-}$ mice, and the percentage of CD4+ T cells producing IFN-γ did not differ between WT B6 and *Ifngr1*$^{-/-}$ mice (Fig 4-10A). The percentage of CD4+ T cells producing IL-4 was significantly lower in *Ifng*$^{-/-}$ mice compared to WT B6 or *Ifngr1*$^{-/-}$ mice (Fig 4-10B; $p < 0.05$ for *Ifng*$^{-/-}$ vs both strains, Dunn's multiple comparisons test). Though not significant, more CD4+ T cells in *Ifngr1*$^{-/-}$ mice produced IL-17a compared to WT B6 and *Ifng*$^{-/-}$ mice (Fig 4-10C), and the percentage of CD4+ T cells expressing both CD25 and Foxp3 was comparable among strains. These results show that IFN-γ signaling does affect CD4+ T cell function at 7 DPI during SINV infection, but impaired signaling does not result in a major change in Th profile.

Function of CD8+ T cells can be evaluated by their production of effector proteins. To examine how IFN-γ signaling affects this process, production of IFN-γ, TNF-α, and granzyme B was examined at 7 DPI in brains of WT B6, *Ifngr1*$^{-/-}$, and *Ifng*$^{-/-}$ mice. As for CD4+ T cells, IFN-γ was not produced by CD8+ T cells in *Ifng*$^{-/-}$ mice, and the percentage of CD8+ T cells producing IFN-γ did not differ between WT B6 and *Ifngr1*$^{-/-}$ mice (Fig 4-11A). The percentage of CD8+ T cells producing TNF-α trended higher in WT B6 mice, though this was not significant (Fig 4-12B). In contrast, CD8+ T cells producing granzyme B were significantly increased in both *Ifngr1*$^{-/-}$ and *Ifng*$^{-/-}$ mice compared to WT B6 mice (Fig 4-12C; $p < 0.01$, Dunn's multiple comparisons test). Furthermore, the mean fluorescence intensity (MFI) of granzyme B produced by CD8+ T

cells was significantly higher in *Ifngr1*$^{-/-}$ mice compared to WT B6 mice (Fig 4-12D; $p < 0.05$, Dunn's multiple comparisons test), indicating that individual CD8+ T cells in the brains of mice with impaired IFN-γ signaling produce more IFN-γ than cells with intact IFN-γ signaling.

Because CD8+ T cell production of granzyme B was significantly increased in *Ifngr1*$^{-/-}$ and *Ifng*$^{-/-}$ mice, we then examined mRNA expression of other granzymes in the brains of the different strains. At 7 DPI, expression of granzyme A (Fig 4-11E) and granzyme B (Fig 4-11F) was significantly lower in *Ifng*$^{-/-}$ mice compared to WT B6 ($p < 0.01$ for granzyme B, Dunn's multiple comparisons test) and *Ifngr1*$^{-/-}$ mice ($p < 0.001$ for both granzyme A and B, Dunn's multiple comparisons test). Expression differences among strains for granzyme K (Fig 4-11G), granzyme M (Fig 4-11H), and perforin (Fig 4-11I) were less pronounced. These results support that IFN-γ may inhibit production of granzyme B by CD8+ T cells in the brain during SINV infection, though this is not seen with granzyme B mRNA expression.

IFN-γ signaling alters the local antibody response during SINV infection

IFN-γ and antibody against the E2 glycoprotein work synergistically to facilitate virus clearance[70]. To determine how IFN-γ signaling influences antibody production, SINV-specific IgM and IgG were measured by ELISA in the sera and brains of WT B6, *Ifngr1*$^{-/-}$, and *Ifng*$^{-/-}$ mice. Serum IgM did not significantly differ over time among strains (Fig 4-12A; $p = 0.7564$, two-way ANOVA), with impaired IFN-γ signaling resulting in less prolonged IgM production in *Ifngr1*$^{-/-}$ and *Ifng*$^{-/-}$ mice and lower levels of SINV-specific IgM at 10 DPI compared to WT B6 mice ($p < 0.05$ for both *Ifngr1*$^{-/-}$ and *Ifng*$^{-/-}$ vs

WT B6, Tukey's multiple comparison test). Serum SINV-specific IgG levels steadily rose through 90 DPI and did not differ among strains (Fig 4-12B; $p = 0.1292$, two-way ANOVA).

In contrast to serum, SINV-specific antibody production in the brain significantly differed among strains over time (Figs 4-12C and 4-12D; $p < 0.0001$ for both IgM and IgG, two way ANOVA). IgM levels were higher in WT B6 brains at 10 and 14 DPI (Fig 4-12C; $p < 0.0001$ for WT B6 vs *Ifngr1*$^{-/-}$ at both time points; $p < 0.001$ and $p < 0.0001$ for WT B6 vs *Ifng*$^{-/-}$ at 10 and 14 DPI, respectively, all Tukey's multiple comparison test). IgG levels steadily increased in the brain of all three strains up to 14 DPI, where levels plateaued in *Ifngr1*$^{-/-}$ and *Ifng*$^{-/-}$ mice (Fig 4-12D). In contrast, IgG in WT B6 brains continued to increase through 21 DPI, where it remained significantly higher than in *Ifngr1*$^{-/-}$ and *Ifng*$^{-/-}$ mice through 90 DPI ($p < .001$, $p < 0.05$, and $p < 0.001$ for 21, 28, and 90 DPI, respectively for WT B6 vs *Ifngr1*$^{-/-}$, $p < 0.001$, $p < 0.001$, and $p < 0.0001$ at 21, 28, and 90 DPI, respectively for WT B6 vs *Ifng*$^{-/-}$, all Tukey's multiple comparison test).

Similar to brains, SINV-specific antibody production in the spinal cord significantly differed among strains over time (Figs 4-12E and 4-12F; $p < 0.01$ for IgM, $p < 0.001$ for IgG, two way ANOVA). IgM levels were higher in WT B6 spinal cords at 10 and 14 DPI (Fig 4-12E; $p < 0.01$ vs *Ifngr1*$^{-/-}$ at both time points; $p < 0.0001$ and $p < 0.001$ vs *Ifng*$^{-/-}$ at 10 and 14 DPI, respectively, all Tukey's multiple comparison test). Also similar to brains, IgG increased through 90 DPI, with *Ifngr1*$^{-/-}$ and *Ifng*$^{-/-}$ mice having significantly lower amounts at 21, 28, and 90 DPI compared to WT B6 mice (Fig 4-12F; $p < .001$, $p < 0.05$, and $p < 0.001$ for 21, 28, and 90 DPI, respectively for WT B6

vs *Ifngr1*$^{-/-}$; $p < 0.001$, $p < 0.001$, and $p < 0.0001$ at 21, 28, and 90 DPI, respectively for WT B6 vs *Ifng*$^{-/-}$, all Tukey's multiple comparisons test). As these data show, IFN-γ signaling did not affect the antibody response in the periphery but did affect production of SINV-specific IgM and IgG at the site of infection.

In mice, there are four IgG subclasses: IgG1, IgG2a, IgG2b, and IgG3[221-223]. Because overall production of IgG in the brain is affected by impaired IFN-γ signaling, we next examined whether only certain subclasses were affected by measuring SINV-specific levels in the brains of WT B6, *Ifngr1*$^{-/-}$, and *Ifng*$^{-/-}$ mice. IgG1 levels did not significantly differ between strains (Fig 4-13A; $p = 0.7824$, two-way ANOVA). IgG2a levels, in contrast, significantly differed among strains over time (Fig 4-13B; $p < 0.0001$, two-way ANOVA) and followed a similar pattern to overall IgG, with production continuing to increase in WT B6 mice while plateauing in *Ifngr1*$^{-/-}$ and *Ifng*$^{-/-}$ mice ($p < 0.05$ for WT B6 vs *Ifngr1*$^{-/-}$ and $p < 0.05$ for WT B6 vs *Ifng*$^{-/-}$ at 10 DPI, $p < 0.0001$ for WT B6 vs both strains at 14, 21, 28, and 90 DPI, all Tukey's multiple comparisons test). IgG2b levels also significantly differed among strains over time (Fig 4-13C; $p < 0.01$, two-way ANOVA). WT B6 mice had increased IgG2b production compared to knockout strains, with significantly higher levels at 14 DPI ($p < 0.01$ for WT B6 vs *Ifngr1*$^{-/-}$ and $p < 0.01$ for WT B6 vs *Ifng*$^{-/-}$, Tukey's multiple comparisons test). SINV infection did not stimulate production of IgG3 in the brains of any strains except for a transient mild increase at 14 DPI in WT B6 mice (Fig 4-13D; $p < 0.05$ for WT B6 vs *Ifngr1*$^{-/-}$ and $p < 0.001$ for WT B6 vs *Ifng*$^{-/-}$, all Tukey's multiple comparison tests) and did not significantly differ among strains overall ($p = 0.0556$, two-way ANOVA). Therefore,

these data show that impaired IFN-γ signaling during SINV infection did not affect production of IgG1 but did decrease production of both IgG2a and IgG2b.

DISCUSSION

IFN-γ affected multiple aspects of disease and the local CNS immune response to SINV infection. Mice with impaired IFN-γ signaling lost less weight and had an altered course of clinical disease compared to WT B6 mice. *In vitro*, multiple antiviral genes were upregulated in SINV-infected neurons by IFN-γ treatment, likely contributing to virus clearance. *In vivo*, these genes were induced at lower levels in the absence of IFN-γ signaling. IFN-γ also had multiple immunomodulatory effects, such as altered cytokine and chemokine signaling in the brain. *Ifngr1*$^{-/-}$ and *Ifng*$^{-/-}$ mice had fewer brain infiltrating CD4+ T cells and B cells producing SINV-specific antibody but more CD8+ T cells producing granzyme B compared to WT B6 mice. Finally, though IFN-γ was capable of clearing viral RNA from neurons *in vitro*, viral RNA clearance from the brain and spinal cord was initiated later in WT B6 mice compared to *Ifngr1*$^{-/-}$ and *Ifng*$^{-/-}$ mice. These findings highlight the multifaceted effects IFN-γ exerts during virus infection.

IFN-γ primarily exerts its antiviral effects through antiviral gene expression upregulation via its signaling pathway. Using microarray, we identified several different genes upregulated by IFN-γ treatment during SINV infection. *Gbp2* and *Irgm1*, genes encoding proteins associated with autophagy, were the most highly induced by IFN-γ signaling in SINV-infected mouse brains and spinal cords. Autophagy is an autonomous

process by which cells can destroy virus or viral replication components present in the cytosol or deliver them to TLR-associated endosomes for induction of the innate immune response, particularly Type I IFNs[224-227]. IRGM associates with four proteins that contribute to autophagy and interacts with mitochondria via cardiolipin, suggesting that it mediates autophagosome biogenesis from the mitochondrial membrane[228,229]. Several RNA viruses target IRGM to inhibit autophagosome maturation or induce autophagosome formation to promote virus replication, including measles virus, CHIK, Japanese encephalitis virus (JEV), HIV, and HCV[229-235]. The localization of GBP2, a guanylate binding protein member of the dynamin protein superfamily implicated in vacuolar processing, to autophagosomes is influenced by IRGM [216,236]. GBP2 inhibits replication of VSV and EMCV *in vitro* and also combats other pathogens, such as protozoa and bacteria[237-241].

Another antiviral protein system that is highly induced by IFN-γ signaling during SINV infection was the 2'-5'-oligoadenylate synthetase (OAS) family. *Oasl2* was identified as a gene of interest by microarray analysis of rat neuronal cells, and *Oas1a* was additionally examined in mouse CNS tissue, as it is considered to have more OAS activity[217]. When bound by dsRNA, 2'-5' OAS proteins catalyze the production of short 2'-5' oligoadenylates (2-5'A) from ATP, which in turn activate latent RNase L, an endonuclease that degrades both cellular and viral ssRNAs[106,242]. Mechanisms by which RNase L can restrict virus propagation include viral genome and mRNA degradation, rRNA degradation (which restricts viral mRNA translation), and amplification of type I IFN signaling[243]. Several neurotropic viruses, including rabies virus and JEV induce this pathway[244]. Similar to autophagy, the 2'-5' OAS/RNase L system is commonly targeted

by viruses via mechanisms such as dsRNA sequestration, 2-5'A degradation, production of inactive or inhibitory 2-5'A, competitive inhibition or binding of RNase L, and genetic avoidance of RNase L cleavage[243].

Two other antiviral genes usually more robustly induced by type I, rather than type II, IFNs, *Rsad2* and *Zc3hav1*, were also examined. *Rsad2* encodes viperin, a protein that associates with the cytosolic face of the endoplasmic reticulum (ER) and with lipid droplets[245,246]. Viperin disrupts lipid rafts and increases plasma membrane fluidity, leading to impaired budding of enveloped viruses such as influenza A and HIV-1[247-249]. It also associates with flavivirus and alphavirus proteins on lipid droplets and the ER, respectively, inhibiting virus replication and assembly[250-253]. Type I IFN production by dendritic cells is also influenced by viperin through modulation of TLR7 and TLR9 signaling[254]. Unsurprisingly, certain viruses utilize viperin to their advantage by disrupting the cytoskeleton to increase virus infectivity or degrading it to circumvent its antiviral effects[255,256]. *Zc3hav1* encodes ZAP, also know as PARP13, a RNA binding protein that modulates the cellular response to stress[257]. ZAP decreases production of several different viruses by recruiting RNA decay factors to degrade viral RNA and inhibiting viral RNA translation[107,258-261]. It also represses the miRNA pathway, leading to upregulation of antiviral transcripts and induction of the antiviral state[262]. Induction of all of these genes during SINV infection highlights the multi-faceted approach by which IFN-γ may mediate virus clearance.

Microarray analysis of brains of SINV-infected WT B6, *Ifngr1*$^{-/-}$, and *Ifng*$^{-/-}$ mice revealed that expression of multiple genes involved in the innate and adaptive immune response were affected by IFN-γ signaling. Compared to WT B6 mice, expression of *Tlr3*

and *Tlr9*, as well as the TLR-associated adaptor protein *Myd88,* were all decreased in mice with impaired IFN-γ signaling. TLR3, which recognizes dsRNA, and TLR9, which recognizes CpG motifs, are expressed intracellularly within endosomes, lysosomes, and multivesicular bodies[263]. Expression of certain intracellular PRR genes, including *Nod1* and the inflammasome-associated *Nlrp3*, were also decreased in mice with IFN-γ-impaired signaling. Signaling through these proteins leads to transcriptional activation of both innate and adaptive immune responses[264]. Innate response effectors include type I IFN's, proinflammatory cytokines, complement, and phagocytosis. Adaptive immune response effectors include T cell activation through induction of dendritic cell maturation and cytokine production, such as IFN-γ.

IFN-γ affects production of the type I IFNs, IFN-α and IFN-β. Local production of type I IFN's is important for the initial control of virus replication, and mice deficient in type I IFN signaling are highly susceptible to many neurotropic viruses[69-72,265]. IFN-α and IFN-β production were decreased in the brains of *Ifngr1*$^{-/-}$ and *Ifng*$^{-/-}$ mice compared to WT B6 mice at 5 and 3 DPI, respectively. Interestingly, both IFN-α and IFN-β levels were significantly higher in the brains of *Ifng*$^{-/-}$ mice at 1 DPI compared to WT B6 and *Ifngr1*$^{-/-}$ mice. Expression of *Stat1* and some of the antiviral ISGs examined were also significantly upregulated in *Ifng*$^{-/-}$ mice at 1 DPI. This might have been driven by higher levels of both infectious virus and viral RNA in the brain and viral RNA in the spinal cord at 1 DPI in these mice. This suggests that IFN-γ plays a role early in infection, even before T cells are able to infiltrate the site of infection. These differences in virus replication and immune gene expression, as well as clinical disease, seen between *Ifng*$^{-/-}$ and *Ifngr1*$^{-/-}$ mice serve as a reminder that the two strains should not be considered

equivalent, and suggest that some IFN-γ signaling still occurs in *Ifngr1*$^{-/-}$ mice, either through the mutated receptor or another mechanism[266-269].

Most of the pathological changes seen with alphavirus encephalomyelitis are associated with the inflammatory effects of infiltrating immune cells, rather than direct virus-induced cell death[39,41,49,55,56,270]. IFN-γ signaling significantly affected expression of several proinflammatory cytokines, including *Tnf*, *Csf2*, *Il1b*, and *Il6*. These genes can be expressed by both infiltrating leukocytes and activated resident microglia to contribute to immune cell recruitment and CNS pathological changes[86]. Upregulation of these genes, particularly *Tnf*, can have a profound effect on clinical disease and provides a possible explanation for the decreased appetites leading to weight loss seen in WT B6 mice compared to *Ifngr1*$^{-/-}$ and *Ifng*$^{-/-}$ mice[271,272]. Future studies microscopically examining brains affected by nonfatal alphavirus encephalomyelitis in the absence of IFN-γ signaling are warranted to better understand this mechanism.

Expression of several chemokines was up-regulated in the brains of WT B6 mice more than in *Ifngr1*$^{-/-}$ and *Ifng*$^{-/-}$ mice, including *Ccl2*, *Ccl5* (RANTES), *Cxcl9*, *Cxcl10*, and *Cxcl13*. CCL-2, RANTES, CXCL9, and CXCL10 all play important roles in microglial activation and leukocyte migration in the CNS during flavivirus, alphavirus, and coronavirus infection and during experimental autoimmune encephalomyelitis[41,91,269,273-278]. CXCL9 and CXCL10 in particular are important for chemotaxis of B cells into the brain during SINV infection, and CXCL13 is important in non-lymphoid tissue formation of B cell follicles for local antibody production[91]. Interestingly, *Ifng*$^{-/-}$ mice have much higher expression of *Ccl1* than WT B6 or *Ifngr1*$^{-/-}$ mice during the first 10 DPI. CCL1, also known as I-309, is an important chemoattractant

of monocytes, natural killer (NK) cells, and regulatory T cells and is generally associated with a Th2 response[279-281]. Upregulation of *Ccl1* has been associated with T cell growth transformation during herpesvirus infection and eosinophil migration into the CNS during bornavirus infection[99,282].

Previous studies have shown that IFN-γ facilitates clearance of infectious virus from neurons during SINV infection[93]. In this study, we found that IFN-γ is capable of clearing both infectious virus and viral RNA in neurons *in vitro*. In examining mice deficient in IFN-γ or IFN-γ receptor, infectious virus was cleared more quickly from the spinal cords of mice with intact IFN-γ signaling. Surprisingly however, clearance of viral RNA was initiated earlier in the brains and spinal cords of *Ifng*$^{-/-}$ and *Ifngr1*$^{-/-}$ mice compared to WT B6 mice. This indicates that while IFN-γ is capable of clearing viral RNA from neurons, alternative effects produced by IFN-γ, likely via immunomodulation, influence viral RNA clearance from the CNS.

During SINV TE infection, CD8+ T cells are the first lymphocyte population to infiltrate the brain[42]. Peak numbers of infiltrating mononuclear cells are reached at 7 DPI in the brain, with CD8+ T cells the predominant population. Following decline in CD8+ T cell numbers, increased numbers of CD4+ T cells and B cells enter the brain. At 7 and/or 10 DPI, fewer CD4+ T cells and CD19+ B cells infiltrated the brain in *Ifngr1*$^{-/-}$ and *Ifng*$^{-/-}$ mice compared to WT B6 mice. Interestingly, at 7 DPI, significantly more CD8+ T cells were present in the brains of mice with impaired IFN-γ signaling compared to mice with intact IFN-γ signaling. This occurred despite WT B6 mice having overall higher numbers of mononuclear cells in the brain at this time. As the effector functions of each of these lymphocyte cell populations can influence both the neuronal damage

inflicted during infection and the clearance and control of the virus, further examination of how these cells functioned in response to IFN-γ signaling was warranted.

CD4+ T cells primarily exert their effects via cytokine secretion, which differentiates the cells into Th subsets and influences the actions of other immune cells, such as activation of CD8+ T cells and antibody class switching in B cells[283]. To understand how IFN-γ influenced the functionality of the CD4+ T cells, we assessed the cytokine profiles of CD4+ T cells at 7 DPI in mice with intact and deficient IFN-γ signaling by flow cytometry and qRT-PCR for mRNA expression. As IFN-γ is the signature cytokine secreted by Th1 cells, these cells could not be defined in *Ifng*$^{-/-}$ mice, and expression of *Il2*, another cytokine associated with Th1 cells, was significantly lower in *Ifng-/-* mice. Despite this, *Ifng*$^{-/-}$ mice did not compensate by skewing to a different Th profile. In fact, IL-4 production, which is used to define Th2 cells, was significantly lower in *Ifng*$^{-/-}$ mice, despite increased *Ccl1* expression, which is associated with a Th2 response. Treg cells, defined by expression of both Foxp3 and CD25, also trended to be lower in *Ifng*$^{-/-}$ mouse brains, and mRNA expression of the regulatory cytokine IL-10 was significantly lower compared to WT B6 and *Ifngr1*$^{-/-}$ mice at 7 DPI. This could be important, as IL-10 promotes the recruitment, proliferation, and cytotoxic activity of CD8+ T cells and promotes antibody class switching in B cells[284-288]. *Ifngr1*$^{-/-}$ mice had significantly increased *Il17a* mRNA expression and trended towards increased IL-17a production in CD4+ T cells compared to WT B6 and *Ifng-/-* mice. Similar results were seen in *Ifngr1*$^{-/-}$ mice infected with NSV and suggest Th17 cells are preferentially expanded[269]. Il-17 has been associated with fatal encephalomyelitis and virus persistence during infection with several viruses, such as SINV NSV, TMEV, JHMV, and HSV-1,

especially in the absence of IFN-γ[56,289-292]. These results show that IFN-γ signaling does affect CD4+ function, through dramatic Th profile skewing is not seen, and reiterates the differences between mice lacking IFN-γ production and mice with impaired receptor function and thus signaling, in the immune response to SINV infection.

CD8+ T cells, frequently known as cytotoxic lymphocytes (CTLs), primarily exert their effector function against virus infections though cytotoxic activity. They secrete proinflammatory cytokines with antiviral activity, such as IFN-γ and TNF-α, and produce granzyme B and perforin[293]. Classically, granzyme B and perforin are known for their contributions to cytolytic activity upon delivery into a target cell via the granule exocytosis pathway, where apoptosis is induced by activation of caspases[294-296]. By specifically targeting infected cells by this mechanism, the immune response can provide a more focused and direct response to virus infection beyond what IFN's can provide. However, this process is classically achieved through direct contact between CTLs and an infected cell expressing MHC Class I molecules. Neurons have at best limited capacity for MHC Class I expression, and induction of apoptosis by CTLs results in loss of valuable cells with limited regenerative capacity[297-301]. Despite this, CD8+ T cells have been shown to form T cell extended processes and directly engage with TMEV-infected neurons, indicating the CD8+ T cells can interact with neurons[83]. Granzymes have long been considered to be exclusively cytotoxic, but recently non-cytotoxic roles of granzymes have become recognized. Though the suggestion of granzymes performing non-apoptotic roles was first made almost 30 years ago, the proinflammatory capacity of granzymes has only been confirmed within the last ten years[302-305]. Mouse granzyme K induces macrophages to release IL-1β and has been suggested to play a pro-

inflammatory, non-cytotoxic role during LCMV infection[306]. Clearance of both WNV and LCMV from neurons is dependent on the granzyme/perforin pathway[307,308].

We found that mice deficient in IFN-γ signaling had more CD8+ T cells producing granzyme B in the brain during peak infiltration time than WT B6 mice. During SINV NSV infection, increased perforin production is also seen in the brains of *Ifngr1*$^{-/-}$ and *Ifng*$^{-/-}$ mice[269]. In contrast, absence of IFN-γ correlates with decreased MHC Class I expression by resident microglia and impaired perforin-mediated effector function during JHMV infection, and IFN-γ has been shown to promote granzyme B production during experimental coronavirus retinopathy[309,310]. Therefore, the effect of IFN-γ on the granule exocytosis pathway during CNS infection appears to be virus-specific, and the mechanisms by which IFN-γ influences granzyme B production during SINV infection remain to be understood.

Recently, granzyme substrates with direct antiviral activity, either viral proteins or host cell proteins essential for virus replication, have been identified. Granzymes A, H, and M have each been shown to cleave viral proteins important in virus replication for Moloney mouse leukemia virus, adenovirus, and HCMV, respectively[311-313]. CD8+ T cells can also recognize neurons latently infected with HSV-1 and inhibit reactivation via a non-cytolytic mechanism[314-316]. Granzymes B and H both cleave the RNA-binding protein La, which is important in viral RNA metabolism for several viruses, including HCV, HBV, and JEV[317-319]. The RNA-binding protein hnRNP K, which modulates viral RNA replication of CHIKV, enterovirus 71, dengue virus, and HIV-1, is a substrate for granzyme B cleavage[320-323]. hnRNP K interacts with SINV nsp2 and subgenomic mRNA, and silencing of hnRNP K leads to decreased SINV RNA replication *in vitro*[324,325]. Based

on these studies, we postulate that the increased granzyme B produced by *Ifngr1*$^{-/-}$ and *Ifng*$^{-/-}$ CD8+ T cells cleaves cellular proteins important for SINV RNA replication and stability to explain the accelerated viral RNA clearance seen in the brain and spinal cord of these mice. Further studies regarding viral RNA clearance, as well as non-cytotoxic roles of granzymes during SINV infection, are warranted.

Previous mouse studies have shown that clearance of infectious SINV is accomplished cooperatively between anti-SINV antibody and IFN-γ, but the mechanisms by which this occurs are not well understood. Production of SINV-specific IgM and IgG in the sera did not significantly differ among WT B6, *Ifngr1*$^{-/-}$, and *Ifng*$^{-/-}$ mice[70]. Here, while we confirmed that IFN-γ signaling does not affect anti-SINV IgM and IgG levels in the serum, both IgM and IgG in the brain and spinal cord were decreased in *Ifngr1*$^{-/-}$ and *Ifng*$^{-/-}$ mice compared to WT B6 mice. Because the number of B cells present in the CLNs did not differ among strains but were significantly lower in the brains of mice with impaired IFN-γ signaling, these findings are likely due to differences in local B cell production of anti-SINV antibody during infection. Expression of chemokine mRNAs *Cxcl9*, *Cxcl10*, and *Cxcl13*, which are all important for inducing migration and promoting survival of antibody-secreting cells (ASCs) during SINV infection[91], were reduced in *Ifngr1*$^{-/-}$ and *Ifng*$^{-/-}$ mouse brains compared to WT B6 mice. Therefore, IFN-γ-induced expression of B cell-associated chemokines affects migration and maintenance of ASCs in the CNS and thus local production of antibody. The promotion of local antibody production provides a mechanism by which IFN-γ may clear infectious SINV from the CNS.

As previously reported, absence of IFN-γ signaling did not affect levels of IgG subclass-specific SINV antibody in the sera of SINV-infected mice[70]. However, the current studies showed that production of IgG2a and IgG2b, but not IgG1, were decreased in the brains of *Ifngr1*$^{-/-}$ and *Ifng*$^{-/-}$ mice compared to WT B6 mice. Our results are consistent with previous observations that Th1 cells producing IFN-γ induce IgG subclass switching towards IgG2a, while Th2 cells producing IL-4 and IL-13 promote subclass switching towards IgG1 and away from IgG2a[326,327]. This also suggests that IgG subclasses IgG2a and IgG2b specifically play a role in antibody-mediated clearance of SINV.

In conclusion, IFN-γ signaling mediates clearance of both infectious SINV and viral RNA from neurons. However, beyond induction of antiviral ISGs, clearance of SINV is also influenced by IFN-γ through modulation of the immune response. During SINV infection in the CNS, IFN-γ promotes local B cell production of anti-SINV IgM and IgG and inhibits infiltration of granzyme B-producing CD8+ T cells. Understanding the non-cytolytic functions of granzyme B/perforin during SINV infection could help better understand the mechanisms by which virus, specifically viral RNA, are cleared from the CNS.

FIGURES

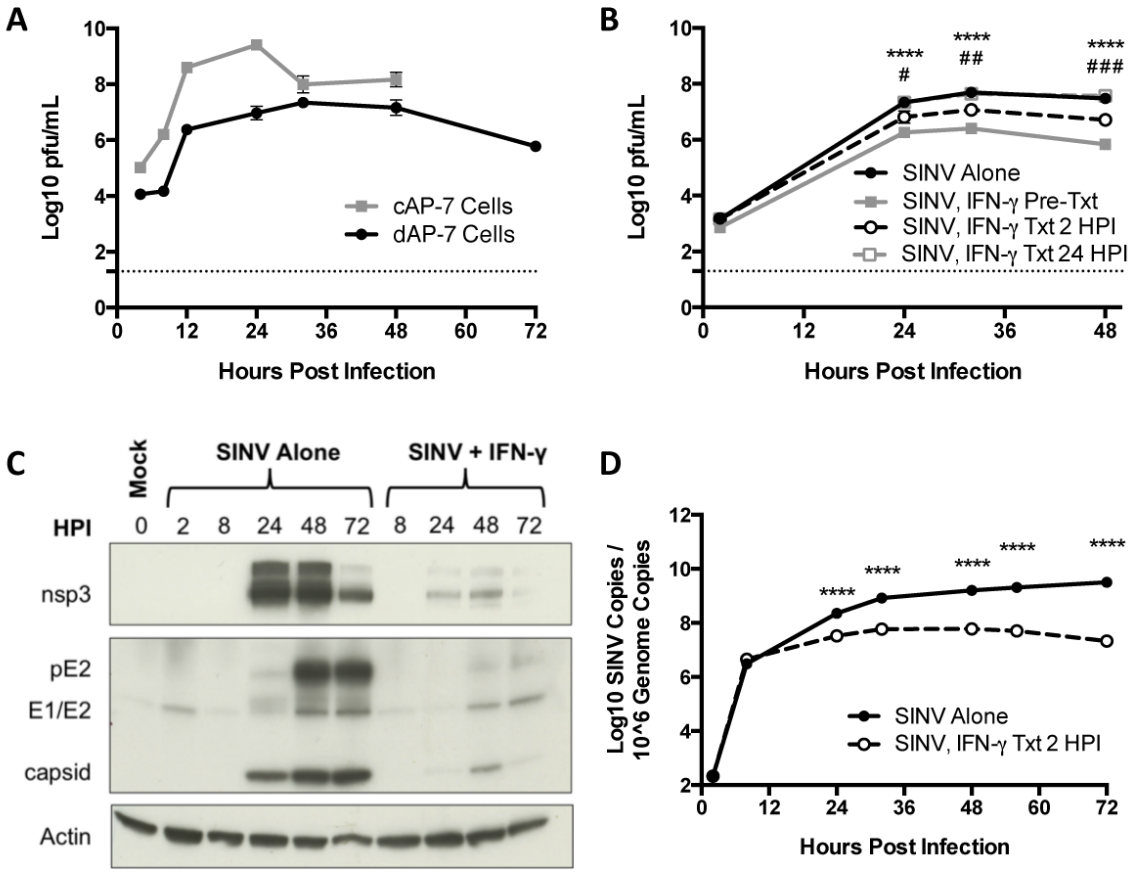

Figure 4-1. Effect of IFN-γ treatment on virus clearance *in vitro*. (**A,B**) Infectious virus titers were measured by plaque assay for cAP-7 (gray line) and dAP-7 (black line) cells (**A**) infected at a MOI of 5, and for dAP-7 cells (**B**) infected with SINV at a MOI of 1 and treated with 500U/mL IFN-γ 2 hours prior to infection (gray square and solid line; SINV, IFN-γ Pre-Txt), at 2 HPI (white circle and black dashed line; SINV, IFN-γ Txt 2 HPI), at 24 HPI (white square and gray dashed line; SINV, INF-γ Txt 24 HPI) or untreated (black circle and solid line; SINV Alone) (n = 3 replicates per cell line per treatment group; data presented as the mean ± SEM; dashed line indicates level of

detection; ****$p < 0.0001$, SINV Alone vs SINV, IFN-γ Pre-Txt; $^{\#}p < 0.05$, $^{\#\#}p < 0.01$, $^{\#\#\#}p < 0.001$, SINV Alone vs SINV, IFN-γ Txt 2 HPI by Tukey's multiple comparisons test). (**C,D**) dAP-7 cells were infected with SINV at a MOI of 1 and were either left untreated or treated with 500U/mL IFN-γ at 2 HPI. (**C**) Nonstructural (nsp3) and structural (pE2, E1/E2, capsid) SINV protein production was evaluated by western blot using beta actin as control. (**D**) Viral RNA levels were evaluated by qPCR in untreated (black circle and solid line) and IFN-γ-treated (white circle and black dashed line) dAP-7 cells (n = 3 replicates per treatment group; data presented as the mean ± SEM; ****$p <$ 0.0001, by Bonferroni's multiple comparisons test).

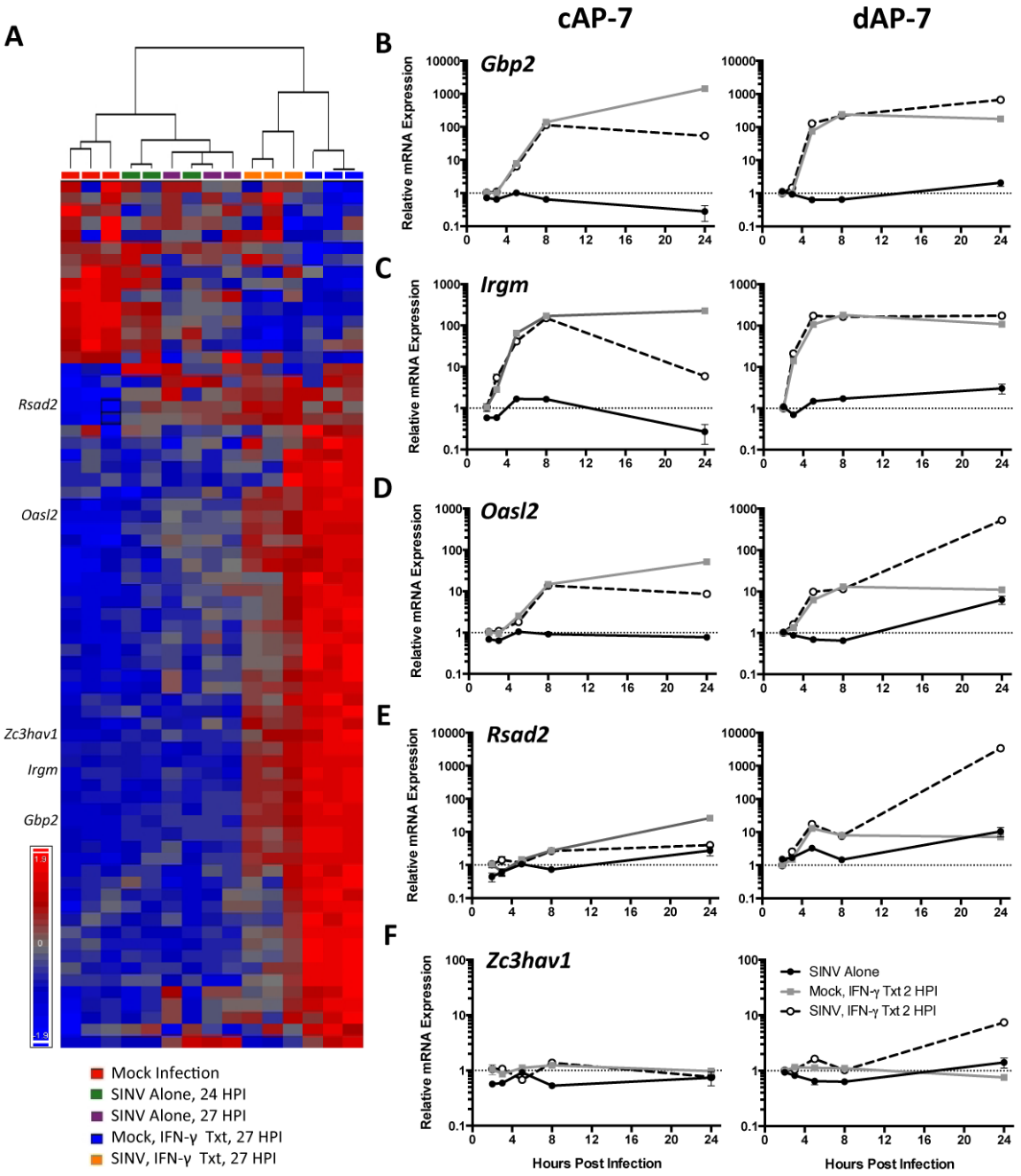

Figure 4-2. Effect of IFN-γ treatment on ISG expression during SINV infection *in vitro*. (**A**) A cluster analysis was performed and a heat map was constructed to display microarray results examining relative gene expression for dCSM14.1 cells that were mock-infected (red), SINV-infected but untreated and collected at 24 HPI (green) or 27 HPI (purple), and mock-infected (blue) or SINV-infected (orange) and treated at 24 HPI

with 100U/mL IFN-γ and collected at 27 HPI. Red represents a positive relative fold-change in gene expression, and blue represents a negative relative fold-change in gene expression. The positions of the five genes with putative antiviral activity are denoted to the left of the heat map. (**B-F**) ISGs selected for further examination by qRT-PCR in cAP-7 (left graphs) and dAP-7 cells (right graphs) infected with SINV at a MOI of 1 and left untreated (black circle and solid line), mock-infected and treated with 500U/mL IFN-γ at 2 HPI (gray square and solid line), or SINV-infected with a MOI of 1 and treated with 500U/mL IFN-γ at 2 HPI (white circle and black dashed line) included *Gbp2* (**B**), *Irgm* (**C**), *Oasl2* (**D**), *Rsad2* (**E**), and *Zc3hav1* (**F**) (n = 3 replicates per group; data represented as mean ± SEM; dashed line indicates gene expression of untreated, mock-infected cells to which other groups were normalized).

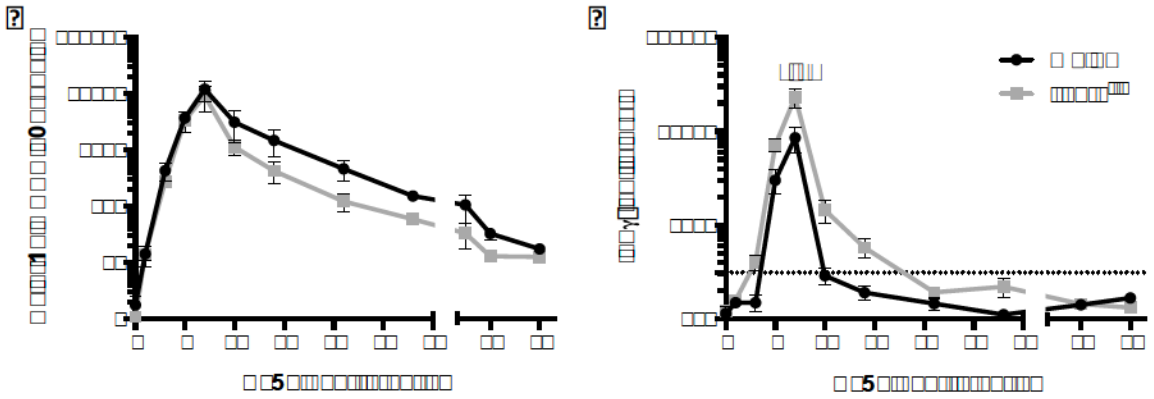

Figure 4-3. *Ifng* mRNA expression and IFN-γ protein production in mice with intact and impaired IFN-γ signaling. (**A**) *Ifng* mRNA expression was determined by qRT-PCR in SINV-infected WT B6 (black circle and line) and *Ifngr1*$^{-/-}$ (gray square and line) mouse brains normalized to mock-infected controls for each strain. (**B**) IFN-γ protein production was measured by ELISA in SINV-infected WT B6 (black circle and line) and *Ifngr1*$^{-/-}$ (gray square and line) mouse brains (n = 3-11 mice per strain per time point; data presented as the mean ± SEM; dotted line represents the limit of detection for the assay; ****$p < 0.0001$ by Bonferroni's multiple comparisons test).

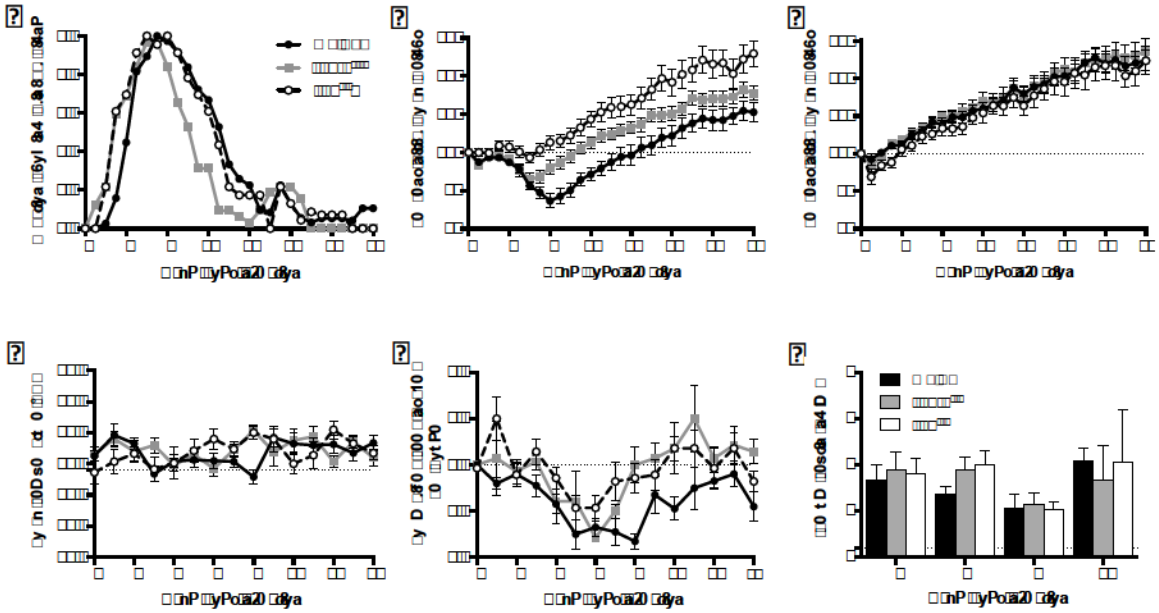

Figure 4-4. Clinical disease in SINV-infected WT B6, *Ifngr1*$^{-/-}$, and *Ifng*$^{-/-}$ mice. (**A**) SINV-infected WT B6 (black circle and solid line), *Ifngr1*$^{-/-}$ (gray square and solid line), and *Ifng*$^{-/-}$ (white circle and black dashed line) mice were evaluated daily for the presence of clinical disease (n = 23-38 mice per strain combined from three to five independent experiments) (**B,C**) Body weights of SINV-infected (**B**) and mock-infected (**C**) mice were measured daily and normalized to the body weight at 0 DPI (n = 13-38 mice per strain combined from three to five independent experiments; dashed line indicates initial body weight). (**D**) Body temperature was measured rectally daily (n = 8 mice per strain; dashed line indicates reported normal rectal temperature for mice). (**E**) Daily feed consumption was measured for 2-3 mice housed per cage, with feed intake of SINV-infected mice normalized first to that of mock-infected mice for each strain for each day and then to the feed intake at 0 DPI for that cage (n = 7-10 cages per strain combined from two independent experiments; dashed line indicates baseline feed intake). (**F**) Serum

leptin levels were measured by ELISA at 0, 5, 7, and 10 DPI in SINV-infected WT B6 (black bars), *Ifngr1*$^{-/-}$ (gray bars), and *Ifng*$^{-/-}$ (white bars) mice (n = 4-11 mice per strain per time point; data presented as the mean ± SEM; dashed line indicates limit of detection).

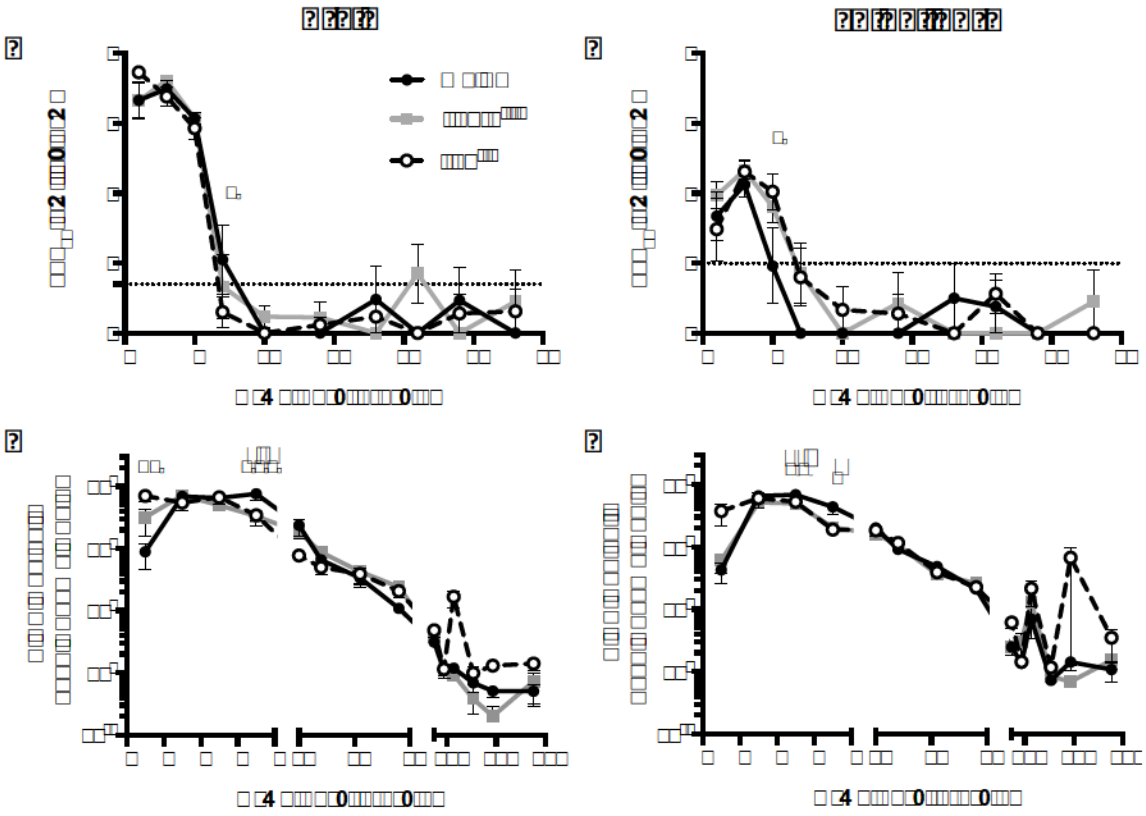

Figure 4-5. Infectious virus and viral RNA clearance in mice with impaired IFN-γ signaling. Infectious virus titers (**A, B**) were examined by plaque assay, and viral RNA levels (**C, D**) were examined by qRT-PCR in brains (**A, C**) and spinal cords (**B, D**) of WT B6 (black circle and solid line), *Ifngr1*$^{-/-}$ (gray square and solid line), and *Ifng*$^{-/-}$ (white circle and black dashed line) mice (n = 3-8 mice per strain per time point; data presented as the mean ± SEM; dashed line indicates limit of detection for the plaque assay; *$p < 0.05$, ***$p < 0.001$, WT B6 vs *Ifngr1*$^{-/-}$; $^{\#}p < 0.05$, $^{\#\#}p < 0.01$, $^{\#\#\#}p < 0.001$, WT B6 vs *Ifng*$^{-/-}$, all by Tukey's multiple comparisons test).

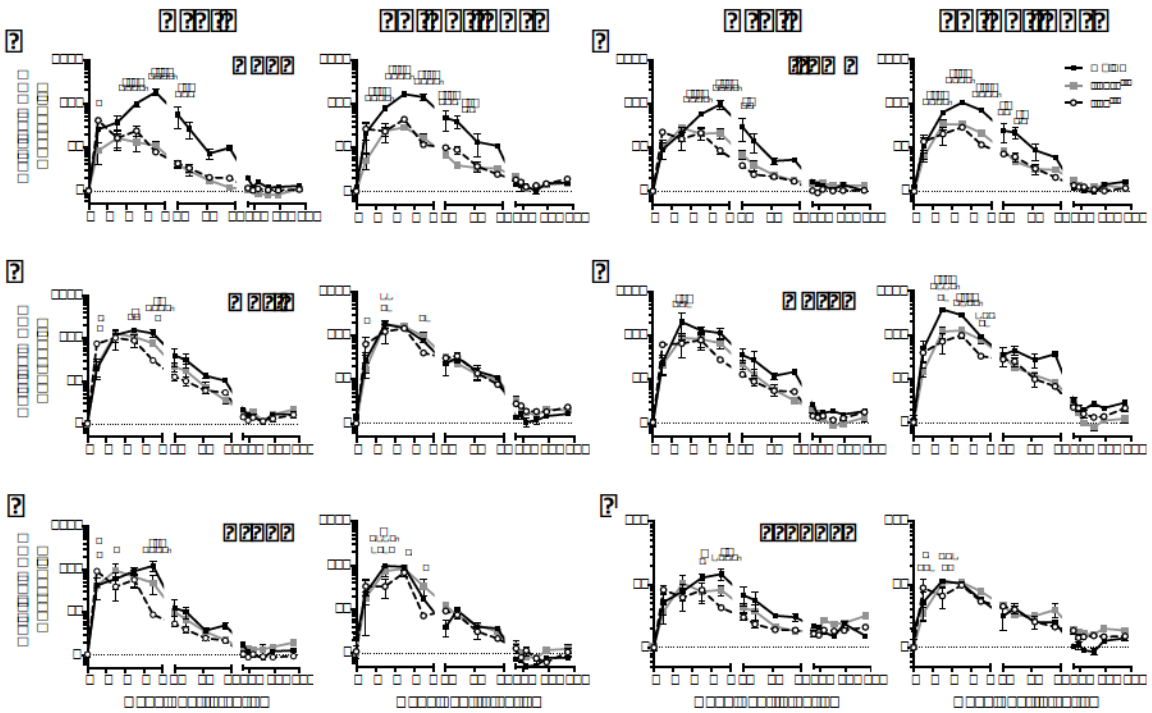

Figure 4-6. ISG expression in SINV-infected mice with impaired IFN-γ signaling. Expression of *Gbp2* (**A**), *Irgm1* (**B**), *Oasl2* (**C**), *Oas1a* (**D**), *Rsad2* (**E**), and *Zc3hav1* (**F**) were examined by qRT-PCR in the brains (left panels) and spinal cords (right panels) of WT B6 (black circle and solid line), *Ifngr1*$^{-/-}$ (gray square and solid line), and *Ifng*$^{-/-}$ (white circle and black dashed line) mice (n = 3-6 mice per strain per time point; data presented as the mean ± SEM; dashed line indicates gene expression of 0 DPI tissue for each strain to which other time points were normalized; *$p < 0.05$, **$p < 0.01$, ***$p < 0.001$, ****$p < 0.0001$, WT B6 vs *Ifngr1*$^{-/-}$; $^{\#}p < 0.05$, $^{\#\#}p < 0.01$, $^{\#\#\#}p < 0.001$, $^{\#\#\#\#}p < 0.0001$ WT B6 vs *Ifng*$^{-/-}$; $^{\dagger}p < 0.05$, $^{\dagger\dagger}p < 0.01$, $^{\dagger\dagger\dagger}p < 0.001$, $^{\dagger\dagger\dagger\dagger}p < 0.0001$, *Ifngr1*$^{-/-}$ vs *Ifng*$^{-/-}$, all by Tukey's multiple comparisons test).

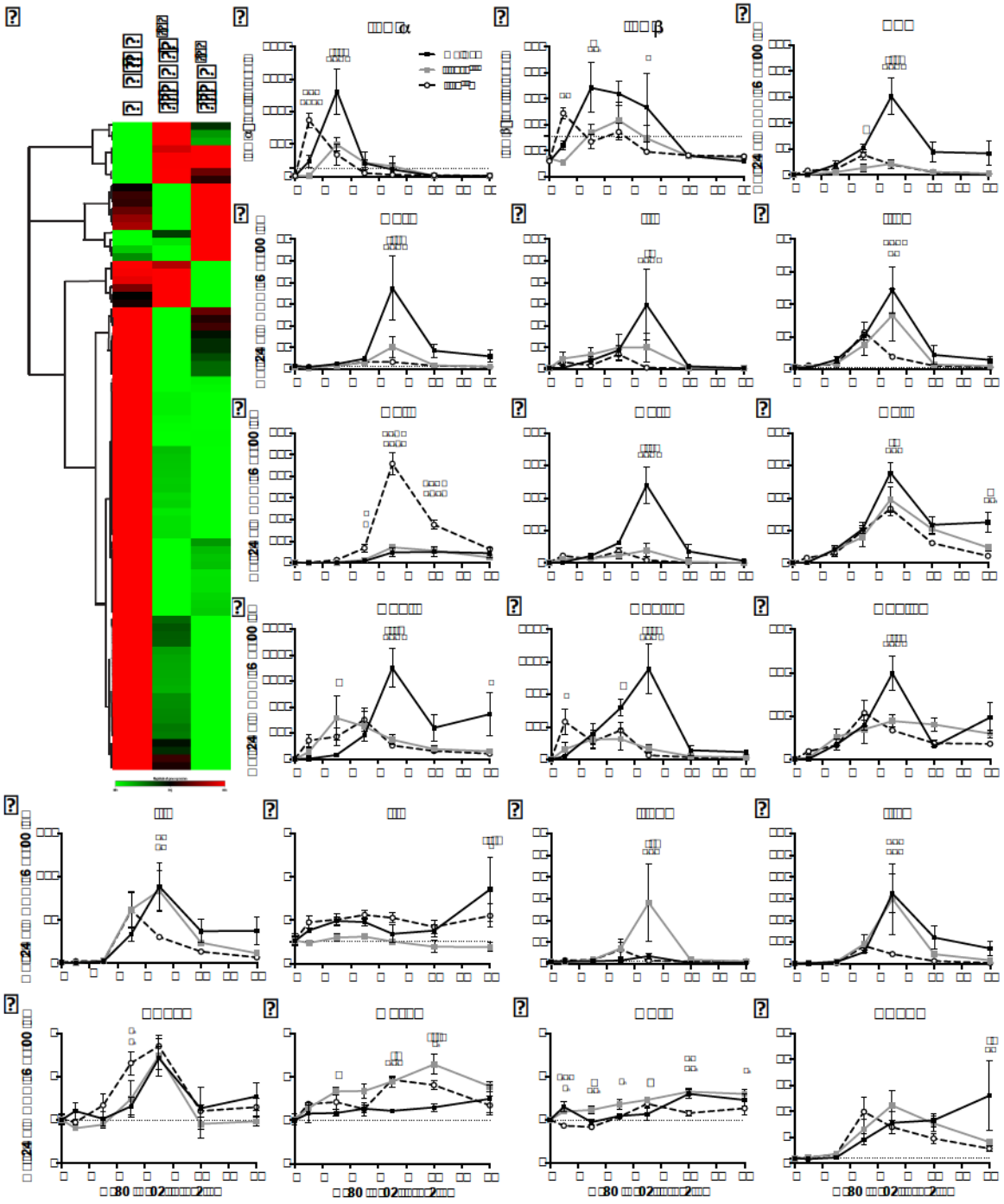

Figure 4-7. Expression of immune response genes in SINV-infected mice with impaired IFN-γ signaling. (**A**) A heat map was constructed to display microarray results examining relative expression of 84 genes in WT B6, *Ifngr1*$^{-/-}$, and *Ifng*$^{-/-}$ mouse brains at 7 DPI. Red represents a positive relative fold-change in gene expression, and green

represents a negative relative fold-change in gene expression. (**B, C**) Protein levels of IFN-α (**B**) and IFN-β (**C**) were examined by ELISA in WT B6 (black circle and solid line), *Ifngr1*$^{-/-}$ (gray square and solid line), and *Ifng*$^{-/-}$ (white circle and black dashed line) mouse brains (n = 3-4 mice per strain per time point; dashed line indicates level of detection of assay). (**D-U**) Selected genes examined for mRNA levels by qRT-PCR in individual WT B6 (black circle and solid line), *Ifngr1*$^{-/-}$ (gray square and solid line), and *Ifng*$^{-/-}$ (white circle and black dashed line) mouse brains included *Tnf* (**D**), *Csf2* (**E**), *Il6* (**F**), *Il1b* (**G**), *Ccl1* (**H**), *Ccl2* (**I**), *Ccl5* (**J**), *Cxcl9* (**K**), *Cxcl10* (**L**), *Cxcl13* (**M**), *Il2* (**N**), *Il4* (**O**), *Il17a* (**P**), *Il10* (**Q**), *Tbx21* (**R**), *Gata3* (**S**), *Rorc* (**T**), and *Foxp3* (**U**) (n = 3-4 mice per strain per time point; data presented as the mean ± SEM; dashed line indicates gene expression of 0 DPI brains for each strain to which other time points were normalized; *$p < 0.05$, **$p < 0.01$, ***$p < 0.001$, ****$p < 0.0001$, WT B6 vs *Ifngr1*$^{-/-}$; $^{\#}p < 0.05$, $^{\#\#}p < 0.01$, $^{\#\#\#}p < 0.001$, $^{\#\#\#\#}p < 0.0001$ WT B6 vs *Ifng*$^{-/-}$; $^{\dagger}p < 0.05$, $^{\dagger\dagger}p < 0.01$, $^{\dagger\dagger\dagger}p < 0.001$, $^{\dagger\dagger\dagger\dagger}p < 0.0001$, *Ifngr1*$^{-/-}$ vs *Ifng*$^{-/-}$, all by Tukey's multiple comparisons test).

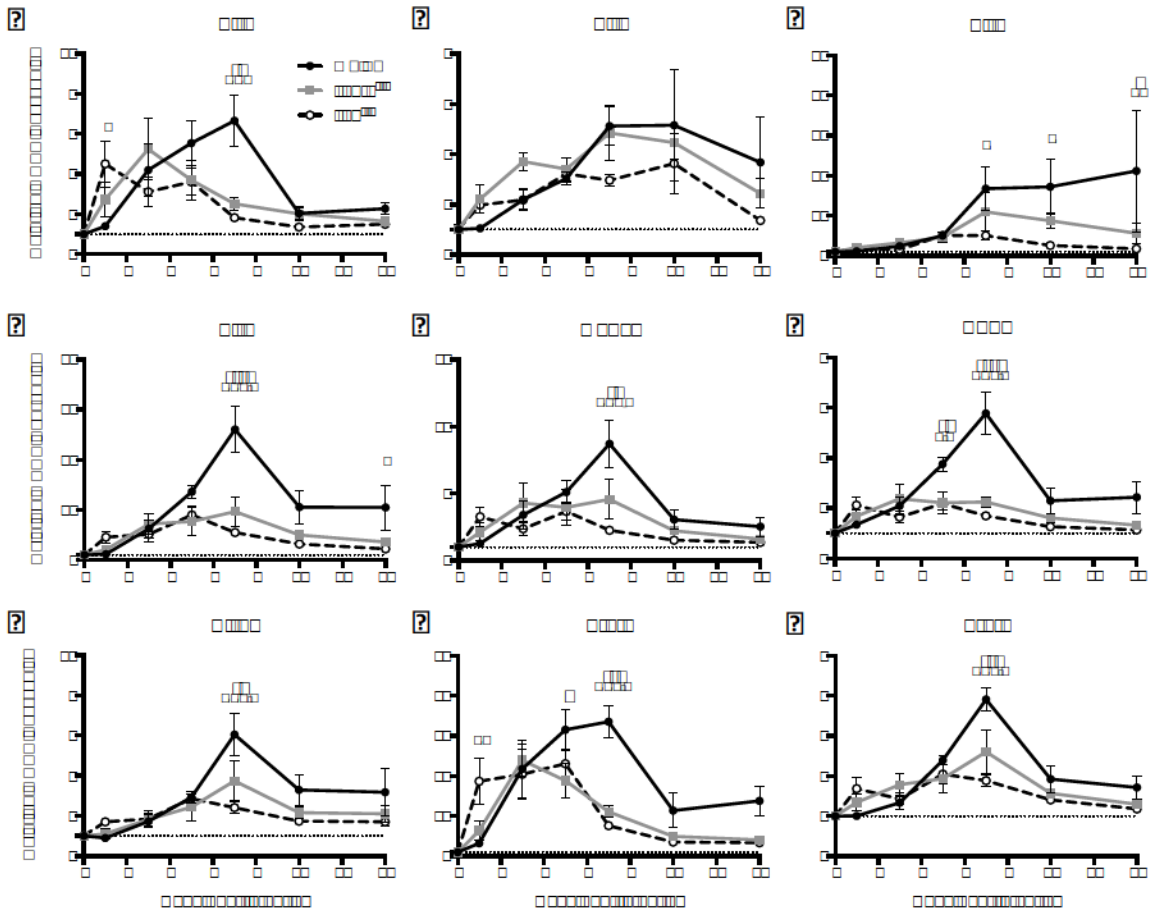

Figure 4-8. Expression of pathogen recognition receptor and associated signaling genes in SINV-infected mice with impaired IFN-γ signaling. Select genes involved in pathogen-associated molecular pattern recognition were examined by qRT-PCR in individual WT B6 (black circle and solid line), *Ifngr1*$^{-/-}$ (gray square and solid line), and *Ifng*$^{-/-}$ (white circle and black dashed line) mouse brains and included *Tlr3* (**A**), *Tlr7* (**B**), *Tlr8* (**C**), *Tlr9* (**D**), *Myd88* (**E**), *Nod1* (**F**), *Nlrp3* (**G**), *Stat1* (**H**), and *Stat3* (**I**) (n = 3-4 mice per strain per time point; data presented as the mean ± SEM; dashed line indicates gene expression of 0 DPI brains for each strain to which other time points were normalized; *$p < 0.05$, **$p < 0.01$, ***$p < 0.001$, ****$p < 0.0001$, WT B6 vs *Ifngr1*$^{-/-}$;

$^{\#}p < 0.05$, $^{\#\#}p < 0.01$, $^{\#\#\#}p < 0.001$, $^{\#\#\#\#}p < 0.0001$ WT B6 vs *Ifng*$^{-/-}$, all by Tukey's multiple comparisons test).

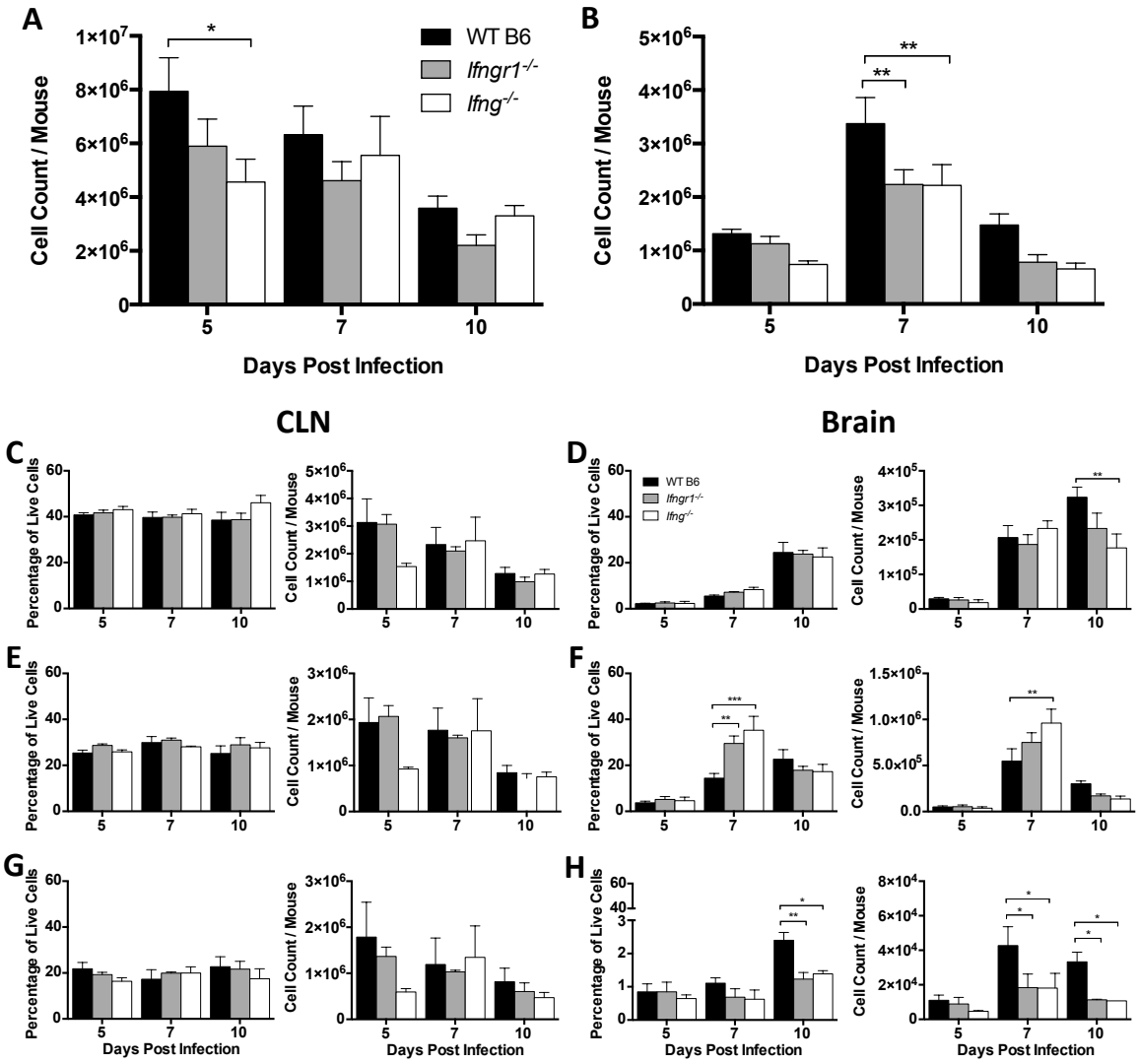

Figure 4-9. Role of IFN-γ signaling in lymphocyte proliferation and infiltration into the brain during SINV infection. (**A, B**) Total live mononuclear cells were evaluated in the CLNs (**A**) and brains (**B**) of WT B6 (black bars), *Ifngr1*$^{-/-}$ (gray bars), and *Ifng*$^{-/-}$ (white bars) mice by trypan blue exclusion at 5, 7, and 10 DPI (n = 3-7 pooled mice per strain per time point from five independent experiments). (**C-H**) Flow cytometry was used to evaluate changes in the CLNs (**C, E, G**) and infiltration into the brain (**D, F, H**) of CD4+ T cells (**C, D**), CD8+ T cells (**E, F**), and CD19+ B cells (**G, H**). Cell data are presented as both percentage of live cells (left graphs) and absolute cell counts (right

graphs) (n = 3-7 pooled mice per strain per time point from three independent experiments; data presented as the mean SEM; *$p < 0.05$, **$p < 0.01$, ***$p < 0.001$, by Tukey's multiple comparisons test).

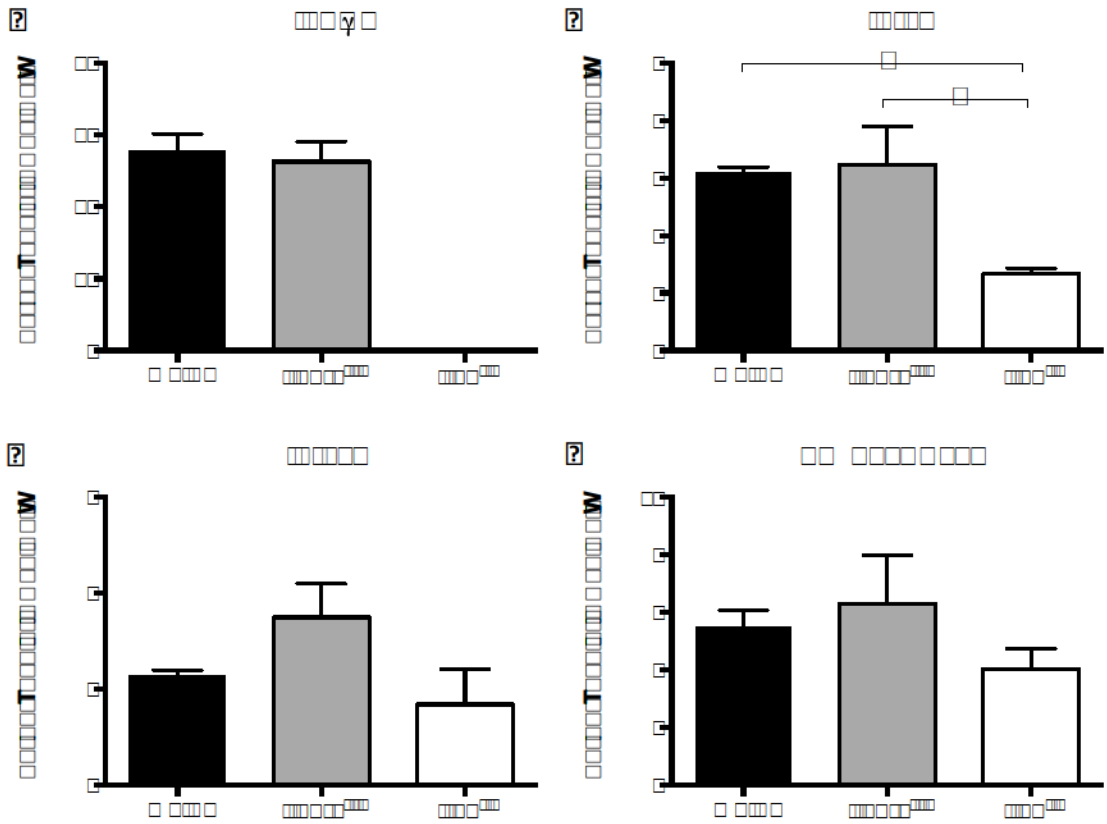

Figure 4-10. T helper cell profiles in brains of mice with impaired IFN-γ signaling at 7 DPI. Flow cytometry was used to examine the percentage of CD4+ T cells producing IFN-γ (**A**), IL-4 (**B**), IL-17a (**C**), or expressing both Foxp3 and CD25 (**D**) in WT B6 (black bars), *Ifngr1*$^{-/-}$ (gray bars), and *Ifng*$^{-/-}$ (white bars) mice at 7 DPI. These markers denoted Th1, Th2, Th17, and Treg cell populations, respectively (n = 3-7 pooled mice per strain per time point from three independent experiments; data presented as the mean SEM; **p* < 0.05 by Dunn's multiple comparisons test).

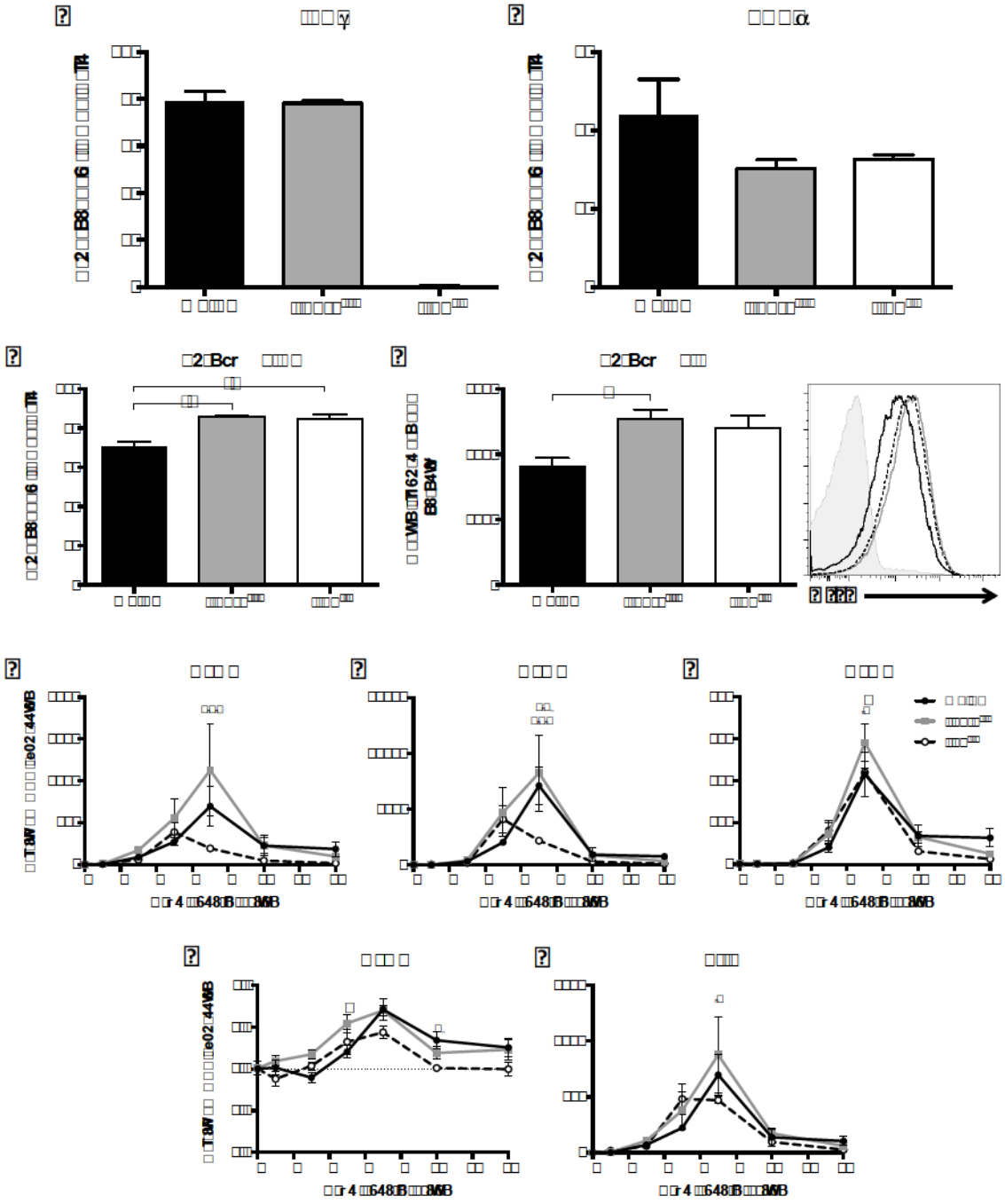

Figure 4-11. CD8+ T cell function during SINV infection in WT B6, *Ifngr1*$^{-/-}$, and *Ifng*$^{-/-}$ mouse brains at 7 DPI. (**A-C**) Flow cytometry was used to evaluate the percentage of CD8+ T cells producing IFN-γ (**A**), TNF-α (**B**), and granzyme B (**C**) in WT B6 (black bars), *Ifngr1*$^{-/-}$ (gray bars), and *Ifng*$^{-/-}$ (white bars) mice at 7 DPI. (**D**) MFI

presented in graph form (left) and as a histogram (right) was used to evaluate the amount of granzyme B produced by individual CD8+ T cells among strains (n = 3-7 pooled mice per strain per time point from three independent experiments; *$p < 0.05$, **p < 0.01 by Dunn's multiple comparisons test). (**E-I**) Relative mRNA expression of granzyme A (**E**), granzyme B (**F**), granzyme K (**G**), granzyme M (**H**), and perforin (**I**) were examined by qRT-PCR in WT B6 (black circle and solid line), *Ifngr1*$^{-/-}$ (gray square and solid line), and *Ifng*$^{-/-}$ (white circle and black dashed line) mouse brains (n = 3-4 mice per strain per time point; data presented as the mean ± SEM; dashed line indicates gene expression of 0 DPI tissue for each strain to which other time points were normalized; *$p < 0.05$, WT B6 vs *Ifngr1*$^{-/-}$; $^{\#\#}p < 0.01$, WT B6 vs *Ifng*$^{-/-}$, $^{\dagger}p < 0.05$, $^{\dagger\dagger\dagger}p < 0.001$, *Ifngr1*$^{-/-}$ vs *Ifng*$^{-/-}$, all by Tukey's multiple comparisons test).

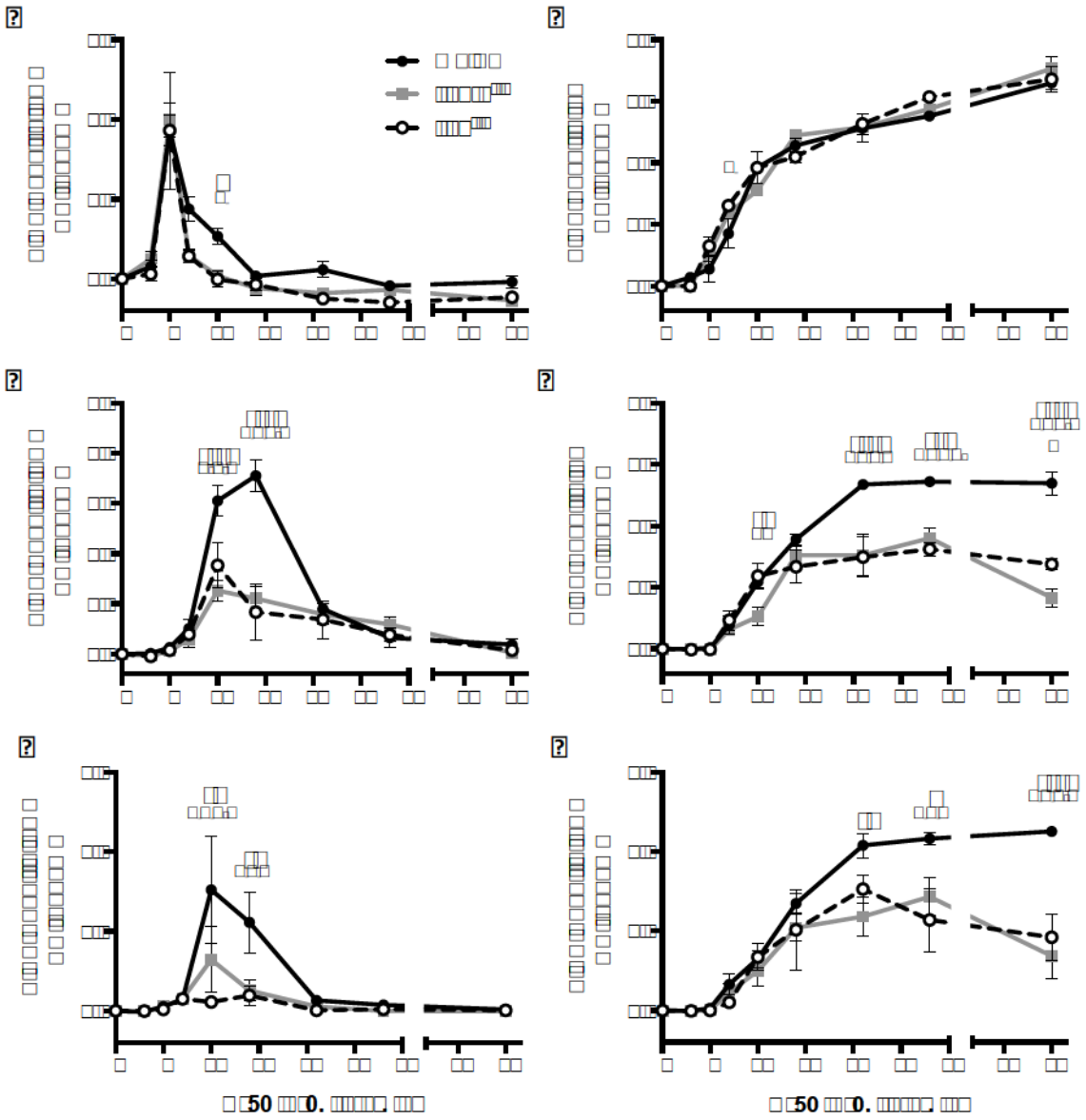

Figure 4-12. Effect of IFN-γ on SINV-specific antibody production. Anti-SINV IgM (**A, C, E**) and IgG (**B, D, F**) were measured in the serum (**A, B**), brains (**C, D**), and spinal cords (**E, F**) of WT B6 (black circle and solid line), *Ifngr1*$^{-/-}$ (gray square and solid line), and *Ifng*$^{-/-}$ (white circle and black dashed line) mice by ELISA (n = 3-4 mice per strain per time point, except for *Ifngr1*$^{-/-}$ 90 DPI spinal cords, where n = 2; data are presented as mean ODs ± SEM; **p* < 0.05, ***p* < 0.01, ****p* < 0.001, *****p* < 0.0001, WT B6 vs

Ifngr1$^{-/-}$; $^{\#}p < 0.05$, $^{\#\#\#}p < 0.001$, $^{\#\#\#\#}p < 0.0001$, WT B6 vs *Ifng*$^{-/-}$; $^{\dagger}p < 0.05$, $^{\dagger\dagger}p < 0.01$, *Ifngr1*$^{-/-}$ vs *Ifng*$^{-/-}$, all by Tukey's multiple comparisons test).

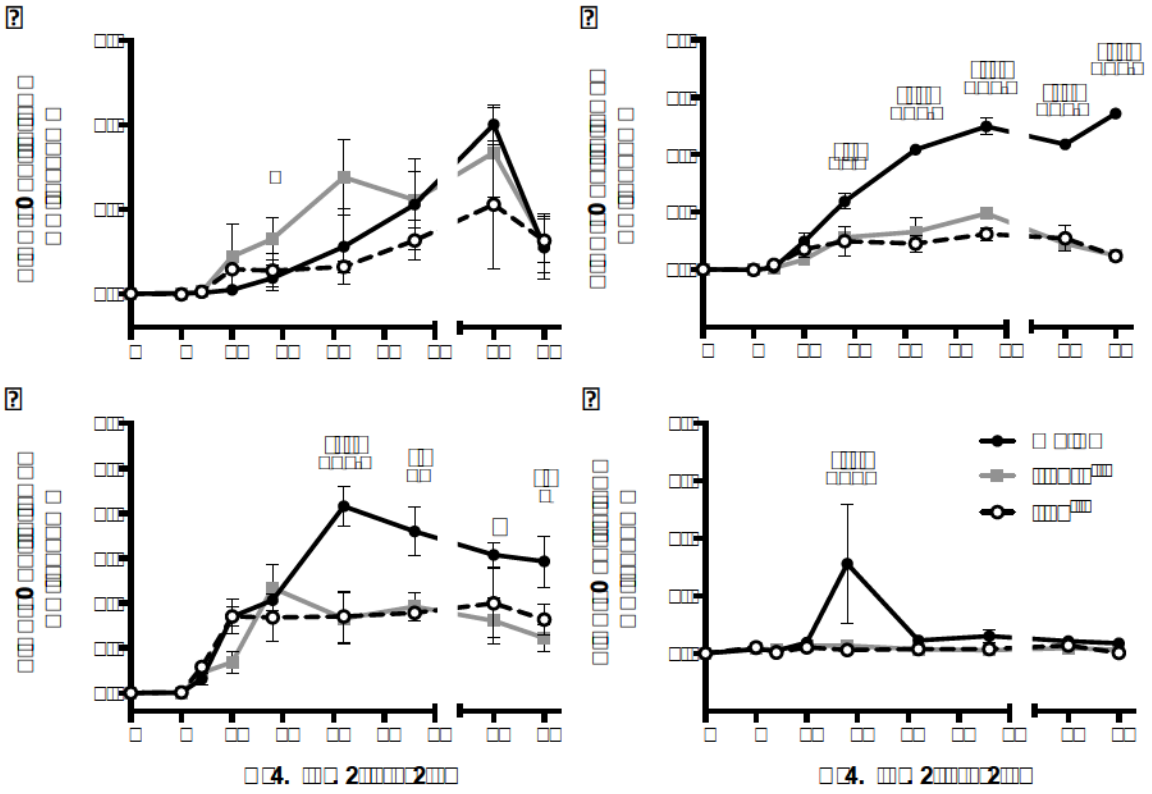

Figure 4-13. Effect of IFN-γ on production of anti-SINV IgG subclasses in the brain. Anti-SINV IgG1 (**A**), IgG2a (**B**), IgG2b (**C**), and IgG3 (**D**) were measured in brains of WT B6 (black circle and solid line), *Ifngr1*$^{-/-}$ (gray square and solid line), and *Ifng*$^{-/-}$ (white circle and black dashed line) mice by ELISA (n = 3-4 mice per strain per time point; data are presented as mean ODs ± SEM; *$p < 0.05$, **$p < 0.01$, ***$p < 0.001$, ****$p < 0.0001$, WT B6 vs *Ifngr1*$^{-/-}$; $^{\#}p < 0.05$, $^{\#\#}p < 0.01$, $^{\#\#\#}p < 0.001$, $^{\#\#\#\#}p < 0.0001$, WT B6 vs *Ifng*$^{-/-}$; $^{\dagger}p < 0.05$, *Ifngr1*$^{-/-}$ vs *Ifng*$^{-/-}$, all by Tukey's multiple comparisons test).

TABLES

[illegible]	SINV + IFN-γ vs Mock Infection	SINV + IFN-γ vs [illegible]	SINV + IFN-γ vs Mock + IFN-γ
[illegible]	[illegible]	[illegible]	[illegible]
[illegible]	[illegible]	[illegible]	[illegible]
Oasl2	[illegible]	[illegible]	[illegible]
Rsad2	[illegible]	[illegible]	[illegible]
Zc3hav1	[illegible]	[illegible]	[illegible]

Table 4-1. Relative fold-change expression of select ISGs in SINV-infected, IFN-γ-treated dCSM14.1 cells

CHAPTER 5:

MEMORY T CELLS REMAIN IN THE BRAIN LONG-TERM FOLLOWING ALPHAVIRUS CLEARANCE

INTRODUCTION

Sindbis virus (SINV) is the prototypic member of the alphaviruses, a genus of enveloped, positive-sense, single stranded RNA viruses belonging to the Togaviridae family[8]. SINV is neurotropic in mice, and when susceptible mice are infected with the nonfatal TE strain, infection in the CNS occurs in the three phases[42]. High levels of both infectious virus and viral RNA characterize Phase 1, which occurs from 0 to approximately 7 or 8 DPI. Phase 2, which occurs from 10 to 60 DPI, is characterized by undetectable infectious virus and high but declining levels of viral RNA. By Phase 3 of infection, which starts around 60 DPI and continues for at least a year following infection, viral RNA has reached a detectable low-level steady state. Because the alphavirus genomic RNA is infectious, the immune system must control persistent viral RNA present in the brain and spinal cord from reactivating and causing disease relapse. Anti-SINV antibody and interferon gamma (IFN-γ) are known to synergistically mediate clearance of infectious SINV, but the immune mechanisms that control RNA clearance and prevent virus reactivation are not well elucidated[24,92].

During acute virus infection, the T cell response can be categorized into three main phases[109]. During the clonal expansion phase in the local draining lymph nodes, activated CD4+ and CD8+ T cells expand primarily via IL-2 production, leave the lymph nodes, and migrate to the site of infection. These cells acquire effector function during this time and can secrete antiviral cytokines such as IFN-γ and tumor necrosis factor alpha (TNF-α) and produce cytotoxic proteins such as granzyme and perforin for CD8+ T cells[110]. Once active virus replication is brought under control, the short-term effector

(T_{EFF}) T cell population contracts considerably, and memory T cells become the predominant population[128].

Memory T cells are generally categorized as central memory (T_{CM}) or effector memory (T_{EM}) cells based on their proliferative and functional capacities[116]. T_{CM} cells express CD62L and home to secondary lymphoid organs; they possess considerable proliferative potential but have little effector capacity. T_{EM} cells in contrast lack CD62L and readily circulate throughout the body; they possess little proliferative capacity but are primed to immediately release effector proteins upon encountering viral antigen to which they are sensitized. Maintenance of these memory T cells is primarily achieved through IL-7 and IL-15 signaling[127]. IL-7 is thought to support T cell survival through promotion of anti-apoptotic protein expression, and IL-15 promotes low-level proliferation of T cells to maintain the memory population pool[132,328].

A recently characterized T cell population found to play an increasingly important role in long-term cellular immunity is the tissue-resident memory T (T_{RM}) cell. T_{RM} cells express CD103 and permanently reside at previous sites of infection without recirculating through the blood or lymph to secondary lymphoid tissues[120]. Similar to T_{EM} cells, they possess a high effector capacity and serve as a first line of defense against reencountered pathogens in nonlymphoid tissues, providing an accelerated antiviral response and presumably virus clearance[121]. T_{RM} presence in tissues has been shown following clearance of several viruses, including vaccinia virus in the skin, LCMV in the intestinal epithelium, salivary glands, and female reproductive tract, VSV in the salivary glands and brain, influenza A in the lung, and herpes simplex virus (HSV) in the skin and

sensory ganglia[117,119,121-126,315,329-331]. The role of T_{RM} cells following initial clearance of SINV in the CNS has not yet been characterized.

Because cellular immunity likely plays a significant role in controlling SINV long-term, it is important to characterize the populations of T cells present in the brains at each phase of SINV infection. We hypothesize that following clearance of infectious virus, memory T cells will be present in the brain and provide protection against virus reactivation through production of antiviral effector cytokines, such as IFN-γ. To test this, we infected C57BL/6 with the nonfatal TE strain of SINV and used flow cytometry to define the different T cell populations and assess their effector capacity.

MATERIALS & METHODS

Sindbis Virus Infection of Mice

Four to six week-old wild-type C57BL/6 mice, mice deficient in IFN-γ receptor 1 (*Ifngr1*$^{-/-}$, strain B6.129S7-*Ifng*^{tm1Ts}/J), and mice deficient in IFN-γ (*Ifng*$^{-/-}$, strain B6.129S7-*Ifngr1*^{tm1Agt}/J, Jackson Labs) were intracranially inoculated with 10^3 pfu of the nonfatal TE strain of SINV diluted in 20μL PBS or 20μL PBS vehicle while under light isoflurane anesthesia[37]. At sacrifice, mice were euthanized by an overdose of isoflurane anesthesia, and cervical lymph nodes (CLNs) and brains were collected. Equal numbers of male and female mice were used in experiments whenever possible. The Johns Hopkins University Institutional Animal Care and Use Committee approved all studies performed.

Mononuclear Cell Isolation

Single cell suspensions were made from CLNs and brains pooled from two to seven mice per strain per time point. CLNs were dissociated in RPMI + 1% FBS using gentleMACS C tubes and Dissociator (Miltenyi Biotech) and filtered through a 70μm-pore-size cell strainer. After pelleting by centrifugation, red blood cells were lysed using an ammonium chloride solution (Sigma-Aldrich or Ebioscience). Remaining cells were filtered through another 70μm strainer, pelleted by centrifugation, and resuspended in PBS + 2mM EDTA (PE buffer) for counting. Brains were placed in RPMI media containing 1% FBS, 1 mg/mL collagenase D (Roche) or 0.5 mg/mL collagenase IV (Worthington labs), and 0.1 mg/mL DNase I (Roche) and dissociated in C tubes using a gentleMACS Dissociator. Tissues were incubated for 30 minutes at 37°C with periodic agitation, and dissociated cells were filtered through a 70μm-pore-size cell strainer and pelleted by centrifugation. Cell pellets were resuspended in 30% supplemented Percoll [9:1 Percoll (GE Healthcare) : 10X salt solution of 80g NaCl, 3g KCl, 0.73g Na_2HPO_4, 0.2g KH_2PO_4, and 20g glucose in 1L dH_2O] in RPMI media in a 15mL conical tube and underlaid with 70% supplemented Percoll in RPMI media. Tubes were centrifuged at 850 x g at 4°C for 30 minutes with slow braking to create a gradient, and cells were collected from the 30/70% interface. Cells were pelleted by centrifugation and resuspended in PE buffer for counting. Live mononuclear cells were quantified by trypan blue exclusion.

Flow Cytometry

10^6 live cells were placed in the wells of a 96-well round bottom plate. A violet LIVE/DEAD Fixable Dead Cell Stain (Life Technologies) diluted in PE buffer was applied to cells for 30 minutes, followed by a 15-minute incubation with anti-mouse CD16/CD32 (BD Pharmingen) diluted in PE buffer to block Fc receptors. Cells were stained with monoclonal antibodies against CD45 (clone 30-F11), CD3 molecular complex (clone 17A2), CD3e (clone 145-2C11), CD4 (clone RM4-5), CD8 (clone 53-6.7), NK1.1 (clone PK136), CD44 (clone IM7), CD62L (clone MEL-14), CD127 (clone A7R34), CD103 (clone 2E7), PD-1 (clone J43), and TIM-3 (clone RMT3-23) from Ebioscience or BD Pharmingen diluted in PBS + 2mM EDTA + 0.5% BSA (FACS Buffer) for 30 minutes on ice. For intracellular staining of Ki67, cells were fixed for 20 minutes using Fixation/Permeabilization solution from the Ebioscience Foxp3/Transcription Factor Staining Buffer kit. Cells were stained for 20 minutes at 4°C with a mouse anti-human monoclonal antibody against Ki67 (clone B56, BD Pharmingen) diluted in Permeabilization Buffer.

For intracytoplasmic cytokine staining (ICS), 2-3 x 10^6 cells were stimulated for four hours at 37°C with 50 ng/mL of phorbol-12-myristate 13-acetate (PMA, Sigma) and 1 μg/mL ionomycin (Sigma) in the presence of brefeldin A (GolgiPlug, BD Pharmingen) in RPMI + 1% FBS. Following LIVE/DEAD and surface antibody staining (see above), cells were fixed for 20 minutes using Fixation/Permeabilization solution from the BD Cytofix/Cytoperm kit. Cells were stained for 30 minutes at 4°C with monoclonal antibodies against IFN-γ (clone XMG1.2), IL-2 (clone JES6-5H4), and TNF-α (clone MP6-XT22) from Ebioscience or BD Pharmingen diluted in BD Perm/Wash buffer.

Cells were resuspended in 200μL FACS Buffer and run on a BD FACSCanto II cytometer using BD FACSDiva software, version 8, and analyses were carried out using FlowJo software, version 8. Polyfunctionality of T cells were analyzed by applying Boolean gating to IL-2, IFN-γ, and TNF-α-gated populations. Cells were characterized as follows: CD4+ T cells ($CD45^{hi}$CD3+CD4+), CD8+ T cells ($CD45^{hi}$CD3+CD8+), NK cells ($CD45^{hi}$CD3-NK1.1+), naïve T cells ($CD44^{lo}$CD62L+), short-term effector T cells (T_{EFF} cells, $CD44^{hi}$CD62L-CD127-), effector memory T cells (T_{EM} cells, $CD44^{hi}$CD62L-CD127+), central memory T cells (T_{CM} cells, $CD44^{hi}$CD62L+CD127+), tissue resident memory T cells (T_{RM} cells, $CD44^{hi}$CD62L-CD103+), proliferating T cells (CD3e+Ki67+), and exhausted T cells ($CD44^{hi}$PD-1+TIM-3+). All flow cytometry data are averaged representations of three to four independent experiments per time point.

Gene mRNA Expression Measurement by Real-Time PCR

Right brain hemispheres from three to four mice per strain per time point were homogenized in Lysing Matrix D tubes (MP Biomedicals) at 6.0 M/s for 40 seconds using a FastPrep-24 homogenizer (MP Biomedicals). Qiagen RNeasy Lipid Tissue Mini kit was used to isolate RNA, and cDNA was synthesized using a High Capacity cDNA Reverse Transcription Kit with random primers (Life Technologies). Quantitative real-time PCR (qRT-PCR) was performed using TaqMan Universal PCR Master Mix (Roche) on a 7500 Fast Real-Time PCR System. IL-7 and IL-15 mRNA was measured using commercially available TaqMan gene expression assays (Integrated DNA Technologies), and relative quantification was performed by the ΔΔCT method using rodent glyceraldehyde-3-phosphate dehydrogenase (*Gapdh*) mRNA for normalization.

Statistics

Statistical analyses were performed using Graphpad Prism 6 software. Time course studies comparing multiple mouse strains were analyzed by two-way ANOVA with Tukey's multiple comparison post-test. A p value of < 0.05 was considered significant for all analyses.

RESULTS

CD4+ and CD8+ T cells produce IFN-γ in the brain throughout SINV infection

As a positive sense, single-stranded RNA virus, SINV RNA is infectious, so low levels that persist in the brain throughout Phase 3 of infection represent a possible nidus from which virus may reactivate[43]. T cells, which remain in brain for at least six months following infection, offer a possible mechanism to control or prevent virus reactivation[42]. IFN-γ plays a critical role in the clearance of virus during Phase 1 of infection, and as a major effector protein produced by both CD4+ and CD8+ cells, we examined its role in the long-term control of SINV.

To determine the source of IFN-γ throughout the course of SINV infection, mice were intracranially infected with SINV TE, and CLNs and brains were collected for flow cytometry. The three main known sources of IFN-γ, CD4+ T cells, CD8+ T cells, and NK cells, were examined for cytokine production during Phase 1 (5 and 7 DPI), Phase 2 (10 and 14 DPI), and Phase 3 (90 DPI) of infection. In the CLNs, few cells produced IFN-γ at

any time point, with none of the cell populations examined emerging as a predominant source of IFN-γ (Figs 5-1A and 5-1C). In contrast, in the brain, NK cells were the predominant source of IFN-γ at 5 DPI, both as percentage of live cells and absolute numbers (Figs 5-1B and 5-1D). IFN-γ-producing cell numbers peaked in the brain at 7 DPI, with CD8+ T cells overtaking NK cells as the predominant source of IFN-γ. By 14 DPI, the number of CD4+ T cells producing IFN-γ was comparable to CD8+ T cells. In Phase 3 of infection, the number of T cells in the brains decreased considerably, with CD8+ and CD4+ T cells continuing to produce the majority of IFN-γ. From these data, NK cells produce the majority of the local IFN-γ early in the course of infection, but CD4+, and especially CD8+ T cells soon take over, becoming the predominant source of IFN-γ during Phases 2 and 3 of infection.

We next characterized the cells producing IFN-γ throughout infection. At all time points examined, less than half the CD4+ T cells, CD8+ T cells, and NK cells in the CLNs were producing IFN-γ (Fig 4-1E). In the brain, the percentage CD4+ and CD8+ T cells producing IFN-γ increased over the course of infection, going from approximately 40 to 60% at 5 and 7 DPI to over 80% at 10, 14, and 90 DPI (Fig 4-1F). In contrast, the percentage of NK cells producing IFN-γ in the brain remained around 20 to 50%, similar to that of the NK cells in the CLNs. The MFIs for IFN-γ produced by CD4+ T cells, CD8+ T cells, and NK cells were assessed as a representation of how much IFN-γ individual cells were producing. In the CLNs, the MFI for IFN-γ remained low and unchanging among cell populations (Figs 4-1G and 4-1I). However in the brain, the MFIs for IFN-γ produced by CD4+ and CD8+ T cells increased over time, with the greatest increase occurring between 7 DPI and 10 DPI (Figs 4-1H and 4-1J). Similar to the CLNs,

the MFI for IFN-γ produced by NK cells in the brain was lower and remained relatively unchanged over time.

Expression of cytokines associated with long-term T cell survival and proliferation are only transiently up-regulated during SINV infection

Long-term survival and proliferation of memory T cells are primarily facilitated by two cytokines: IL-7 and IL-15[127]. Expression of the mRNAs for these cytokines was examined by qRT-PCR in the brains of mice infected with SINV. Compared to 0 DPI, expression of both *Il7* and *Il15* sharply increased following infection, peaking at 7 DPI (Fig 5-2). Expression then abruptly decreased, returning to baseline levels by 28 DPI and remaining there through 180 DPI. These results indicate that at the mRNA level, IL-7 and IL-15 do not remain elevated to support maintenance of memory T cells in the brain during SINV infection.

T_{EM} cells are the predominant T cell population present long-term in the brain during SINV infection

We next sought to characterize the T cells populations present in the CLNs and brain during SINV infection. Using flow cytometry, T cells were defined as naïve T cells, short-term T effector cells (T_{EFF}), effector memory T cells (T_{EM}), or central memory T cells (T_{CM}) at 7, 14, 28, and 90 DPI. Gating schemes used for characterization are shown in Fig 5-3A for CLNs and Fig 5-3B for brains.

In the CLNs, naïve cells predominated in both the CD4+ and CD8+ T cell populations (Fig 5-3C), with far fewer cells showing a T_{EFF} (Fig 5-3D) or T_{EM} (Fig 5-3E)

phenotype. Less than 5% of the CD4+ T cells, but 10 to 15% of the CD8+ T cells in the CLNs were characterized as T_{CM} cells (Fig 5-3F). The T cell population profile in the CLNs did not change over time during SINV infection. In contrast to the CLNs, very few CD4+ or CD8+ T cells were characterized as naïve cells (Fig 5-3G). Early in infection at 7 DPI, T_{EFF} cells were the predominant T cell population in the brain (Fig 5-3H); however as time went on, the percentage of CD4+ and CD8+ T cells characterized as T_{EFF} cells decreased, and the percentage of cells showing a T_{EM} phenotype increased, becoming the predominant T cell population at 90 DPI (Fig 5-3I). T_{CM} cells were rarely found in the brain at any time during infection (Fig 5-3J). Therefore, during SINV infection, while naïve T cells predominate in the CLNs, in the brain the main T cell population transitions from T_{EFF} cells early in infection to T_{EM} cells during the period of long term maintenance and control of SINV reactivation.

Brains from mice with impaired IFN-γ signaling have fewer CD8+ T_{RM} cells

Tissue resident memory (T_{RM}) cells are a recently characterized subset of memory T cells that do not circulate, but instead permanently remain at former sites of infection[120]. The presence of CD103+ T_{RM} cells was assessed in CLNs and brains in WT B6, *Ifngr1*$^{-/-}$, and *Ifng*$^{-/-}$ mice at 7, 14, and 28 DPI to determine what role, if any, IFN-γ played in their development, maintenance, and survival (Fig 5-4A). Very few CD4+ or CD8+ (Fig 5-4B) T_{RM} cells were found in CLNs of SINV-infected mice at any time point. Slightly higher percentages of CD4+ T cells in the brain were characterized as T_{RM} cells, though the numbers did not significantly change over time or differ among mouse strains (Fig 5-4C). Percentages of CD8+ T cells in the brain characterized as T_{RM} cells,

however, did increase over time. WT B6 brains had significantly more CD8+ T_{RM} cells than *Ifngr1*$^{-/-}$ brains at 28 DPI ($p < 0.001$, Tukey's multiple comparisons test) and *Ifng*$^{-/-}$ brains at 14 and 28 DPI ($p < 0.05$ and $p < 0.001$ for 14 and 28 DPI, respectively, Tukey's multiple comparisons test). The results show that IFN-γ signaling promotes the development of CD8+ T_{RM} cells in the brain during SINV infection.

T cells in the brain are proliferative during Phase 1, but not Phases 2 or 3, of SINV infection

To evaluate the proliferative potential of the T cells present in the CLNs and brain over the course of SINV infection, the intranuclear marker Ki67 was measured at 7, 14, 28, and 90 DPI (Fig 5-5A). In the CLNs, less than 10% of the CD4+ or CD8+ T cells were positive for Ki67 at any of the time points (Fig 5-5B). In the brain, the fraction of T cells positive for Ki67 was approximately 50%, but it dropped to less than 10% at all other time points (Fig 5-5C). These findings show that during the period of active virus clearance in the brain, T cells are highly proliferative. However, during Phases 2 and 3, the fraction of T cells that are proliferating is minimal.

Polyfunctionality of T cells in the brain increases over the course of SINV infection

During chronic virus infection, T cells tend to lose their ability to produce effector molecules, potentially making them less efficient at combatting pathogen reactivation[146]. To determine whether this happens over the course of SINV infection, CD4+ and CD8+ T cells were stimulated with PMA and ionomycin and evaluated for their ability to produce three major effector proteins, IL-2, IFN-γ, and TNF-α, at 7, 14, 28, and 90 DPI

(Fig 5-6A). Both CD4+ (Fig 5-6B) and CD8+ (Fig 5-6C) T cells increased in their polyfunctionality over the course of infection. While at 7 DPI, less than 10% of T cells were producing all three cytokines, by 90 DPI, the percentage increased to over 50%.

To further characterize the functionality of T cells in the brain during SINV infection, the MFIs of IL-2, IFN-γ, and TNF-α were quantified (Fig 5-7A). IL-2 production by both CD4+ and CD8+ T cells increased over time, peaking at 90 DPI (Fig 5-7B). For IFN-γ (Fig 5-7C) and TNF-α (Fig 5-7D), MFI values increased throughout Phases 1 and 2 of infection, peaking at 28 DPI, before declining slightly at 90 DPI. These findings show that not only do T cells increase in polyfunctionality over the course of infection, the amount of effector cytokines produced by T cells increases over time as well.

Expression of T cell exhaustion markers decreases during SINV infection

Similar to the production of effector cytokines, T cells tend to increasingly express cell surface markers associated with exhaustion during chronic virus infections[138,139]. To evaluate T cell exhaustion during SINV infection, expression of both PD-1 and TIM-3 were measured on CD4+ and CD8+ T cells in CLNs and brains at 7, 14, 28, and 90 DPI (Fig 5-8A). In CLNs, expression of both PD-1 and TIM-3 was minimal (Fig 5-8B), and far more CD4+ and CD8+ T cells expressed both markers in the brain (Fig 5-8C). Exhaustion marker expression peaked at 14 DPI in CD4+ T cells and at 7 DPI in CD8+ T cells and then decreased. These findings suggest that T cells present in the brain following clearance of infectious virus do not become exhausted and are fully capable of responding to possible virus reemergence.

DISCUSSION

IFN-γ is primarily produced by CD4+ T cells, CD8+ T cells, and NK cells[95,96]. During SINV infection, NK cells are the initial source of IFN-γ in the brain. Because NK cells are innate immune cells, they do not require activation and can respond to infection sooner than cells of the adaptive immune response, and IFN-γ specifically produced by NK cells is important for T cell recruitment to sites of infection[332]. At 7 DPI, when virus clearance is underway, CD8+ T cells become the predominant source of IFN-γ. As infection progresses into Phase 2, CD4+ T cells increase in number as CD8+ T cells decrease, and by 90 DPI, maintenance levels of IFN-γ are produced by both T cell subsets. CD8+ T cells appear to be the predominant source of the IFN-γ that facilitates virus clearance. During Phases 2 and 3, IFN-γ production during viral RNA clearance and control of reactivation is shared between CD4+ and CD8+ T cells.

The percentage of CD4+ T cells, CD8+ T cells, and NK cells producing IFN-γ in the CLNs remained low throughout the course of infection. IFN-γ production by NK cells in the brain was similar. However, while the percentage of CD4+ and CD8+ T cells in the brain producing IFN-γ remained around 50% during Phase 1 of infection, increased percentages of T cells secreting IFN-γ were found as time progressed, attaining greater than 80% by 90 DPI. A similar trend was seen in the amount of IFN-γ produced by individual T cells in the brain over time. These data suggest that CD4+ and CD8+ T cells gain their effector function at the site of infection rather than in the periphery and adapt to increase their effector capacity over course of infection. In contrast, NK cells, which are

part of the innate rather than adaptive immune response, produce consistent amounts of IFN-γ regardless of infection location or time.

Over the course of SINV infection, T_{EM} cells replaced T_{EFF} cells as the predominant CD4+ and CD8+ T cell populations in the brain. T_{EM} cells can survive for several years while undergoing low-level cell turnover to replenish and maintain cell populations[333]. As measured by Ki67 expression, only T cells present in the brain during the height of virus infection were proliferating, with less than 10% of the T cells present in the brain during Phases 2 and 3 cycling. Similar Ki67+ T cell and B cell numbers have been seen during chronic coronavirus and SINV infection, respectively, in the CNS[91,334].

A hallmark of memory T cells is their ability to persist in the absence of continued antigen stimulation, and for many virus infections, T cells are retained in the CNS in the absence of detectable infectious virus[86,335-337]. In some cases, virus may periodically reactivate at low levels and support memory T cell maintenance[338]. Regardless, persistent SINV RNA does not necessarily need to periodically reactivate and produce viral antigen or infectious virus to maintain memory T cell populations in the brain.

Traditionally, memory T cell survival is dependent on IL-7 and homeostatic cell turnover is mediated by IL-15[127]. Surprisingly, mRNA expression of both *Il7* and *Il15* in SINV-infected mouse brains returned to baseline by 28 DPI after peaking at 7 DPI. This suggests that at least at the level of mRNA expression, production of IL-7 and IL-15 does not increase to support long-term maintenance of memory T cells during SINV infection. Expression of IL-15 is mainly regulated post-transcriptionally, with IL-15 protein produced at low levels despite widespread *Il15* mRNA expression[127]. During chronic

CNS infection with certain viruses, CD8+ T cells are able to undergo homeostatic proliferation in the absence of IL-15, indicating memory T cell homeostasis can be mediated in an IL-15-independent manner[334,338]. IL-7-independent mechanisms of T_{EM} maintenance have not been reported, but T_{EM} cells are characterized in part by their expression CD127, the IL-7 receptor, so perhaps constitutive low levels of IL-7 produced by stromal cells are sufficient to mediate T_{EM} survival in the brain[127]. Alternatively, IL-7- and IL-15-dependent maintenance of circulating T_{EM} cells may occur in secondary lymphoid tissues rather than the brain[339].

Over the course of infection, the percentage of CD8+ T cells expressing CD103, a marker for T_{RM} cells in the brain, increased. As permanent residents of previous sites of infection, T_{RM} cells are uniquely situated to provide an immediate and effective response to a pathogen. Priming of these cells is thought to occur in their tissue of residence, as opposed to secondary lymphoid tissues, allowing for a rapid response to local infection[340]. In our model, only CD8+ T_{RM} cells appear to play a local role in virus control, and not CD4+ T cells. Though CD8+ T_{RM} cells are much better described, CD4+ T_{RM} cells play a role in control of other virus and parasitic infections[330,341-344]. T_{RM} cells in the brain do not highly express CD127 nor appear to require IL-7 or IL-15 for survival[117,345]. This provides an alternate explanation on how control of virus reactivation could be achieved in the brain in the absence of upregulation of *Il7* or *Il15* expression.

Previous studies have shown that in a mouse model for influenza, IFN-γ specifically produced by CD4+ T cells is required for generating CD8+ T_{RM} cells in the lung[329]. Brains of mice defective in IFN-γ signaling possessed significantly fewer CD8+ T_{RM} cells compared to wild-type mice with intact signaling, indicating IFN-γ promotes

the presence of T_{RM} cells in the brain. Additionally, IFN-γ secreted by T_{RM} cells helps to recruit CD8+ T_{EM} and B cells to help combat pathogens by up-regulating expression of endothelial vascular cell adhesion molecule 1 (VCAM-1), so the T_{RM} cells in the brains of *Ifngr1*$^{-/-}$ and *Ifng*$^{-/-}$ mice may not be as effective at combatting reactivating virus[121].

Little is known regarding T cell exhaustion in cases of acute virus infection where viral RNA persists following virus clearance. During chronic virus infections, memory T cells tend to lose their effector function capacity over time and show increased rates of apoptosis[146]. The extent of T cell exhaustion is directly proportional to the viral load and duration of virus persistence, suggesting that if persistent SINV RNA were replication competent and prone to reactivation, memory T cells present in the brain would show decreased polyfunctionality and increased inhibitory markers indicative of exhaustion[146,346]. Over the course of infection, the polyfunctionality of SINV-infected T cells in the brain in our mouse model actually increased. As T cells gain polyfunctionality, they exhibit a functional hierarchy for cytokine secretion, with IFN-γ tending to be secreted first, then TNF-α, and finally IL-2, and this hierarchy appears to apply to our model[347]. Furthermore, expression of inhibitory markers PD-1 and TIM-3 decreased over the course of infection. These results indicate that rather than acquiring an exhaustive phenotype, during chronic SINV infection, memory T cells adapt and become more effective at responding to virus reactivation. This suggests that persistent SINV RNA remaining in the brain during Phase 3 of infection rarely reactivates or only does so at extremely low levels, and further studies are warranted to elucidate this.

This study shows that memory T cells do exist in the brain following clearance of infectious virus during SINV infection. CD8+ T_{RM} cells in particular are dependent on

IFN-γ signaling for proper production and function, providing a mechanism by which IFN-γ may control virus reactivation. Furthermore, over time memory T cells do not show signs of exhaustion but rather increase their polyfunctionality. Understanding the long-term maintenance of cellular immunity can assist in developing alphavirus encephalomyelitis treatment and control strategies, such as designing optimal vaccines.

FIGURES

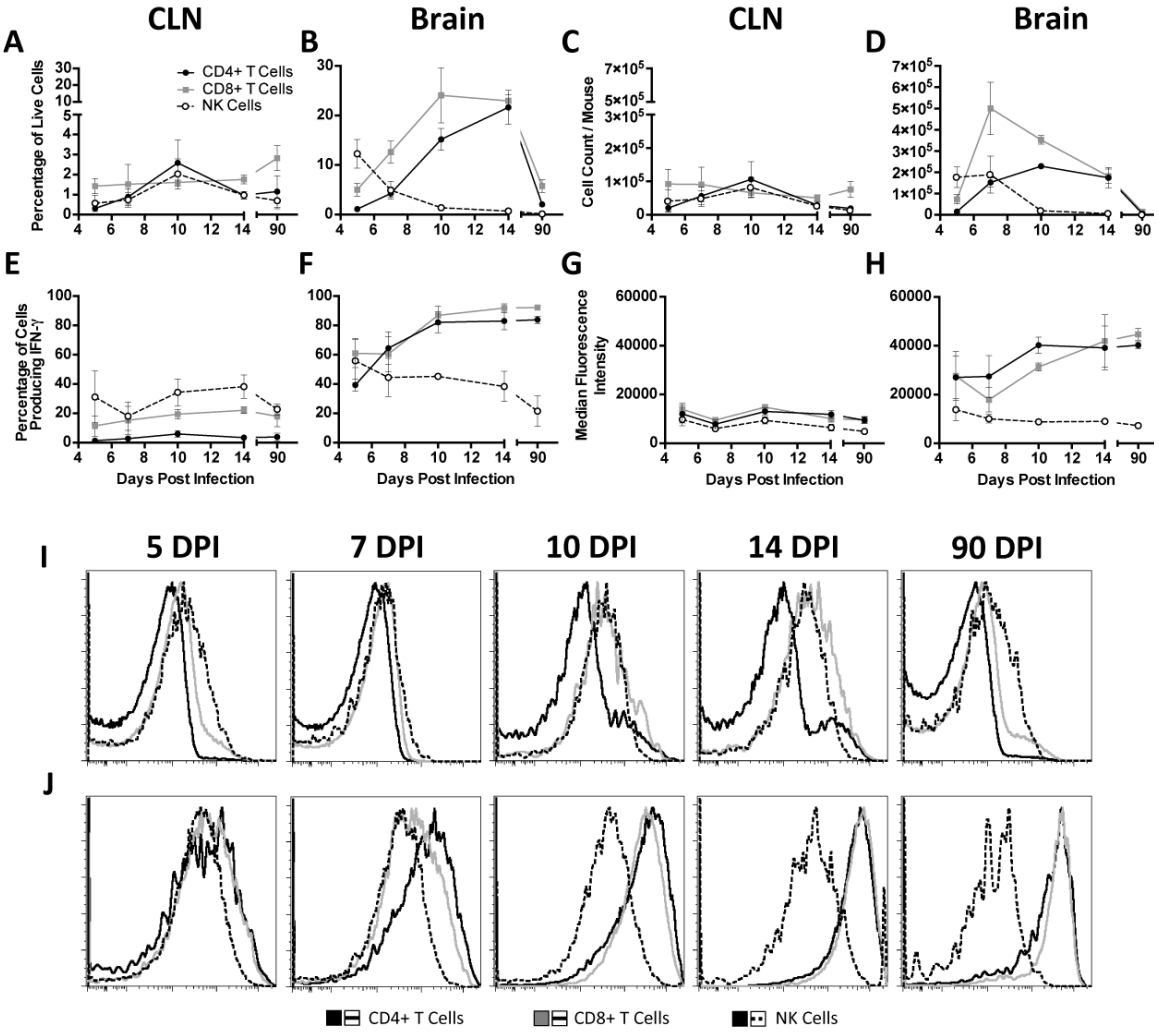

Figure 5-1. Source of IFN-γ during SINV infection. Flow cytometry was used to evaluate what cells were producing IFN-γ in the CLNs (**A, C, E, G, I**) and brains (**B, D, F, H, J**) of WT B6 mice at 5, 7, 10, 14 and 90 DPI. CD4+ T cells (black circle and solid line), CD8+ T cells (gray square and solid line), and NK cells (white circle and black dashed line) producing IFN-γ were examined as both the percentage of live cells (**A, B**) and absolute cell counts (**C, D**). Also evaluated were the percentage of each cell type producing IFN-γ (**E, F**) and the MFI of IFN-γ for each cell type presented in graph form

(**G, H**) and as histograms (**I, J**) (n = 3-7 pooled mice per time point from three independent experiments, except for data from 5 DPI CLNs, which were from two independent experiments; data presented as the mean ± SEM).

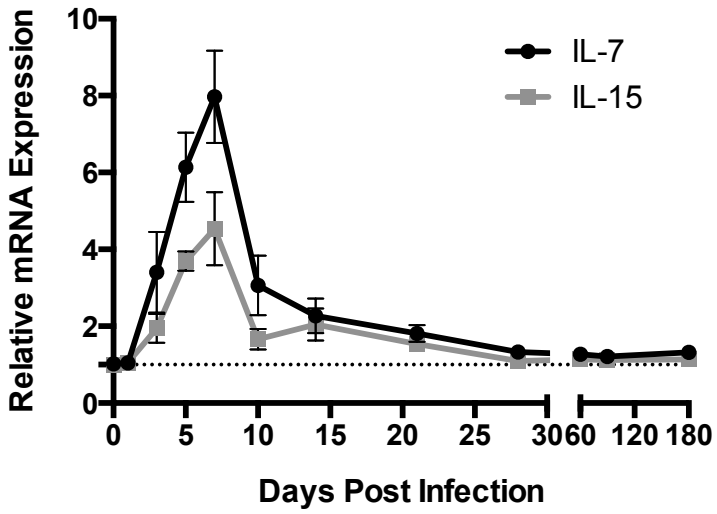

Figure 5-2. Expression of mRNAs for cytokines involved in T cell survival during SINV infection. mRNA expression of *Il7* (black circle and line) and *Il15* (gray square and line) was examined by qRT-PCR in WT B6 mouse brains (n = 3-4 mice per time point; data presented as mean ± SEM; dashed line indicates gene expression of 0 DPI brains to which other time points were normalized).

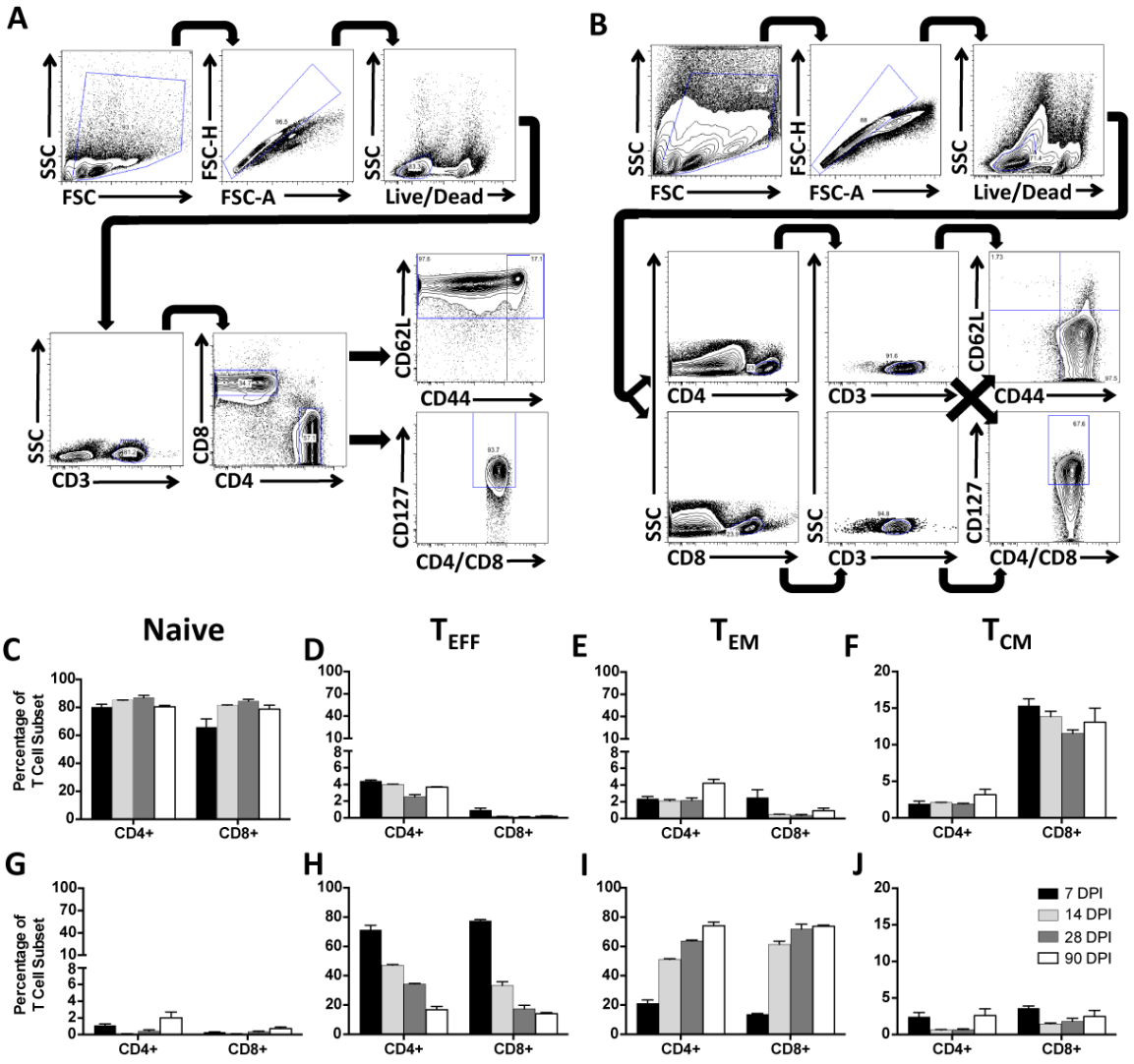

Figure 5-3. Characterization of T cell populations in the CLNs and brain throughout the course of SINV infection. Using the above gating strategies for CLNs (**A**) and brains (**B**), flow cytometry was used to examine different T cell populations in WT B6 mice at 7 (black bars), 14 (light gray bars), 28 (dark gray bars), and 90 (white bars) DPI. The percentage of CD4+ and CD8+ T cells expressing markers characteristic of naïve T cells (**C, G**), T_{EFF} cells (**D, H**), T_{EM} cells (**E, I**), and T_{CM} cells (**F, J**) were evaluated in CLNs (**C-F**) and brains (**G-J**) (n = 3-7 pooled mice per time point from three independent experiments; data presented as the mean ± SEM).

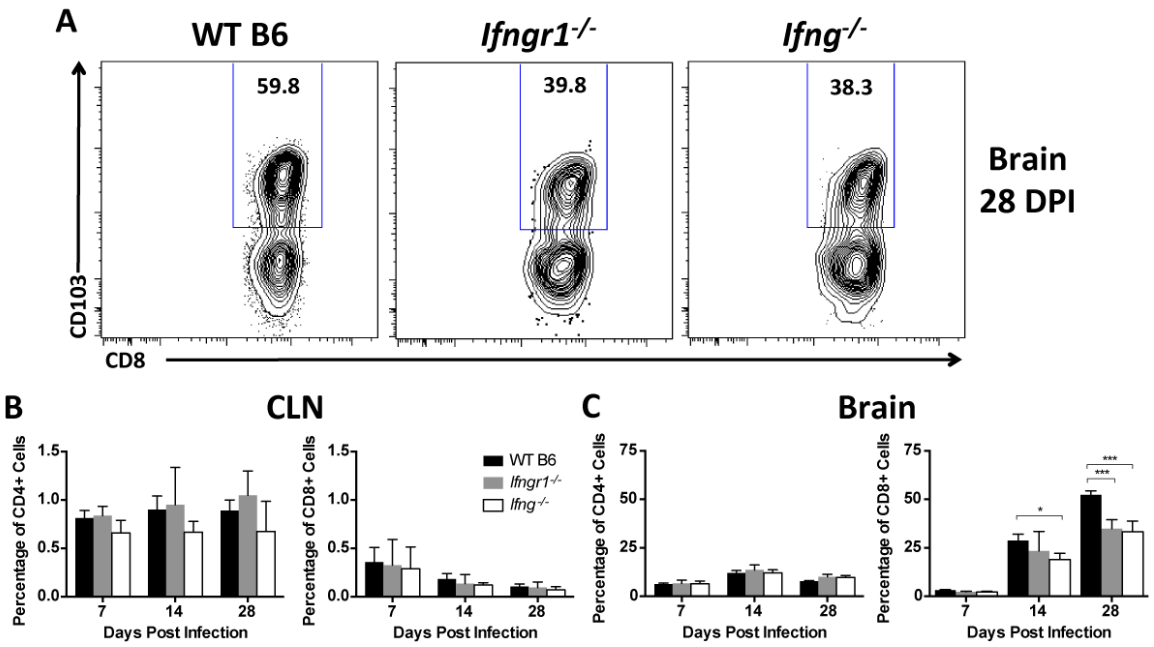

Figure 5-4. Effect of IFN-γ signaling on T_{RM} cell populations. Flow cytometry was used to examine T_{RM} cell populations by gating around CD103+ cells (**A**) at 7, 14, and 28 DPI in the CLNs (**B**) and brains (**C**) of WT B6 (black bars), *Ifngr1*$^{-/-}$ (gray bars), and *Ifng*$^{-/-}$ (white bars) mice, and results are presented as a percentage of CD4+ (left graphs) and CD8+ T cells (right graphs) (n = 2-7 pooled mice per strain per time point from three to four independent experiments; data presented as the mean ± SEM; *$p < 0.05$, ***$p < 0.001$ by Tukey's multiple comparisons test).

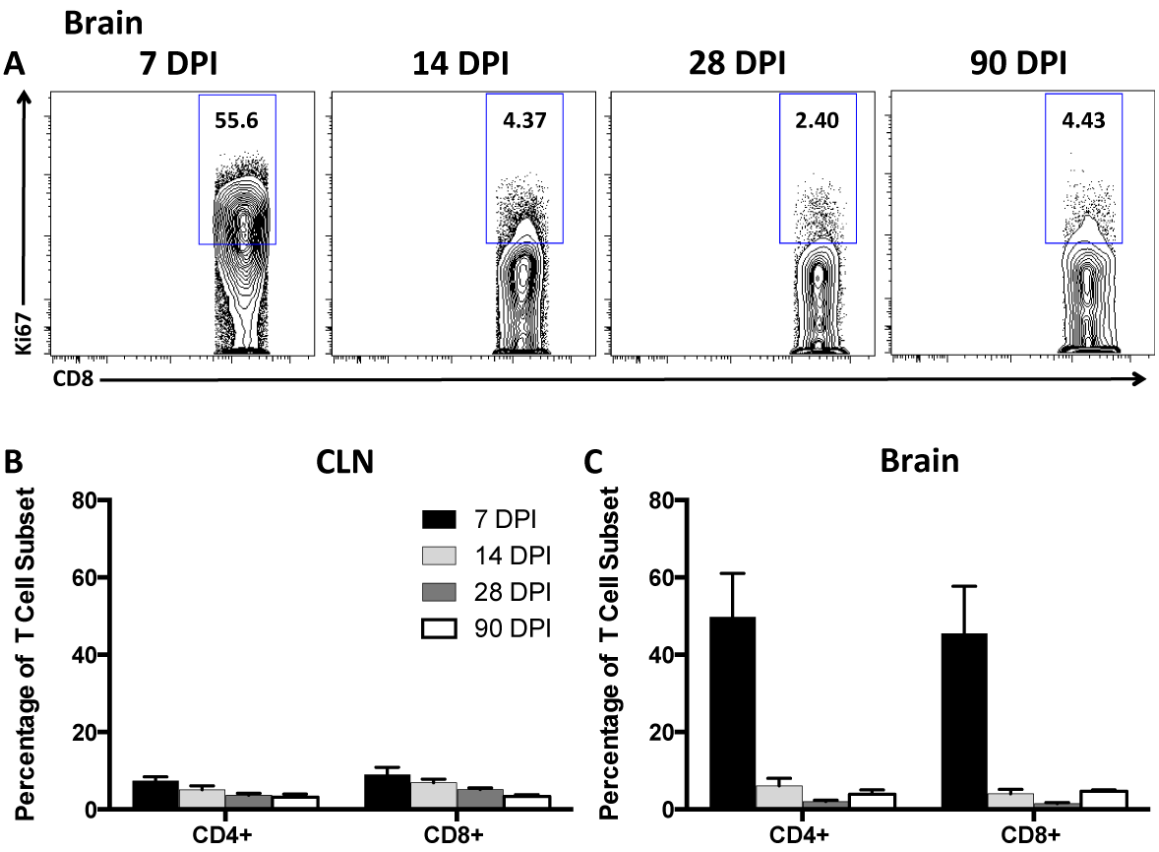

Figure 5-5. Proliferation of T cells in CLNs and brains throughout the course of SINV infection. Flow cytometry was used to evaluate T cell proliferation by gating around Ki67+ cells (**A**) in WT B6 mouse CLNs (**B**) and brains (**C**) at 7 (black bars), 14 (light gray bars), 28 (dark gray bars), and 90 (white bars) DPI, with results presented as a percentage of CD4+ or CD8+ T cells (n = 3-10 pooled mice per time point from three independent experiments; data presented as the mean ± SEM).

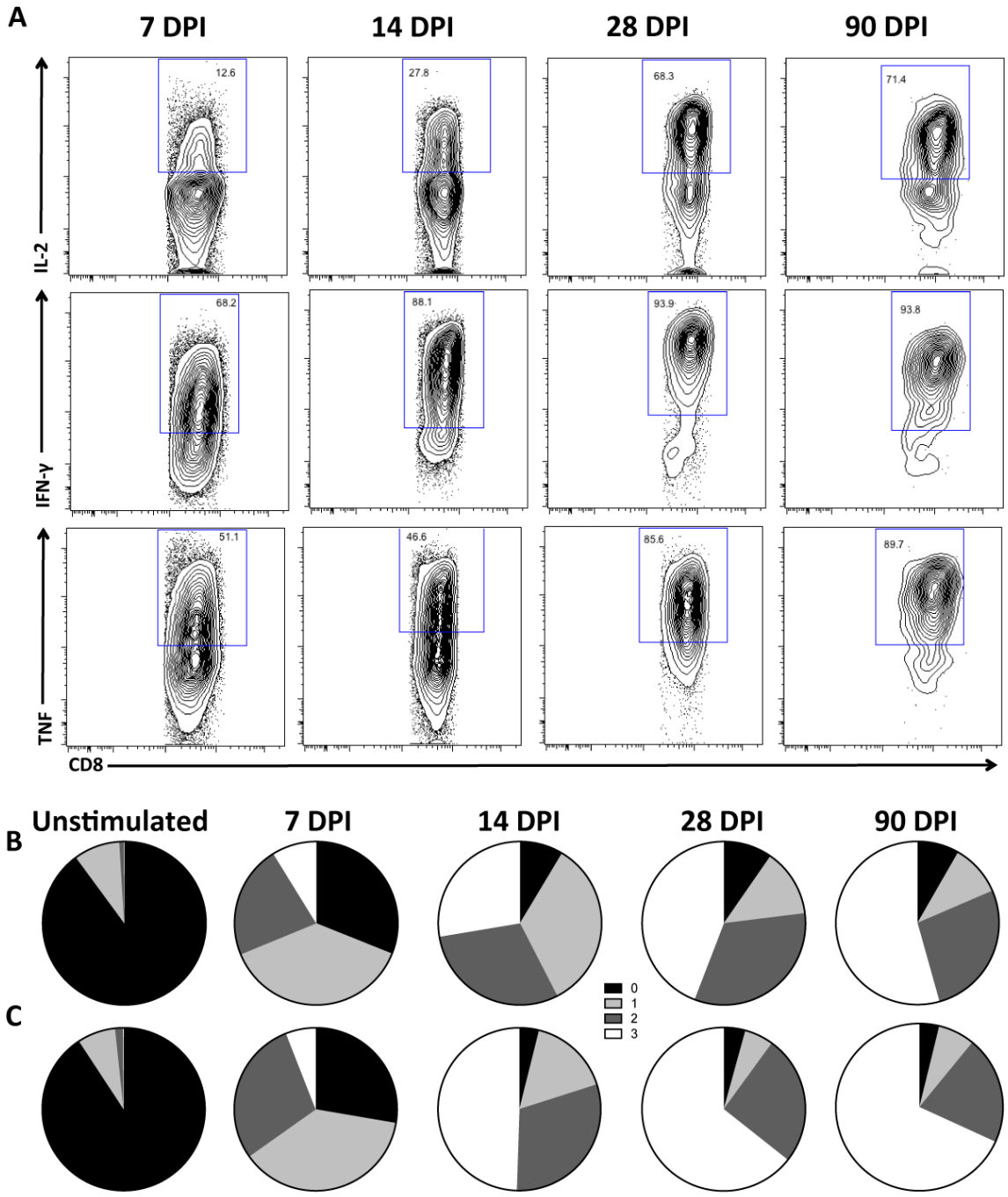

Figure 5-6. Polyfunctionality of T cells in the brain during SINV infection. (**A**) Flow cytometry was used to evaluate the production of IL-2, IFN-γ, and TNF-α by T cells in SINV-infected WT B6 mouse brains at 7, 14, 28, and 90 DPI after being stimulated with PMA and ionomycin. (**B, C**) Boolean gating was used to determine whether stimulated

CD4+ (**B**) and CD8+ (**C**) T cells were producing none of the cytokines (black), or one (light gray), two (dark gray), or all three (white) of the cytokines at each time point, with unstimulated cells from SINV-infected brains provided as a reference (n = 3-10 pooled mice per time point from three independent experiments; data presented as the mean ± SEM).

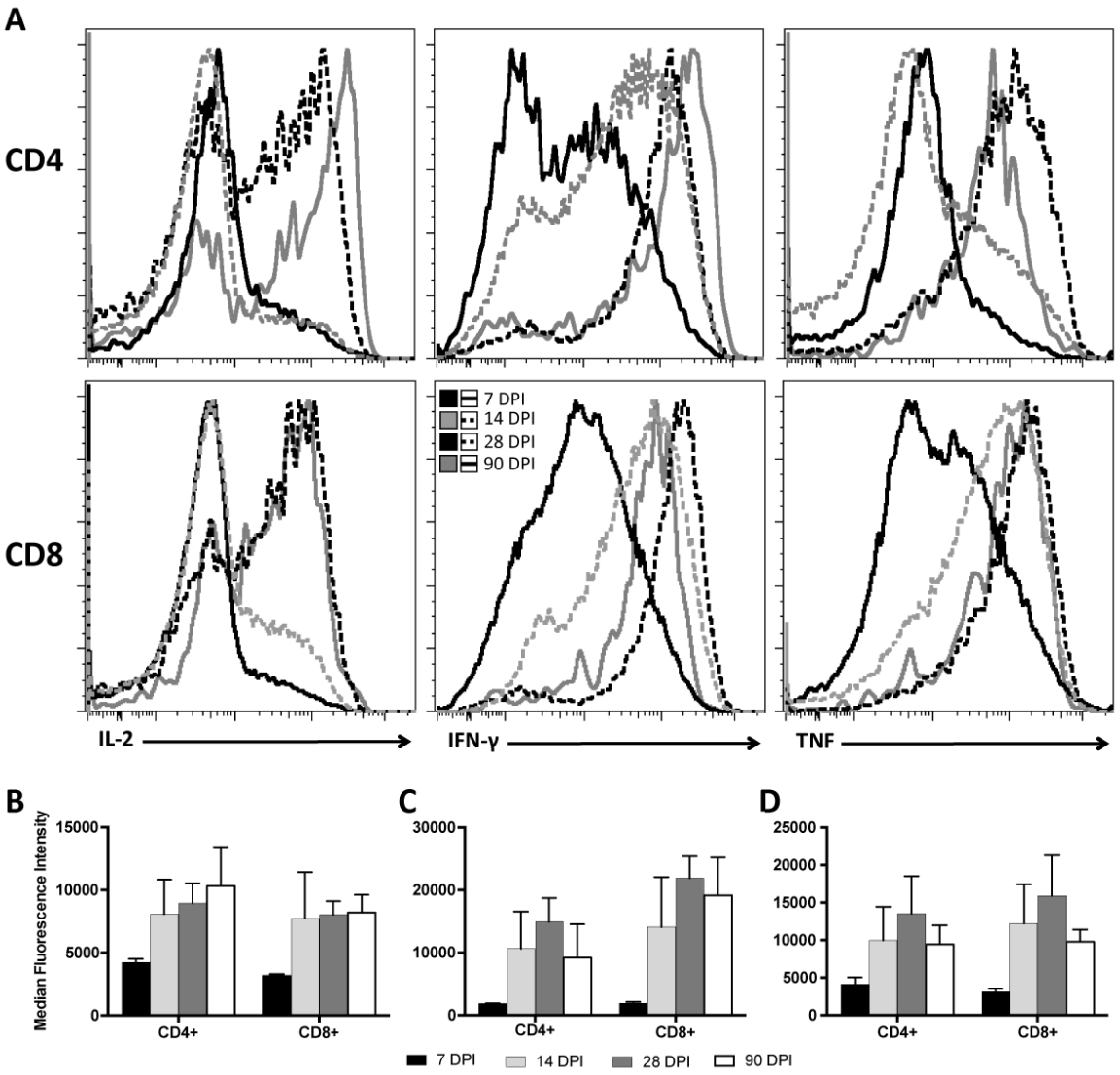

Figure 5-7. Effector function of T cells during SINV infection. (**A**) Histograms of IL-2, IFN-γ, and TNF-α fluorescence of CD4+ and CD8+ T cells in WT B6 mouse brains that indicate how much of each cytokine individual cells were producing at 7 (black solid line), 14 (gray dashed line), 28 (black dashed line), and 90 (gray solid line) DPI. (**B-D**) The MFI was calculated for IL-2 (**B**), IFN-γ (**C**), and TNF-α (**D**) produced by CD4+ and CD8+ T cells at 7 (black bars), 14 (light gray bars), 28 (dark gray bars), and 90 (white bars) DPI (n = 3-10 pooled mice per time point from three independent experiments; data presented as the mean ± SEM).

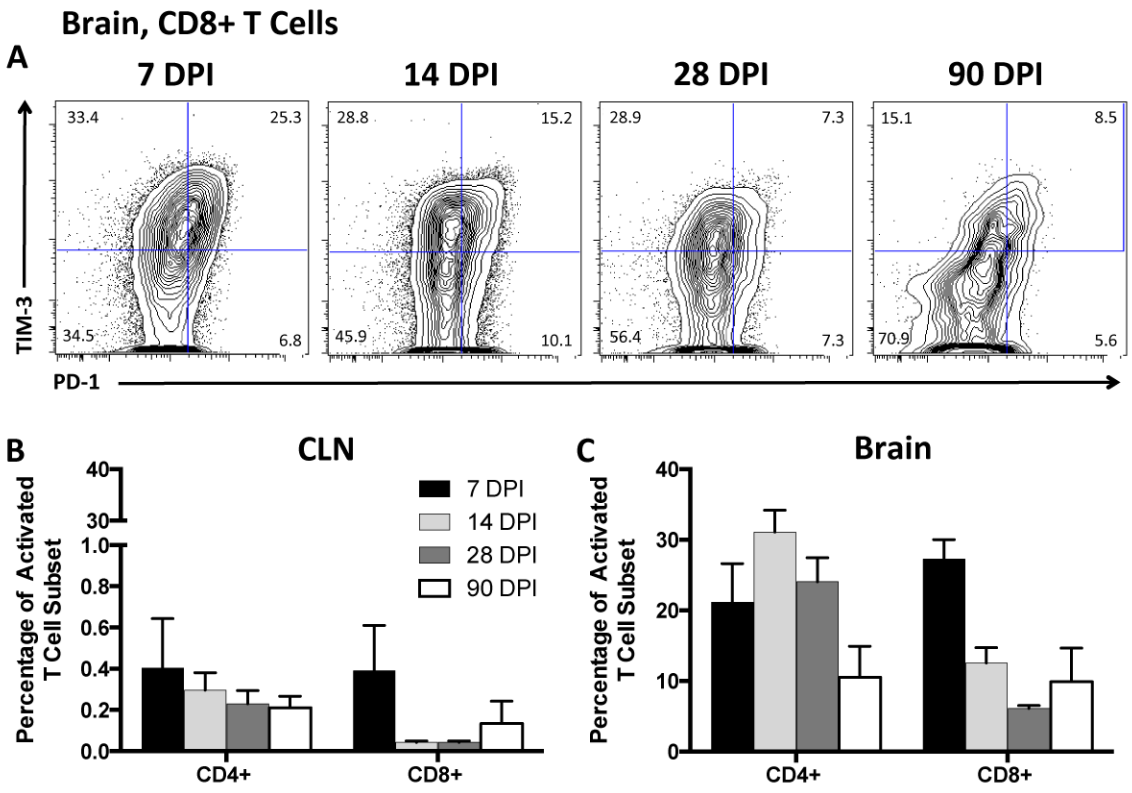

Figure 5-8. T cell exhaustion during SINV infection. Flow cytometry was used to evaluate T cell exhaustion identifying cells expressing both PD-1 and TIM-3 (**A**) in WT B6 mouse CLNs (**B**) and brains (**C**) at 7 (black bars), 14 (light gray bars), 28 (dark gray bars), and 90 (white bars) DPI. Results were presented as a percentage of CD4+ and CD8+ T cells that are PD-1+TIM-3+ (n = 3-7 pooled mice per time point from three independent experiments; data presented as the mean ± SEM).

CHAPTER 6:

GENERAL DISCUSSION AND CONCLUSIONS

The immune system presents a double-edged sword regarding virus infection of the CNS: an adequate immune response is necessary for control and clearance of the virus, yet cytokine production and cytotoxic activity of infiltrating immune cells can cause neuronal damage and death. Because neurons have limited regenerative capacity, loss of this valuable cell population results in neurological deficits. Mice experimentally infected with viruses including TMEV, influenza, and dengue virus or protozoal parasites including *Toxoplasma gondii* develop neurocognitive deficits such as impaired memory or increased anxiety[167-169,348-351]. In our studies, SINV infection resulted in development of disinhibition and hippocampus-dependent memory deficits, which correlated with inflammation and cell death in the brain.

The immune response is well established to mediate most of the CNS pathology observed during fatal alphavirus encephalomyelitis[41,54,56]. In our mouse model of nonfatal alphavirus encephalomyelitis, treatment with a glutamine anatagonist, which inhibits immune cell proliferation, resulted in partial prevention of neurological sequelae. Histopathologic examination resulted in markedly decreased infiltration of inflammatory cells and cell death in the brain, indicating the immune response plays an important role in pathology associated with alphavirus encephalomyelitis. Mice infected with the nonfatal TE strain of SINV develop signs of encephalomyelitis characterized by hunched posture, abnormal gait, and paresis. Inhibiting the immune response by treating mice with the glutamine antagonist DON resulted in fewer mice developing clinical signs of encephalomyelitis by 7 DPI. The findings support the detrimental role inflammation can play during neurotropic virus infection.

We similarly examined clinical disease development during SINV infection in mice deficient in IFN-γ signaling. Numerous studies have been performed to examine the effect IFN-γ signaling has on virus-induced clinical disease using mice deficient in IFN-γ (*Ifng*$^{-/-}$) or IFN-γ receptor (*Ifngr1*$^{-/-}$). Increased mortality is seen in *Ifngr1*$^{-/-}$ or *Ifng*$^{-/-}$ mice during CNS infection with viruses such as JHMV, LCMV, and TMEV[98,292,352,353]. In experimental allergic encephalomyelitis (EAE) and in JHMV-induced autoimmune demyelinating encephalomyelitis, absence of IFN-γ signaling results in more severe demyelinating disease and increased lymphocyte infiltration[354-356]. When mice deficient in both IFN-α/β and IFN-γ receptor are infected with dengue virus, they are significantly more susceptible to developing lethal paralysis and systemic disease than mice deficient in IFN-α/β receptor alone[357]. Infection with other pathogens that do not necessarily target the CNS, such as JHMV, influenza virus, pseudorabies virus (PRV), monkeypox virus, *Mycobacterium bovis*, *Listeria monocytogenes*, and *Leishmania major* also results in more severe clinical disease and/or increased mortality in *Ifngr1*$^{-/-}$ and/or *Ifng*$^{-/-}$ mice[358-363]. Furthermore, neutralization of gamma interferon production in influenza virus-infected mice results in increased weight loss[364]. These studies all indicate that IFN-γ is protective against pathogen-induced clinical disease.

In contrast, in our studies, *Ifngr1*$^{-/-}$ and *Ifng*$^{-/-}$ mice actually lost significantly less weight than WT B6 mice before recovering, indicating that IFN-γ actually exacerbates clinical disease during nonfatal alphavirus encephalomyelitis. The weight loss is likely directly due to decreased feed intake by WT B6 mice relative to *Ifngr1*$^{-/-}$ and *Ifng*$^{-/-}$ mice, but the reason why IFN-γ signaling leads to decreased food consumption remains unknown. *Ifng*$^{-/-}$ mice infected with the Sarafend strain of WNV are protected from

developing limbic seizures in contrast to WT B6 mice[365]. When these mice are treated with seizure-inducing NMDA or kainic acid, seizure responses are diminished or absent compared to WT B6 mice, indicating that IFN-γ plays an important role in regulating the excitatory seizure pathway. Glutamate is the major excitatory neurotransmitter that binds to NMDA and kainic acid receptors (in addition to AMPA receptors), and excitotoxicity induced by glutamate plays a major role in SINV-induced pathology[49,65,366]. In the CNS, IFN-γ receptor complexes with AMPA receptor subunit GluR1 on neurons, forming dendritic beads[367]. Through Jak/STAT signaling via the chimeric receptor, increased calcium influx stimulates nitric oxide production, inducing neuronal toxicity. In contrast, IFN-γ is reported to provide a protective effect against glutamate excitotoxicity in hippocampal neurons during dietary restriction[368]. The potential role IFN-γ-enhanced excitotoxicity plays in alphavirus infection warrants further investigation.

As the quintessential proinflammatory cytokine, IFN-γ plays a multifactorial role in modulation of the immune response during infection. Different virus infections elicit diverse T cell responses via IFN-γ signaling. Increased mortality in *Ifngr1*$^{-/-}$ and *Ifng*$^{-/-}$ mice during EAE is attributed to IFN-γ-mediated suppression of the CD4+ T cell response, which facilitates EAE-induced pathology[369]. When mice are infected with a recombinant rabies virus encoding IFN-γ, fewer CD8+ T cells infiltrate the cortex and cerebellum[370]. Additionally, CD8+ T cells are increased in *Ifng*$^{-/-}$ mice infected with vaccinia virus[371], supporting our finding of *Ifngr1*$^{-/-}$ and *Ifng*$^{-/-}$ mice having more CD8+ T cells in the brain at 7 DPI. The mechanism by which IFN-γ decreases cytotoxic lymphocyte generation is thought to be by limiting IL-2 production, creating a negative feedback loop[358,372]. In our studies, at least at the mRNA level, IL-2 production was not

decreased in WT B6 mouse brains relative to *Ifngr1*$^{-/-}$ and *Ifng*$^{-/-}$ mice during SINV infection. Alternatively, mouse mammary tumor virus (MMTV) infection of *Ifngr1*$^{-/-}$ mice results in no change in CD8+ T cell, CD4+ T cell, or B cell numbers in lymph nodes, nor any difference in virus titers[373], and *Ifng*$^{-/-}$ mice show no difference in CD4 or CD8 T cells in the spinal cord following infection with TMEV[98].

Because neurons are a valuable yet finite and nonrenewable cell population, a noncytolytic mechanism for clearance is essential to maintain neurological integrity. Previous studies have shown that along with anti-SINV antibody, IFN-γ plays an important role in clearance of SINV from neurons and the CNS[24,92,93]. Work from other groups has shown that IFN-γ plays a vital role in the clearance of many different neurotropic virus and bacterial infections, including neurotropic MHV, borna disease virus, HSV, WNV, and *Listeria monocytogenes*[374-378]. As part of this thesis work, we found that IFN-γ affects each of the three major steps of SINV clearance and control (Fig 6-1). First, IFN-γ facilitates infectious virus clearance through, at least in part, modulation of local production of anti-SINV antibody in the CNS. Second, viral RNA clearance is affected by IFN-γ, possibly through its influence on the T cell response in the CNS. And finally, IFN-γ promotes the development of CD8+ T_{RM} cells in the brain throughout Phase 2 of infection, likely helping prevent reactivation of persistent virus.

Antibody is necessary for successful clearance of several viruses, including respiratory syncytial virus, norovirus, hemagglutinating encephalomyelitis virus, MPyV, and rabies virus[379-384]. We found that compared to mice with intact IFN-γ signaling, *Ifngr1*$^{-/-}$ and *Ifng*$^{-/-}$ mice had reduced IgM and IgG production in the brain following SINV infection. This was despite comparable levels of IgM and IgG in the serum, which

has similarly been found in *Ifngr1*$^{-/-}$ and/or *Ifng*$^{-/-}$ mice during SINV and TMEV infection[70,98]. IgG2a and IgG2b in particular were decreased in mice with impaired IFN-γ signaling. During JEV infection, *Ifng*$^{-/-}$ mice have reduced production of IgG2a in response to vaccination, and the IgG2a/c, rather than IFN-γ, confers protection against virus infection[385]. Of the IgG subclasses, IgG2a is most effective at fixing complement and binding to FcγR receptor on macrophages[386,387]. Taken together, these findings suggest IFN-γ enhances anti-SINV antibody-mediated clearance of virus.

In addition to decreased IgM and IgG production in the brain, *Ifngr1*$^{-/-}$ and *Ifng*$^{-/-}$ mice had reduced infiltration of B cells at 7 and 10 DPI compared to WT B6. This was despite comparable numbers of B cells in the CLNs. Previous studies have shown that SINV-specific ASCs infiltrate the brain during SINV infection and serve as the source of local anti-SINV antibody production[91]. Increases in mRNA expression of CXCL9 and CXCL10 has been associated with B cell recruitment to the brain during SINV infection, and increases in CXCL13 mRNA expression is associated with local formation of B cell follicles. All three of these chemokines are induced by IFN-γ and were reduced in mice with impaired IFN-γ signaling. Therefore, IFN-γ signaling promotes the expression of B cell migratory and maintenance chemokines in the brain during SINV infection. This in turn leads to increased infiltration of B cells producing anti-SINV antibodies. Through this mechanism, IFN-γ is able to facilitate clearance of infectious virus from the CNS (Fig 6-1).

Considerably less is known about what factors facilitate viral RNA clearance. When IFN-γ is applied to measles virus-infected brain explant slices, clearance of viral RNA is achieved in the absence of primed leukocytes via the Jak/STAT pathway[100].

Furthermore, when measles virus-primed leukocytes are applied to organotypic explants infected with WNV or MHV, viral RNA of each resident virus is completely eliminated, indicating IFN-γ-mediated viral RNA clearance is antigen-independent. Our *in vitro* findings that IFN-γ is sufficient for clearing SINV RNA from dAP-7 cells corroborate these results. However, when examining IFN-γ-mediated clearance of SINV RNA *in vivo*, we found the opposite effect, with initiation of viral RNA clearance actually accelerated in *Ifngr1*$^{-/-}$ and *Ifng*$^{-/-}$ mice. These findings indicate that influences outside of the neuron were affecting viral RNA clearance, leading us to examine the immune system, particular the T cell response.

In addition to overall increases in CD8+ T cell numbers in the brain at 7 DPI, mice with impaired IFN-γ signaling had more CD8+ T cells producing granzyme B and more granzyme B being produced by individual CD8+ T cells compared to mice with intact IFN-γ signaling. Similarly, more perforin has been detected in brains of *Ifngr1*$^{-/-}$ and *Ifng*$^{-/-}$ mice infected with SINV NSV[269], indicating during SINV infection, IFN-γ inhibits the granzyme-perforin exocytosis pathway by some mechanism. The noncytotoxic functions of granzyme B are becoming increasingly recognized, and this effector protein is no longer considered to exclusively induce cell death upon entry into a recipient cell[296]. Furthermore, several substrates recently identified for granzyme B bind RNA, including viral RNA, allowing for nucleic acid destruction in the absence of neuron death[388]. Therefore, we propose that granzyme B promotes clearance of viral RNA in a non-cytotoxic fashion (Fig 6-1). This mechanism provides an explanation for *Ifngr1*$^{-/-}$ and *Ifng*$^{-/-}$ mice showing accelerated viral RNA clearance from the CNS, despite

IFN-γ being sufficient to clear viral RNA in neurons. Further studies examining the role granzyme B plays in RNA virus clearance are warranted.

Persistent viral RNA from positive-sense RNA viruses presents a potential problem, as the infectious nature of the RNA allows for possible virus reactivation and relapse of disease. When SCID mice are passively transferred hyperimmune serum or monoclonal antibody directed against SINV, they are able to clear both infectious virus and viral RNA[24]. However, when those antibodies are allowed to naturally decay, virus reactivates, indicating that replication-competent viral RNA persists[43]. Viral RNA and/or antigen persistence has been reported following both natural and experimental CNS infection with several flaviviruses and alphaviruses[42,43,389-392]. Virus persistence in acute CNS infections can lead to reactivation, causing neurological signs following apparent recovery, or induce an autoimmune MS-like response through mechanisms such as molecular mimicry or bystander activation[393,394]. Furthermore, latent viruses, such as HSV-1, can reactivate upon exposure to stressors that compromise T cell function[395]. Persistent virus is found in the arthralgic and arthritic alphaviruses such as CHIKV and Ross river virus and is thought to influence chronic arthralgia[7,396-399].

Prevention of virus reactivation is likely achieved through continued presence of immune cells at the previous site of infection[91,400]. Over the course of SINV infection, the primary T cell population in the brain changed from short-term effector T cells (T_{EFF}) to memory T cells, and a small but robust population of CD8+ tissue resident memory T (T_{RM}) cells formed in the brain. T_{RM} cells are phenotypically and functionally distinct from circulating effector memory T (T_{EM}) cells[345]. Upon antigen reactivation, T_{RM} cells produce near-sterilizing immunity by rapidly inducing both the innate and adaptive

immune response, including dendritic cell maturation, NK cell activation, and local antibody production[121]. CD8+ T_{RM} cells present in the respiratory airway following infection with influenza or Sendai virus are able to produce IFN-γ faster than systemic T_{EM} cells, leading to a rapid antigen-dependent decrease in virus replication upon reactivation[331]. While granzyme B production must be induced in T_{EM} cells, T_{RM} cells constitutively produce it, allowing them to deliver immediate effector activity to combat virus[117]. This presents another avenue by which granzyme B may be examined during SINV infection.

The percentage of CD8+ T cells expressing CD103, a marker for T_{RM} cells was decreased in *Ifngr1*$^{-/-}$ and *Ifng*$^{-/-}$ mice during Phase 2 of infection. IFN-γ produced by CD4+ T cells is necessary for generation of lung resident T_{RM} cells following influenza virus infection[329]. As *Ifngr1*$^{-/-}$ and *Ifng*$^{-/-}$ mice cannot produce/respond to IFN-γ and have fewer CD4+ T cells in the brain at 10 DPI compared to WT B6 mice, this provides a possible mechanism for IFN-γ-mediated promotion of CD8+ T_{RM} cell formation in the brain. The reduced CD8+ T_{RM} cell population in mice with impaired IFN-γ signaling could lead in an impaired response to possible virus reactivation. Circulating T_{EM} cells cannot access trigeminal ganglia latently infected with HSV-1, and so T_{RM} cells are responsible for reactivation prevention through the secretion of IFN-γ and noncytotoxic lytic granules[316,401-404]. Indeed, during Phase 3 of infection, transient increases in viral RNA were seen in SINV-infected mice, particularly in *Ifng*$^{-/-}$ brains and spinal cords. Promotion of CD8+ T_{RM} cell development in the brain following Phase 1 of infection provides another mechanism by which IFN-γ controls SINV infection. Therefore, not

only does IFN-γ facilitate clearance of infectious virus and viral RNA, but it also appears to contribute to virus reactivation control (Fig 6-1).

During chronic virus infections, constant exposure to viral antigen leads to T cell exhaustion, exemplified by decreased effector function and increased expression of inhibitory markers[146]. Interestingly, as the course of SINV infection progressed, T cells actually increased in polyfunctionality and production of IFN-γ, TNF-α, and IL-2 effector cytokines and decreased expression of PD-1 and TIM-3 exhaustion markers. This suggests that resident T cells in the brain are not being constantly exposed to virus antigen in a way that induces exhaustion. Our current understanding of the replication competency of SINV RNA is extremely limited. However, during Phase 3 of infection, transient increases in RNA levels were occasionally seen, particularly in the spinal cords of *Ifng*$^{-/-}$ mice, suggesting that viral RNA is capable of replication leading to virus reactivation and requires diligent immune surveillance and control. Further studies examining the nature of viral RNA persistence represent an important avenue to explore in order to better understand immune control of SINV infection.

While most parameters differing between mice with intact and impaired IFN-γ signaling during SINV infection were shared between *Ifngr1*$^{-/-}$ and *Ifng*$^{-/-}$ mice, some virus or immune characteristics only differed in one of the strains (Table 6-1). Most studies in the literature examining the *in vivo* effect of IFN-γ on virus infection utilize either *Ifngr1*$^{-/-}$ or *Ifng*$^{-/-}$ mice, rather than both strains. Previous work on the alphavirus encephalomyelitis mouse model using the neurovirulent NSV strain revealed differing inflammatory responses in *Ifngr1*$^{-/-}$ and *Ifng*$^{-/-}$ mice, including more severe inflammation and increased MHC Class II and *Il17a* expression in *Ifngr1*$^{-/-}$ mice[269]. Similarly disease

severity is increased in *Ifngr1*$^{-/-}$, but not *Ifng*$^{-/-}$, mice infected with vaccinia virus and HSV-1[289]. However, in the previous study, no difference in virus replication was found between *Ifngr1*$^{-/-}$ and *Ifng*$^{-/-}$ mice, while in the current study, *Ifng*$^{-/-}$ showed increased infectious virus and viral RNA at 1 DPI, and both *Ifngr1*$^{-/-}$ and *Ifng*$^{-/-}$ mice showed delayed clearance of infectious virus from the spinal cord. These studies highlight that *Ifngr1*$^{-/-}$ and *Ifng*$^{-/-}$ mice may not necessarily produce the same immune response to virus infection and should therefore not be considered equivalent.

Collectively, the studies presented in this thesis contribute to the understanding of the immunopathogenesis and immune control of alphavirus infection in the CNS. The immune response, particularly IFN-γ, plays a multi-faceted role in the clearance and control of SINV infection. However, as proven by inhibition of the T and B cell response by glutamine antagonism, the immune response is also responsible for the majority of the clinical disease and CNS pathologic changes induced during infection. Understanding the interplay between virus control and tissue damage induced by the immune response is critical for optimal development of potential therapeutics for nonfatal alphavirus encephalomyelitis.

FIGURES

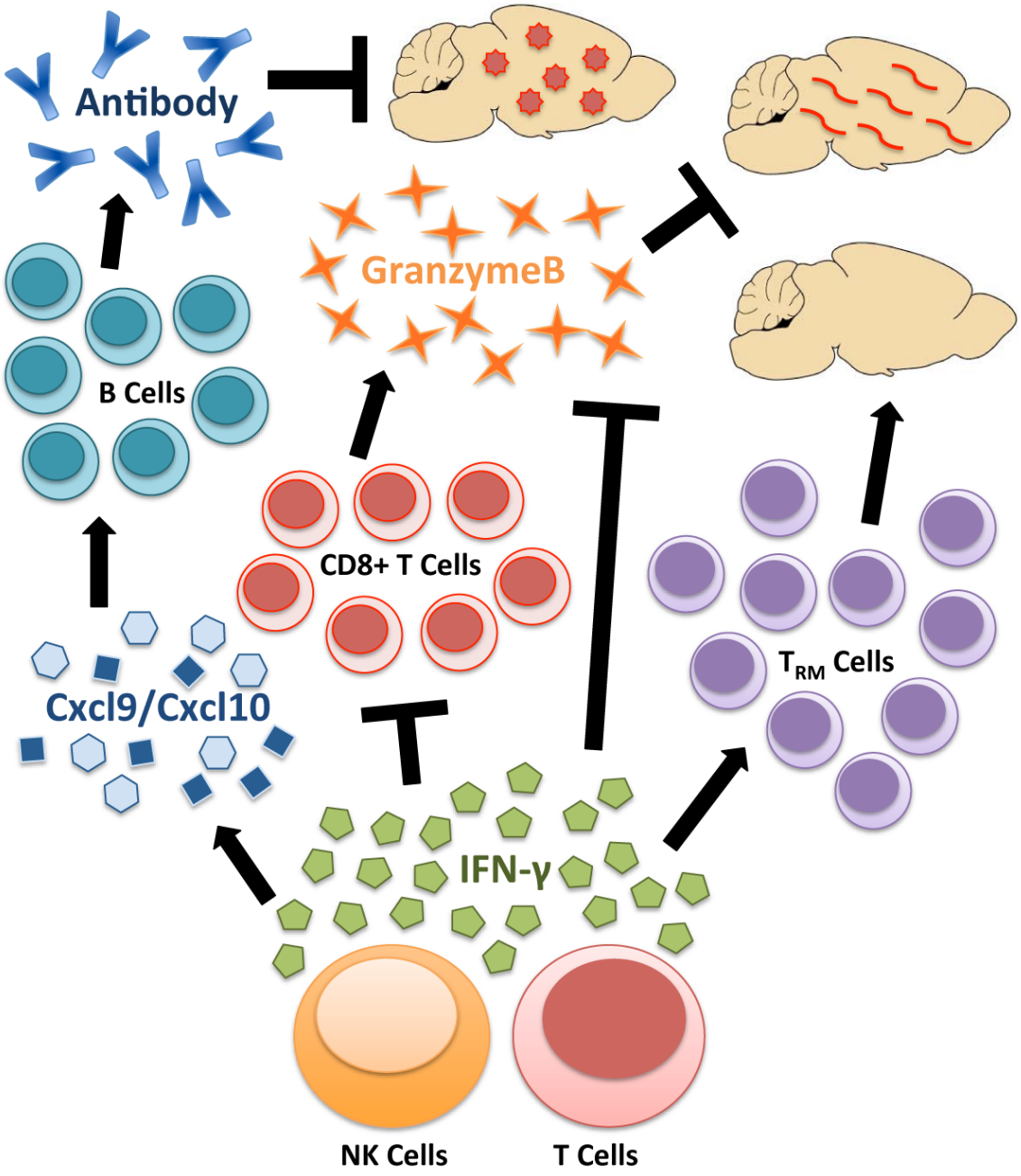

Figure 6-1. Proposed effects of IFN-γ signaling-induced immunomodulation on SINV clearance and control in the CNS. During SINV infection, IFN-γ is primarily produced by NK cells and T cells. IFN-γ signaling upregulates mRNA expression of chemokines CXCL9 and CXCL10, which promote infiltration of B cells into the brain

and local production of SINV-specific antibody. This antibody then inhibits production and promotes clearance of infectious SINV. IFN-γ signaling also inhibits infiltration of CD8+ T cells into the brain and production of granzyme B by CD8+ T cells, which inhibits SINV RNA production in the brain. IFN-γ signaling affects long-term control of SINV and prevents virus reactivation by promoting the development of CD8+ T_{RM} cells in the brain.

TABLES

Unique to *Ifngr1*$^{-/-}$ Mice	Unique to *Ifng*$^{-/-}$ Mice
Faster recovery from clinical disease ↑ *Il17a* expression ↑ IL-17a	↑ Viral RNA in the brain at 1 DPI ↑ Early expression of type I IFNs ↑ *Ccl1* expression ↓ *Il10* expression ↓ *Il2* expression ↓ Il-4
Shared by *Ifngr1*$^{-/-}$ and *Ifng*$^{-/-}$ Mice	
Accelerated development of clinical disease ↓ Weight loss Delayed infectious virus clearance in the spinal cord Faster initiation of viral RNA clearance in the brain and spinal cord ↓ Induction of *Gbp2* and *Irgm1* expression ↓ Expression of proinflammatory cytokines *Tnf, Csf2,* and *Il6* ↓ Expression of *Cxcl9, Cxcl10,* and *Cxcl13* ↓ Expression of PRR mRNAs ↓ CD4+ T cells ↑ CD8+ T cells ↑ Granzyme B ↓ B cells Less prolonged local production of IgM ↓ IgG2a and IgG2b ↓ CD8+ T_{RM} cells	

Table 6-1. Characteristics related to SINV infection in the CNS unique to each knockout mouse strain and shared by both *Ifngr1*$^{-/-}$ and *Ifng*$^{-/-}$ mice compared to WT B6 mice

APPENDICES

APPENDIX A

Gene	SINV Alone, 24 HPI vs Mock Infection	SINV + IFN-γ vs Mock Infection	SINV Alone, 27 HPI vs SINV Alone, 24 HPI	Mock + IFN-γ vs Mock Infection	SINV + IFN-γ vs Mock + IFN-γ	SINV + IFN-γ vs SINV Alone, 27 HPI
A2m	<±1.5	<±1.5	<±1.5	1.52	<±1.5	<±1.5
A3galt2	<±1.5	-2.25	<±1.5	<±1.5	-2.35	<±1.5
Abca1	<±1.5	-1.96	<±1.5	-1.58	<±1.5	<±1.5
Abcb4	2.10	2.24	<±1.5	<±1.5	2.06	<±1.5
Abo2	<±1.5	1.94	<±1.5	<±1.5	<±1.5	<±1.5
Acat2	<±1.5	<±1.5	<±1.5	<±1.5	<±1.5	1.88
Acot12	<±1.5	<±1.5	<±1.5	<±1.5	1.52	<±1.5
Actb	<±1.5	-1.73	<±1.5	<±1.5	-1.77	<±1.5
Adamts1	<±1.5	-2.74	-1.61	<±1.5	-1.89	<±1.5
Adamts5	<±1.5	-2.11	-1.57	<±1.5	<±1.5	<±1.5
Adar	<±1.5	<±1.5	<±1.5	1.66	<±1.5	<±1.5
Adm	-1.68	-3.18	<±1.5	-1.60	-1.98	<±1.5
Adora1	<±1.5	1.93	<±1.5	<±1.5	<±1.5	<±1.5
Adrb2	<±1.5	<±1.5	-1.78	<±1.5	<±1.5	<±1.5
Aer61	<±1.5	<±1.5	<±1.5	<±1.5	-1.61	<±1.5
Afap1	<±1.5	<±1.5	<±1.5	<±1.5	-1.63	<±1.5
Ak2	<±1.5	<±1.5	<±1.5	1.56	-1.65	<±1.5
Ak3l1	<±1.5	-1.80	<±1.5	<±1.5	-2.27	<±1.5
Akap2	<±1.5	<±1.5	<±1.5	1.68	-1.55	<±1.5
Akr1b8	-1.55	<±1.5	<±1.5	<±1.5	-1.67	<±1.5
Amacr	<±1.5	<±1.5	<±1.5	<±1.5	-1.54	<±1.5
Amd1	<±1.5	<±1.5	<±1.5	<±1.5	-1.64	<±1.5
Ampd1	1.55	1.72	<±1.5	<±1.5	<±1.5	<±1.5
Angpt1	<±1.5	<±1.5	<±1.5	<±1.5	-1.67	<±1.5
Angptl2	<±1.5	-1.86	<±1.5	<±1.5	-1.81	<±1.5
Ankrd1	-1.56	-2.87	<±1.5	-3.33	<±1.5	<±1.5
Anxa1	<±1.5	<±1.5	<±1.5	<±1.5	-1.62	<±1.5
Anxa11	<±1.5	<±1.5	<±1.5	<±1.5	-1.55	<±1.5
Apaf1	<±1.5	<±1.5	<±1.5	<±1.5	-1.61	<±1.5
Apol3	<±1.5	<±1.5	<±1.5	9.38	<±1.5	2.66
Apol9a	<±1.5	2.06	<±1.5	4.21	-2.04	<±1.5
Apold1	<±1.5	<±1.5	<±1.5	<±1.5	<±1.5	-1.56
Arg1	<±1.5	<±1.5	<±1.5	<±1.5	-1.57	<±1.5

Gene	SINV Alone, 24 HPI vs Mock Infection	SINV + IFN-γ vs Mock Infection	SINV Alone, 27 HPI vs SINV Alone, 24 HPI	Mock + IFN-γ vs Mock Infection	SINV + IFN-γ vs Mock + IFN-γ	SINV + IFN-γ vs SINV Alone, 27 HPI
Arhgap24	<±1.5	-1.77	<±1.5	<±1.5	-1.64	<±1.5
Arhgap29	<±1.5	<±1.5	<±1.5	1.51	-1.66	<±1.5
Arhgdib	<±1.5	<±1.5	<±1.5	<±1.5	-1.83	<±1.5
Arl6ip5	<±1.5	<±1.5	<±1.5	1.55	<±1.5	<±1.5
Arrdc3	<±1.5	-2.57	<±1.5	<±1.5	-1.73	-1.61
Asl	<±1.5	<±1.5	<±1.5	1.63	<±1.5	<±1.5
Asph	<±1.5	<±1.5	<±1.5	<±1.5	-2.11	<±1.5
Aste1	<±1.5	<±1.5	<±1.5	<±1.5	<±1.5	-1.56
Atf3	2.40	3.41	<±1.5	2.76	<±1.5	<±1.5
Atp2b1	<±1.5	<±1.5	<±1.5	<±1.5	-1.52	<±1.5
Atp2b4	<±1.5	<±1.5	<±1.5	1.61	<±1.5	<±1.5
Atp6v0e1	<±1.5	<±1.5	<±1.5	<±1.5	-1.64	<±1.5
Atp6v1b2	<±1.5	<±1.5	<±1.5	1.74	-1.74	<±1.5
Avpr1a	<±1.5	-1.77	<±1.5	<±1.5	<±1.5	<±1.5
B2m	<±1.5	<±1.5	<±1.5	1.63	<±1.5	<±1.5
B3galnt1	<±1.5	-1.69	<±1.5	<±1.5	-2.25	<±1.5
Baiap2	<±1.5	1.61	<±1.5	<±1.5	<±1.5	<±1.5
Bak1	<±1.5	<±1.5	<±1.5	1.86	-1.60	<±1.5
Bche	<±1.5	<±1.5	1.50	<±1.5	<±1.5	<±1.5
Bdh1	<±1.5	<±1.5	<±1.5	<±1.5	-1.57	<±1.5
Bet1l	<±1.5	<±1.5	<±1.5	<±1.5	-1.70	<±1.5
Bglap	<±1.5	<±1.5	<±1.5	<±1.5	1.71	1.69
Birc2	<±1.5	<±1.5	<±1.5	1.66	<±1.5	<±1.5
Bmp4	<±1.5	-2.77	<±1.5	<±1.5	-1.98	<±1.5
Bmpr1a	<±1.5	-1.85	<±1.5	<±1.5	-1.88	<±1.5
Bmpr1b	<±1.5	<±1.5	<±1.5	1.76	-1.52	<±1.5
Btg1	<±1.5	<±1.5	<±1.5	<±1.5	-1.68	<±1.5
Btg2	<±1.5	-2.28	<±1.5	<±1.5	-1.76	<±1.5
Cacng3	<±1.5	<±1.5	<±1.5	<±1.5	1.59	<±1.5
Casp1	<±1.5	<±1.5	<±1.5	1.89	<±1.5	<±1.5
Casp12	<±1.5	<±1.5	<±1.5	1.98	<±1.5	<±1.5
Casp2	<±1.5	-1.71	<±1.5	<±1.5	-1.57	<±1.5
Casp3	<±1.5	<±1.5	<±1.5	<±1.5	-1.57	<±1.5
Cbr1	<±1.5	<±1.5	<±1.5	<±1.5	-2.17	<±1.5

Gene	SINV Alone, 24 HPI vs Mock Infection	SINV + IFN-γ vs Mock Infection	SINV Alone, 27 HPI vs SINV Alone, 24 HPI	Mock + IFN-γ vs Mock Infection	SINV + IFN-γ vs Mock + IFN-γ	SINV + IFN-γ vs SINV Alone, 27 HPI
Ccl2	<±1.5	<±1.5	<±1.5	1.87	-1.65	<±1.5
Ccl5	2.22	2.94	<±1.5	<±1.5	2.28	<±1.5
Ccl7	<±1.5	<±1.5	<±1.5	2.72	-2.35	<±1.5
Ccr1	<±1.5	<±1.5	<±1.5	2.48	-1.74	<±1.5
Cd14	<±1.5	<±1.5	<±1.5	<±1.5	-2.04	<±1.5
Cd151	<±1.5	-1.68	<±1.5	<±1.5	-1.83	<±1.5
Cd44	<±1.5	<±1.5	<±1.5	<±1.5	-1.57	<±1.5
Cd48	<±1.5	-1.76	<±1.5	<±1.5	-1.82	<±1.5
Cd80	<±1.5	-1.91	-1.57	<±1.5	<±1.5	<±1.5
Cd82	<±1.5	<±1.5	<±1.5	<±1.5	-1.54	<±1.5
Cd97	<±1.5	<±1.5	1.54	<±1.5	<±1.5	<±1.5
Cdc123	<±1.5	<±1.5	<±1.5	<±1.5	-1.52	<±1.5
Cdc25a	<±1.5	<±1.5	<±1.5	<±1.5	-1.58	<±1.5
Cdc26	<±1.5	-1.72	<±1.5	<±1.5	-1.94	<±1.5
Cdc42se1	<±1.5	-1.70	<±1.5	<±1.5	<±1.5	<±1.5
Cdon	<±1.5	-1.69	<±1.5	<±1.5	<±1.5	<±1.5
Cflar	<±1.5	<±1.5	<±1.5	1.65	-1.65	<±1.5
Chac2	<±1.5	<±1.5	-1.63	<±1.5	<±1.5	<±1.5
Chn1	<±1.5	<±1.5	<±1.5	<±1.5	1.50	<±1.5
Cited1	1.64	<±1.5	<±1.5	<±1.5	<±1.5	-1.63
Clcn5	<±1.5	-2.24	<±1.5	<±1.5	-1.73	<±1.5
Cldnd1	<±1.5	-1.65	<±1.5	<±1.5	-1.61	<±1.5
Clic2	<±1.5	1.58	<±1.5	2.37	-1.50	1.70
Cndp2	<±1.5	<±1.5	<±1.5	1.83	-1.51	<±1.5
Cnksr2	<±1.5	<±1.5	<±1.5	-1.74	1.70	<±1.5
Cnksr3	<±1.5	<±1.5	<±1.5	-1.57	<±1.5	<±1.5
Cnot6	<±1.5	<±1.5	<±1.5	<±1.5	-1.54	<±1.5
Col1a2	<±1.5	<±1.5	<±1.5	<±1.5	-1.59	<±1.5
Col3a1	<±1.5	-1.81	<±1.5	<±1.5	<±1.5	<±1.5
Crkrs	<±1.5	<±1.5	<±1.5	<±1.5	-1.52	<±1.5
Crygc	<±1.5	<±1.5	<±1.5	<±1.5	<±1.5	1.68
Csf1	<±1.5	-1.66	<±1.5	<±1.5	-2.28	<±1.5
Csnk1g1	<±1.5	<±1.5	<±1.5	<±1.5	-1.52	<±1.5
Ctgf	-1.92	-3.17	<±1.5	<±1.5	-2.54	<±1.5

Gene	SINV Alone, 24 HPI vs Mock Infection	SINV + IFN-γ vs Mock Infection	SINV Alone, 27 HPI vs SINV Alone, 24 HPI	Mock + IFN-γ vs Mock Infection	SINV + IFN-γ vs Mock + IFN-γ	SINV + IFN-γ vs SINV Alone, 27 HPI
Ctss	<±1.5	1.68	<±1.5	<±1.5	1.82	<±1.5
Cx3cl1	<±1.5	1.64	<±1.5	2.17	<±1.5	<±1.5
Cx3cr1	<±1.5	<±1.5	-1.58	<±1.5	<±1.5	<±1.5
Cxadr	<±1.5	<±1.5	<±1.5	-2.10	<±1.5	<±1.5
Cxcl1	<±1.5	-2.70	<±1.5	-2.26	<±1.5	-1.53
Cxcl10	3.03	7.43	<±1.5	12.91	-1.74	2.23
Cxcl11	<±1.5	7.01	<±1.5	10.77	<±1.5	2.51
Cxcl12	-1.58	<±1.5	<±1.5	<±1.5	-1.53	<±1.5
Cxcl9	<±1.5	12.55	<±1.5	39.34	-3.13	6.14
Cxcr7	<±1.5	<±1.5	<±1.5	<±1.5	-2.32	<±1.5
Cyb5d2	<±1.5	-1.77	<±1.5	<±1.5	<±1.5	<±1.5
Cyp1b1	<±1.5	1.78	<±1.5	2.69	-1.51	<±1.5
Cyr61	-2.08	-3.22	<±1.5	<±1.5	-2.90	<±1.5
Dbnl	<±1.5	<±1.5	<±1.5	1.55	<±1.5	<±1.5
Dcbld2	<±1.5	<±1.5	<±1.5	<±1.5	-1.64	<±1.5
Degs1	<±1.5	<±1.5	<±1.5	<±1.5	-1.60	<±1.5
Dhrs7b	<±1.5	-1.81	<±1.5	<±1.5	-1.75	<±1.5
Dnajb9	<±1.5	-1.66	<±1.5	<±1.5	<±1.5	<±1.5
Dnase1l1	<±1.5	<±1.5	<±1.5	<±1.5	-1.76	<±1.5
Dusp1	-2.21	-5.13	-1.79	<±1.5	-3.38	<±1.5
Dusp6	<±1.5	-2.25	<±1.5	<±1.5	<±1.5	<±1.5
Dyrk1a	<±1.5	<±1.5	<±1.5	<±1.5	-1.59	<±1.5
Ebna1bp2	<±1.5	1.59	<±1.5	<±1.5	<±1.5	<±1.5
Edn1	<±1.5	-3.71	-2.91	<±1.5	-3.19	<±1.5
Ednra	<±1.5	<±1.5	<±1.5	<±1.5	-1.61	<±1.5
Egr2	<±1.5	<±1.5	<±1.5	<±1.5	2.08	<±1.5
Egr3	<±1.5	<±1.5	<±1.5	1.60	<±1.5	<±1.5
Eif2ak3	<±1.5	-2.21	<±1.5	<±1.5	-2.04	<±1.5
Eif4a2	<±1.5	-1.73	<±1.5	<±1.5	<±1.5	<±1.5
Emp1	<±1.5	-1.76	<±1.5	<±1.5	-2.62	<±1.5
Enc1	<±1.5	<±1.5	<±1.5	1.57	<±1.5	<±1.5
Ensa	<±1.5	-2.97	<±1.5	<±1.5	-2.56	-1.79
Ero1l	<±1.5	<±1.5	<±1.5	<±1.5	-1.67	<±1.5
Expi	<±1.5	1.80	<±1.5	2.43	<±1.5	<±1.5

Gene	SINV Alone, 24 HPI vs Mock Infection	SINV + IFN-γ vs Mock Infection	SINV Alone, 27 HPI vs SINV Alone, 24 HPI	Mock + IFN-γ vs Mock Infection	SINV + IFN-γ vs Mock + IFN-γ	SINV + IFN-γ vs SINV Alone, 27 HPI
Extl3	<±1.5	-1.81	<±1.5	<±1.5	-1.94	<±1.5
F3	<±1.5	<±1.5	<±1.5	<±1.5	-2.12	<±1.5
Fabp3	<±1.5	-1.71	<±1.5	<±1.5	-1.77	<±1.5
Fam103a1	<±1.5	-1.70	<±1.5	<±1.5	-1.70	<±1.5
Fam110c	<±1.5	<±1.5	<±1.5	<±1.5	1.65	1.52
Fam26e	<±1.5	<±1.5	<±1.5	<±1.5	-1.64	<±1.5
Fam33a	<±1.5	-3.89	<±1.5	<±1.5	<±1.5	<±1.5
Fam70a	<±1.5	1.61	<±1.5	<±1.5	1.89	<±1.5
Fam71f1	<±1.5	<±1.5	<±1.5	1.78	-1.51	<±1.5
Fam82a2	<±1.5	<±1.5	<±1.5	1.65	<±1.5	<±1.5
Fam96a	<±1.5	-1.68	<±1.5	<±1.5	-1.79	<±1.5
Fas	<±1.5	<±1.5	<±1.5	<±1.5	-1.54	<±1.5
Fat3	<±1.5	-1.88	<±1.5	<±1.5	<±1.5	<±1.5
Fbn1	<±1.5	<±1.5	<±1.5	1.66	-2.06	<±1.5
Fbxo30	<±1.5	1.52	<±1.5	<±1.5	<±1.5	<±1.5
Fgf7	<±1.5	-4.82	<±1.5	-2.75	-1.94	<±1.5
Fgf9	1.52	<±1.5	<±1.5	<±1.5	<±1.5	<±1.5
Fhl4	<±1.5	<±1.5	<±1.5	<±1.5	1.65	<±1.5
Figf	<±1.5	-1.76	<±1.5	<±1.5	<±1.5	<±1.5
Fntb	<±1.5	<±1.5	<±1.5	<±1.5	-1.62	<±1.5
Fosl1	<±1.5	1.52	<±1.5	<±1.5	<±1.5	<±1.5
Foxb1	<±1.5	1.61	<±1.5	<±1.5	1.70	<±1.5
Foxq1	<±1.5	2.23	<±1.5	<±1.5	<±1.5	1.61
Fst	<±1.5	<±1.5	<±1.5	<±1.5	-1.58	<±1.5
Fzd2	<±1.5	<±1.5	<±1.5	<±1.5	<±1.5	1.58
Fzd9	<±1.5	<±1.5	1.77	<±1.5	<±1.5	<±1.5
G3bp2	<±1.5	-1.74	<±1.5	<±1.5	-1.58	<±1.5
Gadd45a	<±1.5	<±1.5	<±1.5	-1.56	1.57	<±1.5
Gadd45b	1.71	2.16	<±1.5	1.81	<±1.5	<±1.5
Galnt7	<±1.5	-2.14	<±1.5	-1.54	<±1.5	<±1.5
Gbp2	1.70	7.46	<±1.5	18.71	-2.51	4.18
Gclm	<±1.5	<±1.5	<±1.5	1.57	-1.78	<±1.5
Gcnt2	<±1.5	-2.29	<±1.5	<±1.5	-2.05	<±1.5
Gcom1	<±1.5	<±1.5	<±1.5	1.53	<±1.5	<±1.5

Gene	SINV Alone, 24 HPI vs Mock Infection	SINV + IFN-γ vs Mock Infection	SINV Alone, 27 HPI vs SINV Alone, 24 HPI	Mock + IFN-γ vs Mock Infection	SINV + IFN-γ vs Mock + IFN-γ	SINV + IFN-γ vs SINV Alone, 27 HPI
Gja1	<±1.5	-1.69	<±1.5	<±1.5	<±1.5	<±1.5
Gja4	<±1.5	<±1.5	<±1.5	3.48	<±1.5	<±1.5
Gja5	<±1.5	<±1.5	<±1.5	<±1.5	-1.88	<±1.5
Glrx1	<±1.5	<±1.5	<±1.5	1.85	-2.09	<±1.5
Glt8d1	<±1.5	<±1.5	<±1.5	<±1.5	-1.65	<±1.5
Gmfb	<±1.5	-1.73	<±1.5	<±1.5	-1.81	<±1.5
Gna13	<±1.5	<±1.5	<±1.5	2.13	<±1.5	<±1.5
Golph3l	<±1.5	-1.72	-1.87	<±1.5	<±1.5	<±1.5
Grb2	<±1.5	<±1.5	<±1.5	<±1.5	1.83	1.52
Grip1	<±1.5	<±1.5	<±1.5	1.55	<±1.5	<±1.5
Grk5	<±1.5	-1.73	<±1.5	<±1.5	-1.57	<±1.5
Gsta2	<±1.5	<±1.5	<±1.5	<±1.5	<±1.5	-1.90
Gstm1	<±1.5	-1.65	<±1.5	<±1.5	-1.78	<±1.5
Gstm2	<±1.5	-1.66	<±1.5	<±1.5	-1.78	<±1.5
Gstm4	<±1.5	<±1.5	<±1.5	<±1.5	-2.01	<±1.5
Gstp1	<±1.5	<±1.5	<±1.5	<±1.5	-1.55	<±1.5
Gtf2a1	1.59	1.74	<±1.5	<±1.5	<±1.5	<±1.5
Guca2a	<±1.5	<±1.5	<±1.5	<±1.5	<±1.5	-1.63
Gzmb	<±1.5	<±1.5	<±1.5	6.37	<±1.5	<±1.5
H2-M10.6	<±1.5	<±1.5	<±1.5	<±1.5	<±1.5	1.58
H2-T24	<±1.5	<±1.5	<±1.5	<±1.5	<±1.5	-2.35
Has2	<±1.5	<±1.5	2.22	<±1.5	-2.04	-1.84
Hbegf	<±1.5	<±1.5	<±1.5	<±1.5	<±1.5	-1.79
Hbp1	<±1.5	-2.02	<±1.5	<±1.5	-1.59	<±1.5
Hcn2	<±1.5	<±1.5	<±1.5	<±1.5	1.52	<±1.5
Hdgfrp2	<±1.5	1.55	<±1.5	<±1.5	1.57	<±1.5
Herpud1	<±1.5	-1.71	<±1.5	<±1.5	<±1.5	<±1.5
Higd1a	<±1.5	<±1.5	<±1.5	<±1.5	-1.66	<±1.5
Hist1h1t	<±1.5	<±1.5	<±1.5	<±1.5	<±1.5	-1.55
Hivep2	<±1.5	<±1.5	1.71	2.21	-1.53	<±1.5
Hk2	<±1.5	<±1.5	<±1.5	1.69	-2.17	<±1.5
Hmgcr	<±1.5	-1.89	<±1.5	<±1.5	-2.04	<±1.5
Hmgcs1	<±1.5	-1.78	<±1.5	<±1.5	-2.21	-1.58
Hmox1	-1.81	<±1.5	<±1.5	1.96	-3.10	<±1.5

Gene	SINV Alone, 24 HPI vs Mock Infection	SINV + IFN-γ vs Mock Infection	SINV Alone, 27 HPI vs SINV Alone, 24 HPI	Mock + IFN-γ vs Mock Infection	SINV + IFN-γ vs Mock + IFN-γ	SINV + IFN-γ vs SINV Alone, 27 HPI
Hnrnpa1	<±1.5	<±1.5	<±1.5	<±1.5	-1.65	<±1.5
Hnrnpa3	-2.55	<±1.5	<±1.5	<±1.5	<±1.5	1.92
Hnrnph2	-1.60	-1.89	<±1.5	<±1.5	-2.12	<±1.5
Hoxa1	<±1.5	<±1.5	<±1.5	<±1.5	1.83	<±1.5
Hpcal1	<±1.5	<±1.5	<±1.5	1.62	<±1.5	<±1.5
Hrsp12	<±1.5	-1.72	<±1.5	<±1.5	<±1.5	<±1.5
Hsd17b1	<±1.5	1.54	<±1.5	<±1.5	<±1.5	<±1.5
Hspa13	<±1.5	-1.77	<±1.5	<±1.5	-1.78	<±1.5
Hspa14	<±1.5	<±1.5	<±1.5	<±1.5	-1.53	<±1.5
Hspa5	<±1.5	-2.00	<±1.5	<±1.5	-2.00	<±1.5
Hspb1	<±1.5	<±1.5	<±1.5	<±1.5	-1.61	<±1.5
Hspb8	<±1.5	<±1.5	<±1.5	1.94	<±1.5	<±1.5
Htr2a	<±1.5	-1.93	<±1.5	<±1.5	-1.64	-1.99
Htr2b	<±1.5	-2.34	<±1.5	<±1.5	<±1.5	<±1.5
Id3	<±1.5	<±1.5	<±1.5	1.97	-2.96	<±1.5
Ier3	-1.79	-2.22	<±1.5	<±1.5	-2.07	<±1.5
Ifi47	<±1.5	21.82	<±1.5	66.98	-3.07	23.65
Ifit1	2.41	4.11	<±1.5	3.64	<±1.5	<±1.5
Ifit3	2.44	2.41	<±1.5	1.80	<±1.5	<±1.5
Il18bp	<±1.5	<±1.5	<±1.5	1.63	<±1.5	<±1.5
Il1a	<±1.5	<±1.5	<±1.5	2.81	<±1.5	<±1.5
Il1r1	<±1.5	-2.08	<±1.5	<±1.5	-2.02	-1.56
Il1rap	<±1.5	<±1.5	<±1.5	1.81	-1.59	<±1.5
Il33	<±1.5	-1.94	<±1.5	<±1.5	-1.89	<±1.5
Il6	<±1.5	-4.49	-2.10	-2.05	-2.19	<±1.5
Il7	<±1.5	1.77	<±1.5	<±1.5	<±1.5	1.53
Il7	<±1.5	<±1.5	<±1.5	<±1.5	<±1.5	1.53
Inhba	<±1.5	-1.88	<±1.5	<±1.5	<±1.5	<±1.5
Inpp1	<±1.5	<±1.5	<±1.5	<±1.5	-1.65	<±1.5
Insig2	<±1.5	-1.70	<±1.5	<±1.5	-1.55	<±1.5
Insl6	<±1.5	<±1.5	<±1.5	<±1.5	<±1.5	-1.66
Ip6k2	<±1.5	-2.03	<±1.5	<±1.5	-1.57	<±1.5
Ireb2	<±1.5	-2.07	<±1.5	<±1.5	-2.16	<±1.5
Irf1	<±1.5	3.36	<±1.5	8.91	-2.66	3.61

Gene	SINV Alone, 24 HPI vs Mock Infection	SINV + IFN-γ vs Mock Infection	SINV Alone, 27 HPI vs SINV Alone, 24 HPI	Mock + IFN-γ vs Mock Infection	SINV + IFN-γ vs Mock + IFN-γ	SINV + IFN-γ vs SINV Alone, 27 HPI
Irf9	<±1.5	<±1.5	<±1.5	2.37	-1.78	1.66
Irgm	<±1.5	6.55	<±1.5	23.71	-3.62	5.49
Irs3	<±1.5	1.55	<±1.5	<±1.5	<±1.5	<±1.5
Itga1	<±1.5	<±1.5	<±1.5	<±1.5	-1.73	<±1.5
Jag1	<±1.5	-2.21	<±1.5	-1.56	<±1.5	<±1.5
Kars	<±1.5	<±1.5	<±1.5	1.50	<±1.5	<±1.5
Kcne3	<±1.5	<±1.5	<±1.5	<±1.5	<±1.5	-1.59
Kcnj16	<±1.5	-2.15	<±1.5	<±1.5	<±1.5	-2.33
Kcns2	<±1.5	2.02	<±1.5	<±1.5	<±1.5	<±1.5
Kdm3a	<±1.5	<±1.5	<±1.5	<±1.5	-1.78	<±1.5
Klf6	<±1.5	-2.19	<±1.5	<±1.5	-2.63	<±1.5
Klhdc3	<±1.5	-1.74	<±1.5	<±1.5	-1.60	<±1.5
Klhl24	<±1.5	-1.83	<±1.5	-1.64	<±1.5	<±1.5
Klrc3	<±1.5	2.96	<±1.5	<±1.5	<±1.5	<±1.5
Kng1l1	<±1.5	<±1.5	<±1.5	<±1.5	<±1.5	-2.42
Kprp	<±1.5	-1.88	-1.62	<±1.5	<±1.5	<±1.5
Laptm4b	<±1.5	-1.96	<±1.5	<±1.5	-1.97	<±1.5
Lbp	<±1.5	<±1.5	<±1.5	<±1.5	-1.68	<±1.5
Lgmn	<±1.5	-1.68	<±1.5	<±1.5	-1.67	<±1.5
Lgr4	<±1.5	-2.04	<±1.5	<±1.5	-2.05	<±1.5
Lipogenin	<±1.5	-1.86	<±1.5	<±1.5	<±1.5	<±1.5
Lmo4	1.52	<±1.5	<±1.5	1.58	<±1.5	<±1.5
Lnpep	<±1.5	<±1.5	<±1.5	<±1.5	-1.66	<±1.5
LOC100125371	<±1.5	-1.94	<±1.5	<±1.5	<±1.5	<±1.5
LOC287167	<±1.5	<±1.5	<±1.5	<±1.5	2.25	<±1.5
LOC288913	<±1.5	<±1.5	<±1.5	<±1.5	<±1.5	1.60
LOC305691	<±1.5	<±1.5	<±1.5	<±1.5	1.99	<±1.5
LOC362921	<±1.5	<±1.5	<±1.5	<±1.5	1.76	1.70
LOC494539	<±1.5	<±1.5	1.55	<±1.5	<±1.5	<±1.5
LOC619574	<±1.5	<±1.5	<±1.5	<±1.5	-1.73	<±1.5
LOC690784	<±1.5	<±1.5	<±1.5	<±1.5	<±1.5	-1.64
Lpar3	<±1.5	<±1.5	<±1.5	<±1.5	<±1.5	-1.73
Lpcat3	<±1.5	<±1.5	<±1.5	<±1.5	-1.76	<±1.5
Lphn2	<±1.5	<±1.5	<±1.5	<±1.5	-1.57	<±1.5

Gene	SINV Alone, 24 HPI vs Mock Infection	SINV + IFN-γ vs Mock Infection	SINV Alone, 27 HPI vs SINV Alone, 24 HPI	Mock + IFN-γ vs Mock Infection	SINV + IFN-γ vs Mock + IFN-γ	SINV + IFN-γ vs SINV Alone, 27 HPI
Lum	-2.01	-4.16	<±1.5	<±1.5	-3.88	<±1.5
Ly49i3	<±1.5	<±1.5	<±1.5	<±1.5	<±1.5	1.77
Ly6c	<±1.5	<±1.5	-1.61	<±1.5	<±1.5	<±1.5
Mafk	<±1.5	1.80	<±1.5	<±1.5	<±1.5	<±1.5
Map2k1ip1	<±1.5	<±1.5	<±1.5	<±1.5	-1.53	<±1.5
Mapk14	<±1.5	<±1.5	<±1.5	<±1.5	-1.62	<±1.5
Mapk6	<±1.5	-2.19	<±1.5	<±1.5	-1.83	<±1.5
Mat2a	<±1.5	<±1.5	<±1.5	<±1.5	<±1.5	-2.25
Mcfd2	<±1.5	-1.67	<±1.5	<±1.5	-1.94	<±1.5
Metrn	<±1.5	<±1.5	<±1.5	<±1.5	1.56	<±1.5
Mfap3	<±1.5	-2.15	<±1.5	<±1.5	-2.11	-2.02
MGC105649	<±1.5	5.80	1.56	17.16	-2.96	4.05
MGC108823	<±1.5	10.79	1.63	44.23	-4.10	7.19
MGC108974	<±1.5	<±1.5	1.84	<±1.5	<±1.5	-1.52
Mid1	<±1.5	<±1.5	<±1.5	-1.60	<±1.5	<±1.5
Minpp1	<±1.5	-1.74	<±1.5	<±1.5	-1.80	<±1.5
Mitd1	<±1.5	1.89	<±1.5	3.72	-1.97	<±1.5
Mllt11	<±1.5	<±1.5	<±1.5	-2.00	1.65	<±1.5
Mmadhc	<±1.5	-1.66	<±1.5	<±1.5	<±1.5	<±1.5
Mmgt2	<±1.5	-1.72	<±1.5	<±1.5	<±1.5	<±1.5
Mmp14	<±1.5	<±1.5	<±1.5	<±1.5	-1.54	<±1.5
Mras	<±1.5	1.56	<±1.5	2.27	<±1.5	<±1.5
mrpl11	<±1.5	<±1.5	<±1.5	<±1.5	-1.79	<±1.5
Mterf	-1.54	-1.90	<±1.5	<±1.5	-2.23	<±1.5
Mx2	1.94	2.38	<±1.5	1.64	<±1.5	<±1.5
Myd88	<±1.5	<±1.5	<±1.5	1.50	<±1.5	<±1.5
Myst2	<±1.5	<±1.5	<±1.5	<±1.5	-1.59	<±1.5
N4bp2l2	<±1.5	<±1.5	<±1.5	<±1.5	-1.78	<±1.5
N5	<±1.5	-1.87	<±1.5	<±1.5	<±1.5	<±1.5
Naaa	<±1.5	<±1.5	<±1.5	<±1.5	1.64	<±1.5
Nampt	<±1.5	1.75	<±1.5	3.95	-2.26	<±1.5
Nampt	<±1.5	<±1.5	<±1.5	<±1.5	<±1.5	<±1.5
Ndst1	<±1.5	<±1.5	<±1.5	<±1.5	-1.54	<±1.5
Nedd9	<±1.5	<±1.5	<±1.5	<±1.5	-2.12	<±1.5

Gene	SINV Alone, 24 HPI vs Mock Infection	SINV + IFN-γ vs Mock Infection	SINV Alone, 27 HPI vs SINV Alone, 24 HPI	Mock + IFN-γ vs Mock Infection	SINV + IFN-γ vs Mock + IFN-γ	SINV + IFN-γ vs SINV Alone, 27 HPI
Nid67	<±1.5	<±1.5	<±1.5	1.75	<±1.5	<±1.5
Nip7	<±1.5	<±1.5	<±1.5	<±1.5	-1.58	<±1.5
Nme7	<±1.5	-1.64	<±1.5	<±1.5	-1.63	<±1.5
Nos2	<±1.5	<±1.5	<±1.5	<±1.5	<±1.5	1.57
Npbwr1	<±1.5	<±1.5	<±1.5	<±1.5	<±1.5	2.16
Npepo	<±1.5	-1.67	<±1.5	<±1.5	<±1.5	<±1.5
Npm2	<±1.5	1.53	<±1.5	<±1.5	<±1.5	<±1.5
Nppb	<±1.5	<±1.5	<±1.5	<±1.5	<±1.5	-2.06
Nppc	<±1.5	1.70	<±1.5	<±1.5	<±1.5	<±1.5
Nr4a1	<±1.5	<±1.5	<±1.5	<±1.5	<±1.5	-1.83
Nras	<±1.5	<±1.5	<±1.5	<±1.5	-1.80	<±1.5
Nrg1	<±1.5	1.61	1.55	<±1.5	<±1.5	<±1.5
Nrp1	<±1.5	<±1.5	<±1.5	<±1.5	-1.65	<±1.5
Nub1	<±1.5	<±1.5	<±1.5	1.53	<±1.5	<±1.5
Nupr1	<±1.5	-1.76	<±1.5	<±1.5	-1.76	<±1.5
Oas1b	<±1.5	3.00	<±1.5	3.98	<±1.5	1.75
Oas1i	<±1.5	2.21	<±1.5	3.70	-1.68	1.66
Oasl	<±1.5	2.05	1.76	<±1.5	1.89	<±1.5
Oasl2	1.70	3.67	<±1.5	6.79	-1.85	1.60
Olr1	<±1.5	2.39	2.16	6.14	-2.57	<±1.5
Olr101	<±1.5	<±1.5	<±1.5	<±1.5	1.92	<±1.5
Olr1014	<±1.5	1.76	<±1.5	<±1.5	1.59	<±1.5
Olr1029	<±1.5	<±1.5	-1.71	<±1.5	<±1.5	<±1.5
Olr1065	<±1.5	<±1.5	<±1.5	<±1.5	<±1.5	-1.53
Olr1077	<±1.5	<±1.5	-2.36	<±1.5	<±1.5	2.18
Olr110	<±1.5	<±1.5	<±1.5	<±1.5	<±1.5	-1.92
Olr1108	<±1.5	<±1.5	<±1.5	<±1.5	<±1.5	1.68
Olr1111	<±1.5	<±1.5	<±1.5	<±1.5	<±1.5	-1.61
Olr1122	<±1.5	<±1.5	-2.16	<±1.5	<±1.5	<±1.5
Olr113	<±1.5	<±1.5	<±1.5	<±1.5	<±1.5	-2.58
Olr1130	<±1.5	<±1.5	<±1.5	<±1.5	1.68	<±1.5
Olr114	<±1.5	<±1.5	<±1.5	<±1.5	<±1.5	-1.63
Olr1147	<±1.5	<±1.5	<±1.5	<±1.5	<±1.5	-1.66
Olr1148	<±1.5	<±1.5	-1.78	<±1.5	<±1.5	<±1.5

Gene	SINV Alone, 24 HPI vs Mock Infection	SINV + IFN-γ vs Mock Infection	SINV Alone, 27 HPI vs SINV Alone, 24 HPI	Mock + IFN-γ vs Mock Infection	SINV + IFN-γ vs Mock + IFN-γ	SINV + IFN-γ vs SINV Alone, 27 HPI
Olr1151	<±1.5	<±1.5	<±1.5	<±1.5	1.57	<±1.5
Olr119	<±1.5	<±1.5	<±1.5	<±1.5	1.66	<±1.5
Olr1196	<±1.5	1.68	<±1.5	<±1.5	<±1.5	<±1.5
Olr1200	<±1.5	<±1.5	<±1.5	<±1.5	<±1.5	-1.57
Olr1202	<±1.5	<±1.5	-2.35	<±1.5	<±1.5	2.63
Olr1219	<±1.5	<±1.5	-1.86	<±1.5	<±1.5	<±1.5
Olr1235	<±1.5	<±1.5	<±1.5	<±1.5	<±1.5	-1.53
Olr128	<±1.5	<±1.5	<±1.5	<±1.5	<±1.5	1.55
Olr1285	<±1.5	<±1.5	<±1.5	<±1.5	<±1.5	1.86
Olr1308	<±1.5	<±1.5	2.26	<±1.5	<±1.5	<±1.5
Olr1313	-2.19	<±1.5	<±1.5	<±1.5	<±1.5	1.55
Olr1316	<±1.5	1.90	<±1.5	<±1.5	1.79	<±1.5
Olr132	<±1.5	<±1.5	<±1.5	<±1.5	<±1.5	-1.69
Olr135	<±1.5	<±1.5	<±1.5	<±1.5	<±1.5	-2.87
Olr1351	<±1.5	1.82	<±1.5	<±1.5	<±1.5	1.63
Olr1386	<±1.5	<±1.5	-1.64	<±1.5	<±1.5	<±1.5
Olr1388	<±1.5	<±1.5	-1.62	<±1.5	<±1.5	<±1.5
Olr1406	<±1.5	<±1.5	<±1.5	<±1.5	<±1.5	-2.65
Olr1442	<±1.5	<±1.5	1.51	<±1.5	<±1.5	<±1.5
Olr1448	<±1.5	<±1.5	<±1.5	<±1.5	<±1.5	2.64
Olr145	<±1.5	<±1.5	<±1.5	<±1.5	<±1.5	-1.68
Olr1450	<±1.5	<±1.5	-2.21	<±1.5	<±1.5	2.79
Olr1485	<±1.5	<±1.5	-1.86	<±1.5	<±1.5	1.80
Olr1498	<±1.5	<±1.5	<±1.5	<±1.5	2.20	1.65
Olr150	<±1.5	<±1.5	-1.70	<±1.5	<±1.5	<±1.5
Olr1529	<±1.5	<±1.5	<±1.5	<±1.5	1.79	1.92
Olr1533	<±1.5	<±1.5	<±1.5	<±1.5	<±1.5	-3.04
Olr1536	<±1.5	<±1.5	<±1.5	<±1.5	<±1.5	-1.81
Olr157	<±1.5	<±1.5	<±1.5	<±1.5	1.64	<±1.5
Olr1605	<±1.5	3.02	<±1.5	<±1.5	4.23	<±1.5
Olr1607	<±1.5	<±1.5	<±1.5	<±1.5	<±1.5	-1.74
Olr161	<±1.5	-2.35	<±1.5	-2.52	-1.64	<±1.5
Olr1625	<±1.5	<±1.5	<±1.5	<±1.5	<±1.5	1.77
Olr1639	<±1.5	<±1.5	<±1.5	<±1.5	1.79	<±1.5

Gene	SINV Alone, 24 HPI vs Mock Infection	SINV + IFN-γ vs Mock Infection	SINV Alone, 27 HPI vs SINV Alone, 24 HPI	Mock + IFN-γ vs Mock Infection	SINV + IFN-γ vs Mock + IFN-γ	SINV + IFN-γ vs SINV Alone, 27 HPI
Olr1643	<±1.5	<±1.5	<±1.5	<±1.5	<±1.5	2.08
Olr1683	<±1.5	<±1.5	<±1.5	<±1.5	<±1.5	-5.46
Olr1684	<±1.5	<±1.5	-2.17	<±1.5	<±1.5	<±1.5
Olr1690	<±1.5	<±1.5	<±1.5	<±1.5	<±1.5	1.52
Olr1705	<±1.5	<±1.5	<±1.5	<±1.5	<±1.5	2.68
Olr1736	<±1.5	<±1.5	<±1.5	<±1.5	<±1.5	-1.78
Olr175	<±1.5	<±1.5	-1.97	<±1.5	<±1.5	2.19
Olr198	<±1.5	<±1.5	<±1.5	<±1.5	1.74	<±1.5
Olr219	<±1.5	<±1.5	<±1.5	<±1.5	<±1.5	-2.19
Olr221	<±1.5	<±1.5	<±1.5	<±1.5	<±1.5	-1.83
Olr242	<±1.5	<±1.5	<±1.5	<±1.5	2.19	<±1.5
Olr302	<±1.5	<±1.5	<±1.5	<±1.5	<±1.5	-1.71
Olr311	<±1.5	<±1.5	<±1.5	<±1.5	2.07	2.25
Olr318	<±1.5	<±1.5	<±1.5	<±1.5	<±1.5	1.70
Olr329	<±1.5	<±1.5	<±1.5	<±1.5	<±1.5	2.71
Olr343	<±1.5	<±1.5	<±1.5	<±1.5	<±1.5	1.83
Olr352	<±1.5	<±1.5	<±1.5	<±1.5	<±1.5	-1.63
Olr358	<±1.5	1.55	<±1.5	<±1.5	<±1.5	<±1.5
Olr374	<±1.5	<±1.5	<±1.5	<±1.5	<±1.5	2.14
Olr376	<±1.5	<±1.5	-1.72	<±1.5	<±1.5	1.72
Olr380	<±1.5	<±1.5	-1.74	<±1.5	<±1.5	2.53
Olr387	<±1.5	<±1.5	2.57	<±1.5	<±1.5	-2.56
Olr404	<±1.5	<±1.5	<±1.5	<±1.5	<±1.5	-1.62
Olr413	<±1.5	<±1.5	-1.73	<±1.5	<±1.5	<±1.5
Olr422	<±1.5	<±1.5	<±1.5	<±1.5	<±1.5	-1.90
Olr427	<±1.5	<±1.5	<±1.5	<±1.5	2.11	<±1.5
Olr47	<±1.5	<±1.5	<±1.5	<±1.5	<±1.5	1.66
Olr514	<±1.5	<±1.5	<±1.5	<±1.5	<±1.5	-1.68
Olr527	<±1.5	<±1.5	-2.32	<±1.5	<±1.5	<±1.5
Olr53	<±1.5	<±1.5	-1.99	<±1.5	<±1.5	<±1.5
Olr530	<±1.5	<±1.5	<±1.5	<±1.5	<±1.5	-2.03
Olr537	<±1.5	<±1.5	<±1.5	<±1.5	<±1.5	-2.05
Olr545	<±1.5	<±1.5	<±1.5	<±1.5	<±1.5	-1.69
Olr602	<±1.5	<±1.5	<±1.5	<±1.5	<±1.5	-2.41

Gene	SINV Alone, 24 HPI vs Mock Infection	SINV + IFN-γ vs Mock Infection	SINV Alone, 27 HPI vs SINV Alone, 24 HPI	Mock + IFN-γ vs Mock Infection	SINV + IFN-γ vs Mock + IFN-γ	SINV + IFN-γ vs SINV Alone, 27 HPI
Olr607	<±1.5	<±1.5	<±1.5	<±1.5	<±1.5	1.54
Olr677	<±1.5	<±1.5	<±1.5	<±1.5	1.66	<±1.5
Olr678	<±1.5	<±1.5	-1.64	<±1.5	<±1.5	1.74
Olr705	<±1.5	<±1.5	<±1.5	<±1.5	<±1.5	1.51
Olr710	<±1.5	<±1.5	<±1.5	<±1.5	2.39	<±1.5
Olr737	<±1.5	<±1.5	-1.81	<±1.5	<±1.5	<±1.5
Olr748	<±1.5	<±1.5	-1.75	<±1.5	<±1.5	<±1.5
Olr756	<±1.5	<±1.5	-1.74	<±1.5	<±1.5	<±1.5
Olr796	<±1.5	<±1.5	-2.33	<±1.5	<±1.5	<±1.5
Olr801	<±1.5	<±1.5	<±1.5	<±1.5	<±1.5	1.71
Olr823	<±1.5	<±1.5	<±1.5	<±1.5	<±1.5	1.93
Olr828	<±1.5	<±1.5	-1.66	<±1.5	<±1.5	<±1.5
Olr838	<±1.5	<±1.5	<±1.5	<±1.5	3.75	<±1.5
Olr857	<±1.5	<±1.5	2.07	<±1.5	<±1.5	-1.62
Olr862	<±1.5	<±1.5	-2.19	<±1.5	<±1.5	<±1.5
Olr920	<±1.5	<±1.5	1.81	<±1.5	<±1.5	1.74
Omd	<±1.5	-2.10	<±1.5	<±1.5	-2.24	<±1.5
Osmr	<±1.5	<±1.5	<±1.5	1.71	-1.62	<±1.5
Parp3	<±1.5	<±1.5	<±1.5	1.61	<±1.5	<±1.5
Pcdhb15	<±1.5	<±1.5	<±1.5	<±1.5	<±1.5	-1.55
Pcdhb19	<±1.5	-1.69	<±1.5	<±1.5	<±1.5	<±1.5
Pdcd10	<±1.5	<±1.5	<±1.5	<±1.5	-1.55	<±1.5
Pde4b	<±1.5	-1.76	<±1.5	-1.62	<±1.5	<±1.5
Pdgfa	<±1.5	<±1.5	<±1.5	<±1.5	-1.61	<±1.5
Pdgfc	<±1.5	-1.80	<±1.5	<±1.5	-1.56	<±1.5
Pdha2	<±1.5	<±1.5	<±1.5	<±1.5	1.73	<±1.5
Pelo	<±1.5	<±1.5	<±1.5	<±1.5	-1.73	<±1.5
Pfkp	<±1.5	<±1.5	<±1.5	2.06	-1.65	<±1.5
Phf11	<±1.5	1.84	<±1.5	1.87	<±1.5	<±1.5
Phlda1	<±1.5	1.60	1.75	<±1.5	<±1.5	<±1.5
Pik3r1	<±1.5	<±1.5	<±1.5	<±1.5	-2.06	<±1.5
Pitx2	<±1.5	<±1.5	<±1.5	<±1.5	1.55	<±1.5
Pkm2	<±1.5	<±1.5	<±1.5	<±1.5	-1.76	<±1.5
Plag1	<±1.5	<±1.5	<±1.5	<±1.5	-1.54	<±1.5

Gene	SINV Alone, 24 HPI vs Mock Infection	SINV + IFN-γ vs Mock Infection	SINV Alone, 27 HPI vs SINV Alone, 24 HPI	Mock + IFN-γ vs Mock Infection	SINV + IFN-γ vs Mock + IFN-γ	SINV + IFN-γ vs SINV Alone, 27 HPI
Plk2	<±1.5	-2.50	<±1.5	<±1.5	-2.21	<±1.5
Plod2	<±1.5	<±1.5	<±1.5	<±1.5	-1.58	<±1.5
Plp1	<±1.5	<±1.5	<±1.5	<±1.5	-1.55	<±1.5
Pmch	<±1.5	<±1.5	<±1.5	<±1.5	1.60	<±1.5
Pnrc1	<±1.5	-2.53	<±1.5	<±1.5	-2.40	<±1.5
Pnrc2	<±1.5	-1.68	<±1.5	<±1.5	-1.69	<±1.5
Polr1c	<±1.5	<±1.5	<±1.5	<±1.5	-1.54	<±1.5
Porf1	<±1.5	<±1.5	<±1.5	<±1.5	<±1.5	-1.52
Ppap2b	<±1.5	<±1.5	<±1.5	<±1.5	-1.56	<±1.5
Ppargc1a	<±1.5	<±1.5	<±1.5	-1.69	<±1.5	<±1.5
Ppm2c	<±1.5	<±1.5	<±1.5	1.75	-1.80	<±1.5
Ppp1cc	<±1.5	<±1.5	<±1.5	<±1.5	-1.75	<±1.5
Ppp1r10	<±1.5	<±1.5	<±1.5	<±1.5	-1.77	<±1.5
Ppp1r3c	<±1.5	-3.09	<±1.5	<±1.5	-2.30	<±1.5
Ppyr1	<±1.5	2.35	<±1.5	<±1.5	<±1.5	<±1.5
Prdm4	<±1.5	<±1.5	<±1.5	<±1.5	-1.73	<±1.5
Prkar2a	<±1.5	<±1.5	<±1.5	<±1.5	-1.64	<±1.5
Prl	<±1.5	<±1.5	<±1.5	<±1.5	1.58	<±1.5
Prps1	<±1.5	<±1.5	-1.59	<±1.5	<±1.5	<±1.5
Prss1	<±1.5	<±1.5	-1.69	<±1.5	<±1.5	<±1.5
Prssl1	<±1.5	1.59	<±1.5	<±1.5	1.63	1.56
Psma2	<±1.5	<±1.5	<±1.5	<±1.5	-1.60	<±1.5
Psmb8	<±1.5	<±1.5	<±1.5	2.11	<±1.5	1.58
Psmb9	<±1.5	2.07	<±1.5	2.87	<±1.5	1.54
Psph	1.54	1.84	<±1.5	<±1.5	1.68	<±1.5
Ptafr	<±1.5	1.58	<±1.5	<±1.5	<±1.5	<±1.5
Ptbp1	<±1.5	-1.70	<±1.5	<±1.5	-1.82	<±1.5
Ptgfr	-1.55	-3.13	<±1.5	<±1.5	-2.56	-1.60
Ptgs2	<±1.5	-1.80	<±1.5	<±1.5	<±1.5	-1.72
Ptpn12	<±1.5	1.67	<±1.5	<±1.5	<±1.5	<±1.5
Ptpn9	<±1.5	<±1.5	<±1.5	1.55	<±1.5	<±1.5
Pxk	<±1.5	<±1.5	<±1.5	1.66	<±1.5	<±1.5
Pxmp2	<±1.5	<±1.5	<±1.5	<±1.5	1.59	<±1.5
Pyroxd1	<±1.5	<±1.5	<±1.5	<±1.5	-1.55	<±1.5

Gene	SINV Alone, 24 HPI vs Mock Infection	SINV + IFN-γ vs Mock Infection	SINV Alone, 27 HPI vs SINV Alone, 24 HPI	Mock + IFN-γ vs Mock Infection	SINV + IFN-γ vs Mock + IFN-γ	SINV + IFN-γ vs SINV Alone, 27 HPI
Qrfp	<±1.5	<±1.5	<±1.5	<±1.5	<±1.5	1.67
Rab27a	<±1.5	<±1.5	<±1.5	<±1.5	<±1.5	-1.89
Rab30	<±1.5	<±1.5	<±1.5	-1.59	<±1.5	<±1.5
Rab3a	<±1.5	<±1.5	<±1.5	-1.57	<±1.5	<±1.5
Rabggtb	<±1.5	<±1.5	<±1.5	<±1.5	-1.79	<±1.5
rCG_59505	<±1.5	-1.69	<±1.5	<±1.5	<±1.5	<±1.5
Rcvrn	<±1.5	<±1.5	<±1.5	<±1.5	<±1.5	1.95
Rdh10	<±1.5	<±1.5	<±1.5	3.11	-2.10	<±1.5
Rdh11	-1.55	<±1.5	<±1.5	<±1.5	<±1.5	<±1.5
Rg9mtd1	<±1.5	<±1.5	<±1.5	<±1.5	<±1.5	-1.89
RGD1304579	<±1.5	<±1.5	<±1.5	1.76	-1.60	<±1.5
RGD1304827	<±1.5	-1.75	<±1.5	<±1.5	<±1.5	<±1.5
RGD1305225	<±1.5	<±1.5	<±1.5	<±1.5	1.64	<±1.5
RGD1307799	<±1.5	<±1.5	<±1.5	<±1.5	-1.60	<±1.5
RGD1308059	<±1.5	-2.03	<±1.5	<±1.5	<±1.5	<±1.5
RGD1309228	<±1.5	<±1.5	<±1.5	<±1.5	<±1.5	-1.52
RGD1309326	<±1.5	<±1.5	1.57	<±1.5	<±1.5	<±1.5
RGD620382	<±1.5	<±1.5	<±1.5	<±1.5	1.58	<±1.5
RGD69425	<±1.5	1.82	<±1.5	<±1.5	1.75	<±1.5
Rho	<±1.5	1.51	<±1.5	<±1.5	<±1.5	<±1.5
Ripk3	<±1.5	<±1.5	<±1.5	1.64	-1.56	<±1.5
Rnase4	<±1.5	-2.29	<±1.5	<±1.5	-2.12	<±1.5
Rnd1	<±1.5	1.69	<±1.5	<±1.5	<±1.5	<±1.5
Rnd3	<±1.5	-1.72	<±1.5	<±1.5	<±1.5	<±1.5
Rpl13a	<±1.5	<±1.5	<±1.5	1.96	-1.83	<±1.5
Rpl28	<±1.5	<±1.5	<±1.5	<±1.5	<±1.5	-2.03
Rsad2	2.06	2.72	<±1.5	2.23	<±1.5	<±1.5
Rsrc1	<±1.5	1.58	<±1.5	<±1.5	<±1.5	<±1.5
Rxfp3	<±1.5	<±1.5	<±1.5	<±1.5	<±1.5	2.19
S100a8	3.26	3.37	<±1.5	<±1.5	3.81	<±1.5
Sblf	<±1.5	-2.13	<±1.5	-1.50	<±1.5	<±1.5
Sc4mol	<±1.5	-1.81	<±1.5	<±1.5	-1.72	<±1.5
Scd	<±1.5	-1.77	<±1.5	<±1.5	-1.52	<±1.5
Scgn	<±1.5	1.51	<±1.5	<±1.5	<±1.5	<±1.5

Gene	SINV Alone, 24 HPI vs Mock Infection	SINV + IFN-γ vs Mock Infection	SINV Alone, 27 HPI vs SINV Alone, 24 HPI	Mock + IFN-γ vs Mock Infection	SINV + IFN-γ vs Mock + IFN-γ	SINV + IFN-γ vs SINV Alone, 27 HPI
Scn3b	<±1.5	<±1.5	<±1.5	1.57	<±1.5	<±1.5
Sdc4	<±1.5	<±1.5	<±1.5	1.82	<±1.5	<±1.5
Sdpr	<±1.5	<±1.5	-1.75	<±1.5	<±1.5	<±1.5
Sectm1b	<±1.5	4.66	<±1.5	17.13	<±1.5	4.95
Sell1l	<±1.5	-1.81	<±1.5	<±1.5	-1.73	<±1.5
Selplg	<±1.5	<±1.5	1.85	<±1.5	<±1.5	<±1.5
Serpinb3	<±1.5	<±1.5	1.59	<±1.5	<±1.5	<±1.5
Serpinc1	<±1.5	<±1.5	<±1.5	<±1.5	1.50	<±1.5
Serpine1	<±1.5	<±1.5	<±1.5	<±1.5	-2.18	<±1.5
Serpinh1	<±1.5	-1.80	<±1.5	<±1.5	-1.70	<±1.5
Sgms2	<±1.5	<±1.5	<±1.5	<±1.5	-1.51	<±1.5
Shmt2	<±1.5	1.51	<±1.5	<±1.5	<±1.5	<±1.5
Slc16a13	<±1.5	-1.77	<±1.5	<±1.5	-1.63	<±1.5
Slc16a3	<±1.5	<±1.5	<±1.5	<±1.5	-2.08	<±1.5
Slc16a7	<±1.5	-2.11	<±1.5	<±1.5	<±1.5	-1.59
Slc20a1	<±1.5	<±1.5	1.78	1.63	<±1.5	<±1.5
Slc23a2	<±1.5	<±1.5	<±1.5	<±1.5	-1.67	<±1.5
Slc29a2	<±1.5	<±1.5	<±1.5	<±1.5	-1.50	<±1.5
Slc2a1	<±1.5	<±1.5	<±1.5	<±1.5	-2.02	<±1.5
Slc38a2	<±1.5	-3.00	<±1.5	<±1.5	-2.01	<±1.5
Slc38a6	<±1.5	-1.75	<±1.5	<±1.5	<±1.5	<±1.5
Slc3a2	<±1.5	1.82	<±1.5	<±1.5	1.81	<±1.5
Slc6a6	<±1.5	-2.21	<±1.5	<±1.5	-2.72	<±1.5
Slc7a13	<±1.5	<±1.5	<±1.5	<±1.5	<±1.5	1.54
Slc7a5	<±1.5	1.63	<±1.5	<±1.5	<±1.5	<±1.5
Slfn3	<±1.5	2.10	<±1.5	4.37	-2.08	1.58
Slfn8	<±1.5	<±1.5	<±1.5	1.52	<±1.5	<±1.5
Sncg	<±1.5	<±1.5	<±1.5	<±1.5	-1.52	<±1.5
Socs3	<±1.5	<±1.5	<±1.5	<±1.5	<±1.5	1.73
Sod2	<±1.5	<±1.5	<±1.5	1.55	<±1.5	<±1.5
Sp100	<±1.5	1.72	<±1.5	2.56	<±1.5	<±1.5
Sp140	<±1.5	2.02	<±1.5	2.92	<±1.5	<±1.5
Spag11b	<±1.5	<±1.5	-2.10	<±1.5	<±1.5	<±1.5
Spetex-2G	<±1.5	<±1.5	<±1.5	<±1.5	8.19	<±1.5

Gene	SINV Alone, 24 HPI vs Mock Infection	SINV + IFN-γ vs Mock Infection	SINV Alone, 27 HPI vs SINV Alone, 24 HPI	Mock + IFN-γ vs Mock Infection	SINV + IFN-γ vs Mock + IFN-γ	SINV + IFN-γ vs SINV Alone, 27 HPI
Sqle	<±1.5	-1.87	<±1.5	<±1.5	-2.57	<±1.5
St3gal4	<±1.5	<±1.5	<±1.5	<±1.5	-2.02	<±1.5
Stat1	<±1.5	1.58	<±1.5	3.34	-2.12	1.67
Stat2	<±1.5	2.47	<±1.5	3.68	<±1.5	1.55
Stat3	<±1.5	<±1.5	<±1.5	1.66	<±1.5	<±1.5
Sult1c2	<±1.5	<±1.5	-2.08	<±1.5	<±1.5	<±1.5
Syne1	<±1.5	<±1.5	<±1.5	-1.59	<±1.5	<±1.5
Synpo	<±1.5	<±1.5	<±1.5	<±1.5	-2.00	<±1.5
Taar8c	<±1.5	<±1.5	<±1.5	<±1.5	<±1.5	1.64
Tada1l	<±1.5	-1.76	<±1.5	<±1.5	-1.74	<±1.5
Tap1	<±1.5	2.49	<±1.5	4.80	-1.93	1.88
Tap2	<±1.5	<±1.5	<±1.5	1.83	<±1.5	<±1.5
Tas2r119	<±1.5	<±1.5	<±1.5	<±1.5	<±1.5	1.78
Tbc1d14	<±1.5	<±1.5	<±1.5	<±1.5	-1.66	<±1.5
Tbp	<±1.5	<±1.5	<±1.5	<±1.5	-1.62	<±1.5
Tdg	<±1.5	<±1.5	<±1.5	<±1.5	-1.55	<±1.5
Terf2ip	<±1.5	-1.77	<±1.5	<±1.5	-2.33	<±1.5
Tf	<±1.5	<±1.5	<±1.5	<±1.5	1.52	<±1.5
Tfpt	<±1.5	1.86	<±1.5	<±1.5	1.55	<±1.5
Tgm2	<±1.5	1.54	<±1.5	2.33	-1.51	<±1.5
Timp1	<±1.5	<±1.5	<±1.5	<±1.5	-2.83	<±1.5
Tlr4	<±1.5	-1.99	-1.89	<±1.5	<±1.5	<±1.5
Tm9sf2	<±1.5	<±1.5	<±1.5	<±1.5	-1.64	<±1.5
Tmem140	<±1.5	<±1.5	-1.69	<±1.5	<±1.5	1.50
Tmem218	<±1.5	-1.74	<±1.5	<±1.5	<±1.5	<±1.5
Tmem50b	<±1.5	<±1.5	<±1.5	<±1.5	-1.53	<±1.5
Tmem77	<±1.5	<±1.5	<±1.5	<±1.5	<±1.5	-2.03
Tnfaip1	<±1.5	<±1.5	<±1.5	<±1.5	-1.67	<±1.5
Tnfrsf11b	<±1.5	-1.68	<±1.5	<±1.5	<±1.5	<±1.5
Tnfrsf1a	<±1.5	<±1.5	<±1.5	<±1.5	-2.00	<±1.5
Tnfsf10	<±1.5	<±1.5	<±1.5	<±1.5	<±1.5	1.94
Tnfsf15	<±1.5	-2.43	-1.75	-1.71	<±1.5	<±1.5
Tnfsf4	<±1.5	<±1.5	<±1.5	<±1.5	<±1.5	-1.56
Tnrc6b	<±1.5	-1.76	<±1.5	<±1.5	<±1.5	<±1.5

Gene	SINV Alone, 24 HPI vs Mock Infection	SINV + IFN-γ vs Mock Infection	SINV Alone, 27 HPI vs SINV Alone, 24 HPI	Mock + IFN-γ vs Mock Infection	SINV + IFN-γ vs Mock + IFN-γ	SINV + IFN-γ vs SINV Alone, 27 HPI
Tomm70a	<±1.5	<±1.5	<±1.5	<±1.5	<±1.5	-1.55
Tp53inp1	<±1.5	-1.72	-1.59	<±1.5	-1.79	<±1.5
Trafd1	<±1.5	<±1.5	<±1.5	1.55	<±1.5	<±1.5
Trib3	<±1.5	<±1.5	<±1.5	<±1.5	1.52	<±1.5
Trim25	<±1.5	<±1.5	<±1.5	<±1.5	-1.65	<±1.5
Tsc22d1	<±1.5	<±1.5	<±1.5	1.72	-1.62	<±1.5
Tsku	<±1.5	<±1.5	<±1.5	<±1.5	-2.67	-1.82
Tssk2	<±1.5	<±1.5	<±1.5	<±1.5	<±1.5	2.18
Tubb3	<±1.5	1.61	<±1.5	5.25	-3.26	1.58
Txndc8	2.16	3.05	<±1.5	<±1.5	3.89	<±1.5
Txnip	<±1.5	<±1.5	<±1.5	1.78	-2.35	<±1.5
Txnrd1	<±1.5	<±1.5	<±1.5	1.57	<±1.5	<±1.5
Ubac1	<±1.5	-1.79	-1.61	<±1.5	-1.69	<±1.5
Ufc1	-1.50	<±1.5	<±1.5	<±1.5	-1.62	<±1.5
Ufm1	<±1.5	<±1.5	<±1.5	<±1.5	-1.81	<±1.5
Ugcg	<±1.5	-1.91	<±1.5	<±1.5	-1.82	<±1.5
Ugdh	<±1.5	1.90	<±1.5	2.76	<±1.5	<±1.5
Unc5c	<±1.5	-1.70	<±1.5	<±1.5	-1.52	<±1.5
Uqcrh	<±1.5	<±1.5	<±1.5	<±1.5	-1.54	<±1.5
Uts2	<±1.5	<±1.5	<±1.5	<±1.5	1.58	<±1.5
V1rc20	<±1.5	<±1.5	<±1.5	<±1.5	<±1.5	1.80
V1rc6	<±1.5	<±1.5	<±1.5	<±1.5	<±1.5	1.64
V1rd24	<±1.5	<±1.5	<±1.5	<±1.5	<±1.5	-2.68
V1re4	<±1.5	<±1.5	<±1.5	<±1.5	-1.70	-1.63
V1re7	<±1.5	<±1.5	<±1.5	<±1.5	<±1.5	-2.24
V1rf6	<±1.5	<±1.5	<±1.5	<±1.5	<±1.5	-2.02
V1rg13	<±1.5	<±1.5	<±1.5	<±1.5	<±1.5	1.73
V1rg16	<±1.5	-1.92	<±1.5	<±1.5	<±1.5	<±1.5
V1rm3	<±1.5	<±1.5	-2.02	<±1.5	<±1.5	<±1.5
Vamp5	<±1.5	<±1.5	<±1.5	<±1.5	-1.56	<±1.5
Vcan	<±1.5	<±1.5	<±1.5	<±1.5	-1.62	<±1.5
Vegfc	<±1.5	-1.70	<±1.5	<±1.5	<±1.5	<±1.5
Vezt	<±1.5	<±1.5	<±1.5	<±1.5	-1.54	<±1.5
Vgll4	<±1.5	-2.22	<±1.5	<±1.5	-1.80	<±1.5

Gene	SINV Alone, 24 HPI vs Mock Infection	SINV + IFN-γ vs Mock Infection	SINV Alone, 27 HPI vs SINV Alone, 24 HPI	Mock + IFN-γ vs Mock Infection	SINV + IFN-γ vs Mock + IFN-γ	SINV + IFN-γ vs SINV Alone, 27 HPI
Vmac	<±1.5	<±1.5	<±1.5	<±1.5	<±1.5	-1.55
Vof16	<±1.5	-2.77	<±1.5	<±1.5	-2.89	<±1.5
Vom2r32	<±1.5	1.88	<±1.5	<±1.5	1.87	1.79
Vsnl1	<±1.5	<±1.5	<±1.5	<±1.5	<±1.5	-1.58
Wars	<±1.5	1.73	<±1.5	2.65	-1.54	<±1.5
Wdr70	<±1.5	1.53	<±1.5	<±1.5	<±1.5	<±1.5
Wisp1	<±1.5	<±1.5	<±1.5	<±1.5	-1.70	<±1.5
Xdh	<±1.5	<±1.5	<±1.5	2.27	-1.82	<±1.5
Zc3hav1	<±1.5	1.74	<±1.5	2.29	<±1.5	<±1.5
Zfp238	<±1.5	<±1.5	<±1.5	<±1.5	-1.70	<±1.5
Zfp386	<±1.5	-1.91	<±1.5	<±1.5	-1.83	<±1.5
Znf292	<±1.5	-1.75	<±1.5	<±1.5	-1.64	<±1.5
Znf294	-1.85	-2.87	<±1.5	<±1.5	-1.68	<±1.5
Znf483	<±1.5	<±1.5	<±1.5	-1.62	<±1.5	<±1.5

Table A-1. Gene list from microarray analysis of SINV-infected, IFN-γ-treated dCSM14.1 cells. Selected genes from a rat exon library showing at least ±1.5 fold-change in gene expression between experiment groups for at least one of the above comparisons. Fold-change expression less than ±1.5 is designated with <±1.5. Fold-change expression ≥ 2.0 is designated by red numbers, and fold-change expression ≥ -2.0 is designated by blue numbers.

APPENDIX B

	Brain		Spinal Cord	
Gene	**WT B6 vs *Ifngr1*$^{-/-}$**	**WT B6 vs *Ifng*$^{-/-}$**	**WT B6 vs *Ifngr1*$^{-/-}$**	**WT B6 vs *Ifng*$^{-/-}$**
Apcs	1.08	1.08	1.14	1.39
C3	-2.13	-3.11	-1.17	-1.49
C5ar1	-1.98	-2.46	-2.07	-1.71
Casp1	-3.38	-2.79	-3.04	-2.37
Ccl12	-2.17	-1.46	-2.00	-1.05
Ccl5	-1.70	-1.70	-1.56	-1.10
Ccr4	1.12	-1.50	1.40	1.71
Ccr5	-2.11	-1.99	-2.29	-1.47
Ccr6	1.22	-1.28	-1.69	1.07
Ccr8	-1.95	-3.50	-2.47	-1.60
Cd14	-1.13	-1.16	1.29	1.69
Cd4	1.00	-1.54	-1.62	-1.09
Cd40	-4.79	-6.77	-5.58	-3.91
Cd40lg	-1.47	-1.53	-1.43	1.26
Cd80	-1.53	-1.71	-1.29	-1.15
Cd86	-2.75	-2.85	-2.43	-1.86
Cd8a	-1.23	-1.29	-1.09	1.65
Crp	-1.58	-1.58	2.30	-1.54
Csf2	-5.70	-5.70	-2.39	-4.29
Cxcl10	-8.01	-6.87	-5.09	-1.92
Cxcr3	1.09	1.02	-1.13	1.48
Ddx58	-1.92	-1.74	-1.71	-1.15
Fasl	-1.33	1.16	-1.66	1.11
Foxp3	-1.29	1.06	1.31	1.67
Gata3	1.30	1.12	1.12	1.38
H2-Q10	-1.29	1.05	1.04	1.65
H2-T23	-4.24	-4.90	-3.62	-2.56
Icam1	-2.82	-3.48	-2.60	-1.95
Ifna2	-1.13	2.07	-1.79	1.05
Ifnar1	-1.19	-1.73	-1.15	-1.08
Ifnb1	-5.31	-2.87	-1.93	-1.15
Ifng	-1.88	-8.58	-2.00	-4.01
Ifngr1	-5.75	-1.56	-6.04	-1.04
Il10	-1.82	-1.36	-1.71	1.12
Il13	-1.45	-1.37	1.54	1.44
Il17a	1.08	1.08	1.14	1.39

Gene	Brain		Spinal Cord	
	WT B6 vs *Ifngr1*$^{-/-}$	WT B6 vs *Ifng*$^{-/-}$	WT B6 vs *Ifngr1*$^{-/-}$	WT B6 vs *Ifng*$^{-/-}$
Il18	-1.14	1.12	-1.19	-1.03
Il1a	-1.11	1.04	1.16	1.43
Il1b	-2.08	-3.01	-1.66	-1.17
Il1r1	-1.02	1.01	-1.13	-1.06
Il2	-2.90	-6.67	-1.11	-3.54
Il23a	1.77	1.55	2.43	2.26
Il4	1.56	1.32	2.85	2.01
Il5	-3.08	-1.25	-2.46	-1.55
Il6	-5.45	-5.19	-1.88	1.16
Irak1	-1.02	-1.11	-1.06	1.05
Irf3	-1.01	1.04	-1.02	1.21
Irf7	-3.06	-3.51	-2.14	-1.51
Itgam	1.04	-1.04	-1.22	-1.13
Jak2	-1.23	-1.24	-1.47	-1.22
Ly96	-1.42	-1.51	-1.62	-1.22
Lyz2	-1.69	-2.57	-1.97	-1.94
Mapk1	1.16	1.17	1.08	1.17
Mapk8	1.14	1.36	1.23	1.27
Mbl2	1.14	4.22	-3.15	-2.23
Mpo	-1.41	-1.65	-1.11	1.84
Mx1	-3.49	-2.92	-2.39	1.03
Myd88	-2.88	-4.35	-1.44	-1.03
Nfkb1	-1.26	-1.38	-1.14	1.03
Nfkbia	-1.51	-1.61	-1.60	-1.24
Nlrp3	-2.47	-2.10	-1.93	-1.71
Nod1	-3.21	-3.29	-2.62	-1.94
Nod2	-3.08	-3.25	-2.68	-2.74
Rag1	-1.85	-1.21	1.45	2.52
Rorc	1.12	1.02	1.87	1.41
Slc11a1	-2.95	-3.80	-2.50	-2.21
Stat1	-2.89	-2.61	-2.31	-1.65
Stat3	-1.76	-2.12	-1.34	-1.32
Stat4	-1.37	-1.32	-1.24	1.23
Stat6	-1.85	-2.50	-1.68	-1.56
Tbx21	-1.47	-1.83	-1.32	1.03
Ticam1	-1.42	-2.01	-1.16	-1.40
Tlr1	-1.53	-1.32	-1.64	-1.19

	Brain		Spinal Cord	
Gene	**WT B6 vs *Ifngr1*$^{-/-}$**	**WT B6 vs *Ifng*$^{-/-}$**	**WT B6 vs *Ifngr1*$^{-/-}$**	**WT B6 vs *Ifng*$^{-/-}$**
Tlr2	-1.83	-2.01	-1.73	-1.35
Tlr3	-1.87	-1.33	-2.14	-1.40
Tlr4	-2.15	-2.30	-2.18	-1.83
Tlr5	-1.42	-1.75	1.24	1.36
Tlr6	-2.52	-1.75	-2.32	-1.51
Tlr7	-1.75	-1.38	-1.67	-1.34
Tlr8	-3.69	-3.20	-2.68	-2.44
Tlr9	-4.61	-8.30	-4.18	-3.10
Tnf	-4.34	-5.50	-4.01	-3.28
Traf6	-1.14	-1.37	-1.21	-1.05
Tyk2	1.01	-1.17	-1.27	-1.25

Table B-1. Gene list from microarray analysis using Mouse Innate & Adaptive Immune Responses RT² Profiler PCR Array on WT B6, *Ifngr1*$^{-/-}$, and *Ifng*$^{-/-}$ mouse brains and spinal cords at 7 DPI. Fold-change expression ≥ 2.0 is designated by red numbers, and fold-change expression ≥ -2.0 is designated by blue numbers.

REFERENCES

1. Ryman, K. D. & Klimstra, W. B. Host responses to alphavirus infection. *Immunol. Rev.* **225,** 27–45 (2008).
2. Hollidge, B. S., González-Scarano, F. & Soldan, S. S. Arboviral encephalitides: transmission, emergence, and pathogenesis. *J Neuroimmune Pharmacol* **5,** 428–442 (2010).
3. Willems, W. R. *et al.* Semliki forest virus: cause of a fatal case of human encephalitis. *Science* **203,** 1127–1129 (1979).
4. Ganesan, K. *et al.* Chikungunya encephalomyeloradiculitis: report of 2 cases with neuroimaging and 1 case with autopsy findings. *AJNR Am J Neuroradiol* **29,** 1636–1637 (2008).
5. Alla, S. A. O. & Combe, B. Arthritis after infection with Chikungunya virus. *Best Prac Res Clin Rheumatol* **25,** 337–346 (2011).
6. Sane, J. *et al.* Prolonged myalgia in Sindbis virus infection: case description and in vitro infection of myotubes and myoblasts. *J. Infect. Dis.* **206,** 407–414 (2012).
7. Hawman, D. W. *et al.* Chronic joint disease caused by persistent Chikungunya virus infection is controlled by the adaptive immune response. *J. Virol.* **87,** 13878–13888 (2013).
8. Griffin, D. E. Alphaviruses. In *Fields Virology* Edn. 7 (eds. Knipe, D. M. & Howley, P. M.) **1**, 652–686 (Lippincott Williams & Wilkins, 2013).
9. Weaver, S. C. *et al.* Re-emergence of epidemic Venezuelan equine

encephalomyelitis in South America. VEE Study Group. *Lancet* **348,** 436–440 (1996).

10. Lubelczyk, C. *et al.* An Epizootic of Eastern Equine Encephalitis Virus, Maine, USA in 2009: Outbreak Description and Entomological Studies. *Am. J. Trop. Med. Hyg.* **88,** 95–102 (2013).

11. Molaei, G., Armstrong, P. M., Graham, A. C., Kramer, L. D. & Andreadis, T. G. Insights into the recent emergence and expansion of eastern equine encephalitis virus in a new focus in the Northern New England USA. *Parasit Vectors* **8**, 516 (2015). doi:10.1186/s13071-015-1145-2

12. Calisher, C. H. Medically important arboviruses of the United States and Canada. *Clin. Microbiol. Rev.* **7,** 89–116 (1994).

13. Steele, K. E. *et al.* Alphavirus encephalitides. In *Medical Aspects of Biological Warfare* (ed. Dembek, Z. F.) 241-270 (Office of the Surgeon General, US Army Medical Department Center and School, Borden Institute, 2007).

14. Bruyn, H. B. & Lennette, E. H. Western equine encephalitis in infants; a report on three cases with sequelae. *Calif Med* **79,** 362–366 (1953).

15. Finley, K. H., Longshore, W. A., Palmer, R. J., Cook, R. E. & Riggs, N. Western equine and St. Louis encephalitis; preliminary report of a clinical follow-up study in California. *Neurology* **5,** 223–235 (1955).

16. Palmer, R. J. & Finley, K. H. Sequelae of encephalitis; report of a study after the California epidemic. *Calif Med* **84,** 98–100 (1956).

17. Earnest, M. P., Goolishian, H. A., Calverley, J. R., Hayes, R. O. & Hill, H. R. Neurologic, intellectual, and psychologic sequelae following western

encephalitis. A follow-up study of 35 cases. *Neurology* **21,** 969–974 (1971).

18. Villari, P., Spielman, A., Komar, N., McDowell, M. & Timperi, R. J. The economic burden imposed by a residual case of eastern encephalitis. *Am. J. Trop. Med. Hyg.* **52,** 8–13 (1995).

19. Go, Y. Y., Balasuriya, U. B. R. & Lee, C-K. Zoonotic encephalitides caused by arboviruses: transmission and epidemiology of alphaviruses and flaviviruses. *Clin Exp Vaccine Res* **3,** 58–20 (2014).

20. Griffin, D. E. Emergence and re-emergence of viral diseases of the central nervous system. *Prog Neurobiol* **91,** 95–101 (2010).

21. Strauss, J. H. & Strauss, E. G. The alphaviruses: gene expression, replication, and evolution. *Microbiol. Rev.* **58,** 491–562 (1994).

22. Kuhn, R. T. Togaviridae. In *Fields Virology* Edn. 7 (eds. Knipe, D. M. & Howley, P. M.) **1**, 629-650 (Lippincott Williams & Wilkins, 2013).

23. Rice, C. M. & Strauss, J. H. Nucleotide sequence of the 26S mRNA of Sindbis virus and deduced sequence of the encoded virus structural proteins. *Proc. Natl. Acad. Sci. U.S.A.* **78**, 2062-2066 (1981).

24. Levine, B. *et al.* Antibody-mediated clearance of alphavirus infection from neurons. *Science* **254,** 856–860 (1991).

25. Griffin, D., Levine, B., Tyor, W., Ubol, S. & Després, P. The role of antibody in recovery from alphavirus encephalitis. *Immunol. Rev.* **159,** 155–161 (1997).

26. Taylor, R. M., Hurlbut, H. S., Work, T. H., Kingston, J. R. & Frothingham, T. E. Sindbis virus: a newly recognized arthropod-transmitted virus. *Am. J. Trop. Med. Hyg.* **4,** 844–862 (1955).

27. Johnson, R. T. Virus invasion of the central nervous system: a study of Sindbis virus infection in the mouse using fluorescent antibody. *Am. J. of Pathol.* **46,** 929–943 (1965).

28. Johnson, R. T., McFarland, H. F. & Levy, S. E. Age-dependent resistance to viral encephalitis: studies of infections due to Sindbis virus in mice. *J. Infect. Dis.* **125,** 257–262 (1972).

29. Griffin, D. E. Role of the immune response in age-dependent resistance of mice to encephalitis due to Sindbis virus. *J. Infect. Dis.* **133,** 456–464 (1976).

30. Griffin, D. E., Levine, B., Tyor, W. R., Tucker, P. C. & Hardwick, J. M. Age-dependent susceptibility to fatal encephalitis: alphavirus infection of neurons. *Arch. Virol. Suppl.* **9,** 31–39 (1994).

31. Oliver, K. R., Scallan, M. F., Dyson, H. & Fazakerley, J. K. Susceptibility to a neurotropic virus and its changing distribution in the developing brain is a function of CNS maturity. *J. Neurovirol.* **3,** 38–48 (1997).

32. Schultz, K. L. W., Vernon, P. S. & Griffin, D. E. Differentiation of neurons restricts arbovirus replication and increases expression of the alpha isoform of IRF-7. *J. Virol.* **89,** 48–60 (2014).

33. Sherman, L. A. & Griffin, D. E. Pathogenesis of encephalitis induced in newborn mice by virulent and avirulent strains of Sindbis virus. *J. Virol.* **64,** 2041–2046 (1990).

34. Griffin, D. E. & Johnson, R. T. Role of the immune response in recovery from Sindbis virus encephalitis in mice. *J. Immunol.* **118,** 1070–1075 (1977).

35. Jackson, A. C., Moench, T. R., Griffin, D. E. & Johnson, R. T. The pathogenesis

of spinal cord involvement in the encephalomyelitis of mice caused by neuroadapted Sindbis virus infection. *Lab. Invest.* **56,** 418–423 (1987).

36. Tucker, P. C., Strauss, E. G., Kuhn, R. J., Strauss, J. H. & Griffin, D. E. Viral determinants of age-dependent virulence of Sindbis virus for mice. *J. Virol.* **67,** 4605–4610 (1993).

37. Lustig, S. *et al.* Molecular basis of Sindbis virus neurovirulence in mice. *J. Virol.* **62,** 2329–2336 (1988).

38. Dropulic, L. K., Hardwick, J. M. & Griffin, D. E. A single amino acid change in the E2 glycoprotein of Sindbis virus confers neurovirulence by altering an early step of virus replication. *J. Virol.* **71,** 6100–6105 (1997).

39. Rowell, J. F. J. & Griffin, D. E. The inflammatory response to nonfatal Sindbis virus infection of the nervous system is more severe in SJL than in BALB/c mice and is associated with low levels of IL-4 mRNA and high levels of IL-10-producing CD4+ T cells. *J. Immunol.* **162,** 1624–1632 (1999).

40. Thach, D. C., Kimura, T. & Griffin, D. E. Differences between C57BL/6 and BALB/cBy mice in mortality and virus replication after intranasal infection with neuroadapted Sindbis virus. *J. Virol.* **74,** 6156–6161 (2000).

41. Kulcsar, K. A., Baxter, V. K., Abraham, R., Nelson, A. & Griffin, D. E. Distinct Immune Responses in Resistant and Susceptible Strains of Mice during Neurovirulent Alphavirus Encephalomyelitis. *J. Virol.* **89,** 8280–8291 (2015).

42. Metcalf, T. U. & Griffin, D. E. Alphavirus-induced encephalomyelitis: antibody-secreting cells and viral clearance from the nervous system. *J. Virol.* **85,** 11490–11501 (2011).

43. Levine, B. & Griffin, D. E. Persistence of viral RNA in mouse brains after recovery from acute alphavirus encephalitis. *J. Virol.* **66,** 6429–6435 (1992).

44. Tyor, W. R., Wesselingh, S. & Levine, B. Long term intraparenchymal Ig secretion after acute viral encephalitis in mice. *J. Immunol.* **149,** 4016-4020**.** (1992).

45. Griffin, D. E. Viral encephalomyelitis. *PLoS Pathog* **7,** e1002004 (2011).

46. Lewis, J., Wesselingh, S. L., Griffin, D. E. & Hardwick, J. M. Alphavirus-induced apoptosis in mouse brains correlates with neurovirulence. *J. Virol.* **70,** 1828–1835 (1996).

47. Lewis, J. *et al.* Inhibition of virus-induced neuronal apoptosis by Bax. *Nat. Med.* **5,** 832–835 (1999).

48. Havert, M. B., Schofield, B., Griffin, D. E. & Irani, D. N. Activation of divergent neuronal cell death pathways in different target cell populations during neuroadapted Sindbis virus infection of mice. *J. Virol.* **74,** 5352–5356 (2000).

49. Greene, I. P., Lee, E.-Y., Prow, N., Ngwang, B. & Griffin, D. E. Protection from fatal viral encephalomyelitis: AMPA receptor antagonists have a direct effect on the inflammatory response to infection. *Proc. Natl. Acad. Sci. U.S.A.* **105,** 3575–3580 (2008).

50. Conrady, C. D., Drevets, D. A. & Carr, D. J. J. Herpes simplex type I (HSV-1) infection of the nervous system: Is an immune response a good thing? *J. Neuroimmunol.* **220,** 1–9 (2010).

51. Tilleux, S. & Hermans, E. Neuroinflammation and regulation of glial glutamate uptake in neurological disorders. *J. Neurosci. Res.* **85,** 2059–2070 (2007).

52. Greenlee, J. E. The equine encephalitides. In *Handbook of Clinical Neurology: Neurovirology* 3rd series. Vol. **123** (eds. Tselis, A. C. & Booss, J.) 417–432 (Elsevier B.V., 2014).

53. Hatanpaa, K. J. & Kim, J. H. Neuropathology of viral infections. In *Handbook of Clinical Neurology: Neurovirology* 3rd series. Vol. **123** (eds. Tselis, A. C. & Booss, J.) 193–214 (Elsevier B.V., 2014).

54. Kimura, T. & Griffin, D. E. Extensive immune-mediated hippocampal damage in mice surviving infection with neuroadapted Sindbis virus. *Virology* **311,** 28–39 (2003).

55. Rowell, J. F. & Griffin, D. E. Contribution of T cells to mortality in neurovirulent Sindbis virus encephalomyelitis. *J. Neuroimmunol.* **127,** 106–114 (2002).

56. Kulcsar, K. A., Baxter, V. K., Greene, I. P. & Griffin, D. E. Interleukin 10 modulation of pathogenic Th17 cells during fatal alphavirus encephalomyelitis. *Proc. Natl. Acad. Sci. U.S.A.* **111,** 16053–16058 (2014).

57. Sattler, R. & Tymianski, M. Molecular mechanisms of glutamate receptor-mediated excitotoxic neuronal cell death. *Mol. Neurobiol.* **24,** 107–129 (2001).

58. Lee, J. M., Zipfel, G. J. & Choi, D. W. The changing landscape of ischaemic brain injury mechanisms. *Nature* **399,** A7–14 (1999).

59. Nicotera, P. & Orrenius, S. The role of calcium in apoptosis. *Cell Calcium* **23,** 173–180 (1998).

60. Nadler, J. V., Perry, B. W. & Cotman, C. W. Intraventricular kainic acid preferentially destroys hippocampal pyramidal cells. *Nature* **271,** 676–677

(1978).

61. Olney, J. W., Fuller, T. & de Gubareff, T. Acute dendrotoxic changes in the hippocampus of kainate treated rats. *Brain Res.* **176,** 91–100 (1979).

62. Rothstein, J. D., Jin, L., Dykes-Hoberg, M. & Kuncl, R. W. Chronic inhibition of glutamate uptake produces a model of slow neurotoxicity. *Proc. Natl. Acad. Sci. U.S.A.* **90,** 6591–6595 (1993).

63. Carriedo, S. G., Sensi, S. L., Yin, H. Z. & Weiss, J. H. AMPA exposures induce mitochondrial Ca(2+) overload and ROS generation in spinal motor neurons in vitro. *J. Neurosci.* **20,** 240–250 (2000).

64. Darman, J. Viral-induced spinal motor neuron death is non-cell-autonomous and involves glutamate excitotoxicity. *J. Neurosci.* **24,** 7566–7575 (2004).

65. Nargi-Aizenman, J. L. *et al.* Glutamate receptor antagonists protect from virus-induced neural degeneration. *Ann Neurol.* **55,** 541–549 (2004).

66. Griffin, D. E., Levine, B., Tyor, W. R. & Irani, D. N. The immune response in viral encephalitis. *Semin. Immunol.* **4,** 111–119 (1992).

67. Kimura, T. & Griffin, D. E. The role of CD8(+) T cells and major histocompatibility complex class I expression in the central nervous system of mice infected with neurovirulent Sindbis virus. *J. Virol.* **74,** 6117–6125 (2000).

68. Préhaud, C., Mégret, F., Lafage, M. & Lafon, M. Virus infection switches TLR-3-positive human neurons to become strong producers of beta interferon. *J. Virol.* **79,** 12893–12904 (2005).

69. Byrnes, A. P., Durbin, J. E. & Griffin, D. E. Control of Sindbis virus infection by antibody in interferon-deficient mice. *J. Virol.* **74,** 3905–3908 (2000).

70. Burdeinick-Kerr, R., Wind, J. & Griffin, D. E. Synergistic roles of antibody and interferon in noncytolytic clearance of Sindbis virus from different regions of the central nervous system. *J. Virol.* **81,** 5628–5636 (2007).

71. Ireland, D. D. C., Stohlman, S. A., Hinton, D. R., Atkinson, R. & Bergmann, C. C. Type I interferons are essential in controlling neurotropic coronavirus infection irrespective of functional CD8 T cells. *J. Virol.* **82,** 300–310 (2008).

72. Müller, U., Steinhoff, U., Reis, L. F., Hemmi, S. & Pavlovic, J. Functional role of type I and type II interferons in antiviral defense. *Science* **264**, 1918-1921 (1994).

73. Fiette, L. *et al.* Theiler's virus infection of 129Sv mice that lack the interferon alpha/beta or interferon gamma receptors. *J. Exp. Med.* **181,** 2069–2076 (1995).

74. Ryman, K. D., Klimstra, W. B., Nguyen, K. B. & Biron, C. A. Alpha/beta interferon protects adult mice from fatal Sindbis virus infection and is an important determinant of cell and tissue tropism. *J. Virol* **74**, 3366-3378 (2000).

75. Samuel, M. A. & Diamond, M. S. Alpha/beta interferon protects against lethal West Nile virus infection by restricting cellular tropism and enhancing neuronal survival. *J. Virol.* **79,** 13350–13361 (2005).

76. Wesselingh, S. L., Levine, B., Fox, R. J., Choi, S. & Griffin, D. E. Intracerebral cytokine mRNA expression during fatal and nonfatal alphavirus encephalitis suggests a predominant type 2 T cell response. *J. Immunol.* **152,** 1289–1297 (1994).

77. Asensio, V. C. & Campbell, I. L. Chemokine gene expression in the brains of mice with lymphocytic choriomeningitis. *J. Virol.* **71,** 7832–7840 (1997).

78. Parra, B., Hinton, D. R., Lin, M. T., Cua, D. J. & Stohlman, S. A. Kinetics of cytokine mRNA expression in the central nervous system following lethal and nonlethal coronavirus-induced acute encephalomyelitis. *Virology* **233,** 260–270 (1997).

79. Frolov, I., Akhrymuk, M., Akhrymuk, I., Atasheva, S. & Frolova, E. I. Early events in alphavirus replication determine the outcome of infection. *J. Virol.* **86,** 5055–5066 (2012).

80. Harling-Berg, C. J., Park, T. J. & Knopf, P. M. Role of the cervical lymphatics in the Th2-type hierarchy of CNS immune regulation. *J. Neuroimmunol.* **101,** 111–127 (1999).

81. Weller, R. O., Djuanda, E., Yow, H.-Y. & Carare, R. O. Lymphatic drainage of the brain and the pathophysiology of neurological disease. *Acta Neuropathol.* **117,** 1–14 (2009).

82. Stohlman, S. A., Bergmann, C. C., Lin, M. T., Cua, D. J. & Hinton, D. R. CTL effector function within the central nervous system requires CD4+ T cells. *J. Immunol.* **160,** 2896–2904 (1998).

83. McDole, J. R. *et al.* Rapid formation of extended processes and engagement of Theiler's virus-infected neurons by CNS-infiltrating CD8 T cells. *Am. J. Pathol.* **177,** 1823–1833 (2010).

84. Bergmann, C. C., Lane, T. E. & Stohlman, S. A. Coronavirus infection of the central nervous system: host–virus stand-off. *Nat Rev Micro* **4,** 121–132 (2006).

85. Tyor, W. R., Moench, T. R. & Griffin, D. E. Characterization of the local and systemic B cell response of normal and athymic nude mice with Sindbis virus

encephalitis. *J. Neuroimmunol.* **24,** 207–215 (1989).

86. Griffin, D. E. Immune responses to RNA-virus infections of the CNS. *Nat Rev Immunol* **3,** 493–502 (2003).

87. Després, P., Griffin, J. W. & Griffin, D. E. Effects of anti-E2 monoclonal antibody on sindbis virus replication in AT3 cells expressing bcl-2. *J. Virol.* **69,** 7006–7014 (1995).

88. Griffin, D. E. Immunoglobulins in the cerebrospinal fluid: changes during acute viral encephalitis in mice. *J. Immunol.* **126,** 27–31 (1981).

89. Griffin, D. E., Hess, J. L. & Moench, T. R. Immune responses in the central nervous system. *Toxicologic Pathology* **15,** 294–302 (1987).

90. Knopf, P. M. *et al.* Antigen-dependent intrathecal antibody synthesis in the normal rat brain: tissue entry and local retention of antigen-specific B cells. *J. Immunol.* **161,** 692–701 (1998).

91. Metcalf, T. U., Baxter, V. K., Nilaratanakul, V. & Griffin, D. E. Recruitment and retention of B cells in the central nervous system in response to alphavirus encephalomyelitis. *J. Virol.* **87,** 2420–2429 (2013).

92. Binder, G. K. Interferon-gamma-mediated site-specific clearance of alphavirus from CNS neurons. *Science* **293,** 303–306 (2001).

93. Burdeinick-Kerr, R. & Griffin, D. E. Gamma interferon-dependent, noncytolytic clearance of sindbis virus infection from neurons in vitro. *J. Virol.* **79,** 5374–5385 (2005).

94. Hirsch, R. L. & Griffin, D. E. The pathogenesis of Sindbis virus infection in athymic nude mice. *J. Immunol.* **123,** 1215–1218 (1979).

95. Farrar, W. L., Johnson, H. M. & Farrar, J. J. Regulation of the production of immune interferon and cytotoxic T lymphocytes by interleukin 2. *J. Immunol.* **126,** 1120–1125 (1981).

96. Trinchieri, G. *et al.* Response of resting human peripheral blood natural killer cells to interleukin 2. *J. Exp. Med.* **160,** 1147–1169 (1984).

97. Rottenberg, M. & Kristensson, K. Effects of interferon-γ on neuronal infections. *Viral Immunol.* **15,** 247–260 (2002).

98. Rodriguez, M. *et al.* Gamma interferon is critical for neuronal viral clearance and protection in a susceptible mouse strain following early intracranial Theiler's murine encephalomyelitis virus infection. *J. Virol.* **77,** 12252–12265 (2003).

99. Hausmann, J. *et al.* CD8 T cells require gamma interferon to clear borna disease virus from the brain and prevent immune system-mediated neuronal damage. *J. Virol.* **79,** 13509–13518 (2005).

100. Stubblefield Park, S. R., Widness, M., Levine, A. D. & Patterson, C. E. T cell-, interleukin-12-, and gamma interferon-driven viral clearance in measles virus-infected brain tissue. *J. Virol.* **85,** 3664–3676 (2011).

101. O'Donnell, L. A. *et al.* STAT1-independent control of a neurotropic measles virus challenge in primary neurons and infected mice. *J. Immunol.* **188,** 1915–1923 (2012).

102. Shen, F. H. *et al.* Enterovirus 71 infection increases expression of interferon-gamma-inducible protein 10 which protects mice by reducing viral burden in multiple tissues. *J. Gen. Virol.* **94,** 1019–1027 (2013).

103. Tau, G. & Rothman, P. Biologic functions of the IFN-gamma receptors. *Allergy*

54, 1233–1251 (1999).

104. Burdeinick-Kerr, R., Govindarajan, D. & Griffin, D. E. Noncytolytic Clearance of Sindbis Virus Infection from Neurons by Gamma Interferon Is Dependent on Jak/Stat Signaling. *J. Virol.* **83,** 3429–3435 (2009).

105. Farrar, M. A. & Schreiber, R. D. The molecular cell biology of interferon-gamma and its receptor. *Annu. Rev. Immunol.* **11,** 571–611 (1993).

106. Samuel, C. E. Antiviral actions of interferons. *Clin. Microbiol. Rev.* **14,** 778–809 (2001).

107. Bick, M. J. *et al.* Expression of the zinc-finger antiviral protein inhibits alphavirus replication. *J. Virol.* **77,** 11555–11562 (2003).

108. Wacher, C. *et al.* Coordinated regulation and widespread cellular expression of interferon-stimulated genes (ISG) ISG-49, ISG-54, and ISG-56 in the central nervous system after infection with distinct viruses. *J. Virol.* **81,** 860–871 (2007).

109. Wherry, E. J. & Ahmed, R. Memory CD8 T-cell differentiation during viral infection. *J. Virol.* **78,** 5535–5545 (2004).

110. Cho, B. K., Wang, C., Sugawa, S., Eisen, H. N. & Chen, J. Functional differences between memory and naive CD8 T cells. *Proc. Natl. Acad. Sci. U.S.A.* **96,** 2976–2981 (1999).

111. Mosmann, T. R. & Coffman, R. L. TH1 and TH2 cells: different patterns of lymphokine secretion lead to different functional properties. *Annu. Rev. Immunol.* **7,** 145–173 (1989).

112. Badovinac, V. P., Porter, B. B. & Harty, J. T. Programmed contraction of CD8(+) T cells after infection. *Nat. Immunol.* **3,** 619–626 (2002).

113. Kaech, S. M., Wherry, E. J. & Ahmed, R. Effector and memory T-cell differentiation: implications for vaccine development. *Nat Rev Immunol* **2,** 251–262 (2002).

114. Busch, D. H., Pilip, I. M., Vijh, S. & Pamer, E. G. Coordinate regulation of complex T cell populations responding to bacterial infection. *Immunity* **8,** 353–362 (1998).

115. Murali-Krishna, K. *et al.* Counting antigen-specific CD8 T cells: a reevaluation of bystander activation during viral infection. *Immunity* **8,** 177–187 (1998).

116. Sallusto, F., Lenig, D., Förster, R., Lipp, M. & Lanzavecchia, A. Two subsets of memory T lymphocytes with distinct homing potentials and effector functions. *Nature* **401,** 708–712 (1999).

117. Wakim, L. M., Woodward-Davis, A. & Bevan, M. J. Memory T cells persisting within the brain after local infection show functional adaptations to their tissue of residence. *Proc. Natl. Acad. Sci. U.S.A.* **107,** 17872–17879 (2010).

118. Casey, K. A. *et al.* Antigen-independent differentiation and maintenance of effector-like resident memory T cells in tissues. *J. Immunol.* **188,** 4866–4875 (2012).

119. Mackay, L. K. *et al.* The developmental pathway for CD103(+)CD8+ tissue-resident memory T cells of skin. *Nat. Immunol.* **14,** 1294–1301 (2013).

120. Schenkel, J. M. & Masopust, D. Tissue-resident memory T cells. *Immunity* **41,** 886–897 (2014).

121. Schenkel, J. M., Fraser, K. A., Beura, L. K. & Pauken, K. E. Resident memory CD8 T cells trigger protective innate and adaptive immune responses. *Science*

346, 98-101 (2014). doi:10.1126/science.1257530

122. Gebhardt, T. *et al.* Memory T cells in nonlymphoid tissue that provide enhanced local immunity during infection with herpes simplex virus. *Nat. Immunol.* **10,** 524–530 (2009).

123. Masopust, D. *et al.* Dynamic T cell migration program provides resident memory within intestinal epithelium. *J. Exp. Med.* **207,** 553–564 (2010).

124. Hofmann, M. & Pircher, H. E-cadherin promotes accumulation of a unique memory CD8 T-cell population in murine salivary glands. *Proc. Natl. Acad. Sci. U.S.A.* **108,** 16741–16746 (2011).

125. Jiang, X. *et al.* Skin infection generates non-migratory memory CD8+ T(RM) cells providing global skin immunity. *Nature* **483,** 227–231 (2012).

126. Skon, C. N. *et al.* Transcriptional downregulation of S1pr1 is required for the establishment of resident memory CD8+ T cells. *Nat. Immunol.* **14,** 1285–1293 (2013).

127. Schluns, K. S. & Lefrançois, L. Cytokine control of memory T-cell development and survival. *Nat Rev Immunol* **3,** 269–279 (2003).

128. Kaech, S. M. *et al.* Selective expression of the interleukin 7 receptor identifies effector CD8 T cells that give rise to long-lived memory cells. *Nat. Immunol.* **4,** 1191–1198 (2003).

129. Akashi, K., Kondo, M., Freeden-Jeffry, von, U., Murray, R. & Weissman, I. L. Bcl-2 rescues T lymphopoiesis in interleukin-7 receptor-deficient mice. *Cell* **89,** 1033–1041 (1997).

130. Maraskovsky, E. *et al.* Bcl-2 can rescue T lymphocyte development in

interleukin-7 receptor-deficient mice but not in mutant rag-1-/- mice. *Cell* **89,** 1011–1019 (1997).

131. Kim, K., Lee, C. K., Sayers, T. J., Muegge, K. & Durum, S. K. The trophic action of IL-7 on pro-T cells: inhibition of apoptosis of pro-T1, -T2, and -T3 cells correlates with Bcl-2 and Bax levels and is independent of Fas and p53 pathways. *J. Immunol.* **160,** 5735–5741 (1998).

132. Vella, A. T., Dow, S., Potter, T. A., Kappler, J. & Marrack, P. Cytokine-induced survival of activated T cells in vitro and in vivo. *Proc. Natl. Acad. Sci. U.S.A.* **95,** 3810–3815 (1998).

133. Zhang, X., Sun, S., Hwang, I., Tough, D. F. & Sprent, J. Potent and selective stimulation of memory-phenotype CD8+ T cells in vivo by IL-15. *Immunity* **8**, 591–599 (1998).

134. Schluns, K. S., Williams, K., Ma, A. & Zheng, X. X. Cutting edge: requirement for IL-15 in the generation of primary and memory antigen-specific CD8 T cells. *J. Immunol.* **168**, 4827-4831 (2002). doi:10.4049/jimmunol.168.10.4827

135. Zajac, A. J. *et al.* Viral immune evasion due to persistence of activated T cells without effector function. *J. Exp. Med.* **188,** 2205–2213 (1998).

136. Fuller, M. J. & Zajac, A. J. Ablation of CD8 and CD4 T cell responses by high viral loads. *J. Immunol.* **170**, 477-486 (2003). doi:10.4049/jimmunol.170.1.477

137. Wherry, E. J., Blattman, J. N. & Murali-Krishna, K. Viral persistence alters CD8 T-cell immunodominance and tissue distribution and results in distinct stages of functional impairment. *J. Virol.* **77**, 4911–4927 (2003). doi:10.1128/JVI.77.8.4911-4927.2003

138. Blackburn, S. D. *et al.* Coregulation of CD8+ T cell exhaustion by multiple inhibitory receptors during chronic viral infection. *Nat. Immunol.* **10,** 29–37 (2009).

139. Crawford, A. & Wherry, E. J. The diversity of costimulatory and inhibitory receptor pathways and the regulation of antiviral T cell responses. *Curr. Opin. Immunol.* **21,** 179–186 (2009).

140. Moskophidis, D., Lechner, F., Pircher, H. & Zinkernagel, R. M. Virus persistence in acutely infected immunocompetent mice by exhaustion of antiviral cytotoxic effector T cells. *Nature* **362,** 758–761 (1993).

141. Oxenius, A., Zinkernagel, R. M. & Hengartner, H. Comparison of activation versus induction of unresponsiveness of virus-specific CD4+ and CD8+ T cells upon acute versus persistent viral infection. *Immunity* **9**, 449–457 (1998).

142. Brooks, D. G., Teyton, L., Oldstone, M. B. A. & McGavern, D. B. Intrinsic functional dysregulation of CD4 T cells occurs rapidly following persistent viral infection. *J. Virol.* **79,** 10514–10527 (2005).

143. Urbani, S. *et al.* Outcome of acute hepatitis C is related to virus-specific CD4 function and maturation of antiviral memory CD8 responses. *Hepatology* **44,** 126–139 (2006).

144. Kaufmann, D. E. *et al.* Upregulation of CTLA-4 by HIV-specific CD4+ T cells correlates with disease progression and defines a reversible immune dysfunction. *Nat. Immunol.* **8,** 1246–1254 (2007).

145. Virgin, H. W., Wherry, E. J. & Ahmed, R. Redefining chronic viral infection. *Cell* **138,** 30–50 (2009).

146. Wherry, E. J. T cell exhaustion. *Nat. Immunol.* **12**, 492-499 (2011). doi:10.1038/ni.2035

147. Gubler, D. J. The global emergence/resurgence of arboviral diseases as public health problems. *Arch. Med. Res.* **33,** 330–342 (2002).

148. van den Hurk, A. F., Ritchie, S. A. & Mackenzie, J. S. Ecology and Geographical Expansion of Japanese Encephalitis Virus. *Annu. Rev. Entomol.* **54,** 17–35 (2009).

149. Lambrechts, L., Scott, T. W. & Gubler, D. J. Consequences of the expanding global distribution of *Aedes albopictus* for dengue virus transmission. *PLoS Negl Trop Dis* **4,** e646 (2010).

150. Weaver, S. C. & Reisen, W. K. Present and future arboviral threats. *Antiviral Res.* **85,** 328–345 (2010).

151. León, C. A. Sequelae of Venezuelan equine encephalitis in humans: a four year follow-up. *Int J Epidemiol* **4,** 131–140 (1975).

152. Silverman, M. A. *et al.* Eastern equine encephalitis in children, Massachusetts and New Hampshire, USA, 1970–2010. *Emerg. Infect. Dis.* **19,** 194–201 (2013).

153. Potter, M. C., Yuan, C., Ottenritter, C., Mughal, M. & van Praag, H. Exercise is not beneficial and may accelerate symptom onset in a mouse model of Huntington's disease. *PLoS Curr* **2,** RRN1201 (2010).

154. Marlatt, M. W., Potter, M. C., Lucassen, P. J. & van Praag, H. Running throughout middle-age improves memory function, hippocampal neurogenesis, and BDNF levels in female C57BL/6J mice. *Devel Neurobio* **72,** 943–952 (2012).

155. Okun, E. *et al.* Toll-like receptor 3 inhibits memory retention and constrains adult hippocampal neurogenesis. *Proc. Natl. Acad. Sci. U.S.A.* **107,** 15625–15630 (2010).

156. Melnikova, T. *et al.* Cycloxygenase-2 activity promotes cognitive deficits but not increased amyloid burden in a model of Alzheimer's disease in a sex-dimorphic pattern. *Neuroscience* **141,** 1149–1162 (2006).

157. Millichap, J. G. Etiologic Classification of Attention-Deficit/Hyperactivity Disorder. *Pediatrics* **121,** e358–e365 (2008).

158. Adhikari, A. Distributed circuits underlying anxiety. *Front Behav Neurosci* **8,** 112 (2014).

159. Provenzale, J. M., vanLandingham, K. E., Lewis, D. V., Mukundan, S., Jr & White, L. E. Extrahippocampal involvement in human herpesvirus 6 encephalitis depicted at MR imaging. *Radiology* **249,** 955–963 (2008).

160. Nozyce, M. L. A Behavioral and cognitive profile of clinically stable HIV-infected children. *Pediatrics* **117,** 763–770 (2006).

161. Phillips, R. G. & LeDoux, J. E. Differential contribution of amygdala and hippocampus to cued and contextual fear conditioning. *Behav. Neurosci.* **106,** 274–285 (1992).

162. Sanders, M. J., Wiltgen, B. J. & Fanselow, M. S. The place of the hippocampus in fear conditioning. *Eur. J. Pharmacol.* **463,** 217–223 (2003).

163. Kim, J. J. & Jung, M. W. Neural circuits and mechanisms involved in Pavlovian fear conditioning: A critical review. *Neurosci Biobehav Rev* **30,** 188–202 (2006).

164. Wiltgen, B. J. Context Fear Learning in the Absence of the Hippocampus. *J.*

Neurosci. **26,** 5484–5491 (2006).

165. Crawley, J. N. *What's wrong with my mouse? : behavioral phenotyping of transgenic and knockout mice*. Edn. 2 (Wiley-Interscience, 2007).

166. Maren, S., Phan, K. L. & Liberzon, I. The contextual brain: implications for fear conditioning, extinction and psychopathology. *Nat. Rev. Neurosci.* **14**, 417-428 (2013). doi:10.1038/nrn3492

167. Amaral, D. C. *et al.* Intracerebral infection with dengue-3 virus induces meningoencephalitis and behavioral changes that precede lethality in mice. *J Neuroinflammation* **8,** 23 (2011).

168. Jurgens, H. A., Amancherla, K. & Johnson, R. W. Influenza infection induces neuroinflammation, alters hippocampal neuron morphology, and impairs cognition in adult mice. *J. Neurosci.* **32,** 3958–3968 (2012).

169. Umpierre, A. D. *et al.* Impaired cognitive ability and anxiety-like behavior following acute seizures in the Theiler's virus model of temporal lobe epilepsy. *Neurobiology of Disease* **64,** 98–106 (2014).

170. Rozdilsky, B., Robertson, H. E. & Chorney, J. Western encephalitis: report of eight fatal cases. Saskatchewan epidemic, 1965. *Can Med Assoc J* **98,** 79–86 (1968).

171. Schultz, D. R., Barthal, J. S. & Garrett, G. Western equine encephalitis with rapid onset of parkinsonism. *Neurology* **27,** 1095–1096 (1977).

172. Przelomski, M. M., O'Rourke, E., Grady, G. F., Berardi, V. P. & Markley, H. G. Eastern equine encephalitis in Massachusetts: a report of 16 cases, 1970-1984. *Neurology* **38,** 736–739 (1988).

173. Deresiewicz, R. L., Thaler, S. J., Hsu, L. & Zamani, A. A. Clinical and neuroradiographic manifestations of eastern equine encephalitis. *N. Engl. J. Med.* **336,** 1867–1874 (1997).

174. Rivas, F. *et al.* Epidemic Venezuelan equine encephalitis in La Guajira, Colombia, 1995. *J. Infect. Dis.* **175,** 828–832 (1997).

175. Lury, K. & Castillo, M. Eastern equine encephalitis: CT and MRI findings in one case. *Emerg Radiol* **11,** 1–3 (2004).

176. Harvala, H. *et al.* Case report: Eastern equine encephalitis virus imported to the UK. *J. Med. Virol.* **81,** 305–308 (2009).

177. Reddy, A. J., Woods, C. W. & Welty-Wolf, K. E. Eastern equine encephalitis leading to multi-organ failure and sepsis. *J. Clin. Virol.* **42,** 418–421 (2008).

178. Mancao, M. Y. *et al.* Eastern Equine Encephalitis virus infection and hemophagocytic lymphohistiocytosis in A 5-month-old infant. *Pediatr. Infect. Dis. J.* **28,** 543–545 (2009).

179. Vilcarromero, S. *et al.* Venezuelan equine encephalitis and 2 human deaths, Peru. *Emerg. Infect. Dis.* **16,** 553–556 (2010).

180. Ethier, M. & Rogg, J. Eastern equine encephalitis: MRI findings in two patients. *Med Health R I* **95,** 227–229 (2012).

181. Muñiz, A. E. Venezuelan equine encephalitis in a teenager visiting Central America. *Pediatr Emerg Care* **28,** 372–375 (2012).

182. Babi, M. A., Raleigh, T., Shapiro, R. E., McSherry, J. & Applebee, A. MRI and encephalography in fatal eastern equine encephalitis. *Neurology* **83,** 1483–1483 (2014).

183. Baig, B., Mehta, T., Khalid, N. & Chhabra, L. Eastern equine encephalitis: a classical case. *Conn Med* **78,** 529–531 (2014).

184. Lindenberg, R. & Haymaker, W. Tissue reactions in the grey matter of the central nervous system. In *Histology and Histopathology of the Nervous System* (eds. Haymaker, W. & Adams, R. D.) 973-1219 (Charles C. Thomas, Springfield, IL, 1982).

185. Gleiser, C. A., Gochenour, W. S. & Berge, T. O. The comparative pathology of experimental Venezuelan equine encephalomyelitis infection in different animal hosts. *J. Infect. Dis.* **110**, 80-97 (1962).

186. Del Piero, F., Wilkins, P. A., Dubovi, E. J., Biolatti, B. & Cantile, C. Clinical, pathologic, immunohistochemical, and virologic findings of eastern equine encephalomyelitis in two horses. *Vet. Pathol.* **38,** 451–456 (2001).

187. Newsholme, E. A., Crabtree, B. & Ardawi, M. S. Glutamine metabolism in lymphocytes: its biochemical, physiological and clinical importance. *Q J Exp Physiol* **70,** 473–489 (1985).

188. Souba, W. W. Glutamine and cancer. *Ann. Surg.* **218,** 715–728 (1993).

189. Colombo, S. L. *et al.* Anaphase-promoting complex/cyclosome-Cdh1 coordinates glycolysis and glutaminolysis with transition to S phase in human T lymphocytes. *Proc. Natl. Acad. Sci. U.S.A.* **107,** 18868–18873 (2010).

190. Wang, R. *et al.* The transcription factor Myc controls metabolic reprogramming upon T lymphocyte activation. *Immunity* **35,** 871–882 (2011).

191. Thangavelu, K., Chong, Q. Y., Low, B. C. & Sivaraman, J. Structural basis for the active site inhibition mechanism of human kidney-type glutaminase (KGA).

Sci. Rep. **4,** 3827 (2014).

192. Carr, E. L. *et al.* Glutamine uptake and metabolism are coordinately regulated by ERK/MAPK during T lymphocyte activation. *J. Immunol.* **185,** 1037–1044 (2010).

193. Maciolek, J. A., Pasternak, J. A. & Wilson, H. L. Metabolism of activated T lymphocytes. *Curr. Opin. Immunol.* **27,** 60–74 (2014).

194. Gordon, E. B. *et al.* Targeting glutamine metabolism rescues mice from late-stage cerebral malaria. *Proc. Natl. Acad. Sci. U.S.A.* **112,** 13075–13080 (2015).

195. Sklaroff, R. B., Casper, E. S., Magill, G. B. & Young, C. W. Phase I study of 6-diazo-5-oxo-L-norleucine (DON). *Cancer Treat Rep* **64,** 1247–1251 (1980).

196. Kovach, J. S. *et al.* Phase I and pharmacokinetic studies of DON. *Cancer Treat Rep* **65,** 1031–1036 (1981).

197. Earhart, R. H., Koeller, J. M. & Davis, H. L. Phase I trial of 6-diazo-5-oxo-L-norleucine (DON) administered by 5-day courses. *Cancer Treat Rep* **66,** 1215–1217 (1982).

198. Earhart, R. H. *et al.* Phase II trial of 6-diazo-5-oxo-L-norleucine versus aclacinomycin-A in advanced sarcomas and mesotheliomas. *Invest New Drugs* **8,** 113–119 (1990).

199. Shijie, J. *et al.* Blockade of glutamate release from microglia attenuates experimental autoimmune encephalomyelitis in mice. *Tohoku J. Exp. Med.* **217,** 87–92 (2009).

200. Shelton, L. M., Huysentruyt, L. C. & Seyfried, T. N. Glutamine targeting inhibits systemic metastasis in the VM-M3 murine tumor model. *Int. J. Cancer* **127,**

2478–2485 (2010).

201. Rudy, J. W. Contextual conditioning and auditory cue conditioning dissociate during development. *Behav. Neurosci.* **107,** 887–891 (1993).

202. Phillips, R. G. & LeDoux, J. E. Lesions of the dorsal hippocampal formation interfere with background but not foreground contextual fear conditioning. *Learn. Mem.* **1,** 34–44 (1994).

203. Logue, S. F., Paylor, R. & Wehner, J. M. Hippocampal lesions cause learning deficits in inbred mice in the Morris water maze and conditioned-fear task. *Behav. Neurosci.* **111,** 104–113 (1997).

204. Holt, W. & Maren, S. Muscimol inactivation of the dorsal hippocampus impairs contextual retrieval of fear memory. *J. Neurosci.* **19,** 9054–9062 (1999).

205. Gould, T. J., McCarthy, M. M. & Keith, R. A. MK-801 disrupts acquisition of contextual fear conditioning but enhances memory consolidation of cued fear conditioning. *Behav Pharmacol* **13,** 287–294 (2002).

206. Goeldner, C., Reiss, D., Wichmann, J., Kieffer, B. L. & Ouagazzal, A.-M. Neurobiology of Learning and Memory. *Neurobiol Learn Mem* **91,** 393–401 (2009).

207. McArthur, J. C., Steiner, J., Sacktor, N. & Nath, A. HIV-associated neurocognitive disorders: 'mind the gap'. *Ann Neurol.* **67**, 699-714 (2010). doi:10.1002/ana.22053

208. Fitting, S. *et al.* Synaptic dysfunction in the hippocampus accompanies learning and memory deficits in human immunodeficiency virus type-1 Tat transgenic mice. *Biol. Psychiatry* **73,** 443–453 (2013).

209. Potter, M. C., Figuera-Losada, M., Rojas, C. & Slusher, B. S. Targeting the glutamatergic system for the treatment of HIV-associated neurocognitive disorders. *J Neuroimmune Pharmacol* **8,** 594–607 (2013).

210. Griffin, D. E. Recovery from viral encephalomyelitis: immune-mediated noncytolytic virus clearance from neurons. *Immunol Res* **47,** 123–133 (2010).

211. Murrell, J. R. & Hunter, D. D. An olfactory sensory neuron line, odora, properly targets olfactory proteins and responds to odorants. *J. Neurosci.* **19,** 8260–8270 (1999).

212. Durand, M. M., Chugani, D. C., Mahmoudi, M. & Phelps, M. E. Characterization of neuron-like cell line immortalized from primary rat mesencephalon cultures. *Soc. Neurosci. Abstr.* **16,** 40 (1990).

213. Zhong, L. T., Kane, D. J. & Bredesen, D. E. BCL-2 blocks glutamate toxicity in neural cell lines. *Brain Res. Mol. Brain Res.* **19,** 353–355 (1993).

214. Park, E. & Griffin, D. E. The nsP3 macro domain is important for Sindbis virus replication in neurons and neurovirulence in mice. *Virology* **388,** 305–314 (2009).

215. Jackson, A. C., Moench, T. R., Trapp, B. D. & Griffin, D. E. Basis of neurovirulence in Sindbis virus encephalomyelitis of mice. *Lab. Invest.* **58,** 503–509 (1988).

216. Traver, M. K. *et al.* Immunity-related GTPase M (IRGM) proteins influence the localization of guanylate-binding protein 2 (GBP2) by modulating macroautophagy. *J. Biol. Chem.* **286,** 30471–30480 (2011).

217. Eskildsen, S. Characterization of the 2‘-5’-oligoadenylate synthetase ubiquitin-

like family. *Nucleic Acids Res.* **31,** 3166–3173 (2003).

218. Mattijssen, S. & Pruijn, G. J. M. Viperin, a key player in the antiviral response. *Microbes Infect.* **14,** 419–426 (2012).

219. Karki, S. *et al.* Multiple interferon stimulated genes synergize with the zinc Finger antiviral protein to mediate anti-alphavirus activity. *PLoS ONE* **7,** e37398 (2012).

220. Schroder, K., Sweet, M. J. & Hume, D. A. Signal integration between IFNγ and TLR signaling pathways in macrophages. *Immunobiology* **211,** 511–524 (2006).

221. Fahey, J. L., Wunderlich, J. & Mishell, R. The immunoglbulins of mice II. Two subclasses of mouse 7S γ2-globulins: γ2a- and γ2b-globulins. *J. Exp. Med.* **120,** 243–251 (1964).

222. Nussenzweig, R. S., Merryman, C. & Benacerraf, B. Electrophoretic separation and properties of mouse antihapten antibodies involved in passive cutaneous anaphylaxis and passive hemolysis. *J. Exp. Med.* **120,** 315–328 (1964).

223. Grey, H. M., Hirst, J. W. & Cohn, M. A new mouse immunoglobulin: IgG3. *J. Exp. Med.* **133,** 289–304 (1971).

224. Levine, B. Eating oneself and uninvited guests: autophagy-related pathways in cellular defense. *Cell* **120,** 159–162 (2005).

225. Lee, H. K., Lund, J. M., Ramanathan, B. & Mizushima, N. Autophagy-dependent viral recognition by plasmacytoid dendritic cells. *Science* **315**, 1398-1401 (2007). doi:10.1126/science.ll37949

226. Petkova, D. S., Viret, C. & Faure, M. IRGM in autophagy and viral infections. *Front Immunol* **3,** 426 (2012).

227. Richetta, C. & Faure, M. Autophagy in antiviral innate immunity. *Cell. Microbiol.* **15,** 368–376 (2013).

228. Hailey, D. W. *et al.* Mitochondria supply membranes for autophagosome biogenesis during starvation. *Cell* **141,** 656–667 (2010).

229. Grégoire, I. P. *et al.* IRGM Is a common target of RNA viruses that subvert the autophagy network. *PLoS Pathog* **7,** e1002422 (2011).

230. Joubert, P.-E. *et al.* Autophagy induction by the pathogen receptor CD46. *Cell Host Microbe* **6,** 354–366 (2009).

231. Kyei, G. B. *et al.* Autophagy pathway intersects with HIV-1 biosynthesis and regulates viral yields in macrophages. *J. Cell Biol.* **186,** 255–268 (2009).

232. Meiffren, G., Joubert, P. E., Grégoire, I. P. & Codogno, P. Pathogen recognition by the cell surface receptor CD46 induces autophagy. *Autophagy* **6**, 299-300 (2010). doi:10.4161/auto.6.2.11132

233. Krejbich-Trotot, P. *et al.* Chikungunya triggers an autophagic process which promotes viral replication. *Virol. J.* **8,** 432 (2011).

234. Joubert, P.-E. *et al.* Chikungunya-induced cell death is limited by ER and oxidative stress-induced autophagy. *Autophagy* **8,** 1261–1263 (2012).

235. Wang, X. *et al.* Capsid, membrane and NS3 are the major viral proteins involved in autophagy induced by Japanese encephalitis virus. *Vet. Microbiol.* **178,** 217–229 (2015).

236. Haldar, A. K. *et al.* IRG and GBP host resistance factors target aberrant, "non-self" vacuoles characterized by the missing of ‘self’ IRGM proteins. *PLoS Pathog* **9,** e1003414 (2013).

237. Carter, C. C., Gorbacheva, V. Y. & Vestal, D. J. Inhibition of VSV and EMCV replication by the interferon-induced GTPase, mGBP-2: differential requirement for wild-type GTP binding domain. *Arch Virol* **150,** 1213–1220 (2005).

238. KylAniemi, M. K., Haveri, A., Vuola, J. M., Puolakkainen, M. & Lahesmaa, R. Gene expression signatures characterizing the development of lymphocyte response during experimental Chlamydia pneumoniae infection. *Microb. Pathog.* **46,** 235–242 (2009).

239. Gautam, A. *et al.* Interleukin-10 alters effector functions of multiple genes induced by *Borrelia burgdorferi* in macrophages to regulate Lyme disease inflammation. *Infect. Immun.* **79,** 4876–4892 (2011).

240. Degrandi, D. *et al.* Murine guanylate binding protein 2 (mGBP2) controls Toxoplasma gondii replication. *Proc. Natl. Acad. Sci. U.S.A.* **110,** 294–299 (2013).

241. Meunier, E. *et al.* Guanylate-binding proteins promote activation of the AIM2 inflammasome during infection with Francisella novicida. *Nat. Immunol.* **16,** 476–484 (2015).

242. Pulit-Penaloza, J. A., Scherbik, S. V. & Brinton, M. A. Activation of Oas1a gene expression by type I IFN requires both STAT1 and STAT2 while only STAT2 is required for Oas1b activation. *Virology* **425,** 71–81 (2012).

243. Drappier, M. & Michiels, T. Inhibition of the OAS/RNase L pathway by viruses. *Curr Opin Virol* **15,** 19–26 (2015).

244. Saha, S. & Rangarajan, P. N. Common host genes are activated in mouse brain by Japanese encephalitis and rabies viruses. *J. Gen. Virol.* **84,** 1729–1735 (2003).

245. Hinson, E. R. & Cresswell, P. The antiviral protein, viperin, localizes to lipid droplets via its N-terminal amphipathic alpha-helix. *Proc. Natl. Acad. Sci. U.S.A.* **106,** 20452–20457 (2009).

246. Hinson, E. R. & Cresswell, P. The N-terminal amphipathic α-helix of viperin mediates localization to the cytosolic face of the endoplasmic reticulum and inhibits protein secretion. *J. Biol. Chem.* **284**, 4705–4712 (2009).

247. Wang, X., Hinson, E. R. & Cresswell, P. The interferon-inducible protein viperin inhibits influenza virus release by perturbing lipid rafts. *Cell Host Microbe* **2,** 96–105 (2007).

248. Nasr, N. *et al.* HIV-1 infection of human macrophages directly induces viperin which inhibits viral production. *Blood* **120,** 778–788 (2012).

249. Tan, K. S. *et al.* In vivo and in vitro studies on the antiviral activities of viperin against influenza H1N1 virus infection. *J. Gen. Virol.* **93,** 1269–1277 (2012).

250. Miyanari, Y. *et al.* The lipid droplet is an important organelle for hepatitis C virus production. *Nat. Cell Biol.* **9,** 1089–1097 (2007).

251. Helbig, K. J. *et al.* The antiviral protein viperin inhibits hepatitis C virus replication via interaction with nonstructural protein 5A. *Hepatology* **54,** 1506–1517 (2011).

252. Helbig, K. J. & Beard, M. R. The role of viperin in the innate antiviral response. *J. Mol. Biol.* **426,** 1210–1219 (2014).

253. Teng, T.-S. *et al.* Viperin restricts chikungunya virus replication and pathology. *J. Clin. Invest.* **122,** 4447–4460 (2012).

254. Saitoh, T. *et al.* Antiviral protein Viperin promotes Toll-like receptor 7- and

Toll-like receptor 9-mediated type I interferon production in plasmacytoid dendritic cells. *Immunity* **34,** 352–363 (2011).

255. Chan, Y.-L., Chang, T.-H., Liao, C.-L. & Lin, Y.-L. The cellular antiviral protein viperin is attenuated by proteasome-mediated protein degradation in Japanese encephalitis virus-infected cells. *J. Virol.* **82,** 10455–10464 (2008).

256. Seo, J. Y., Yaneva, R., Hinson, E. R. & Cresswell, P. Human cytomegalovirus directly induces the antiviral protein viperin to enhance infectivity. *Science* **332,** 1093-1097 (2011).

257. Todorova, T., Bock, F. J. & Chang, P. Poly(ADP-ribose) polymerase-13 and RNA regulation in immunity and cancer. *Trends Mol Med* **21,** 373–384 (2015).

258. Müller, S. *et al.* Inhibition of filovirus replication by the zinc finger antiviral protein. *J. Virol.* **81,** 2391–2400 (2007).

259. Zhu, Y. *et al.* Zinc-finger antiviral protein inhibits HIV-1 infection by selectively targeting multiply spliced viral mRNAs for degradation. *Proc. Natl. Acad. Sci. U.S.A.* **108,** 15834–15839 (2011).

260. Zhu, Y., Wang, X., Goff, S. P. & Gao, G. Translational repression precedes and is required for ZAP-mediated mRNA decay. *EMBO J.* **31,** 4236–4246 (2012).

261. Mao, R. *et al.* Inhibition of hepatitis B virus replication by the host zinc finger antiviral protein. *PLoS Pathog* **9,** e1003494–18 (2013).

262. Seo, G. J. *et al.* Reciprocal inhibition between intracellular antiviral signaling and the RNAi machinery in mammalian cells. *Cell Host Microbe* **14,** 435–445 (2013).

263. Blasius, A. L. & Beutler, B. Intracellular toll-like receptors. *Immunity* **32,** 305–

315 (2010).

264. Pasare, C. & Medzhitov, R. Toll-like receptors: linking innate and adaptive immunity. In *Mechanisms of Lymphocyte Activation and Immune Regulation* (eds. Gupta, S., Paul, W. E. & Fauci, A. S.) **560,** 11–18 (Springer US, 2005).

265. Grieder, F. B. & Vogel, S. N. Role of interferon and interferon regulatory factors in early protection against Venezuelan equine encephalitis virus infection. *Virology* **257,** 106–118 (1999).

266. Soh, J., Donnelly, R. J., Kotenko, S., Mariano, T. M. & Cook, J. R. Identification and sequence of an accessory factor required for activation of the human interferon γ receptor. *Cell* **76,** 793–802 (1994).

267. Kotenko, S. V. *et al.* Interaction between the components of the interferon gamma receptor complex. *J. Biol. Chem.* **270,** 20915–20921 (1995).

268. Leon, C., Nandan, D. & Lopez, M. Annexin V Associates with the IFN-γ Receptor and Regulates IFN-γ Signaling. *J. Immunol.* **176**, 5934-5942 (2006). doi:10.4049/jimmunol.176.10.5934

269. Lee, E.-Y., Schultz, K. L. W. & Griffin, D. E. Mice deficient in interferon-gamma or interferon-gamma receptor 1 have distinct inflammatory responses to acute viral encephalomyelitis. *PLoS ONE* **8,** e76412 (2013).

270. Charles, P. C., Trgovcich, J., Davis, N. L. & Johnston, R. E. Immunopathogenesis and immune modulation of Venezuelan equine encephalitis virus-induced disease in the mouse. *Virology* **284,** 190–202 (2001).

271. Feuerstein, G. Z., Liu, T. & Barone, F. C. Cytokines, inflammation, and brain injury: role of tumor necrosis factor-alpha. *Cerebrovasc Brain Metab Rev* **6,**

341–360 (1994).

272. Fehr, A. R. *et al.* The nsp3 macrodomain promotes virulence in mice with coronavirus-induced encephalitis. *J. Virol.* **89,** 1523–1536 (2015).

273. Tran, E. H., Prince, E. N. & Owens, T. IFN-γ shapes immune invasion of the central nervous system via regulation of chemokines. *J. Immunol.* **164**, 2759-2768 (2000). doi:10.4049/jimmunol.164.5.2759

274. Palus, M. *et al.* Mice with different susceptibility to tick-borne encephalitis virus infection show selective neutralizing antibody response and inflammatory reaction in the central nervous system. *J Neuroinflammation* **10,** 77 (2013).

275. Trujillo, J. A., Fleming, E. L. & Perlman, S. Transgenic CCL2 expression in the central nervous system results in a dysregulated immune response and enhanced lethality after coronavirus infection. *J. Virol.* **87,** 2376–2389 (2013).

276. Hussmann, K. L. & Fredericksen, B. L. Differential induction of CCL5 by pathogenic and non-pathogenic strains of West Nile virus in brain endothelial cells and astrocytes. *J. Gen. Virol.* **95,** 862–867 (2014).

277. Quick, E. D., Leser, J. S., Clarke, P. & Tyler, K. L. Activation of intrinsic immune responses and microglial phagocytosis in an ex vivo spinal cord slice culture model of West Nile virus infection. *J. Virol.* **88,** 13005–13014 (2014).

278. Bardina, S. V. *et al.* Differential roles of chemokines CCL2 and CCL7 in monocytosis and leukocyte migration during West Nile virus infection. *J. Immunol.* **195,** 4306–4318 (2015).

279. Miller, M. D. & Krangel, M. S. The human cytokine I-309 is a monocyte chemoattractant. *Proc. Natl. Acad. Sci. U.S.A.* **89,** 2950–2954 (1992).

280. D'Ambrosio, D., Iellem, A. & Bonecchi, R. Cutting edge: selective up-regulation of chemokine receptors CCR4 and CCR8 upon activation of polarized human type 2 Th cells. *J. Immunol.* **161**, 5111-5115 (1998).

281. Colantonio, L., Iellem, A., Sinigaglia, F. & D'Ambrosio, D. Skin-homing CLA+ T cells and regulatory CD25+ T cells represent major subsets of human peripheral blood memory T cells migrating in response to CCL1/I-309. *Eur. J. Immunol.* **32,** 3506–3514 (2002).

282. Tamgüney, G., Van Snick, J. & Fickenscher, H. Autocrine stimulation of rhadinovirus-transformed T cells by the chemokine CCL1/I-309. *Oncogene* **23,** 8475–8485 (2004).

283. Zhu, J. & Paul, W. E. CD4 T cells: fates, functions, and faults. *Blood* **112,** 1557–1569 (2008).

284. Jinquan, T., Larsen, C. G., Gesser, B., Matsushima, K. & Thestrup-Pedersen, K. Human IL-10 is a chemoattractant for CD8+ T lymphocytes and an inhibitor of IL-8-induced CD4+ T lymphocyte migration. *J. Immunol.* **151,** 4545–4551 (1993).

285. Groux, H., Bigler, M., de Vries, J. E. & Roncarolo, M. G. Inhibitory and stimulatory effects of IL-10 on human CD8+ T cells. *J. Immunol.* **160,** 3188–3193 (1998).

286. Rowbottom, A. W., Lepper, M. A., Garland, R. J., Cox, C. V. & Corley, E. G. Interleukin-10-induced CD8 cell proliferation. *Immunology* **98,** 80–89 (1999).

287. Santin, A. D. *et al.* Interleukin-10 increases Th1 cytokine production and cytotoxic potential in human papillomavirus-specific CD8(+) cytotoxic T

lymphocytes. *J. Virol.* **74,** 4729–4737 (2000).

288. Moore, K. W., de Waal Malefyt, R., Coffman, R. L. & O'Garra, A. Interleukin-10 and the interleukin-10 receptor. *Annu. Rev. Immunol.* **19,** 683–765 (2001).

289. Cantin, E., Tanamachi, B. & Openshaw, H. Role for gamma interferon in control of herpes simplex virus type 1 reactivation. *J. Virol.* **73,** 3418–3423 (1999).

290. Hou, W., Kang, H. S. & Kim, B. S. Th17 cells enhance viral persistence and inhibit T cell cytotoxicity in a model of chronic virus infection. *J. Exp. Med.* **206,** 313–328 (2009).

291. Kim, B. S. *et al.* IL-1 signal affects both protection and pathogenesis of virus-induced chronic CNS demyelinating disease. *J Neuroinflammation* **9,** 217 (2012).

292. Savarin, C. *et al.* IFN-γ protects from lethal IL-17 mediated viral encephalomyelitis independent of neutrophils. *J Neuroinflammation* **9,** 104 (2012).

293. Fong, T. A. & Mosmann, T. R. Alloreactive murine CD8+ T cell clones secrete the Th1 pattern of cytokines. *J. Immunol.* **144,** 1744–1752 (1990).

294. Fischer, U., Jänicke, R. U. & Schulze-Osthoff, K. Many cuts to ruin: a comprehensive update of caspase substrates. *Cell Death and Differentiation* **10,** 76–100 (2003).

295. Taylor, R. C., Cullen, S. P. & Martin, S. J. Apoptosis: controlled demolition at the cellular level. *Nat. Rev. Mol. Cell Biol.* **9,** 231–241 (2008).

296. Afonina, I. S., Cullen, S. P. & Martin, S. J. Cytotoxic and non-cytotoxic roles of the CTL/NK protease granzyme B. *Immunol. Rev.* **235,** 105–116 (2010).

297. Joly, E., Mucke, L. & Oldstone, M. B. Viral persistence in neurons explained by

lack of major histocompatibility class I expression. *Science* **253,** 1283–1285 (1991).

298. Neumann, H., Cavalié, A., Jenne, D. E. & Wekerle, H. Induction of MHC class I genes in neurons. *Science* **269,** 549–552 (1995).

299. Rall, G. F., Mucke, L. & Oldstone, M. B. Consequences of cytotoxic T lymphocyte interaction with major histocompatibility complex class I-expressing neurons in vivo. *J. Exp. Med.* **182,** 1201–1212 (1995).

300. Corriveau, R. A., Huh, G. S. & Shatz, C. J. Regulation of class I MHC gene expression in the developing and mature CNS by neural activity. *Neuron* **21,** 505–520 (1998).

301. Horwitz, M. S., Evans, C. F., Klier, F. G. & Oldstone, M. B. Detailed in vivo analysis of interferon-gamma induced major histocompatibility complex expression in the central nervous system: astrocytes fail to express major histocompatibility complex class I and II molecules. *Lab. Invest.* **79,** 235–242 (1999).

302. Kramer, M. D. & Simon, M. M. Are proteinases functional molecules of T lymphocytes? *Immunol. Today* **8,** 140–142 (1987).

303. Metkar, S. S. *et al.* Human and mouse granzyme A induce a proinflammatory cytokine response. *Immunity* **29,** 720–733 (2008).

304. Lieberman, J. Granzyme A activates another way to die. *Immunol. Rev.* **235,** 93–104 (2010).

305. Afonina, I. S. *et al.* Granzyme B-dependent proteolysis acts as a switch to enhance the proinflammatory activity of IL-1α. *Molecular Cell* **44,** 265–278

(2011).

306. Joeckel, L. T. *et al.* Mouse granzyme K has pro-inflammatory potential. *Cell Death Differ.* **18,** 1112–1119 (2011).

307. Zajac, A. J., Dye, J. M. & Quinn, D. G. Control of lymphocytic choriomeningitis virus infection in granzyme B deficient mice. *Virology* **305**, 1–9 (2003). doi:10.1006/viro.2002.1754

308. Shrestha, B., Samuel, M. A. & Diamond, M. S. CD8+ T cells require perforin to clear West Nile virus from infected neurons. *J. Virol.* **80,** 119–129 (2006).

309. Bergmann, C. C. *et al.* Perforin-mediated effector function within the central nervous system requires IFN-γ-mediated MHC up-regulation. *J. Immunol.* **170,** 3204–3213 (2003).

310. Hooks, J. J. The critical role of IFN-γ in experimental coronavirus retinopathy. *Invest. Ophthalmol. Vis. Sci.* **44,** 3402–3408 (2003).

311. Simon, H. G., Fruth, U., Kramer, M. D. & Simon, M. M. A secretable serine proteinase with highly restricted specificity from cytolytic T lymphocytes inactivates retrovirus-associated reverse transcriptase. *FEBS Letters* **223,** 352–360 (1987).

312. Andrade, F., Fellows, E., Jenne, D. E., Rosen, A. & Young, C. S. H. Granzyme H destroys the function of critical adenoviral proteins required for viral DNA replication and granzyme B inhibition. *EMBO J.* **26,** 2148–2157 (2007).

313. van Domselaar, R. *et al.* Noncytotoxic inhibition of cytomegalovirus replication through NK cell protease granzyme M-mediated cleavage of viral phosphoprotein 71. *J. Immunol.* **185,** 7605–7613 (2010).

314. Decman, V., Kinchington, P. R., Harvey, S. A. K. & Hendricks, R. L. Gamma interferon can block herpes simplex virus type 1 reactivation from latency, even in the presence of late gene expression. *J. Virol.* **79,** 10339–10347 (2005).

315. Verjans, G. M. G. M. *et al.* Selective retention of herpes simplex virus-specific T cells in latently infected human trigeminal ganglia. *Proc. Natl. Acad. Sci. U.S.A.* **104,** 3496–3501 (2007).

316. Knickelbein, J. E. *et al.* Noncytotoxic lytic granule-mediated CD8+ T cell inhibition of HSV-1 reactivation from neuronal latency. *Science* **322,** 268–271 (2008).

317. Ehlers, I. *et al.* Functional characterization of the interaction between human La and hepatitis B virus RNA. *J. Biol. Chem.* **279,** 43437–43447 (2004).

318. Romero, V., Fellows, E., Jenne, D. E. & Andrade, F. Cleavage of La protein by granzyme H induces cytoplasmic translocation and interferes with La-mediated HCV-IRES translational activity. *Cell Death and Differentiation* **16,** 340–348 (2009).

319. Vashist, S., Anantpadma, M., Sharma, H. & Vrati, S. La protein binds the predicted loop structures in the 3' non-coding region of Japanese encephalitis virus genome: role in virus replication. *J. Gen. Virol.* **90,** 1343–1352 (2009).

320. Lin, J.-Y. *et al.* Heterogeneous nuclear ribonuclear protein K interacts with the enterovirus 71 5' untranslated region and participates in virus replication. *J. Gen. Virol.* **89,** 2540–2549 (2008).

321. Wolf, D. *et al.* HIV Nef enhances Tat-mediated viral transcription through a hnRNP-K-nucleated signaling complex. *Cell Host Microbe* **4,** 398–408 (2008).

322. Kanlaya, R., Pattanakitsakul, S.-N., Sinchaikul, S., Chen, S.-T. & Thongboonkerd, V. Vimentin interacts with heterogeneous nuclear ribonucleoproteins and dengue nonstructural protein 1 and is important for viral replication and release. *Mol Biosyst* **6,** 795–806 (2010).

323. Bouraï, M. *et al.* Mapping of Chikungunya virus interactions with host proteins identified nsP2 as a highly connected viral component. *J. Virol.* **86,** 3121–3134 (2012).

324. Burnham, A. J., Gong, L. & Hardy, R. W. Heterogeneous nuclear ribonuclear protein K interacts with Sindbis virus nonstructural proteins and viral subgenomic mRNA. *Virology* **367,** 212–221 (2007).

325. Varjak, M. *et al.* Magnetic fractionation and proteomic dissection of cellular organelles occupied by the late replication complexes of Semliki Forest virus. *J. Virol.* **87,** 10295–10312 (2013).

326. Snapper, C. M. & Paul, W. E. Interferon-gamma and B cell stimulatory factor-1 reciprocally regulate Ig isotype production. *Science* **236**, 944-947 (1987).

327. Stevens, T. L. *et al.* Regulation of antibody isotype secretion by subsets of antigen-specific helper T cells. *Nature* **334,** 255–258 (1988).

328. Vella, A., Teague, T. K., Ihle, J. & Kappler, J. Interleukin 4 (IL-4) or IL-7 prevents the death of resting T cells: Stat6 is probably not required for the effect of IL-4. *J. Exp. Med.* **186**, 325–330 (1997).

329. Laidlaw, B. J. *et al.* CD4+ T cell help guides formation of CD103+ lung-resident memory CD8+ T cells during influenza viral infection. *Immunity* **41,** 633–645 (2014).

330. Beura, L. K. *et al.* Lymphocytic choriomeningitis virus persistence promotes effector-like memory differentiation and enhances mucosal T cell distribution. *J. Leukoc. Biol.* **97,** 217–225 (2015).

331. McMaster, S. R., Wilson, J. J., Wang, H. & Kohlmeier, J. E. Airway-resident memory CD8 T cells provide antigen-specific protection against respiratory virus challenge through rapid IFN-γ production. *J. Immunol.* **195,** 203–209 (2015).

332. Ge, M. Q. *et al.* NK cells regulate CD8+ T cell priming and dendritic cell migration during influenza A infection by IFN-γ and perforin-dependent mechanisms. *J. Immunol.* **189,** 2099–2109 (2012).

333. Homann, D., Teyton, L. & Oldstone, M. B. Differential regulation of antiviral T-cell immunity results in stable CD8+ but declining CD4+ T-cell memory. *Nat. Med.* **7,** 913–919 (2001).

334. Zuo, J., Stohlman, S. A., Parra, G. I. & Bergmann, C. C. IL-15 independent maintenance of virus-specific CD8+ T cells in the CNS during chronic infection. *J. Neuroimmunol.* **207,** 32–38 (2009).

335. Hawke, S., Stevenson, P. G. & Freeman, S. Long-term persistence of activated cytotoxic T lymphocytes after viral infection of the central nervous system. *J. Exp. Med.* **187**, 1575-1582 (1998).

336. van der Most, R. G. & Krishna, K. M. Prolonged presence of effector-memory CD8 T cells in the central nervous system after dengue virus encephalitis. *Int. Immunol.* **15**, 119-125 (2003).

337. Ramakrishna, C. & Stohlman, S. A. Differential regulation of primary and secondary CD8+ T cells in the central nervous system. *J. Immunol.* **173**, 6265-

6273 (2004). doi:10.4049/jimmunol.173.10.6265

338. Obar, J. J., Crist, S. G. & Leung, E. K. IL-15-independent proliferative renewal of memory CD8+ T cells in latent gammaherpesvirus infection. *J. Immunol.* **173**, 2705-2714 (2004). doi:10.4049/jimmunol.173.4.2705

339. Sprent, C. D. S. J. Homeostasis of naive and memory T cells. *Immunity* **29,** 848–862 (2008).

340. Wakim, L. M., Waithman, J., van Rooijen, N., Heath, W. R. & Carbone, F. R. Dendritic cell-induced memory T cell activation in nonlymphoid tissues. *Science* **319,** 198–202 (2008).

341. Booth, J. S. & Toapanta, F. R. Characterization and functional properties of gastric tissue-resident memory T cells from children, adults, and the elderly. *Front Immunol* **5**, 294 (2014). doi:10.3389/fimmu.2014.00294

342. Turner, D. L. & Farber, D. L. Mucosal resident memory CD4 T cells in protection and immunopathology. *Front Immunol* **5**, 331 (2014). doi:10.3389/fimmu.2014.00331

343. Glennie, N. D. *et al.* Skin-resident memory CD4+ T cells enhance protection against Leishmania major infection. *J. Exp. Med.* **212,** 1405–1414 (2015).

344. Watanabe, R. *et al.* Human skin is protected by four functionally and phenotypically discrete populations of resident and recirculating memory T cells. *Sci Transl Med* **7,** 279ra39–279ra39 (2015).

345. Wakim, L. M. *et al.* The molecular signature of tissue resident memory CD8 T cells isolated from the brain. *J. Immunol.* **189,** 3462–3471 (2012).

346. Kahan, S. M., Wherry, E. J. & Zajac, A. J. T cell exhaustion during persistent

viral infections. *Virology* **479-480,** 180–193 (2015).

347. La Gruta, N. L., Turner, S. J. & Doherty, P. C. Hierarchies in cytokine expression profiles for acute and resolving influenza virus-specific CD8+ T cell responses: correlation of cytokine profile and TCR avidity. *J. Immunol.* **172,** 5553–5560 (2004).

348. Hermes, G. *et al.* Neurological and behavioral abnormalities, ventricular dilatation, altered cellular functions, inflammation, and neuronal injury in brains of mice due to common, persistent, parasitic infection. *J Neuroinflammation* **5,** 48 (2008).

349. Kannan, G. *et al. Toxoplasma gondii* strain-dependent effects on mouse behaviour. *Folia Parasitol.* **57,** 151–155 (2010).

350. Howe, C. L., LaFrance-Corey, R. G., Sundsbak, R. S. & LaFrance, S. J. Inflammatory monocytes damage the hippocampus during acute picornavirus infection of the brain. *J Neuroinflammation* **9,** 50 (2012).

351. de Miranda, A. S. *et al.* Dengue-3 encephalitis promotes anxiety-like behavior in mice. *Behav. Brain Res.* **230,** 237–242 (2012).

352. Parra, B. *et al.* IFN-γ is required for viral clearance from central nervous system oligodendroglia. *J. Immunol.* **162,** 1641–1647 (1999).

353. Henrichsen, P., Bartholdy, C., Christensen, J. P. & Thomsen, A. R. Impaired virus control and severe CD8+ T-cell-mediated immunopathology in chimeric mice deficient in gamma interferon receptor expression on both parenchymal and hematopoietic cells. *J. Virol.* **79,** 10073–10076 (2005).

354. Krakowski, M. & Owens, T. Interferon-γ confers resistance to experimental

allergic encephalomyelitis. *Eur. J. Immunol.* **26,** 1641–1646 (1996).

355. Willenborg, D. O., Fordham, S., Bernard, C. C., Cowden, W. B. & Ramshaw, I. A. IFN-gamma plays a critical down-regulatory role in the induction and effector phase of myelin oligodendrocyte glycoprotein-induced autoimmune encephalomyelitis. *J. Immunol.* **157,** 3223–3227 (1996).

356. Pewe, L., Haring, J. & Perlman, S. CD4 T-cell-mediated demyelination is increased in the absence of gamma interferon in mice infected with mouse hepatitis virus. *J. Virol.* **76**, 7329–7333 (2002). doi:10.1128/JVI.76.14.7329-7333.2002

357. Prestwood, T. R. *et al.* Gamma interferon (IFN-γ) receptor restricts systemic dengue virus replication and prevents paralysis in IFN-α/β receptor-deficient mice. *J. Virol.* **86,** 12561–12570 (2012).

358. Dalton, D. K. *et al.* Multiple defects of immune cell function in mice with disrupted interferon-gamma genes. *Science* **259,** 1739–1742 (1993).

359. Huang, S. *et al.* Immune response in mice that lack the interferon-gamma receptor. *Science* **259,** 1742–1745 (1993).

360. Schijns, V. E. *et al.* IFN-gamma receptor-deficient mice generate antiviral Th1-characteristic cytokine profiles but altered antibody responses. *J. Immunol.* **153,** 2029–2037 (1994).

361. Kyuwa, S. *et al.* Murine coronavirus-induced subacute fatal peritonitis in C57BL/6 mice deficient in gamma interferon. *J. Virol.* **72,** 9286–9290 (1998).

362. Brown, D. M., Lee, S., Garcia-Hernandez, M. de L. L. & Swain, S. L. Multifunctional CD4 cells expressing gamma interferon and perforin mediate

protection against lethal influenza virus infection. *J. Virol.* **86,** 6792–6803 (2012).

363. Earl, P. L., Americo, J. L. & Moss, B. Lethal monkeypox virus infection of CAST/EiJ mice is associated with a deficient gamma interferon response. *J. Virol.* **86,** 9105–9112 (2012).

364. Teijaro, J. R., Verhoeven, D., Page, C. A., Turner, D. & Farber, D. L. Memory CD4 T cells direct protective responses to influenza virus in the lungs through helper-independent mechanisms. *J. Virol.* **84,** 9217–9226 (2010).

365. Getts, D. R. *et al.* Role of IFN-gamma in an experimental murine model of West Nile virus-induced seizures. *J. Neurochem.* **103,** 1019–1030 (2007).

366. Nargi-Aizenman, J. L. & Griffin, D. E. Sindbis virus-induced neuronal death is both necrotic and apoptotic and is ameliorated by N-methyl-D-aspartate receptor antagonists. *J. Virol.* **75,** 7114–7121 (2001).

367. Mizuno, T. *et al.* Interferon-gamma directly induces neurotoxicity through a neuron specific, calcium-permeable complex of IFN-gamma receptor and AMPA GluR1 receptor. *FASEB J.* **22,** 1797–1806 (2008).

368. Lee, J., Kim, S. J., Son, T. G., Chan, S. L. & Mattson, M. P. Interferon-gamma is up-regulated in the hippocampus in response to intermittent fasting and protects hippocampal neurons against excitotoxicity. *J. Neurosci. Res.* **83,** 1552–1557 (2006).

369. Chu, C. Q., Wittmer, S. & Dalton, D. K. Failure to suppress the expansion of the activated CD4 T cell population in interferon γ–deficient mice leads to exacerbation of experimental autoimmune encephalomyelitis. *J. Exp. Med.* **192**,

123-128 (2000).

370. Barkhouse, D. A. *et al.* Expression of interferon gamma by a recombinant rabies virus strongly attenuates the pathogenicity of the virus via induction of type I interferon. *J. Virol.* **89,** 312–322 (2015).

371. Remakus, S. & Sigal, L. J. Gamma interferon and perforin control the strength, but not the hierarchy, of immunodominance of an antiviral CD8+ T cell response. *J. Virol.* **85,** 12578–12584 (2011).

372. Hidalgo, L. G., Urmson, J. & Halloran, P. F. IFN-gamma decreases CTL generation by limiting IL-2 production: A feedback loop controlling effector cell production. *Am. J. Transplant.* **5,** 651–661 (2005).

373. Maillard, I., Launois, P., Xenarios, I. & Louis, J. A. Immune response to mouse mammary tumor virus in mice lacking the alpha/beta interferon or the gamma interferon receptor. *J. Virol.* **72**, 2638–2646 (1998).

374. Pearce, B. D., Hobbs, M. V., McGraw, T. S. & Buchmeier, M. J. Cytokine induction during T-cell-mediated clearance of mouse hepatitis virus from neurons in vivo. *J. Virol.* **68,** 5483–5495 (1994).

375. Geiger, K. D. *et al.* Cytokine-mediated survival from lethal herpes simplex virus infection: role of programmed neuronal death. *Proc. Natl. Acad. Sci. U.S.A.* **92,** 3411–3415 (1995).

376. Hallensleben, W. & Staeheli, P. Inhibition of Borna disease virus multiplication by interferon: cell line differences in susceptibility. *Arch Virol* **144,** 1209–1216 (1999).

377. Jin, Y., Lundkvist, G., Dons, L., Kristensson, K. & Rottenberg, M. E. Interferon-

gamma mediates neuronal killing of intracellular bacteria. *Scand. J. Immunol.* **60,** 437–448 (2004).

378. Klein, R. S. & Diamond, M. S. Immunological headgear: antiviral immune responses protect against neuroinvasive West Nile virus. *Trends Mol Med* **14,** 286–294 (2008).

379. Prince, G. A. *et al.* Mechanism of antibody-mediated viral clearance in immunotherapy of respiratory syncytial virus infection of cotton rats. *J. Virol.* **64,** 3091–3092 (1990).

380. Dietzschold, B. Antibody-mediated clearance of viruses from the mammalian central nervous system. *Trends Microbiol.* **1,** 63–66 (1993).

381. Szomolanyi-Tsuda, E. & Welsh, R. M. T cell-independent antibody-mediated clearance of polyoma virus in T cell-deficient mice. *J. Exp. Med.* **183,** 403–411 (1996).

382. Hirano, N., Taira, H., Sato, S., Hashikawa, T. & Tohyama, K. Antibody-mediated virus clearance from neurons of rats infected with hemagglutinating encephalomyelitis virus. *Adv Exp Med Biol* **581,** 391–394 (2006).

383. Chachu, K. A. *et al.* Antibody is critical for the clearance of murine norovirus infection. *J. Virol.* **82,** 6610–6617 (2008).

384. Hooper, D. C., Phares, T. W., Fabis, M. J. & Roy, A. The production of antibody by invading B cells is required for the clearance of rabies virus from the central nervous system. *PLoS Negl Trop Dis* **3,** e535 (2009).

385. Chen, H.-W. *et al.* A poorly neutralizing IgG2a/c response elicited by a DNA vaccine protects mice against Japanese encephalitis virus. *J. Gen. Virol.* **95,**

1983–1990 (2014).

386. Neuberger, M. S. & Rajewsky, K. Activation of mouse complement by monoclonal mouse antibodies. *Eur. J. Immunol.* **11,** 1012–1016 (1981).

387. Kipps, T. J., Parham, P., Punt, J. & Herzenberg, L. A. Importance of immunoglobulin isotype in human antibody-dependent, cell-mediated cytotoxicity directed by murine monoclonal antibodies. *J. Exp. Med.* **161,** 1–17 (1985).

388. van Domselaar, R. & Bovenschen, N. Cell death-independent functions of granzymes: hit viruses where it hurts. *Rev. Med. Virol.* **21,** 301–314 (2011).

389. Ravi, V. *et al.* Persistence of Japanese encephalitis virus in the human nervous system. *J. Med. Virol.* **40,** 326–329 (1993).

390. Donnelly, S. M., Sheahan, B. J. & Atkins, G. J. Long-term effects of Semliki Forest virus infection in the mouse central nervous system. *Neuropathol Appl Neurobiol* **23,** 235–241 (1997).

391. Appler, K. K. *et al.* Persistence of West Nile virus in the central nervous system and periphery of mice. *PLoS ONE* **5,** e10649 (2010).

392. Brooke, C. B., Deming, D. J., Whitmore, A. C., White, L. J. & Johnston, R. E. T cells facilitate recovery from Venezuelan equine encephalitis virus-induced encephalomyelitis in the absence of antibody. *J. Virol.* **84,** 4556–4568 (2010).

393. Münz, C., Lünemann, J. D., Getts, M. T. & Miller, S. D. Antiviral immune responses: triggers of or triggered by autoimmunity? *Nat Rev Immunol* **9,** 246–258 (2009).

394. Reuter, D. & Schneider-Schaulies, J. Measles virus infection of the CNS: human

disease, animal models, and approaches to therapy. *Med. Microbiol. Immunol.* **199,** 261–271 (2010).

395. Freeman, M. L., Sheridan, B. S. & Bonneau, R. H. Psychological stress compromises CD8+ T cell control of latent herpes simplex virus type 1 infections. *J. Immunol.* **179**, 322-328 (2007). doi:10.4049/jimmunol.179.1.322

396. Linn, M. L., Aaskov, J. G. & Suhrbier, A. Antibody-dependent enhancement and persistence in macrophages of an arbovirus associated with arthritis. *J. Gen. Virol.* **77,** 407–411 (1996).

397. Suhrbier, A. & La Linn, M. Clinical and pathologic aspects of arthritis due to Ross River virus and other alphaviruses. *Curr Opin Rheumatol* **16,** 374–379 (2004).

398. Hoarau, J. J. *et al.* Persistent chronic inflammation and infection by Chikungunya arthritogenic alphavirus in spite of a robust host immune response. *J. Immunol.* **184,** 5914–5927 (2010).

399. Morrison, T. E. *et al.* A mouse model of chikungunya virus-induced musculoskeletal inflammatory disease: evidence of arthritis, tenosynovitis, myositis, and persistence. *Am. J. Pathol.* **178,** 32–40 (2011).

400. Stewart, B. S., Demarest, V. L., Wong, S. J., Green, S. & Bernard, K. A. Persistence of virus-specific immune responses in the central nervous system of mice after West Nile virus infection. *BMC Immunol.* **12,** 6 (2011).

401. Liu, T., Khanna, K. M., Chen, X., Fink, D. J. & Hendricks, R. L. CD8(+) T cells can block herpes simplex virus type 1 (HSV-1) reactivation from latency in sensory neurons. *J. Exp. Med.* **191,** 1459–1466 (2000).

402. Liu, T., Khanna, K. M., Carriere, B. N. & Hendricks, R. L. Gamma interferon can prevent herpes simplex virus type 1 reactivation from latency in sensory neurons. *J. Virol.* **75,** 11178–11184 (2001).

403. Khanna, K. M., Lepisto, A. J., Decman, V. & Hendricks, R. L. Immune control of herpes simplex virus during latency. *Curr. Opin. Immunol.* **16,** 463–469 (2004).

404. Himmelein, S. *et al.* Circulating herpes simplex type 1 (HSV-1)-specific CD8+ T cells do not access HSV-1 latently infected trigeminal ganglia. *Herpesviridae* **2,** 5 (2011).

CURRICULUM VITAE
The Johns Hopkins University School of Medicine

Victoria K. Baxter **January 2016**

EDUCATION

Doctor of Philosophy, Johns Hopkins University School of Medicine — Expected 2016
Graduate Program in Cellular and Molecular Medicine
Mentor: Diane E. Griffin, MD, PhD

Doctor of Veterinary Medicine, Texas A&M University — 2010
Summa Cum Laude

Bachelor of Science, Texas A&M University — 2006
Genetics
Summa Cum Laude, University Honors

RESEARCH EXPERIENCE

Doctoral Thesis Research, Johns Hopkins University School of Medicine and Bloomberg School of Public Health, Department of Molecular Microbiology and Immunology, Baltimore, MD

Laboratory of Diane Griffin, MD, PhD — 2011-2016

- Examined the immunopathogenesis and clearance of Sindbis virus in the central nervous system during nonfatal alphavirus encephalomyelitis
- Determined mice develop persistent neurological sequelae following alphavirus infection
- Determined glutamine antagonist treatment mitigates development of clinical disease and central nervous system pathology but delays virus clearance
- Identified the role interferon gamma plays in viral RNA clearance and the mechanisms by which it facilitates virus clearance
- Identified memory T cells present in the brain following clearance of infectious alphavirus

Veterinary Student Research Externship, University of Missouri, Department of Veterinary Pathobiology, Columbia, MO

Laboratory of Matthew H. Myles, DVM, PhD — 2009

- Developed a recombinant hemagglutinin-neuraminidase protein of Sendai virus for use in a diagnostic test

Veterinary Student Research Fellowship, Texas A&M University College of Veterinary Medicine and Health Science Center, Department of Microbial and Molecular Pathogenesis, College Station, TX

Laboratory of James E. Samuel, PhD 2007-2010

- Compared clinical and cytokine profiles between *Coxiella burnetii* isolates during persistent and reactivated Q fever in mice
- Developed a mouse model for intratracheal *Coxiella burnetii* infection

Undergraduate Student Research, Texas A&M University, Department of Biochemistry and Biophysics, College Station, TX

Laboratory of Susan Colette Daubner, PhD 2003-2006

- Examined the mechanism of 14-3-3 protein activity on tyrosine hydroxylase

Summer Undergraduate Medical Research Fellowship, University of Texas Southwestern Medical Center, Department of Neurology, Dallas, TX

Laboratory of Ramon Diaz-Arrastia, MD, PhD 2005

- Examined genetic biomarkers in traumatic brain injury outcome

AWARDS, SCHOLARSHIPS, AND FELLOWSHIPS

American Society for Virology Student Travel Award 2015

- Scholarship awarded to support travel to the 2015 American Society for Virology 34th Annual Meeting at Western University in London, Ontario

NIH T32 Training Grant for Veterinarians in Biomedical Research, Johns Hopkins University School of Medicine 2011-2014

- NIH T32 OD011089, PI MC Zink
- Postdoctoral fellowship in laboratory animal medicine

Burroughs Wellcome Fund Career Award for Medical Scientists 2014
Institutional Nomination, Johns Hopkins University

- Selected as one of five applicants by the Johns Hopkins University Internal Review Committee for nomination to submit an application to the Burroughs Wellcome Fund Career Award for Medical Scientists.

National Institute of Neurological Disorders and Stroke Travel Award 2013

- NINDS 1R13NS084525, PI DE Griffin
- Scholarship awarded to a postdoctoral fellow to support travel to the 2013 Infections of the Nervous System: Pathogenesis to Worldwide Impact Gordon Research Conference in Hong Kong

John C. Clarke Award, Texas A&M College of Veterinary Medicine 2010

- Annually presented to the top five academically-ranked students of the graduating Texas A&M College of Veterinary Medicine DVM class

Mike Keeling Memorial Veterinary Scholarship, Texas A&M College of Veterinary Medicine 2010

- Presented to a veterinary student with academic achievement and an interest in laboratory animal or special species medicine

Texas A&M College of Veterinary Medicine Academic and Excellence Award 2010

- Awarded to the top three academically-ranked students in the fourth year DVM class

Red Finley and Glory and Mojo Neshiem Memorial Scholarship, Texas A&M College of Veterinary Medicine 2010

- Presented to a veterinary student who has displayed excellent empathy and compassion to both owner and pet as well as aptitude and ability in either small animal medicine or oncology

Phi Zeta Induction, Eta Chapter, Texas A&M College of Veterinary Medicine 2009

- Election into the Honor Society of Veterinary Medicine during third year of curriculum as part of the scholastic top 10% of the College of Veterinary Medicine Class of 2010

Danny Davis Memorial Scholarship, Texas A&M College of Veterinary Medicine 2008

- Awarded to veterinary students who have best demonstrated exemplary dedication, perseverance, and loyalty to the study of veterinary medicine

Charles River Laboratories Student Veterinarian Travel Award 2008

- Travel scholarship awarded to a veterinary student displaying interest and aptitude in the field of laboratory animal medicine

Texas A&M College of Veterinary Medicine Class of 1975 Endowed Scholarship 2006-2007

- Scholarship to study at Texas A&M University College of Veterinary Medicine

NIH T35 Veterinary Medical Student Research Training Grant, Texas A&M Agrilife 2007

- NIH T35 RR019530, PI LG Adams
- Summer veterinary student research fellowship

Phi Beta Kappa Induction, Kappa Chapter, Texas A&M University 2006

- Academic honor society with membership granted to the top 10% of college graduates of the university

Texas A&M College of Agriculture and Life Sciences Senior Merit Award 2006

- Presented to a graduating senior in recognition of an outstanding record of academic achievement and distinguished leadership

Nestor R. Bottino Award for Undergraduate Research, Texas A&M University 2006

- Departmental award from the Texas A&M Department of Biochemistry & Biophysics presented to a graduating senior who has shown aptitude and excellence in research during their undergraduate career

Phi Kappa Phi Induction, Chapter 53, Texas A&M University 2006

- Academic honor society that extends membership to the top 10% of the university class

Texas A&M Chapter of Gamma Sigma Delta Outstanding Junior Award 2005

- Award of merit from the Honor Society of Agriculture presented to a junior in the College of Agriculture for academic achievement

McFadden Scholarship, Texas A&M University 2003-2006

- College scholarship for study at Texas A&M University awarded to high school seniors in recognition of outstanding academic achievement

PUBLICATIONS

Olson EJ, Shaw GC, Hutchinson EK, Schultz-Darken N, Bolton ID, Parker J, Morrison JF, **Baxter VK**, Metcalf Pate KA, Mankowski JL, Carlson CS (2015) Bone disease in the common marmoset: Radiographic and histological findings. *Vet Pathol* 52(5):883-93.

Kulcsar KA, **Baxter VK**, Abraham R, Nelson A, Griffin DE. (2015) Distinct immune responses in resistant and susceptible strains of mice during neurovirulent alphavirus encephalomyelitis. *J Virol.* 89(16):8280-8289.

Potter MC*, **Baxter VK***, Mathey RW, Alt J, Rojas C, Griffin DE, Slusher BS (2015) Neurological sequelae induced by alphavirus infection of the CNS are attenuated by treatment with the glutamine antagonist 6-diazo-5-oxo-l-norleucine. *J Neurovirol*. 21(2):159-173. *Co-first authorship

Kulcsar KA, **Baxter VK**, Greene IP, Griffin DE (2014) Interleukin-10 modulation of pathogenic Th17 cells during fatal alphavirus encephalomyelitis. *PNAS.* 111(45):16053-16058.

Johnson NM, Egner PN, **Baxter VK**, Sporn MB, Wible RS, Sutter TR, Groopman JD, Kensler TW, Roebuck BD (2014) Complete protection against aflatoxin B1-induced hepatocellular carcinoma with a synthetic oleanane triterpenoid: molecular signature and genotoxicity threshold. *Cancer Prev Res.* 7(7):658-665.

Baxter VK, Shaw GC, Sotuyo NP, Carlson CS, Olson EJ, Zink MC, Mankowski JL, Adams RJ, Hutchinson EK, Metcalf Pate KA (2013) Serum albumin and body weight as biomarkers for the antemortem identification of bone and gastrointestinal disease in the common marmoset. *PLoS ONE*. 8(12):e82747.

Metcalf TU, **Baxter VK**, Nilaratanakul V, Griffin DE (2013) Recruitment and retention of B cells in the CNS in response to alphavirus encephalomyelitis. *J Virol*. 87(5):2420-2429.

Diaz-Arrastia R, **Baxter VK** (2006) Genetic factors in outcome after traumatic brain injury: what the Human Genome Project can tell us about brain trauma. *J Head Trauma Rehabil*. 21(4):361-374.

PUBLICATIONS IN PRESS

Baxter VK, Griffin DE. "Animal Models." In*: Viral Pathogenesis: From Essentials to Systems Biology, 3rd ed*. N Nathanson and M Katze (Eds.). Academic Press. *Available January 29, 2016.*

Moats CR, **Baxter VK**, Pate NM, Watson J. Parasite burdens, clinical disease, and immune responses during *Myocoptes musculinus* infestations in aging C57BL/6 and *Rag1-/-* mice. *Comp Med*

ORAL PRESENTATIONS

Baxter VK, Potter MC, Slusher BS, Griffin DE. Persistent neurological sequelae in a mouse model of nonfatal alphavirus encephalomyelitis. 2015 National Meeting of the American Association of Laboratory Animal Science. Phoenix, AZ. November 1-5, 2015.

Baxter VK, Griffin DE. The role of interferon gamma in alphavirus clearance from the central nervous system. 34rd Annual Meeting of the American Society for Virology. London, Ontario. July 11-15, 2015.

Baxter VK. The Laboratory Animal Professional's Guide to the World of Vaccine Immunology: What Do I Need to Know About Cell-Mediated Immunity? 2014 National Meeting of the American Association of Laboratory Animal Science. San Antonio, TX. October 19-23, 2014.

Baxter VK, Griffin DE. The effect of interferon gamma on the immunopathogenesis of nonfatal alphavirus encephalomyelitis. 33rd Annual Meeting of the American Society for Virology. Fort Collins, CO. June 21-24, 2014.

Baxter VK, Potter MC, Slusher BS, Griffin DE. Neurological sequelae in a mouse model of alphavirus encephalomyelitis. 2013 Infections of the Nervous System: Pathogenesis and Worldwide Impact Gordon Research Conference. Hong Kong, China. July 7-12, 2013.

Baxter VK, Hutchinson EK, Shaw GC, Metcalf Pate KA. Clinical and biochemical characterization of Bone and Gut Syndrome in the common marmoset (*Callathrix jacchus*). 2012 National Meeting of the American Association of Laboratory Animal Science. Minneapolis, MN. November 4-8, 2012.

Andoh M, **Baxter VK**, Chen C, Russell-Lodrigue KE, Zhang G, Samuel JE. Route of infection and phylogenetic group-specific virulence of isolates determines disease outcome in a Q fever mouse model. 2007 National Meeting of the American Society for Rickettsiology. Colorado Springs, CO. September 8-11, 2007.

POSTER PRESENTATIONS

Moats CR, **Baxter VK**, Pate NM, Watson J. Ectoparasite burden, clinical disease, and immune responses over the infestation in C57BL/6 and *Rag1-/-* mice. 2015 National Meeting of the American Association of Laboratory Animal Science. Phoenix, AZ. November 1-5, 2015.

Baxter VK, Potter MC, Slusher BS, Griffin DE. Delayed virus clearance and immune cell infiltration in a mouse model of alphavirus encephalomyelitis treated with a glutamine antagonist. 2014 Annual Meeting of the Society for Neuroscience. Washington, D.C. November 15-19, 2014.

Baxter VK, Griffin DE. The effect of interferon gamma on the immunopathogenesis of nonfatal alphavirus encephalomyelitis. 2014 Merial-NIH Veterinary Scholars Program Symposium. Ithaca, NY. July 31-August 3, 2014.

Abraham R, Kulcsar KA, **Baxter VK**, Nelson A, Griffin DE. Characterization of the antiviral and immune responses to fatal Alphavirus encephalomyelitis in susceptible C57Bl/6J and resistant Balb/cJ mice. 114th General Meeting of the American Society for Microbiology. Boston, MA. May 17-20, 2014.

Baxter VK, Potter MC, Mathey RW, Slusher BS, Griffin DE. Characterization and inhibition of neurological sequelae induced by alphavirus infection. 2013 Symposium of the International Society for Neurovirology. Washington, D.C. October 29-November 2, 2013.

Baxter VK, Sotuyo NP, Shaw GC, Hutchinson EK, Metcalf Pate KA. Progressive body weight trends predict development of Bone and Gastrointestinal Syndrome in the common marmoset (*Callithrix jacchus*). 2013 National Meeting of the American Association of Laboratory Animal Science. Baltimore, MD. October 27-31, 2013.

Baxter VK, Potter MC, Slusher BS, Griffin DE. Neurological sequelae in a mouse model of alphavirus encephalomyelitis. 2013 Infections of the Nervous System: Pathogenesis and Worldwide Impact Gordon Research Conference. Hong Kong, China. July 7-12, 2013.

Potter MC, **Baxter VK,** Wozniak KM, Griffin DE, Slusher BS. Behavioral characterization of Sindbis virus infected mice. 2013 Annual Meeting of the International Behavioral Neuroscience Society. Malahide, County Dublin, Ireland. June 25-30, 2013.

Baxter VK, Schultz KLW, Metcalf TU, Griffin DE. Interferon gamma-stimulated gene expression in the CNS of Sindbis virus-infected mice. 2012 Department of Molecular Microbiology and Immunology Retreat. Hershey Park, PA. September 15-16, 2012.

Baxter VK, Garcia-Garcia JC, Borroto CJ, Peters LA, Dumler JS, Scorpio DG. Role of MMP9 in the immunopathogenesis of *Anaplasma phagocytophilum* infection in a human granulocytic anaplasmosis mouse model. 2012 National Meeting of the American Society of Rickettsiology. Park City, UT. July 28-31, 2012.

Baxter VK, Metcalf Pate KA, Shaw G, Hutchinson E. Characterization and diagnosis of Bone and Gut Syndrome in the common marmoset (*Callathrix jacchus*). 2012 ACLAM Forum. St. Pete's Beach, FL. May 6-9, 2012.

Baxter VK, Brayton C, Karim B, Watson, J. Omphalitis in immunomodulated weanling mice. 2011 National Meeting of the American Association of Laboratory Animal Science. San Diego, CA. October 2-6, 2011.

Baxter VK, Arenas A, Russell-Lodrigue KE, Weeks BR. Epitheliotropic lymphoma in a cornsnake. 2008 National Meeting of the American College of Veterinary Pathologists. San Antonio, TX. November 15-19, 2008.

Baxter VK, Andoh M, Russell-Lodrigue KE, Samuel JE. Infectivity and inflammatory responses during persistent and reactivated Q fever in mice. 2007 Merck-Merial NIH Veterinary Scholars Symposium. Bethesda, MD. August 2-5, 2007.

Baxter VK, Daubner SC. Identification of the mechanism of 14-3-3 protein activity on tyrosine hydroxylase. Texas A&M University Student Research Week. College Station, TX. March 27-31, 2006.

TEACHING & ACADEMIC SERVICE

2014-present	Course Mentor, Regulations That Govern Animal Research course, Johns Hopkins School of Medicine
2012-present	Lecture Presenter, LAM/Path Integrated Problem Solving course, Johns Hopkins School of Medicine
2010-present	Veterinary Postdoctoral Training Program Admissions Committee Member, Johns Hopkins School of Medicine, Department of Molecular and Comparative Pathobiology
2015	On-Site Seminar Coordinator, The Laboratory Animal Professional's Guide to the Science Behind Common Alternatives to Animal Models, 2015 National Meeting of the American Association of Laboratory Animal Science
2015	Laboratory Assistant, Clinical Examination and Clinical Pathology & Specimen Collection Labs, Mouse Pathobiology and Phenotyping Shortcourse 2015
2015	Remote Site Facilitator for Continuing Education Seminar, District of Columbia Academy of Veterinary Medicine
2014-2015	ACLAM Boards Eligibility Project Research Co-Mentor for Cassandra Moats, Clinical Resident in Laboratory Animal Medicine at Johns Hopkins School of Medicine

2013-2015	Laboratory Mentor, Lab of Diane Griffin, Johns Hopkins Bloomberg School of Public Health, Department of Molecular Microbiology and Immunology ▪ Alicia Braxton, veterinary student research externship, 2015 ▪ Elizabeth Troisi, PhD research rotation, 2015 ▪ Julia Zhao, MHS thesis project, 2014-2015
2013-2014	Senior Trainee in Laboratory Animal Medicine, Johns Hopkins School of Medicine Department of Molecular and Comparative Pathobiology
2013-2014	Teaching Assistant, Fundamental Virology course, Johns Hopkins Bloomberg School of Public Health
2013-2014	Laboratory Animal Medicine Regulations Club Coordinator, Johns Hopkins School of Medicine Department of Molecular and Comparative Pathobiology
2010-2014	Veterinary Trainee in Laboratory Animal Medicine, Institutional Animal Care and Use Committee, Johns Hopkins University ▪ Animal Use Protocol Veterinary Reviewer, 2010-2014 ▪ Lecturer and Laboratory Instructor for Rodent Surgery and Class lab, 2010-2011
2012	Cellular and Molecular Medicine Program Pollard Scholar, Principles of Immunology I course, Johns Hopkins Bloomberg School of Public Health
2012	Lecture Presenter, The Use of Animals in Biomedical Research, Introduction to Research Ethics II course, Johns Hopkins School of Medicine
2010-2011	Teaching Assistant, Third Year Medical Student Surgery Lab, Minimally Invasive Surgical Training Center, Johns Hopkins School of Medicine
2010	Laboratory Assistant, Clinical Examination and Clinical Pathology & Specimen Collection Labs, Mouse Pathobiology and Phenotyping Shortcourse 2010
2010	Laboratory Assistant, Mouse Necropsy Lab, Summer Internship Program, Johns Hopkins School of Medicine
2007-2009	Research Committee Student Chair, Texas Veterinary Medical Association

2007-2009	Texas A&M College of Veterinary Medicine Open House ▪ Small Animal Hospital Chair, 2008, 2009 ▪ Endoscopy Room Chair, 2008 ▪ Anatomy Room Co-Chair, 2007
2008	Laboratory Instructor, Mouse Intubation Lab, Department of Molecular and Microbial Pathogenesis, Texas A&M Health Science Center

PROFESSIONAL MEMBERSHIP

District of Columbia Academy of Veterinary Medicine	2015-present
American College of Laboratory Animal Medicine, Diplomate	2014-present
American Society for Virology	2014-present
American Association for Advancement in Science	2012-present
American Association of Laboratory Animal Science	2010-present
American Society of Laboratory Animal Practitioners	2007-present
Society for Neuroscience	2014-2015
International Society for Neurovirology	2013-2014
American Veterinary Medical Association	2006-2013
Texas Veterinary Medical Association	2010-2011
Texas A&M Student Chapter of American Society of Laboratory Animal Practitioners ▪ President, 2008-2009 ▪ Vice President, 2007-2008 ▪ Co-founder, 2007	2007-2010
Texas A&M Student Chapter of American College of Veterinary Pathologists ▪ President, 2008-2009	2006-2010
Texas A&M Biochemistry and Genetics Society ▪ Treasurer, 2004-2006	2003-2006